RPP-RPT-58948, Rev. 0

Model Package Report System Model for the WMA C Performance Assessment and RCRA Closure Analysis Version 1.0

Author Name:
S. Mehta – INTERA, Inc.
M. P. Bergeron – Washington River Protection Solutions, LLC
Richland, WA 99352
U.S. Department of Energy Contract DE-AC27-08RV14800

EDT/ECN:	DRCF	UC:	
Cost Center:		Charge Code:	
B&R Code:		Total Pages:	~~177~~ 180 TM 08/17/16

Key Words: Performance Assessment, Waste Management Area C, PA, WMA C, single-shell tank, STOMP, GoldSim, process-level model, systems-level model, modeling codes, vadose zone, groundwater unsaturated flow, groundwater flow, contaminant transport, radiological dose, risk, hazard impacts, hazard quotient, hazard index, DOE Order 435.1, Washington Administrative Code, RCRA

Abstract: This model package report documents the development of a system-level model for the Waste Management Area C Performance Assessment and Resource Conservation and Recovery Act of 1976 Closure Analysis in order to support landfill closure of Waste Management Area C per the Federal and State regulations.

TRADEMARK DISCLAIMER. Reference herein to any specific commercial product, process, or service by trade name, trademark, manufacturer, or otherwise, does not necessarily constitute or imply its endorsement, recommendation, or favoring by the United States Government or any agency thereof or its contractors or subcontractors.

APPROVED
By Janis Aardal at 8:35 am, Aug 17, 2016

Release Approval Date

DATE:
Aug 17, 2016
HANFORD RELEASE

Release Stamp

Approved For Public Release

RPP-RPT-58948
Revision 0

Model Package Report System Model for the WMA C Performance Assessment and RCRA Closure Analysis Version 1.0

Prepared by:
S. Mehta
INTERA, Inc.

Prepared for:
Washington River Protection Solutions, LLC

Date:
August 2016

Approved for public release; distribution unlimited

Version History

Version	Date	Author	Change Description
Draft A	30-Nov-2015	S. Mehta	Initial draft for DOE-ORP review
Draft B	28-Jan-2016	S. Mehta	Incorporates updates based on review comments from DOE-ORP and changes to Intruder Scenario description and associated figures. Minor edits to radon flux description.
Rev. 0	26-July-2016	S. Mehta	Incorporates updates based on review comments from LFRG review. Also includes signature cover sheet to meet new QA requirements for Model Package Reports.

ENVIRONMENTAL MODEL PACKAGE REPORT COVER PAGE

Section 1 - Completed by Responsible Manager

Project:
Waste Management Area C Performance Assessment

Date:
7/26/2016

Environmental Model Name and Version:
System Model for the WMA C Performance Assessment

RELEASE/ISSUE

Section 2 - Completed by Preparer

Document Number: RPP-RPT-58948 Revision No.: 0

Revision History

Revision No.	Description	Date	Affected Pages
0	Initial Version	NA	NA

Section 3 - Completed by Responsible Manager

Document Control	Yes	No
1. Is document intended to be controlled within the Document Management Control System (DMCS)?	◉	○
2. Does document contain scientific and technical information intended for public use?	○	◉
3. Does document contain controlled-use information?	○	◉

Section 4 - Training and Software Installation Approval (Completed Prior to Model Implementation)

Modeler-Required Training Completed:

Print	Position	Signature	Date
WE Nichols (Training Coordinator)	Principal Engineer		26 Jul 2016

Implementation Software Installation and Checkout Certified:

Print	Position	Signature	Date
WE Nichols (Training Coordinator)	Principal Engineer		26 Jul 2016

Section 5 - Document Review & Approval

Print	Position	Signature	Date
Sunil Mehta (Model Developer)	Principal Scientist		07/26/16
Amena Mayenna (Model Checker)	Environmental Engineer		07/26/16
Raziuddin Khaleel (Model Senior Reviewer)	Principal Scientist		07/27/16

Page 1 of 1 A-6006-960 (REV 0)

EXECUTIVE SUMMARY

This model package report documents the development of a system-level model for the Waste Management Area C Performance Assessment and Resource Conservation and Recovery Act of 1976 (RCRA) Closure Analysis in order to support safe closure of Waste Management Area C as per the Federal and State regulations. Instead of performing calculations using specialized process-level models for each part of the subsystem, a single model is developed for computationally efficient evaluation of the total system through coupling of processes at various scales that are relevant for evaluating the long-term performance and for comparison to the performance objectives. Some of the important submodels/processes that are included within the system model calculation architecture are: (a) waste form degradation and release from various residual inventory-containing sources at closure (tanks and ancillary equipment); (b) flow and transport of contaminants through the vadose zone and saturated zone using an abstraction approach; (c) air-pathway transport of volatile contaminants; (d) calculation of effective dose and risk from exposure of radionuclides and chemicals at the assessment point for various exposure scenarios; (e) calculation of acute and chronic dose to the inadvertent intruder; and (f) radon flux calculation from residual waste.

One of the primary goals of the system model is to evaluate the uncertainty in calculated dose at the point of compliance due to uncertainty in input parameters and in recognition of environmental processes that are inherently uncertain. Uncertainty analysis is undertaken to understand which uncertain factors (parameters or processes) exert the greatest influence on the model results. The objective of the uncertainty analysis is to support the determination that there is a reasonable expectation of meeting the performance objectives.

CONTENTS

1 PURPOSE 1-1

1.1 NEED 1-1

1.2 BACKGROUND 1-1

1.3 DOCUMENT ORGANIZATION 1-5

2 MODEL OBJECTIVES 2-1

3 MODEL CONCEPTUALIZATION 3-1

3.1 FEATURES, EVENTS, AND PROCESSES 3-1

3.2 SOURCE TERM AND ENGINEERED FEATURES 3-5

3.2.1 100-Series Tanks 3-9

3.2.2 200-Series Tanks 3-10

3.2.3 244-CR Process Tank Vault 3-10

3.2.4 Pipelines 3-10

3.2.5 Gas-Phase Diffusive Flux 3-14

3.3 CONCEPTUAL MODEL FOR TRANSPORT ALONG GROUNDWATER PATHWAY 3-14

3.4 CONCEPTUAL MODEL FOR TRANSPORT ALONG ATMOSPHERIC PATHWAY 3-16

4 MODEL IMPLEMENTATION 4-1

4.1 SOFTWARE 4-1

4.2 SOURCE TERM IMPLEMENTATION 4-2

4.2.1 Sorption of Contaminants to Grout and Concrete 4-4

4.2.2 Source Term Mathematical Model 4-5

4.3 ABSTRACTION APPROACH FOR IMPLEMENTING GROUNDWATER TRANSPORT PATHWAY 4-9

4.4 IMPLEMENTATION OF ATMOSPHERIC TRANSPORT PATHWAY 4-23

4.4.1 Mathematical Modeling of First Step 4-32

4.4.2 Gas Tortuosity 4-33

4.4.3 Mathematical Modeling of Second Step 4-36

4.4.4 Horizontal and Vertical Plume Dispersivity in Air 4-37

4.5 IMPLEMENTATION OF INADVERTENT INTRUDER SCENARIO 4-38

4.6 PARAMETERIZATION 4-41

4.6.1 Selection of Radionuclides for System-Level Model 4-41

4.6.2 Selection of Chemicals for System-Level Model 4-42

5 MODEL SENSITIVITY AND UNCERTAINTY ANALYSIS 5-1

5.1 SENSITIVITY ANALYSIS 5-1

5.2 UNCERTAINTY ANALYSIS 5-1

5.2.1 Parameter Uncertainty Distributions 5-2

5.2.2 Development of Vadose Zone Flow Fields and Propagation of Uncertainty 5-29

6 MODEL LIMITATIONS 6-1

7 GOLDSIM© SOFTWARE 7-1

8 MODEL CONFIGURATION MANAGEMENT 8-1

9 MODEL RECOMMENDATIONS 9-1

10 REFERENCES 10-1

APPENDIX A – RESULTS ILLUSTRATING VADOSE ZONE FLOW-FIELD UNCERTAINTY RANGE ..... A-i

FIGURES

Figure 1-1. Location of Waste Management Area C in Relation to Hanford Site..... 1-3

Figure 1-2. Conceptual Model of Closure of Waste Management Area C..... 1-4

Figure 2-1. Overview of the Analysis of Performance for the Waste Management Area C Performance Assessment..... 2-1

Figure 2-2. Complementary Use of Subsurface Transport Over Multiple Phases and GoldSim© in the Evaluation of Parts of the Performance Assessment. 2-2

Figure 3-1. Schematic Conceptual Representation of Waste Management Area C and Various Pathways..... 3-2

Figure 3-2. Conceptual Model of the Waste Management Area C Site Showing Stratigraphy. 3-3

Figure 3-3. Aerial View of Waste Management Area C Showing Surface Features and the Surrounding Area. 3-4

Figure 3-4. Computer-Aided Modeling Results Showing Distribution of Residual Waste for a Retrieved Tank..... 3-7

Figure 3-5. Conceptual Model of Tank after Site Closure..... 3-8

Figure 3-6. Engineered Structure at the Base of the C-100-Series Tank..... 3-11

Figure 3-7. C-100-Series Tank Corner Features..... 3-12

Figure 3-8. C-200-Series Tank Cross-Section. 3-13

Figure 3-9. Schematic of the 244-CR Process Tank Vault in Waste Management Area C. 3-14

Figure 3-10. Location of Active and Existing Pipelines Along with New and Existing Facilities for Waste Fractionization Operations (1961 to 1978)..... 3-15

Figure 4-1. Three-Dimensional Subsurface Transport Over Multiple Phases (STOMP©)-Based Model Node Locations for Waste Management Area C along with Location of Cross-section Lines..... 4-12

Figure 4-2. Northwest-Southeast Trending Geologic Cross-sections Through the Tank Farm Using Information from Three-Dimensional Subsurface Transport Over Multiple Phases (STOMP©)-Based Model..... 4-13

Figure 4-3. Moisture Content Distribution below Tank 241-C-105 at Various Times during (a) Surface Barrier Design Time Period of 500 years Following Closure and (b) Post-Surface Barrier Design Time Period. 4-15

Figure 4-4. Vertical Darcy Flux Distribution below Tank 241-C-105 at Various Times..... 4-16

Figure 4-5. Representative Hydrostratigraphic Column for (a) 100-Series and (b) 200-Series Tanks. 4-17

Figure 4-6. Representative Flow Field Applied Under 100-Series Tank for the Base Case (Intact Tank condition)..... 4-20

Figure 4-7. Representative Flow Field Applied Under 200-Series Tank for the Base Case (Intact Tank condition)..... 4-21

Figure 4-8. Representative Flow Field Applied for Degraded Tank Conditions for (a) 100-Series Tank and (b) 200-Series Tank. 4-22

Figure 4-9. Implementation of Aquifer Pathway for a Given Source Area Along with Points of Evaluation of Concentrations..... 4-23

Figure 4-10. Vertical Darcy Flux Extracted from Three-Dimensional Subsurface Transport Over Multiple Phases (STOMP©)-Based Model Nodes Located below Tanks 241-C-105, 241-C-112, and 241-C-201 along with Their Location in Waste Management Area C. 4-25

Figure 4-11. Comparison between Three-Dimensional Subsurface Transport Over Multiple Phases (STOMP©)-Based Model Prediction and GoldSim©-Based One-Dimensional Abstraction Model Prediction for Nodes Located in H1 Gravelly Sand Unit..... 4-26

Figure 4-12. Comparison between Three-Dimensional Subsurface Transport Over Multiple Phases (STOMP©)-Based Model Prediction and GoldSim©-Based One-Dimensional Abstraction Model Prediction for Nodes Located in H2 Sand Unit and H3 Gravelly Sand Unit. 4-27

Figure 4-13. Comparison between Three-Dimensional Subsurface Transport Over Multiple Phases (STOMP©)-Based Model Prediction and GoldSim©-Based One-Dimensional Abstraction Model Prediction in the Saturated Zone at 100 meter Distance from the Waste Management Area C Fenceline. 4-28

Figure 4-14. Atmospheric Transport Pathway Considered for Release from Tank Sources.... 4-32

Figure 4-15. Atmospheric Transport Pathway from a Source to the Receptor Located at the Point of Calculation Along the Centerline of the Gas Plume. 4-34

Figure 4-16. A Schematic of Gaseous Plume Movement Based on Gaussian Distribution in the Horizontal and Vertical Directions. 4-35

Figure 4-17. Comparison of Measured Tortuosity (i.e., Ratio of Diffusion Coefficient in Soil [D_{ef}] to that in Free Air [D_0]) with Fitted Tortuosity Models..... 4-36

Figure 5-1. Cumulative Distribution Function of Normalized Inventory of Technetium-99 for Retrieved Tanks, and the Average Cumulative Distribution Function. 5-8

Figure 5-2. Cumulative Distribution Function of Normalized Inventory of Various Analytes for the Retrieved Tanks along with the Average Cumulative Distribution Function. 5-9

Figure 5-3. Cumulative Distribution Function of Normalized Residual Volume for the Retrieved Tanks along with the Average Cumulative Distribution Function..... 5-19

Figure 5-4. Fitted Log-Normal Distribution to the Saturated Hydraulic Conductivity Dataset Used for H2 Unit. 5-21

Figure 5-5. Fitted Log-Normal Distribution to the van Genuchten “Alpha” Parameter Dataset Used for H2 Unit. 5-22

Figure 5-6. Fitted Log-Normal Distribution to the van Genuchten “*n*” Parameter Dataset Used for H2 Unit. 5-23

Figure 5-7. 200 Realizations of Unsaturated Hydraulic Conductivity as a Function of Matric Potential for H2 Unit. Red line indicates the Composite curve used in the Base Case. 5-24

Figure 5-8. 200 Realizations of Soil-Moisture as a Function of Matric Potential for H2 Unit. Red line indicates the Composite curve used in the Base Case. 5-25

Figure 5-9. Fitted Log-Normal Distribution to the Saturated Hydraulic Conductivity Dataset Used for H1/H3 Units. 5-27

Figure 5-10. Fitted Log-Normal Distribution to the van Genuchten “Alpha” Parameter Dataset Used for H1/H3 Units. 5-28

Figure 5-11. Fitted Log-Normal Distribution to the van Genuchten “*n*” Parameter Dataset Used for H1/H3 Units. 5-29

Figure 5-12. 200 Realizations of Unsaturated Hydraulic Conductivity as a Function of Matric Potential for H1/H3 Units. Red line indicates the Composite curve used in the Base Case. 5-30

Figure 5-13. 200 Realizations of Soil-Moisture as a Function of Matric Potential for H1/H3 Units. Red line indicates the Composite curve used in the Base Case. .. 5-31

Figure 5-14. Cumulative Distribution Function of Pore Water Velocity from 200 Realizations for the H2 Unit. 5-36

Figure 5-15. Cumulative Distribution Function of Pore Water Velocity from 200 Realizations for the H1/H3 Unit. 5-37

Figure 5-16. Cumulative Distribution Function of Pore Water Velocity from 200 Realizations for the Backfill Unit. 5-38

Figure 5-17. Normalized Darcy Flux for Node 66 during (a) Early Post-Closure Period (b) Late Post-Closure Period. 5-41

Figure 5-18. Normalized Darcy Flux for Deeper Nodes during (a) Early Post-Closure Period (b) Late Post-Closure Period. 5-42

Figure 5-19. Normalized Moisture Content for Node 66 during (a) Early Post-Closure Period (b) Late Post-Closure Period. 5-43

Figure 5-20. Normalized Moisture Content for Deeper Nodes during (a) Early Post-Closure Period (b) Late Post-Closure Period. 5-44

Figure 5-21. Comparison between Darcy Flux Calculated using Regression Equation and that Obtained from Three-Dimensional Subsurface Transport Over Multiple Phases Based Model Simulation for the 5th Percentile Hydraulic Property Case for (a) H1 Unit under 100-Series Tank (Node 66); (b) H2 Unit under 100-Series Tank (Node 47); (c) H1 Unit under 200-Series Tank (Node 66); and (d) H2 Unit under 200-Series Tank (Node 43). 5-47

TABLES

Table 4-1. Hydrostratigraphic Unit Thickness Under the Tanks Taken From the Three-Dimensional Subsurface Transport Over Multiple Phases (STOMP©)-Based Model. 4-14

Table 4-2. Vertical Grid Discretization and Flow Field for the System-Level Model. 4-18

Table 4-3. Diffusion Coefficients in Air at 20 °C and 1 Atm. 4-31

Table 4-4. Henry's Law Constants. 4-31

Table 4-5. Descriptions of the Inadvertent Intruder Scenarios Evaluated in the Waste Management Area C Performance Assessment. 4-39

Table 4-6. List of Radionuclides Considered for the Performance Assessment. 4-43

Table 4-7. Estimated Inventory of Radionuclides (in Curies) at Closure of Waste Management Area C (Decay Corrected to January 1, 2020) Used in the Calculation. 4-45

Table 4-8. List of Chemicals Considered for the RCRA Closure Analysis. 4-48

Table 4-9. Estimated Inventory of Chemicals (in Kilograms) at Closure at Waste Management Area C Used in the RCRA Closure Analysis Calculations. 4-49

Table 4-10. Parameters Used in Developing Source Term Model. 4-51

Table 4-11. K_d Values (mL/g) for Grout/Concrete Used for Waste Management Area C Performance Assessment. 4-52

Table 4-12. K_d Values (mL/g) for Sand Material. 4-54

Table 5-1. Spatial and Temporal Uncertainty in Recharge Rates Considered for Waste Management Area C. 5-6

Table 5-2. Uncertainty Distributions Developed for H1/H3 Hydraulic Properties. 5-26

Table 5-3. Uncertainty Distributions Developed for Backfill Hydraulic Properties. 5-33

Table 5-4. Uncertainty in K_d Values (mL/g) for Sand As a Triangular Distribution. 5-34

Table 5-5. van Genuchten-Mualem Parameters Corresponding to the Percentiles Selected from the Vertical Pore Water Velocity Cumulative Distribution Functions. 5-39

Table 5-6. Recharge Rate Used in Scaling Flow Field. 5-39

Table 5-7. Example of Normalized Darcy Flux at Calendar Year 2300 from Selected Three-Dimensional STOMP©-based Model Nodes under Tank 241-C-105 Using 5th Percentile Hydraulic Property. 5-40

Table 5-8. Regression Equations for Scaling Darcy Flux for 100-Series Tank. 5-45

Table 5-9. Regression Equations for Scaling Darcy Flux for 200-Series Tank. 5-45

Table 5-10. Regression Equations for Scaling Volumetric Moisture Content. 5-46

TERMS

1-D	one dimensional
244-CR vault	244-CR Process Tank Vault
3-D	three-dimensional
BBI	Best-Basis Inventory
CDF	cumulative distribution function
CHPRC	CH2M HILL Plateau Remediation Company
COPC	constituent of potential concern
CPGWM	Central Plateau Groundwater Model
DOE	U.S. Department of Energy
EMMA	Environmental Model Management Archive
FEP	Feature, event, or process
HISI	Hanford Information Systems Inventory
HSU	hydrostratigraphic unit
PA	performance assessment
RCA	Resource Conservation and Recovery Act of 1976 (RCRA) Closure Analysis
RCRA	Resource Conservation and Recovery Act of 1976
RSD	relative standard deviation
SD	standard deviation
SST	single-shell tank
TWINS	Tank Waste Information Network System
WMA	Waste Management Area

1 PURPOSE

A system-level model is developed to assess the long-term performance of Waste Management Area (WMA) C following closure. The purpose of the system model is to evaluate the impact of features, processes, and events that are deemed to be relevant at both the spatial and temporal scale of the analysis on release of contaminants from the residual waste, their transport through the geosphere, and eventual impact on the biosphere at the point of compliance. Instead of performing calculations using specialized codes for each part of the subsystem, a single model is developed for computationally efficient evaluation of the total system through coupling of processes at various scales that are relevant for evaluating the long-term performance and for comparison to the performance objectives.

1.1 NEED

A performance assessment (PA) of Single-Shell Tank (SST) WMA C located at the U.S. Department of Energy's (DOE's) Hanford Site in southeastern Washington is being conducted to satisfy the requirements of the Hanford Federal Facility Agreement and Consent Order (Ecology et al. 1989), as well as other Federal requirements and State-approved closure plans and permits. The WMA C PA assesses the fate, transport, and impacts of radionuclides and hazardous chemicals within residual wastes left in tanks and ancillary equipment and facilities in their assumed closed configuration and the subsequent potential risks to humans into the far future.

The system model is developed to support two documents, one related to PA in terms of radiological dose impacts and the other related to the environmental impacts from hazardous chemicals in the residual inventory. The part of the PA focused on radiological impacts is being developed to meet the requirements for a closure authorization under DOE O 435.1, Radioactive Waste Management. The second part of the analysis will evaluate human health and environmental impacts from hazardous chemical inventories in residual wastes remaining in WMA C tanks and ancillary equipment to meet the requirements for permitted closure under the Resource Conservation and Recovery Act of 1976 (RCRA).

System-level modeling is needed to evaluate the long-term impacts from slow release of contaminants from the residual inventories at closure. The time scale of analysis is up to 10,000 years and needs to consider the combined effects of contaminants in the aquifer from various source terms leading to eventual exposure to a Reference Person. In addition, a probabilistic analysis is required to evaluate the impact of parameter uncertainty in estimating dose for the PA, which requires a system model.

1.2 BACKGROUND

WMA C is one of seven WMAs (A-AX, B-BX-BY, C, S-SX, T, TX-TY, and U) containing 149 SSTs built from 1943 to 1964. In general, the WMA C boundary is represented by the fenceline surrounding 241-C Tank Farm (C Farm) (Figure 1-1). WMA C contains 12 100-series

SSTs and 4 200-series SSTs that were constructed in 1943 to 1944 along with associated ancillary equipment (i.e., diversion boxes, pipes). It was placed in service in 1946 and used to store and transfer waste until mid-1980. Additional ancillary equipment (244-CR Process Tank Vault [244-CR vault] and CR diversion boxes) were added in the early 1950s.

During its operational history, a number of confirmed or suspected waste release events have occurred at WMA C. These included suspected tank leaks and known unplanned releases from waste transfer lines and systems.

Pumping of liquid waste in preparation for removing the tanks from service began in 1976. Currently, the pumpable liquid wastes have been removed from the C Farm tanks and all tanks have been stabilized on an interim basis. Since 2003, there has been a concerted effort to retrieve the waste from the SSTs within WMA C. At present, waste retrieval has been completed for 13 of the 16 tanks. Retrieval is underway for SSTs 241-C-102 (C-102), 241-C-105 (C-105), and 241-C-111 (C-111).

Figure 1-2 illustrates the closure concept for WMA C following tank waste retrieval. Surface facilities will be removed and retrieved SSTs and accessible ancillary equipment with significant void spaces will be filled with grout. Waste transfer pipelines are also expected to be left in place. An engineered surface cover system will be placed over the tank farm and will be monitoring using existing wells.

The PA modeling considered reduction of net infiltration from the presence of an engineered cover (surface barrier) over WMA C. The surface barrier is assumed to remain intact and allow only negligible amounts of net infiltration for the first 500 years (i.e., 2020 to 2520), coinciding with an estimated 500-year barrier design life, which includes a 100-year institutional control time period.

For the purpose of assessing the long-term performance, a closure date of 2020 is assumed for WMA C. In the post-closure assessment, three time periods of barrier performance are considered, as follows.

- A 100-year institutional control period when the engineered surface cover (overlying WMA C) is working to its full barrier capability resulting in 0.5 mm/yr recharge rate under the base of WMA C.

- An additional time period of 400 years after the institutional control period during which the full barrier capability results in 0.5 mm/yr recharge rate under the base of WMA C.

- A time period after 500 years after closure during which the surface cover barrier function is assumed to be fully degraded at the start of the time period (assuming a design life of 500 years).

Under DOE O 435.1, the dose performance objectives must be complied with for 1,000 years after site closure. The post-compliance period (beyond 1,000 years) up to 10,000 years is considered for the purpose of evaluating uncertainty and sensitivity on dose estimates.

Figure 1-1. Location of Waste Management Area C in Relation to Hanford Site.

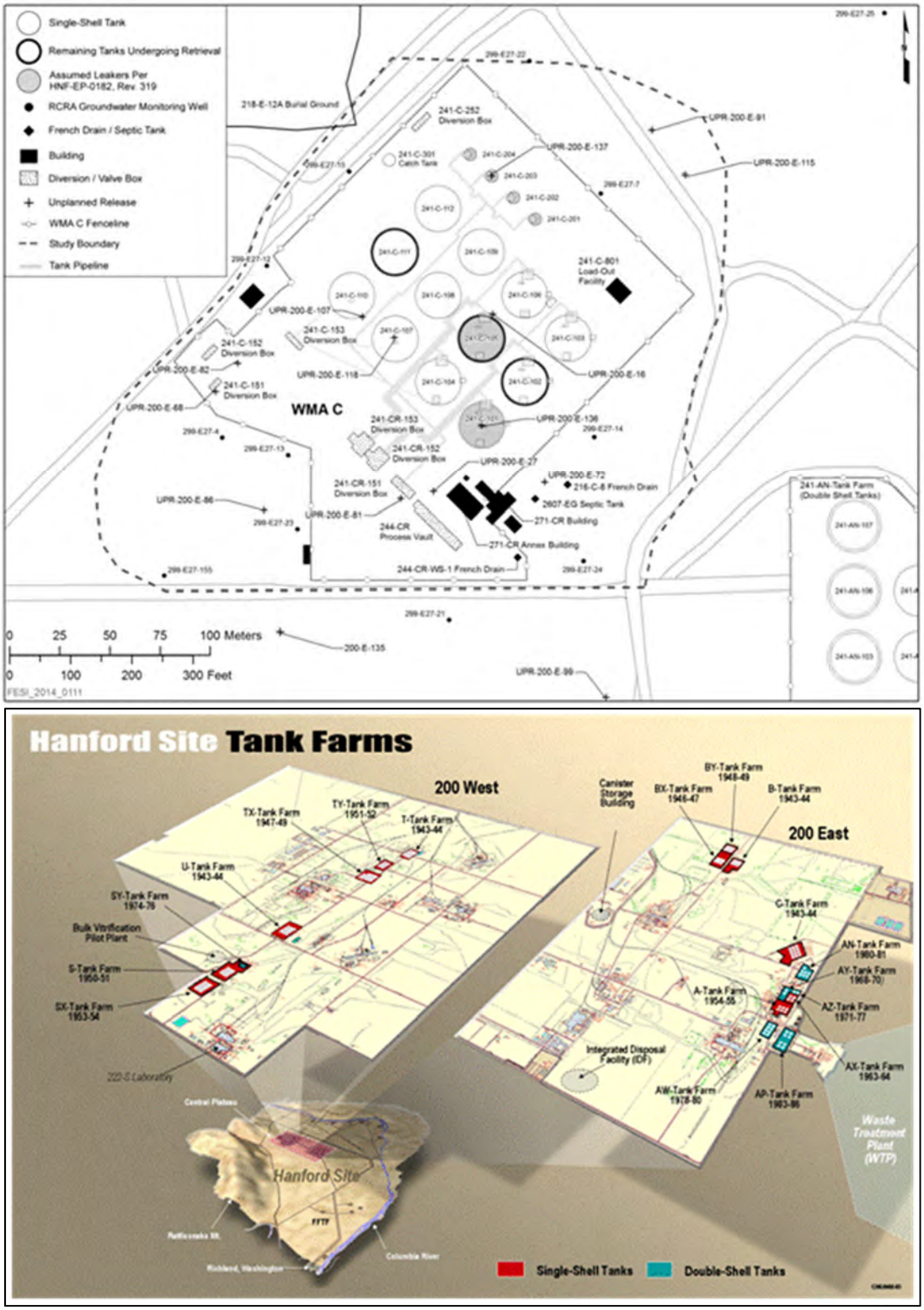

RCRA = Resource Conservation and Recovery Act of 1976 WMA = Waste Management Area

Reference: HNF-EP-0182, 2014, "Waste Tank Summary Report for Month Ending July 31, 2014," Rev. 319.

Figure 1-2. Conceptual Model of Closure of Waste Management Area C.

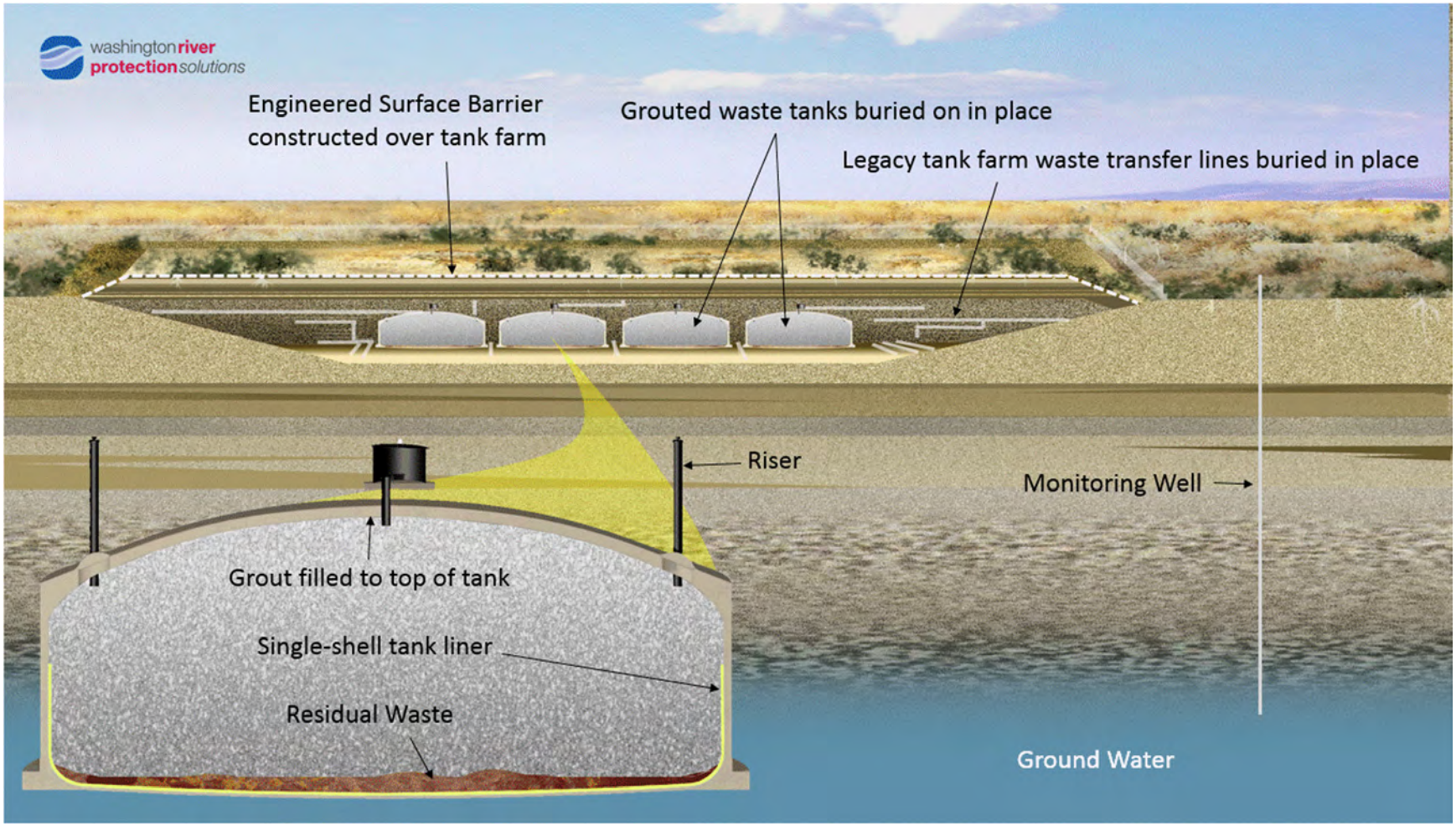

1.3 DOCUMENT ORGANIZATION

The model package report is organized into three parts: (1) basis for development of the model, including the identification of objectives; (2) software qualifications; and (3) model implementation and parameterization. Section 2 presents the modeling objectives. Section 3 presents the relevant Features, Events, and Processes (FEPs) that affect flow and transport in WMA C, along with the modeling assumptions and the source characteristics of the residual contamination. Section 4 describes the modeling implementation details, initial conditions, boundary conditions, and parameter values. Section 5 discusses the use of the GoldSim©[1] software to conduct the analysis. Section 6 identifies the limitations of the model, and the applicability of the results, and Section 7 provides the details related to configuration management of the model inputs and outputs including the software used.

[1] GoldSim© simulation software is copyrighted by GoldSim Technology Group LLC of Issaquah, Washington (see http://www.goldsim.com).

This page intentionally left blank.

2 MODEL OBJECTIVES

The major pathways for contamination entering the environment are the groundwater pathway, the air pathway, and a hypothetical inadvertent intruder pathway (through drill cuttings brought to the surface). Figure 2-1 shows the various pathways of possible exposure evaluated in the PA. For the RCRA Closure Analysis (RCA) only the groundwater pathway is evaluated. The most important exposure pathway for hydrologic transport is groundwater use for drinking water, irrigation, livestock watering, and biotic transport. Under the groundwater pathway, it is assumed that moisture from rain and snowfall enters the subsurface, contacts waste, and carries dissolved contaminants through the thick heterogeneous vadose zone to the unconfined aquifer. During the compliance and post-compliance periods, a receptor is assumed to reside 100 m downgradient from the southeastern edge of the WMA fenceline.

Figure 2-1. Overview of the Analysis of Performance for the Waste Management Area C Performance Assessment.

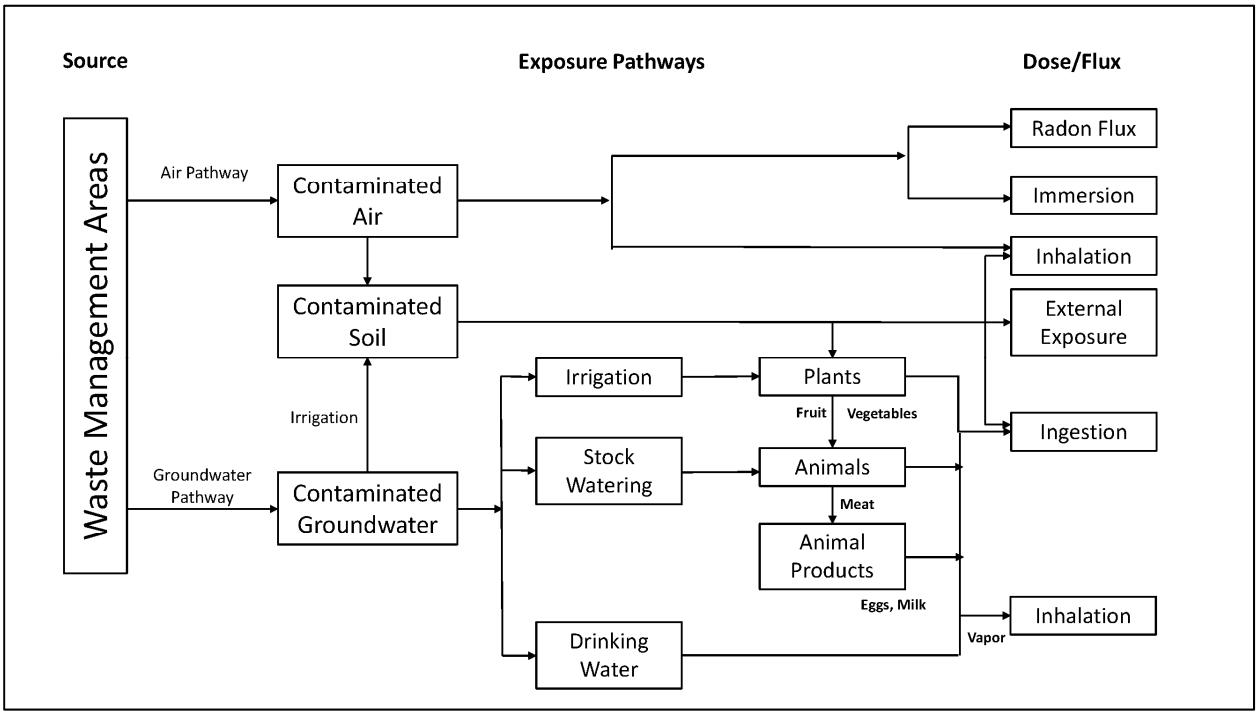

WMA = Waste Management Area

The modeling to support the PA and RCA is being conducted using complementary approaches, including both deterministic and probabilistic approaches for simulating contaminant releases to groundwater (Figure 2-2). Since a variety of mass transport and exposure scenario calculations are needed to support the PA and RCA requirements, the methodology conducts some calculations using a process-level model while other calculations are conducted using the system-level model.

Figure 2-2. Complementary Use of Subsurface Transport Over Multiple Phases and GoldSim© in the Evaluation of Parts of the Performance Assessment.

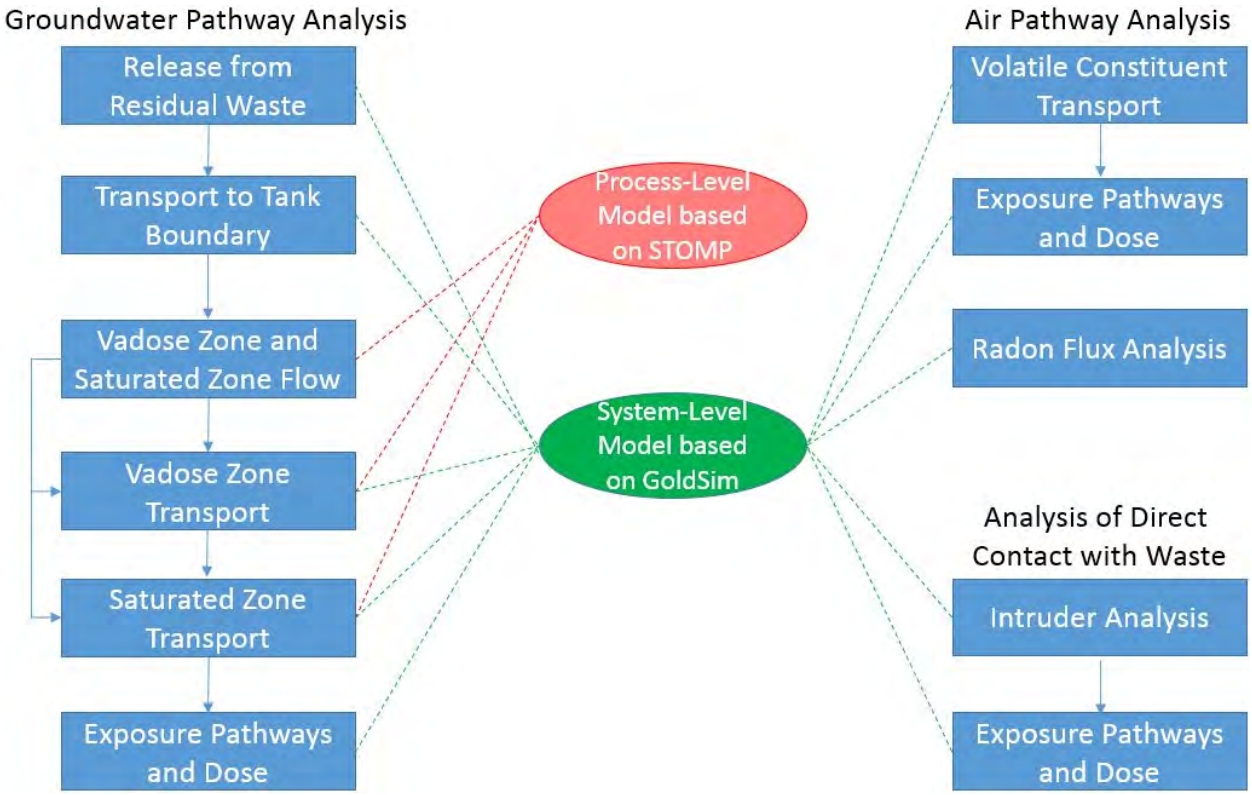

GoldSim© simulation software is copyrighted by GoldSim Technology Group LLC of Issaquah, Washington (see http://www.goldsim.com).
Subsurface Transport Over Multiple Phases (STOMP©) is copyrighted by Battelle Memorial Institute, 1996.

A three-dimensional (3-D) process-level flow and contaminant transport numerical model has been developed using Subsurface Transport Over Multiple Phases (STOMP©)[2] to evaluate the contaminant transport through the vadose zone and saturated zone and to calculate the groundwater concentration at the receptor location. All other calculations that are needed to satisfy the requirements of the PA and RCA are undertaken using the system-level model. The system-level model developed using GoldSim© is used for:

- Source term modeling to evaluate release from residual waste within the grouted tanks and ancillary equipment and to provide input to the 3-D process model developed using STOMP© code

- Modeling transport of contaminants through the vadose zone and saturated zone using an abstraction approach

- Modeling transport of volatile contaminants along the air pathway including calculation of radon flux at the surface of WMA C

[2] Subsurface Transport Over Multiple Phases (STOMP©) is copyrighted by Battelle Memorial Institute, 1996.

- Calculating radiological dose and risk through implementation of exposure scenarios

- Inadvertent intruder analysis.

The description of the 3-D flow and contaminant transport model developed using STOMP© are presented in a separate document (RPP-RPT-58949, "Model Package Report Flow and Contaminant Transport Numerical Model used in WMA C Performance Assessment and RCRA Closure Analysis"). The current report discusses the system-level model that is implemented using GoldSim©.

This page intentionally left blank.

3 MODEL CONCEPTUALIZATION

This section describes the modeling methodology for the determination of the WMA C residual waste impacts using the system model. This methodology uses conceptual models that are based on the physical system and expected contaminant migration pathways.

Figure 3-1 provides a schematic representation of both WMA C as it will exist at closure and the contaminant migration pathways evaluated in this PA. WMA C is composed of man-made and natural components. The man-made components of the system that influence contaminant migration include a closure surface barrier, the WMA C tanks, pipelines, and infrastructure, and the distribution of waste in those components. The natural components of the system that influence contaminant migration are a number of mostly horizontal stratigraphic layers within the vadose zone and an underlying stratigraphic layer that is part of the unconfined aquifer. Figure 3-2 illustrates the stratigraphy for the WMA C site, which has a thick vadose zone with the water table within the undifferentiated Hanford formation and Cold Creek gravels and a predominantly south/southeastwardly groundwater flow.

Figure 3-3 shows an aerial view of WMA C, and surrounding disturbed, undisturbed, and resurfaced areas. Also shown is the location of WMA A, where the 100 m point of analysis downgradient of WMA C is located. This location represents the assumed location of a hypothetical well that supplies water for drinking and irrigation in the all-pathway dose scenario calculations.

For performing contaminant transport calculations using the system model, an abstraction approach is undertaken, where the flow field based on the results from the 3-D model developed using STOMP© is considered for the system model. Detailed representations of the geological system and hydraulic properties are implemented in the 3-D model developed using STOMP©, so that relevant features and processes on water flow and radionuclide transport in groundwater can be evaluated. However, the model for evaluating flow requires significant computational time, limiting its ability to fully address parameter uncertainties at the system level. The abstraction approach assures that, for a specific set of input parameters for flow, the flow field in both models is consistent, differing only in the discretization of the two models.

3.1 FEATURES, EVENTS, AND PROCESSES

The landfill closure of WMA C is assumed to occur at year 2020, at which time the tanks are assumed to be filled with grout and covered with a final closure cover. It is assumed that institutional control and societal memory is retained for the first 100 years after the year of closure. The point of analysis for all pathways and groundwater protection analyses is 100 m from the downgradient boundary of WMA C. In order to ensure consistency in the analysis, hazardous chemicals are also evaluated at this point in the companion report that addresses these requirements.

Figure 3-1. Schematic Conceptual Representation of Waste Management Area C and Various Pathways.

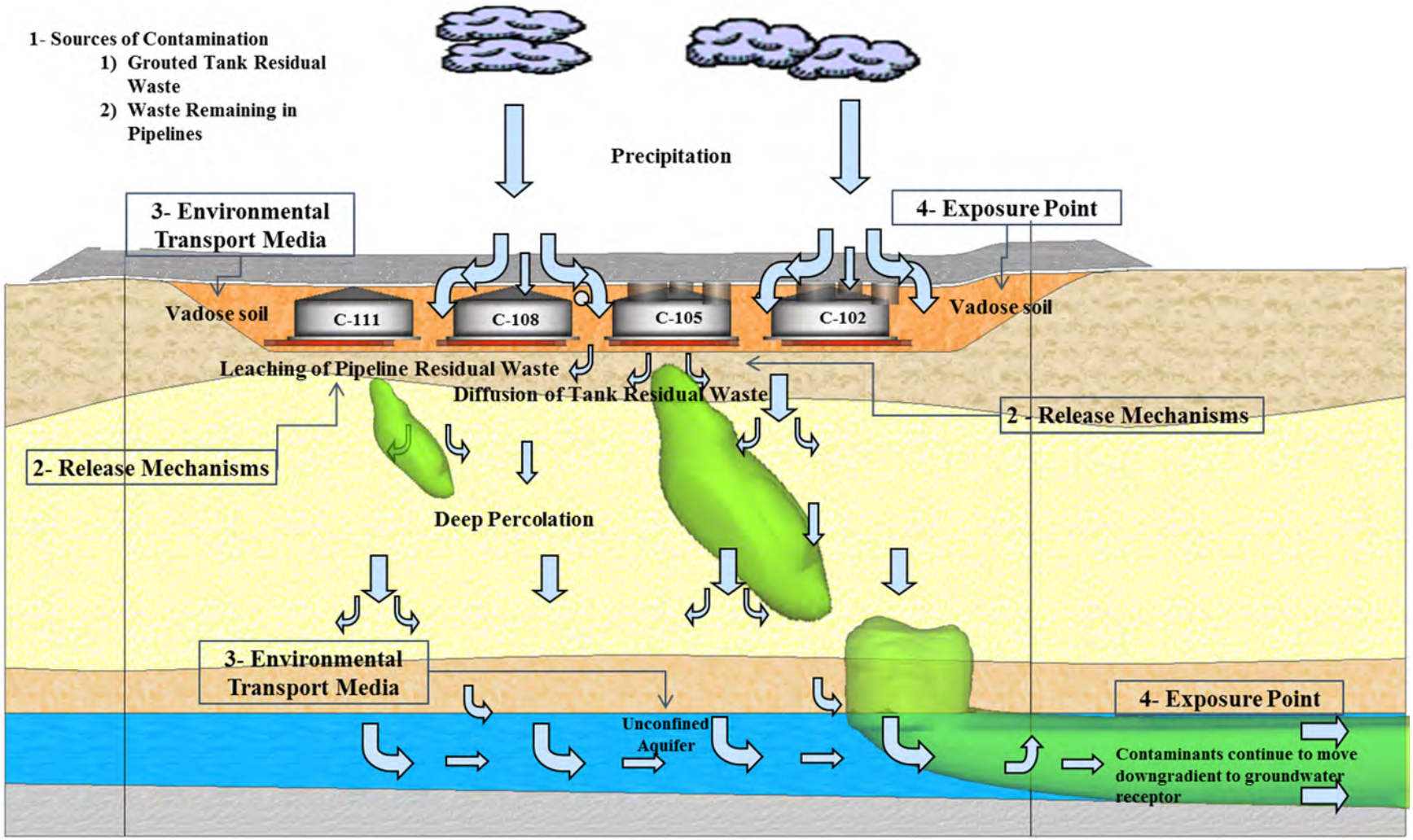

Figure 3-2. Conceptual Model of the Waste Management Area C Site Showing Stratigraphy.

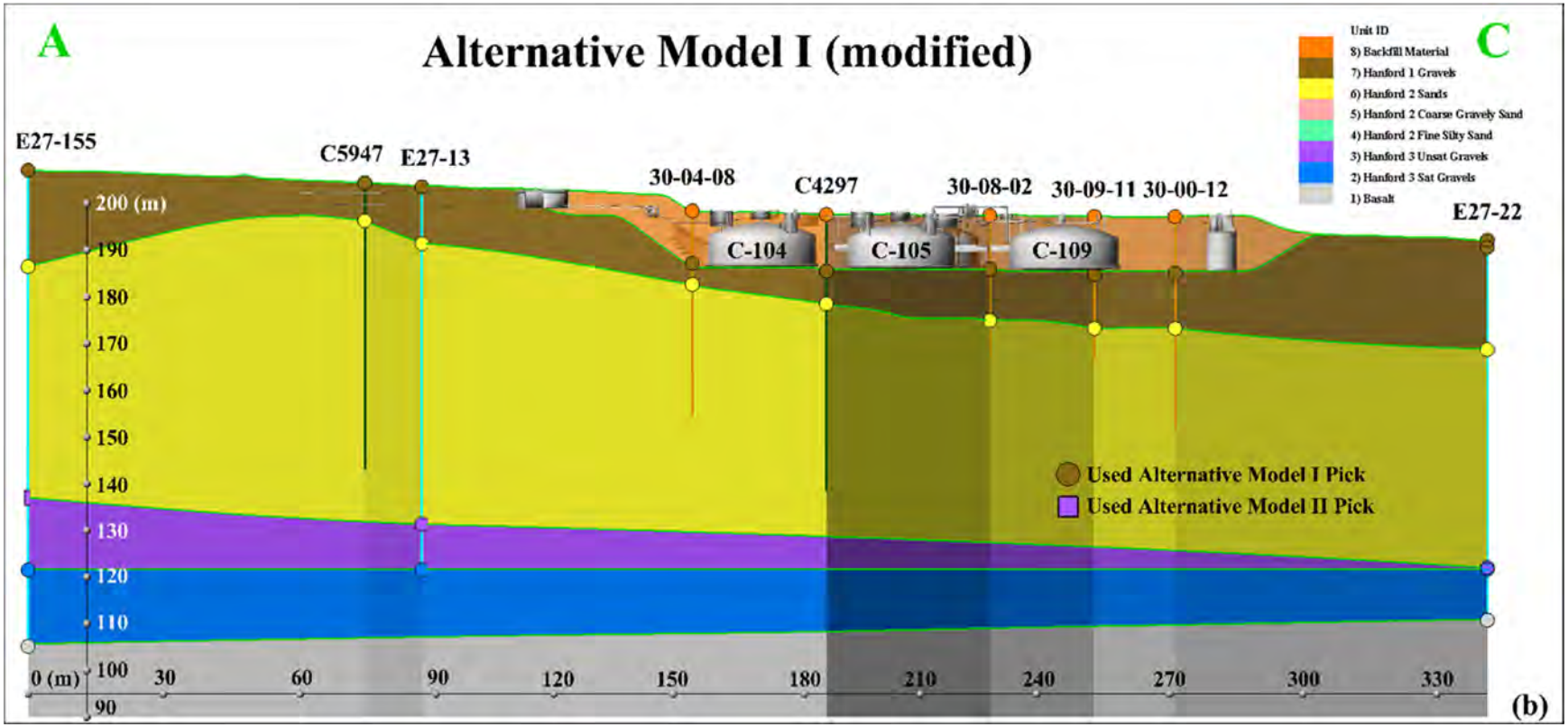

Figure 3-3. Aerial View of Waste Management Area C Showing Surface Features and the Surrounding Area.

WMA = Waste Management Area

Several key safety functions and related FEPs characterize the conceptual models for release and transport of radionuclides in WMA C for the post-closure period. The conceptual models and relevant parameters for fate and transport modeling are developed for the following four time periods:

- Pre-operations and initial construction period (before 1945) representing the time when the tank farm ground remained undisturbed from the Hanford Manhattan Project mission
- Operations period representing tank farm construction, current, and immediate future conditions of the tank farm (1945 to 2020)
- Closure and post-closure period during the assumed design life of the intact surface barrier (2020 to 2520) when the tanks become grouted and radionuclides begin to diffuse out of the grout
- Post-closure period beyond assumed design life of the surface barrier (2520 to 12120) when the performance of the surface barrier is assumed to degrade.

A 1,000-year post-closure period is considered in the WMA C PA for the purpose of evaluating compliance with DOE O 435.1 performance objectives; a 10,000-year post-closure period is considered for the purpose of evaluating uncertainty in the results.

For the system-level model calculations, following FEPs are included:

- The process of waste form degradation and release of contaminants from the grouted tanks and ancillary equipment to the outside of the tank
- Contaminant transport through the natural environment
- Transport of volatiles through the air pathway
- Calculation of radiological dose and risk to the receptor (a reasonably maximally exposed individual)
- Consideration of uncertainty in input parameters and evaluation of uncertainty in dose calculations
- Evaluation of inadvertent intruder scenario
- Account for decay and in-growth of daughter isotopes.

3.2 SOURCE TERM AND ENGINEERED FEATURES

The source term considers processes associated with release of contaminants from residual waste into the natural environment. Separate source terms are considered for each of the

twelve 100-series tanks, four 200-series tanks, C-301 catch tank, 244-CR vault, and pipelines, resulting in 19 separate source terms. The inventory used in the source term model includes the current estimate of the inventory and residual volume. Source terms for pits and diversion boxes are not explicitly considered but are incorporated as part of the pipeline source term.

Both mineral phase solubility-limited and matrix degradation rate-limited processes are considered for release of contaminant from the waste. These conceptual models are based on observations made through multi-year leaching tests and identification of mineral phases. The following release models are considered based on empirical evidence:

- a matrix-degradation-rate-based release of ^{99}Tc,
- solubility-controlled releases of uranium, and
- dissolved concentration limits for chromium.

The engineered features that are considered in the source term calculations are the tank structure, pipeline area,[3] infill grout material, and the emplaced surface cover at closure. The modified RCRA cover reduces the net infiltration that percolates to the buried tank structures and ancillary equipment. The infill grout material provides not only structural stability to the tank configuration, but also provides a relatively impermeable barrier to flow leading to flow diversion around the tank, as long as the grout is not physically degraded. The infill grout material also controls the chemical conditions of the pore water that contacts the residual waste through mineral phase dissolution and precipitation (e.g., dissolution of portlandite and precipitation of calcite).

The source term processes that are considered in the post-closure period include releases of contaminants from residual waste and their transport to the underlying vadose zone via either diffusion or advection. The key processes that are expected to affect release of contaminants from tank residuals include:

- Leaching of contaminants from the tank waste residual layer into the pore water associated with the tank residuals

- Diffusive transport of contaminants through the tank wall grout and concrete layer, along the tortuous continuous connections, to vadose zone soil outside the tank

- Ongoing chemical and physical degradation of the tank wall concrete and grout layer

- Ongoing dissolution and degradation of emplaced grout in the tank leading to eventual formation of cracks

- Advective flow of water potentially influencing the source term once a sufficient number of cracks form in the engineered barriers.

[3] Individual pipelines are not treated as separate sources. Instead, the inventory associated with the pipeline source term is distributed uniformly over the area at WMA C that contains pipelines.

The distribution of residual waste volume within the retrieved tanks has been estimated by a variety of techniques that have involved video observations and computer/CAD modeling (e.g., RPP-CALC-54266, "Post-Hard Heel Retrieval Camera/CAD Modeling System Waste Volume Estimate for Tank 241-C-108"). The result of one such attempt is presented in Figure 3-4. Spatial distribution of residual waste volumes are estimated for the tank dish bottom, tank walls and stiffener rings, and in-tank equipment for the retrieved tanks, and are summarized in RPP-RPT-42323, "Hanford C-Farm Tank and Ancillary Equipment Residual Waste Inventory Estimates." The estimates indicate that the majority of residual waste is located in the tank dish bottom (>80% for the 100-series tanks and >50% for the 200-series tanks), with minor amounts associated with the in-tank equipment.

Figure 3-4. Computer-Aided Modeling Results Showing Distribution of Residual Waste for a Retrieved Tank.

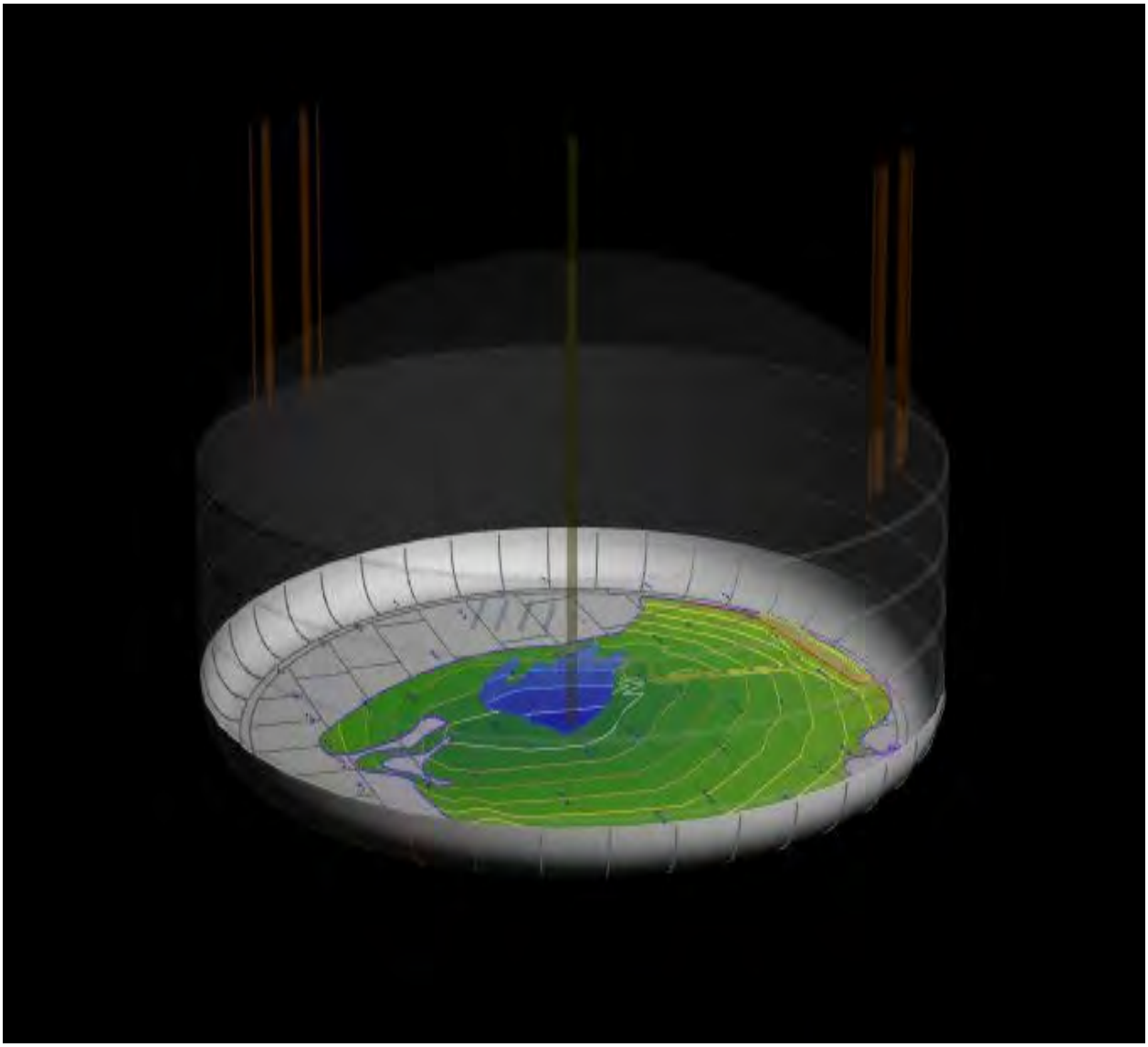

For the purpose of developing a source release model for tanks and the 244-CR vault, the residual waste volume is conceptualized to be present as a thin layer at the base of the tank (Figure 3-5). The estimated residual waste volume is assumed to be spread across the circular tank dish bottom area. The residual waste is conceptualized to be sludge-like, with a texture similar to a hardened paleosol. It is assumed to be fully saturated with a porosity of 40% based on evaluation of sludge waste phase from the retrieved tanks (Tank Waste Information Network Systems [TWINS], Queried 02/10/2014, [WMA C Tanks, wt% water in sludge/solid waste type], http://twins.pnl.gov/twins.htm). The variability associated with residual volume is considered in the uncertainty analysis.

Figure 3-5. Conceptual Model of Tank after Site Closure.

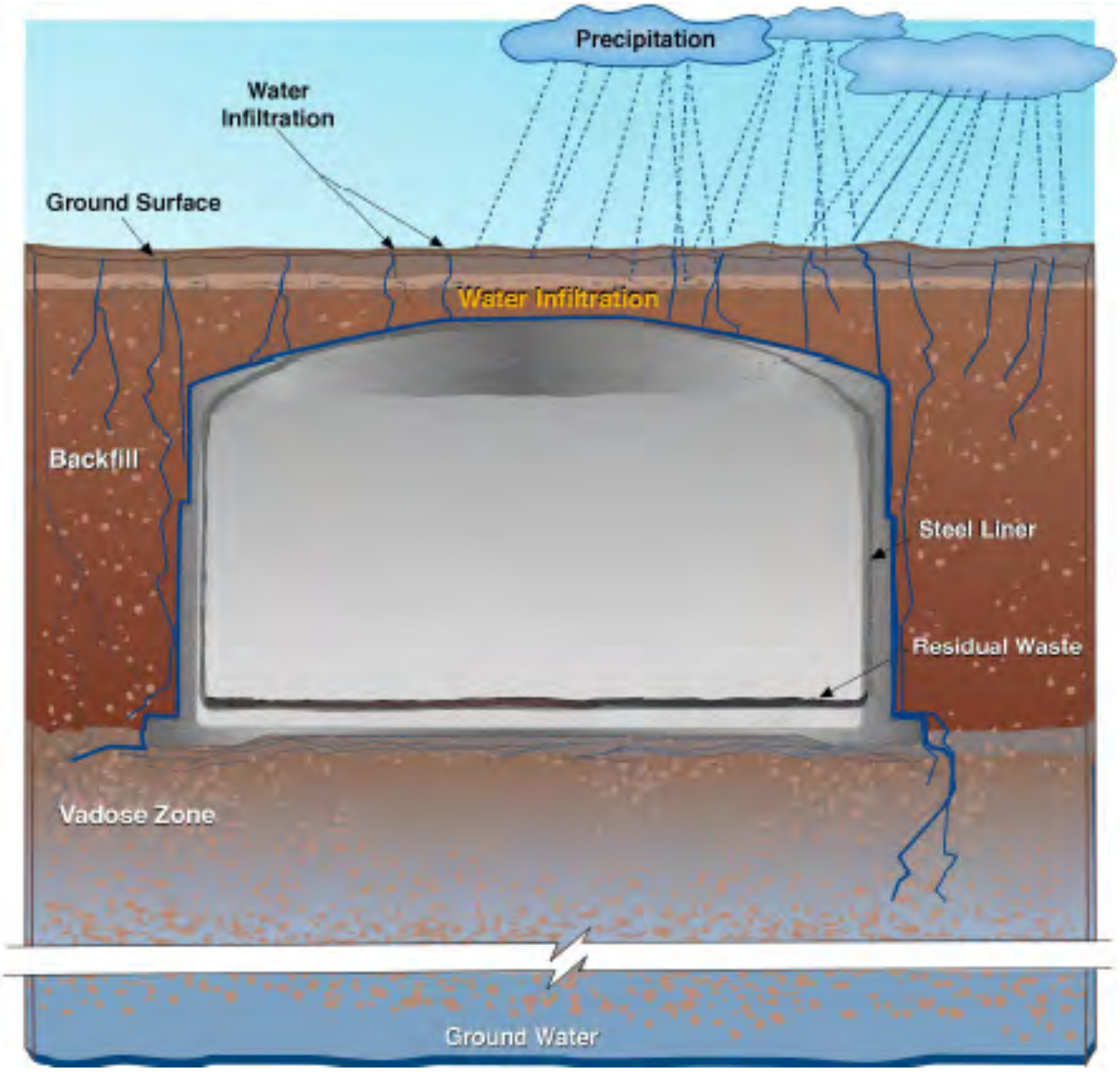

While the tank is intact, it will divert any water that infiltrates through the surface cover. Therefore, the transport mechanism for release of contaminants from the residual tank waste to the underlying vadose zone is primarily diffusive. The dissolved concentration of contaminants in the residual waste pore volume is controlled by the waste characteristics, such as waste form degradation and dissolution of solubility controlling mineral phases. The presence of continuous water connections is assumed across the grout and concrete layers for the diffusive transport to occur in the aqueous phase.

The source release model for the pipelines is quite different from the tanks. Instead of modeling discrete source terms, a single source area reflective of the approximate areal distribution of the waste transfer pipelines is considered. This is the assessed area of the tank farm where pipelines are generally present. The estimated residual inventory is uniformly spread over this area. Unlike tanks, the pipelines are assumed not to be filled with grout at closure, and due to limited information on the condition of the pipeline material, no credit is taken for the structural integrity of the pipeline. Therefore, both advective and diffusive releases are considered from the pipelines. More details related to the source conceptualization are discussed below.

3.2.1 100-Series Tanks

The C-100-series tanks consist of a concrete base slab with a steel-plate lining. They have an inside diameter of 22.9 m (75 ft) and an internal height of 5.5 m (18 ft) from the bottom metal sheets to the top of the metal side plates, which is also the spring line for the dome. The tanks are buried underground with approximately 2.1 m (7 ft) of backfill over the top of the dome to provide shielding from radiation exposure. The details of the engineered structure at the base of the C-100-series tanks are shown in Figures 3-6 and 3-7. The structures were built by installing a reinforced concrete base that is at least 0.15 m (6 in.) thick followed by 0.05 m (2 in.) of additional grout on top, over which carbon steel liner was emplaced. Following the completion of the bottom of the tank, the sidewalls of the metal liner were welded together and the liner was encased in sidewall concrete approximately 0.3 m (1 ft) thick. A concrete dome approximately 0.38 m (1.25 ft) thick was erected on top of the tank with a 3-ply waterproof membrane applied to the top of the dome.

The carbon steel liner thickness varies, from 0.375-in. thick at the base of the tank to 0.25-in. thick along the sides. As shown in Figure 3-7, the residual waste layer is conceptualized to be located on top of the carbon steel liner. Although the carbon steel liner was designed to hold the waste in place and act as a barrier to the transport of contaminants, no credit is taken for the liner due to lack of information on its present condition. Recent studies related to characterization of the corrosion behavior of the carbon steel liner (WHC-EP-0772, “Characterization of the Corrosion Behavior of the Carbon Steel Liner in Hanford Site Single-Shell Tanks”) determined several likely corrosion processes within the tank environment that could lead to degradation of steel. Some of the likely corrosion processes are pitting and crevice corrosion, stress corrosion cracking, general corrosion, and galvanic cell corrosion. These are discussed in more detail in RPP-RPT-46879, “Corrosion and Structural Degradation within Engineered System in Waste Management Area C.” These processes lead to uncertainties regarding the state of the carbon steel liner; consequently, no credit is taken in the source term model for its presence. As a result, the residual waste layer is conceptualized to overlie the 0.05 m (2 in.)-thick grout layer that is

underlain by a 0.15 m (6 in.)-thick base slab concrete layer. The source term model represents the shortest possible vertical diffusive transport path length from residual waste layer to outside of the tank, which is the combined thickness of grout and base slab concrete layer of 0.2 m (8 in.). The diffusive area is taken to be the base area of the tank. The aqueous concentration of contaminants in the residual waste provide the upstream boundary concentration for diffusive transport with a zero concentration boundary being applied in the far-field (at the water table depth). The source term release calculations are performed using the system model.

3.2.2 200-Series Tanks

The details of the engineered structure at the base of the C-200-series tanks is presented in Figure 3-8. The 200-series tanks have an internal diameter of 6.1 m (20 ft) and an operating depth of 7.3 m (24 ft). Other than the changed dimensions, the basic construction of the 200-series tanks is similar to the 100-series tanks. The 200-series tanks also have a base concrete slab over which a grout layer and a steel liner is present. The thickness of the base concrete slab is 0.15 m (6 in.), while the grout layer is 0.025 m (1 in.), leading to a combined thickness of 0.175 m (7 in.). Because the thickness differences are minor between the 100-series and 200-series tanks, a constant thickness of 0.2 m (8 in.) is applied to all the tanks for simplifying the diffusive transport calculations. Note that this thickness is conservative for diffusive release calculations as it ignores thickness of overlying steel liner (or steel corrosion products) and the residual waste (sludge) layer.

3.2.3 244-CR Process Tank Vault

The configuration of the 244-CR vault, which is located in the southwest corner of the C Farm complex, is shown in Figure 3-9. The vault is a two-level, underground, reinforced concrete structure. The lower level consists of four cells, each equipped with a concrete sump. The exterior walls and dividing walls between the cells are 0.61 m (2 ft) thick, with each cell housing a steel tank. The cells housing tanks CR-011 and CR-001 are each 26 ft long by 22 ft wide. The cells housing tanks CR-002 and CR-003 are each 20 ft long by 16 ft wide. Although the cells are distinct, for the purpose of source term modeling their inventory is assumed to be uniformly distributed over the rectangular footprint of the 244-CR vault of ~28 m (92 ft) length and 5.8 m (19 ft) width. The residual waste layer is conceptualized to be present over the grouted base of the tank, and the diffusive thickness is conservatively taken to be 0.2 m (8 in.) to be consistent with the path lengths assumed for the 100-series and 200-series tanks.

3.2.4 Pipelines

An extensive network of transfer lines connects the various components of the tank farms. These pipelines carried a variety of process wastes, typically in a slurry form. The initial tank farm waste-transfer pipelines installed in 1944 to 1945 were direct-buried (not encased) pipelines, with some on concrete slabs. Typical burial depth was 1 m (3 ft). After 1947, all pipelines installed either were concrete encased or pipe-in-pipe encased. The primary pipe used was typically carbon or stainless steel. Figure 3-10 shows the areal extent of active and existing pipelines in WMA C during the 1961 to 1978 time period.

Figure 3-6. Engineered Structure at the Base of the C-100-Series Tank.

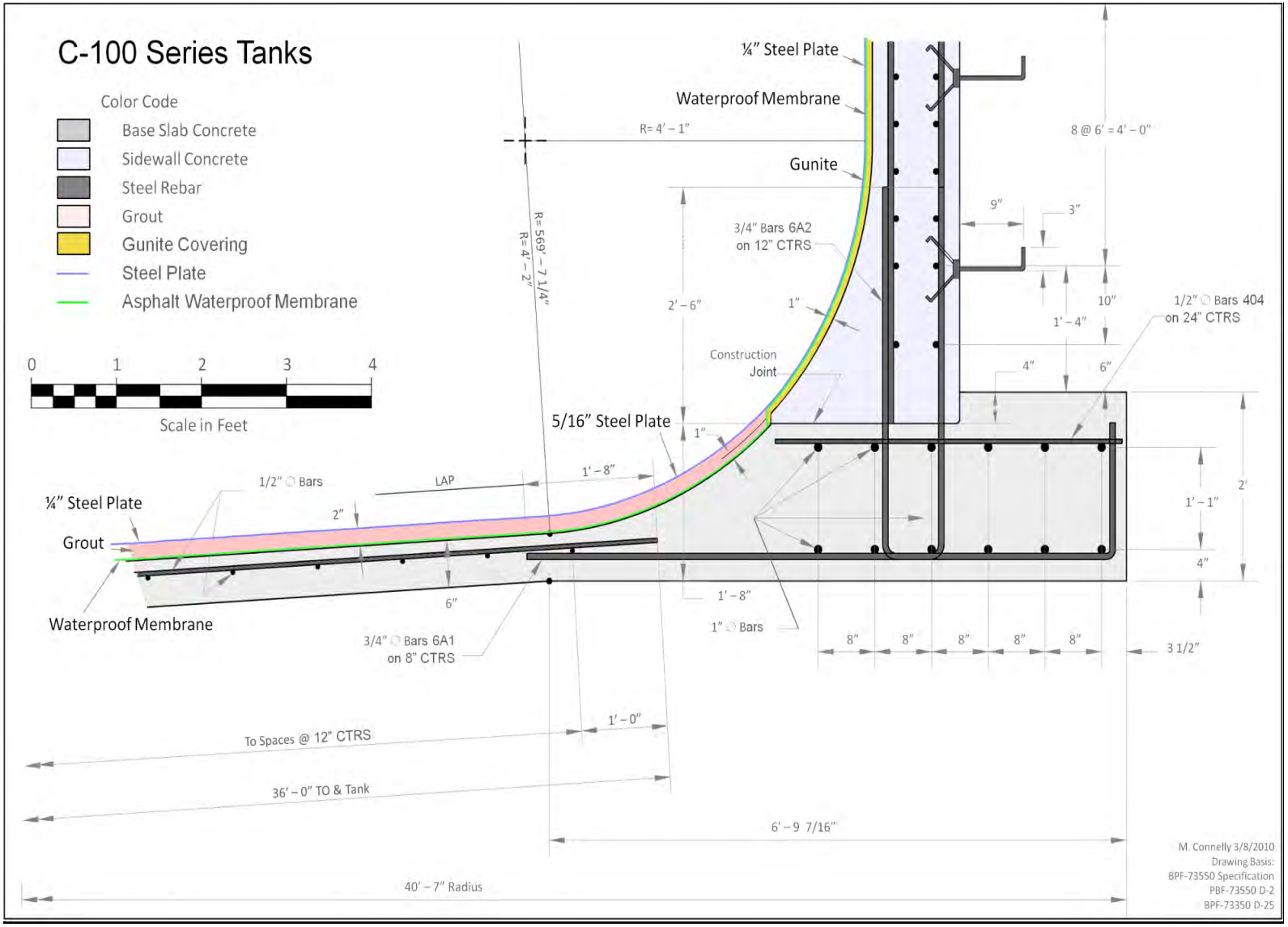

Reference: BPF-73550, "Specifications For Construction of Composite Storage Tanks Bldg. No. 241 Hanford Engineer Works Project 9536."

Figure 3-7. C-100-Series Tank Corner Features.

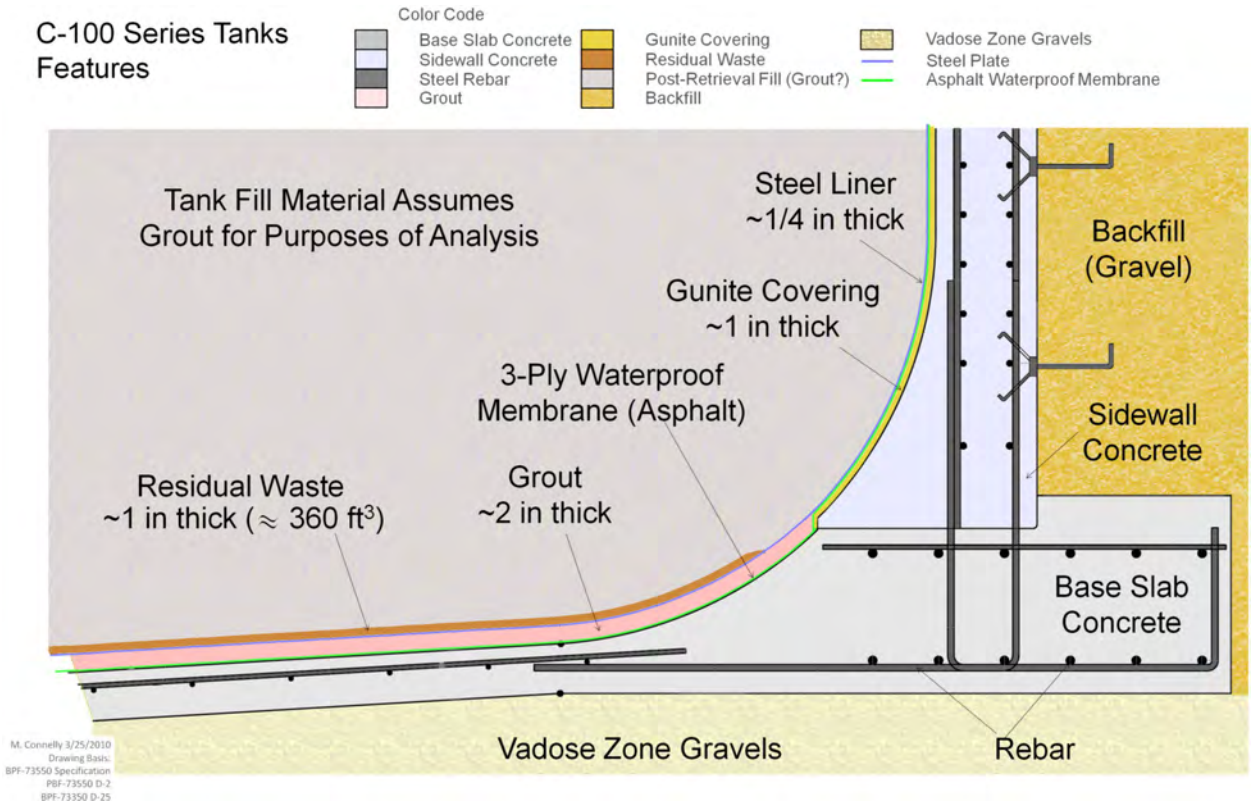

Reference: BPF-73550, "Specifications For Construction of Composite Storage Tanks Bldg. No. 241 Hanford Engineer Works Project 9536."

As discussed in RPP-PLAN-47559, "Single-Shell Tank Waste Management Area C Pipeline Feasibility Evaluation," approximately 7 miles and 200 separate pipelines with different diameters and lengths comprise the abandoned pipelines in WMA C. Appendix A of RPP-PLAN-47559 compiles the information on various pipeline segments, indicating that the pipeline diameters typically vary from 0.05 m (2 in.) to 0.15 m (6 in.), with 0.076 m (3 in.) pipe diameter being the most common.

The residual pipeline inventory is based on the assumption of fully plugged cascade lines, one known plugged pipeline, and 5% full remaining pipelines. Although the source inventory within the pipeline is spatially variable, for the purpose of the source release calculations the pipeline residual inventory is assumed to be uniformly distributed over a square area of 150 m side length. This square area of 225,000 m^2 areal extent roughly coincides with the pipeline extent area shown in Figure 3-10. The contaminated thickness in the vertical direction is taken to be 0.076 m (3 in.), which is the most common pipeline diameter. The residual inventory is conceptualized to be uniformly distributed within this volume mixed in with the bulk soil (backfill). No credit is taken for the pipeline material (carbon steel or stainless steel) as a barrier or any grout-fill that may occur in the future for transport. Therefore, the mass release is both advective and diffusive.

Figure 3-8. C-200-Series Tank Cross-Section.

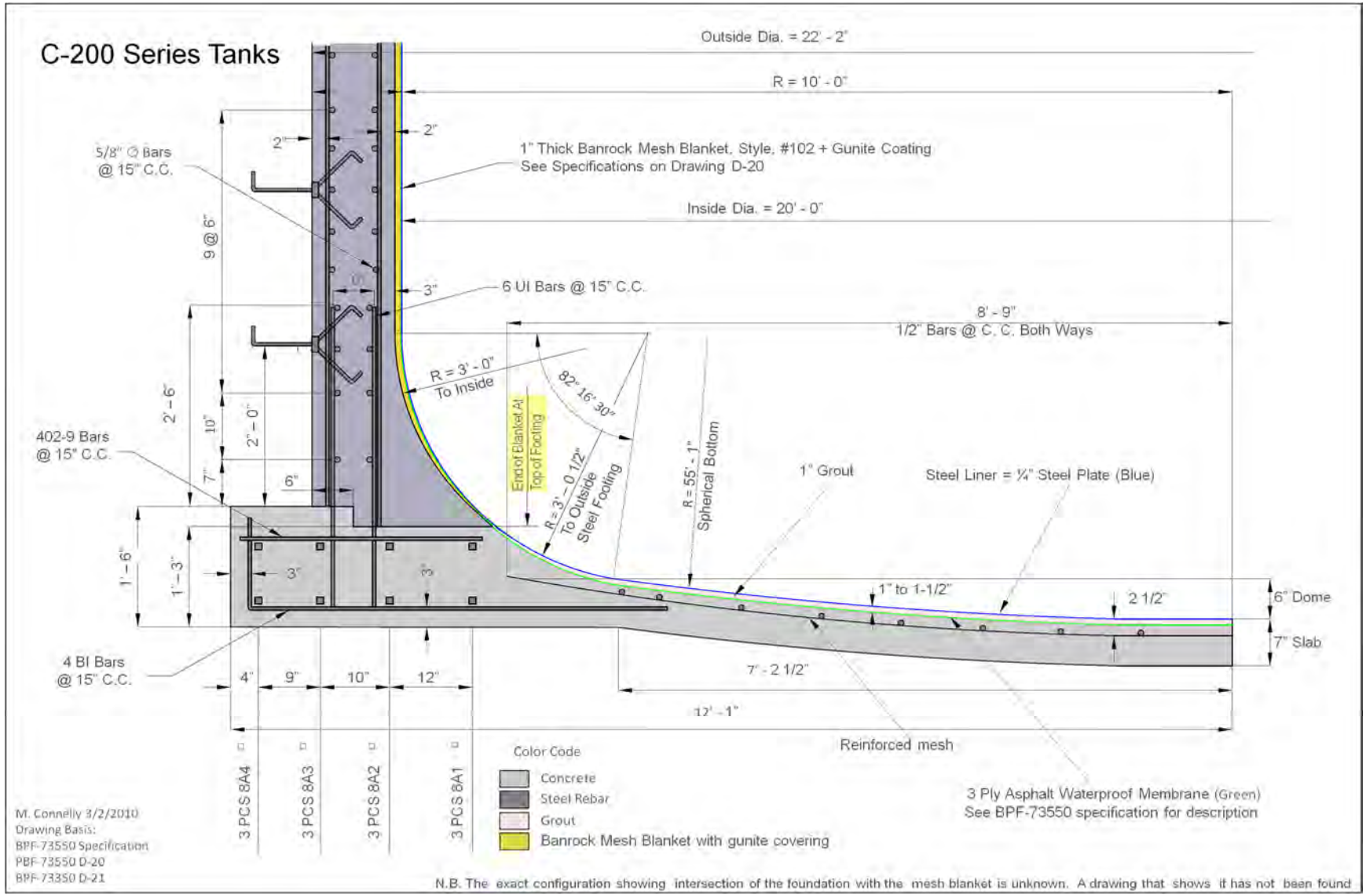

Reference: BPF-73550, "Specifications For Construction of Composite Storage Tanks Bldg. No. 241 Hanford Engineer Works Project 9536."

Figure 3-9. Schematic of the 244-CR Process Tank Vault in Waste Management Area C.

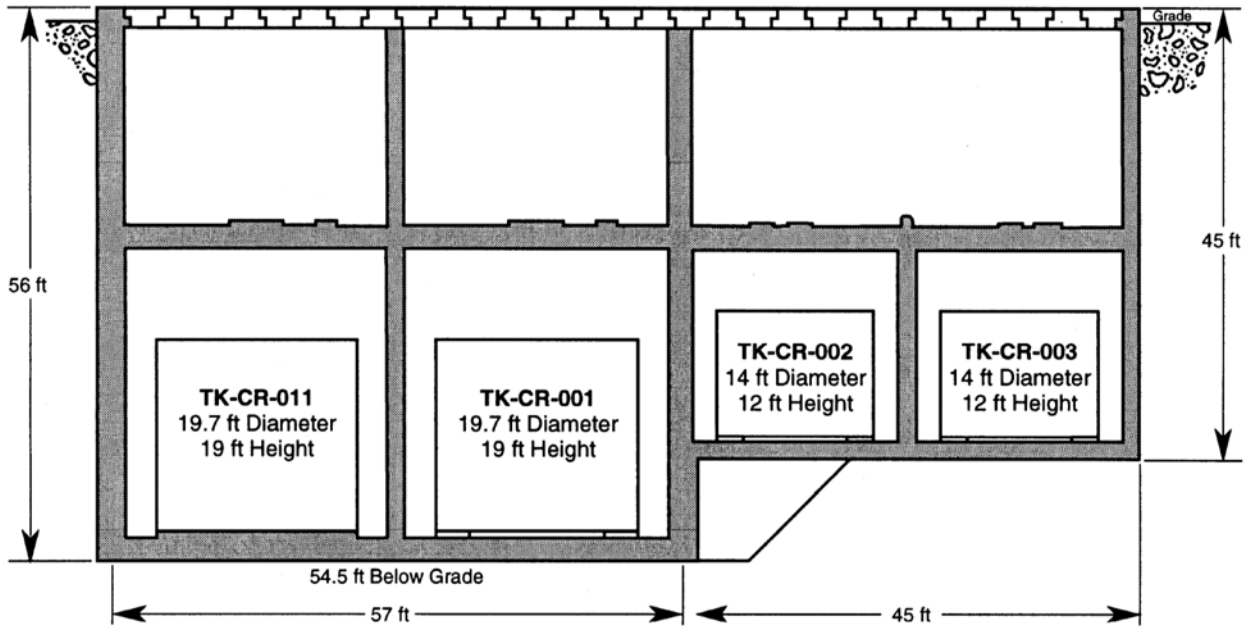

3.2.5 Gas-Phase Diffusive Flux

While the infill grout is intact, upward gaseous diffusion of volatile contaminants is modeled from the residual waste layer towards the atmosphere. The air content within the infill grout is assumed to be 6% based on characterization information for possible Hanford grout formulations (WSRC-TR-2005-00195, "Summary of Grout Development and Testing for Single Shell Tank Closure at Hanford"). Upward diffusive gas phase transport through the tank is modeled to occur along a 10-m-long pathway towards the land surface. This pathway is split into a lower 5-m thickness composed of infill grout material followed by another 5-m thickness of soil overburden. For the purpose of diffusive release calculations, the porosity and saturation of the infill grout and soil overburden are fixed over time. The surface barrier that will be emplaced at closure over the tank farm will provide additional depth to the waste. For performing the air pathway calculations, this thickness is conservatively ignored.

3.3 CONCEPTUAL MODEL FOR TRANSPORT ALONG GROUNDWATER PATHWAY

The conceptual model of the groundwater pathway considers a diffusion-controlled release of radionuclides from the grouted tanks and ancillary equipment and an advection-controlled release from the pipelines, vertical transport through the thick vadose zone to the water table, and then transport laterally through the aquifer to a hypothetical well located 100 m downgradient.

Once contaminants enter the vadose zone, the low recharge (infiltration rate) controlled by the surface cover system, the thickness of the vadose zone between the base of the tanks and the

unconfined aquifer, and the soil-contaminant interaction, prevent all but the least-reactive contaminants from reaching the unconfined aquifer for thousands of years. The saturated zone (aquifer) beneath WMA C can be viewed as a natural barrier, because as recharge containing contaminants enters the aquifer, the leachate mixes with groundwater and becomes more dilute. This dilution in concentration lowers the exposure point concentration and consequent dose to a receptor. Thus the transport of radionuclides to the groundwater is a complicated process that depends on data and assumptions relevant to the following physical systems: (1) engineered features of WMA C, (2) surface features of WMA C, (3) the vadose zone beneath WMA C, and (4) the saturated zone (groundwater) beneath WMA C.

Figure 3-10. Location of Active and Existing Pipelines Along with New and Existing Facilities for Waste Fractionization Operations (1961 to 1978).

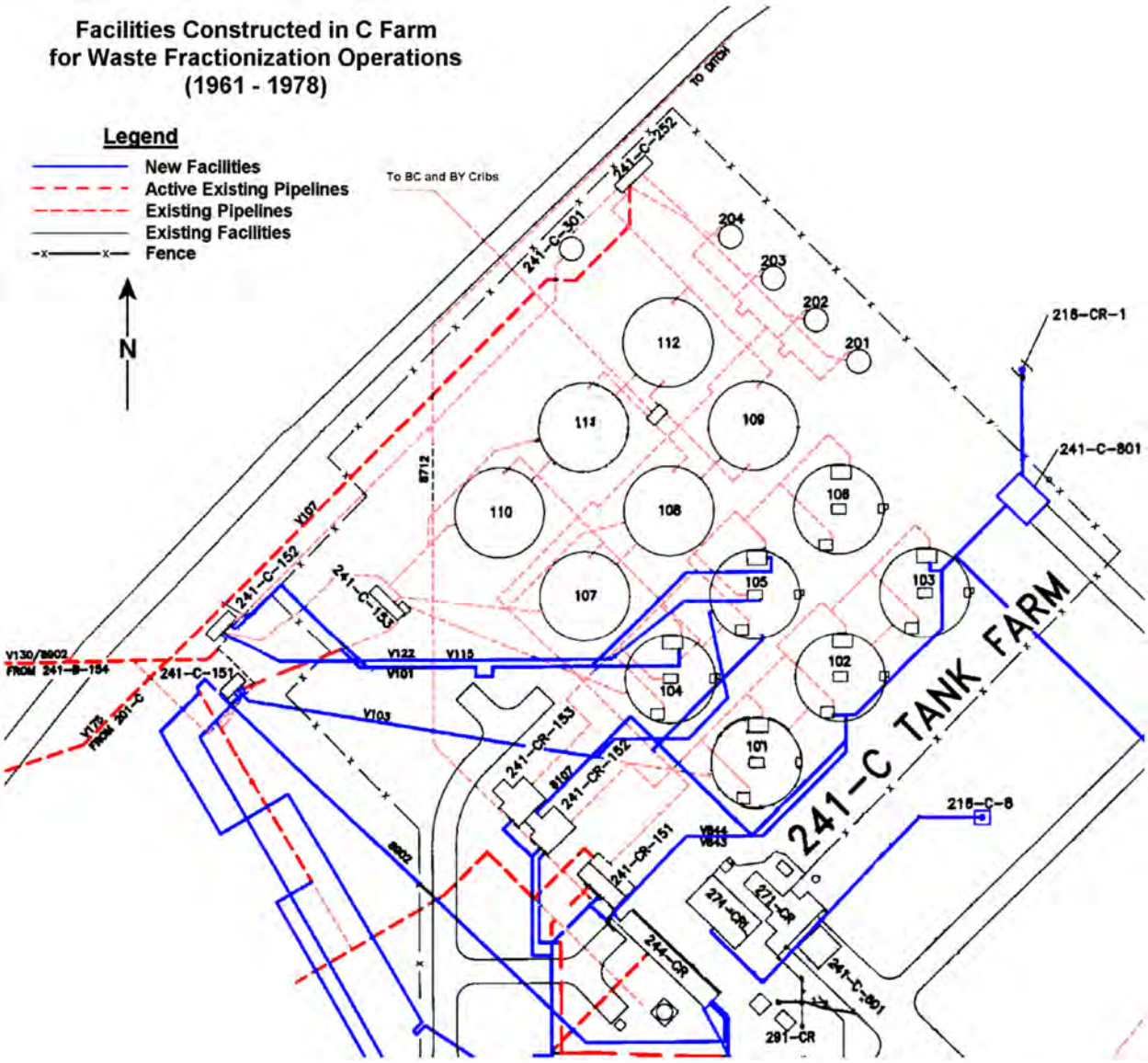

The vadose zone underlying WMA C consists of heterogeneous layers of sedimentary units that vary in thickness at different locations. From top to bottom, the hydrostratigraphic units (HSUs) overlying the basalt beneath WMA C are as follows:

- Backfill
- Hanford formation unit 1 (H1) (gravel-dominated)
- Hanford formation unit 2 (H2) (sand-dominated)
- Hanford formation unit 3 (H3) (gravel-dominated) (Note that this unit is often referred to as undifferentiated Hanford H3, Cold Creek, and Ringold gravel in the vicinity of WMA C).

Conceptually, and for the purpose of simplification, these layers have been combined into equivalent homogeneous medium units with macroscopic flow properties. The porous media continuum assumption (an extended form of Darcy's Law for vadose zone applications) and the soil relative permeability/saturation/capillary pressure relations provide the basis for vadose zone flow and transport modeling. Conceptually, for simplification, each heterogeneous geologic unit is represented by an equivalent homogeneous medium having macroscopic flow and transport properties. In the model domain, the hydraulic properties describing fluid flow and transport characteristics associated with each geologic unit are thus approximated by average upscaled (effective) parameters.

3.4 CONCEPTUAL MODEL FOR TRANSPORT ALONG ATMOSPHERIC PATHWAY

Gases and vapors can potentially diffuse upward from the residual waste in the WMA C tanks and ancillary equipment to the ground surface. The principal mechanism by which contaminants migrate from the waste to the ground surface is gaseous diffusion along the air-filled pore spaces that are assumed to be continuous.

Of the contaminants contained in WMA C wastes at closure, four of them could potentially originate as gas from the residual wastes:

- Carbon-14 as CO_2 gas
- Hydrogen-3 as H_2 gas
- Iodine-129 as I_2 gas
- Radon-222 as radon gas.

Due to small inventory of these radionuclides in the tank residuals, the dose contribution from the air pathway is expected to be negligible (compared to the groundwater pathway), and therefore a simplified and conservative conceptual model is considered. Since tanks will be fully grouted at closure and the residual waste layer is conceptualized to be present near the base of the tank, it is assumed that grout will behave as a porous medium, and gases could slowly

emanate and diffuse through the tortuous pathway along the gas-filled pore space. The releases would be controlled by the partitioning of the radionuclides among the aqueous phase, solid phase, and gaseous phase, and therefore modeled by considering the following equilibrium coefficients:

- K_d for solid/water phase partitioning
- Henry's law constant (K_h) for air/water partitioning.

The atmospheric transport pathway calculations are conducted in two steps:

1. Gaseous fluxes emitted from each source term (tanks and ancillary equipment) are calculated by assuming a zero concentration boundary at the surface. This is conceptually equivalent to having a large enough wind speed near the ground surface of WMA C that the air parcel is renewed constantly, thereby maximizing the diffusive gradient.

    - Upward diffusive gas phase transport through the SSTs, 244-CR vault, and C-301 catch tank is modeled to occur along a 10-m-long pathway towards the land surface. This pathway is split into a lower 5-m thickness composed of infill grout material, followed by another 5-m thickness of soil overburden. The diffusive area is taken to be the base area of each source term. The surface barrier that will be emplaced at closure will provide additional diffusive pathway length but, for performing the air pathway calculations, this thickness is conservatively ignored. The diffusive length chosen is the minimum thickness over which gas-phase diffusion is likely to occur through the tortuous air-filled pore volume (defined by the air content). The 5-m thickness through the infill grout only considers the thickness up to the spring line of the tank, which is likely to remain as the minimum path length under other conceptualizations for transport along the air pathway.

    - The air content within the infill grout is assumed to be 6% based on characterization information for possible Hanford grout formulations (WSRC-TR-2005-00195). The air content of the soil overburden is calculated by taking the difference in the backfill porosity and soil moisture content, which varies as a function of time. The air content of the infill grout is assumed to be fixed over time, even though studies have indicated that chemical transformation of initial grout material will likely cause porosity reduction over time due to increased molar volume of the newly formed mineral phases. The effective diffusion coefficient for each gas is calculated separately by taking its binary diffusion coefficient in free air, under atmospheric pressure of 1 atm. and a temperature of 20 °C, and multiplying with the gas tortuosity.

    - The calculations consider equilibrium partitioning of contaminants among solid, water, and air phases. Assumed grout K_d values are applied for the 5-m diffusive pathway calculations within the infill tank grout material, while no sorption is assumed for the 5-m pathway length considered through the soil backfill material.

- For the pipelines, the gas phase diffusive calculations are performed in a similar manner to that described above, except for consideration of the 5-m diffusive path length along the grout infill material. For pipeline analysis, only the 5-m diffusive path length along the soil overburden is considered.

2. The gas-phase diffusive mass flux arriving at the surface for each source area (twelve 100-series tanks, four 200-series tanks, CR-Vaults, C-301 catch tank, and the pipelines) is transported (except for radon), assuming advection and dispersion via wind movement to the receptor placed 100 m downwind from the WMA C fenceline. The air mixing height is assumed to be 2 m, which is an approximate height of an adult. Horizontal air dispersion is considered along the transport pathway, which is based on the expected air turbulence in and around WMA C.

4 MODEL IMPLEMENTATION

The system-level model is implemented using GoldSim© software ("GoldSim Contaminant Transport Module User's Guide" [GoldSim Technology Group 2014a]; "GoldSim Distributed Processing Module User's Guide" [GoldSim Technology Group 2014b]; "GoldSim Probabilistic Simulation Environment User's Guide" [GoldSim Technology Group 2014c]).

4.1 SOFTWARE

The WMA C PA relies on two primary controlled-use software packages to simulate the flow and transport in the subsurface, simulate source term releases, conduct inadvertent intruder calculations, and simulate air-pathway transport in order to calculate doses resulting from the disposal of waste at the facility. These primary software packages are STOMP© and GoldSim© Pro, which are qualified for controlled use at the Hanford Site in accordance with their respective software management and testing plans. These software packages are registered in the Hanford Information Systems Inventory (HISI). HISI provides the platform for tracking all software in use at the Hanford Site. For safety software (which includes STOMP© and GoldSim© Pro), the HISI entry is used to record approval for use of software versions, to maintain a registry of authorized users, and to log all instances of the software's usage. Software is maintained using the established Hanford Site configuration management system, MKS Integrity®[4], which is the Hanford Site standard for preserving and managing source code and executable versions of software. MKS Integrity® provides a "checkpoint" feature that locks files at particular points, such as when an executable has passed quality assurance testing, been documented in an acceptance test report, and been approved for use.

Software development of Goldsim© Pro meets ASME NQA-1-2000, "Quality Assurance Requirements for Nuclear Facility Applications" software requirements, as well as the requirements specified under DOE O 414.1D, Quality Assurance for Safety Software. Goldsim© Pro use at the Hanford Site is managed and controlled such that the computational needs filled by use of Goldsim© Pro (and any associated utility codes) and the specific roles and responsibilities for management, the modeling staff, and subcontractors have been identified and traced. These responsibilities include the following:

- modeler training,
- source code installation and testing,
- preserving the software and verification test results,
- validation and verification that the Goldsim© Pro quality assurance documentation demonstrate that Goldsim© Pro meets identified modeling needs and purposes,

[4] MKS Integrity, Integrity, and all other PTC product names and logos are trademarks or registered trademarks of Parametric Technology Corporation or its subsidiaries in the United States and in other countries.

- reporting and documenting any software errors (none were encountered during the development of the WMA C PA),

- management of the Goldsim© Pro input files, and

- contingency and disaster recovery (which was not encountered during the development of the WMA C PA).

Acceptance and installation tests of the Goldsim© Pro simulation software demonstrate that it is appropriate for its intended uses for the WMA C PA and that it has been successfully installed on the computing systems used to conduct WMA C PA modeling.

4.2 SOURCE TERM IMPLEMENTATION

Waste form degradation and release mechanisms of tank residual waste were evaluated experimentally for ^{99}Tc, uranium, and chromium. These experiments were conducted under static and under slowly flowing conditions as described in "Single-pass flow-through test elucidation of weathering behavior and evaluation of contaminant release models for Hanford tank residual radioactive waste" (Cantrell et al. 2013) and "Thermodynamic Model for Uranium Release from Hanford Site Tank Residual Waste" (Cantrell et al. 2011). Based on the results of the experiments and detailed evaluations, the following source release base models are implemented.

To make the source release model for ^{99}Tc consistent with the observations, an initial 6% fraction of the ^{99}Tc inventory is considered to be instantaneously available for release, while the remaining 94% fraction undergoes relatively slower release at the fractional rate of 6×10^{-4} day^{-1}.

The following solubility controls are imposed on the uranium concentrations.

- Apply a solubility limit of 1×10^{-4} M for 1,000 years (equivalent to a reaction progress of 0.2) based on the assumption that amorphous uranium mineral phases such as $Na_2U_2O_7$(am) control the solubility.

- After 1,000 years, apply the solubility limit of 1×10^{-6} M, assuming $CaUO_4$ as the solubility-controlling mineral phase under $Ca(OH)_2$ saturated conditions (infill grout saturated and intact-tank conditions).

- If and when the tank is assumed to be degraded such that flow rates are fast enough not to equilibrate with the infill grout material and are $CaCO_3$ saturated (vadose zone water), then apply a solubility limit of 1×10^{-4} M for 1,000 years. Beyond this time, apply solubility limit of 2×10^{-5} M based on the long-term uranium concentrations assuming minimal influence of $Ca(OH)_2$ water (Cantrell et al. 2011).

For chromium, a constant high dissolved concentration limit of 2,000 µg/L is imposed. This value is at the high end of observed values in tank 241-C-202 leachate.

Observations of retrieved tanks show that the residual waste is primarily distributed on the tank bottoms (see Section 5.2 of RPP-RPT-42323). Consequently, the residual waste is conceptualized to be distributed in a uniform layer at the base of the tank. As long as tank wall integrity is maintained and the infill grout is not physically degraded, the primary contaminant transport process will be diffusive. The shortest diffusive pathway for release to the near-field environment is through the base of the tank. The diffusive thickness being considered is the 8-in. combined thickness of concrete and grout layer located at the base of the tank (ignoring the steel plate). The aqueous phase diffusive transport will occur along the water phase within the pore spaces of the grout and concrete layer. The effective diffusion coefficient of contaminant (which includes effects of tortuosity) along with sorption behavior within the grout and concrete layer are going to control the diffusive mass flux besides the concentration gradient.

The effective diffusion coefficient of mobile contaminants (such as ^{99}Tc) through the combined grout and concrete base mat is considered a key parameter that controls the diffusive flux. Over the past decade, several experiments have been conducted to determine the effective diffusion coefficient through concrete for relatively mobile contaminants under unsaturated conditions. The results of various experiments are presented in PNNL-23841, “Radionuclide Migration through Sediment and Concrete: 16 Years of Investigations.” Of particular interest are the sediment-concrete half-cell experiments conducted in Year 2008 (for a period of 351 days) with ^{99}Tc and stable iodine. The concentration profiles developed in the concrete are analyzed by fitting the analytical solution to Fick’s second law, with the assumption of zero concentration downstream boundary condition, and deriving a bulk diffusion coefficient for the media. This bulk diffusion coefficient implicitly incorporates the effects of porosity and tortuosity due to diffusion that primarily occurs along the water films in the concrete. For the purpose of modeling mass transport along the water (liquid) phase the effective diffusion coefficient in the water phase is needed (instead of bulk diffusion coefficient), which can be derived by multiplying bulk diffusion coefficient with the moisture content. Since the moisture content of the base mat concrete and grout material is not known and would likely change with time due to slow but steady physical and chemical degradation, the effective diffusion coefficient is chosen conservatively to be the same as the measured bulk diffusion coefficient for the purpose of source-term modeling. In other words, the reduction due to multiplying with moisture content is not applied for calculating the diffusive flux. Note that the effective diffusion coefficient incorporates the effects of tortuosity resulting from transport along water films in the porous media.

The calculated effective diffusion coefficients of ^{99}Tc derived from the experimental results range from 6.6×10^{-9} cm^2/s to 1.6×10^{-7} cm^2/s, with a median value of about 3×10^{-8} cm^2/s. No particular measurable trend exists to indicate whether the effective diffusion coefficient varies with moisture content of the sediment. The highest ^{99}Tc diffusivities were predominantly observed in the non-carbonated concrete cores contacting spiked sediments. A clear effect from the addition of iron was not observed. In general, the increased carbonation reduced diffusion coefficients. For the purpose of the PA base case calculations, a best-estimate value of 3×10^{-8} cm^2/s is chosen for the effective diffusion coefficient in concrete. This value is applied to all species diffusing through the concrete.

4.2.1 Sorption of Contaminants to Grout and Concrete

A linear sorption isotherm (using a K_d approach) is used to represent sorption within the grout and concrete layer for various contaminants as they undergo diffusive (and advective) transport through the tank. Development of a sophisticated sorption model depends on the availability of complete sets of experimental data, including measurement of isotherm, and dependence on solid to liquid ratio under conditions that are applicable to the near-field environment. It is noted that presently the vast majority of sorption values on cementitious material are still results from single-point measurements, and information on uptake mechanisms and uptake controlling phases in cement systems are lacking to a large extent (NAGRA NTB 02-20, "Cementitious Near-Field Sorption Data Base for Performance Assessment of an ILW Repository in Opalinus Clay"). The macroscopic studies would have to be complemented by studies performed on a molecular level to discern uptake processes. Due to these limitations, the available sorption databases typically rely on expert judgment in selecting realistic and defensible sorption values. As a result, a simple linear sorption isotherm approach based on empirical information that is commensurate with the level of knowledge is applicable.

As described below, selections for values of K_d have been made based on review of past reports that are focused on developing internally consistent cement sorption databases for cementitious near-field material (hardened cement paste) based on composition of cement porewaters and stage of cement degradation.

- Conditions in the closed tank farm are expected to be moderately oxidizing, owing to the position of the waste in unsaturated conditions. Where data are available to differentiate between oxidizing and reducing conditions, oxidizing conditions are preferred. It should be noted that in all cases, this leads to the selection of lower values for K_d compared to reducing conditions.

- Composition of the cementitious material (grout or concrete) may have different chemical compositions, and therefore differ in contaminant uptake mechanisms and cement phases. Due to lack of information, the differences in sorption between various types of cements and concretes are ignored here.

- The selected K_d values are based on the assumption of $Ca(OH)_2$-saturated waters contacting the waste, and therefore represent the so-called stage II of the chemical degradation of cementitious material. In this stage, chemical composition of the alkali-depleted cement pore water is controlled by the solubility of portlandite. The impact on K_d values during evolution of chemical conditions from stage I (higher alkali content and pH) to stage II is expected to be minor and incorporated within the uncertainty range.

- The reviews of SKB Rapport R-05-75, "Assessment of uncertainty intervals for sorption coefficients, SFR-1 uppföljning av SAFE" and NIROND-TR 2008-23 E, "Review of sorption values for the cementitious near field of a near surface radioactive waste disposal facility, Project near surface disposal of category A waste at Dessel" are more recent, and represent critical reviews and independent data from NAGRA NTB 02-20 and

PSI Bericht Nr. 95-06, "Sorption Databases for the Cementitious Near-Field of a L/ILW Repository for Performance Assessment." Where appropriate values are available from these more recent references, they are preferred to the older ones.

- When literature values are absent from these references, a value of zero has been assigned to the analyte. At this stage of the PA, no attempt has been made to draw chemical equivalences between similar analytes to justify nonzero K_d values. As necessary, the chemical equivalences suggested by SKB Rapport R-05-75 may be used to update K_d values.

- When there was significant disagreement between literature sources, the more conservative (lower) K_d value was chosen. This occurs, for instance, in a preference for NAGRA NTB 02-20 data for oxidizing conditions, compared to values from more recent references.

4.2.2 Source Term Mathematical Model

The source term model is implemented in GoldSim© using its Contaminant Transport Module. The Contaminant Transport Module allows the user to dynamically model mass transport using a compartment-based model of the system. The Contaminant Transport Module includes the following key features (GoldSim 2014a).

- Radioactive decay chains can be simulated, taking into account ingrowth and decay.

- A large built-in database exists for radionuclide decay data (species, decay rates, and radioactive progeny) for over 1,300 radionuclides and their corresponding stable elements. The data is based on "ICRP Publication 107: Nuclear Decay Data for Dosimetric Calculations" (ICRP 2008).

- Specialized elements in GoldSim© called Source and Cells are available to model key release mechanisms from source terms that include waste form degradation rate and solubility control.

- Both advective and diffusive transport mechanisms can be explicitly represented using the "Cell" pathway element by specifying the flow rates for advective transport and the diffusion coefficient and geometric factors for diffusive transport. Media properties through which advection and diffusion occur also need to be specified.

- When multiple Cells are linked together via advective and diffusive mechanisms, the behavior of the Cell network is mathematically described using a coupled system of ordinary differential equations in time. A network of Cells is mathematically equivalent to a finite difference network of nodes. GoldSim© numerically solves the coupled system of equations to compute the contaminant mass present in each Cell and the mass fluxes between Cells as a function of time. The solution technique uses a backwards-difference (fully implicit) algorithm for each cell-net and each species decay-chain family.

The basic mass balance equation for Cell *i* is as follows:

$$m'_{is} = -m_{is}\lambda_s + \sum_{p=1}^{NP_s} m_{ip}\lambda_p f_{ps} R_{sp}\left(\frac{A_s}{A_p}\right) + \sum_{c=1}^{NF_i} f_{cs} + S_{is} \quad (4\text{-}1)$$

Where:

m'_{is} = rate of increase of mass of species s in Cell i (M/T)
m_{is} = mass of species s in Cell i (M)
λ_s = decay rate of species s (T^{-1})
NP_s = Number of direct parents for species s
f_{ps} = fraction of parent p which decays into species s
R_{sp} = stoichiometric ratio of moles of species s produced per mole of species p decayed
A_s = molecular (or atomic) weight of species s (M/mol)
A_p = molecular (or atomic) weight of species p (M/mol)
NF_i = number of mass flux links from/to Cell i
f_{cs} = influx rate of species s (into cell i) through mass flux link c (M/T)
S_{is} = rate of direct input of species s to Cell i from external source (M/T).

The first term on the right-hand side in Equation 4-1 represents decay (or chemical reaction), the second term represents ingrowth, the third term represents mass transfer in or out of the Cell via mass flux links, and the fourth term represents the rate of direct input to the Cell from other sources.

Equation 4-1 couples in two ways to other mass balance equations: 1) through the ingrowth terms, which couple all species in a decay chain; and 2) through the mass flux terms, which couple all Cells that are connected by mass flux links. Representation of the mass flux terms (f_{cs}) is the most complex part of the above equation, and is described in detail below in terms of advective mass flux and diffusive mass flux.

Advective mass flux from Cell i to Cell j for species s is computed as follows:

$$f_{s,i\to j} = c_{ims}\, q \quad (4\text{-}2)$$

Where:

q = the rate of advection of water for the mass flux link i to j (L^3/T)
c_{ims} = the total dissolved concentration of species s in medium m within Cell i (M/L^3).

Diffusive mass flux links are used to transport mass through a stagnant or slowly moving fluid via the process of molecular diffusion. Diffusive mass transport is proportional to a concentration difference, with mass diffusing from high concentration to low concentration. The constant of proportionality is referred to as the diffusive conductance:

Diffusive Mass Rate = (Diffusive Conductance) × (Concentration Difference)

In this equation, the Diffusive Mass Rate has dimensions of mass/time, the Diffusive Conductance has dimensions of volume/time, and the Concentration Difference has dimensions of mass/volume. Diffusive Conductance is a function of the properties of the species and fluids involved and the geometry of the diffusive process. For diffusion through a single fluid, the Diffusive Conductance for species s (D_s) is computed as:

$$D_s = \frac{(A\, d\, \tau\ \theta)}{L} \tag{4-3}$$

Where:

A = mean cross-sectional area of the connection (L^2)
d = free-water diffusivity of species s
τ = tortuosity of continuous liquid film in the porous medium t
θ = moisture content (porosity times saturation)
L = diffusive length.

The diffusive flux f_s from pathway i to pathway j is computed as follows:

$$f_{s,i\rightarrow j} = D_s(C_{ims} - C_{jms}) \tag{4-4}$$

Where C_{ims} and C_{jms} are the dissolved concentrations of species s for medium m in Cell i and j.

The diffusion can occur in either direction, so the flux can be positive or negative. When media properties differ across a boundary, such as when diffusion occurs between tank wall concrete layer and the surrounding soil, the diffusive conductance is calculated using a harmonic average of the physical properties of the two cell pathways as follows:

$$D_s = \frac{A}{\frac{L_i}{d_{msi}\theta_i\tau_{Pi}} + \frac{L_j}{d_{msj}\theta_j\tau_{Pj}}} \tag{4-5}$$

Where:

A = the area of the diffusive mass flux link (L^2)
L_i = diffusive length for the diffusive mass flux link in Cell i (L)
L_j = diffusive length for the diffusive mass flux link in Cell j (L)
d_{msi} = free-water diffusivity of species s for fluid m in Cell i (L^2/T)
d_{msj} = free-water diffusivity of species s for fluid m in Cell j (L^2/T)
τ_{Pi} = tortuosity for the porous medium for Cell i
τ_{Pj} = tortuosity for the porous medium for Cell j
θ_i = moisture content of porous media in Cell i
θ_j = moisture content of porous media in Cell j.

When mass enters a Cell, it is instantaneously partitioned among the media present in the Cell. The partitioning is controlled by the partition coefficients defined for each species in each

medium, and the quantity of each medium present. In the absence of solubility limits, the concentration of the species s in medium m in Cell i is computed by GoldSim© as follows:

$$C_{ims} = \left(\frac{K_{mrs}}{\sum_{g=1}^{NM_i} K_{grs}.VM_{ig}}\right) m_{is} \tag{4-6}$$

Where:

C_{ims} = concentration of species s in medium m in Cell i ([M/L^3] for Fluids or [M/M] for solids)
m_{is} = mass of species s in Cell i (M)
K_{mrs} = partition coefficient between medium m and Reference Fluid r for species s (L^3/L^3) for Fluids or (L^3/M) for Solids
K_{grs} = partition coefficient between medium g and Reference Fluid r for species s (L^3/L^3) for Fluids or (L^3/M) for Solids
VM_{ig} = quantity (volume or mass) of medium g in Cell I (L^3 for Fluids or M for Solids)
NM_i = the number of media in Cell i.

When a solubility constraint is applied for a species in a Cell, the Cell has a saturation capacity with respect to that species, which represents the maximum amount of species mass the Cell can contain before the species will start to precipitate out of solution. It is calculated as:

$$msat_{is} = sol_{sr} \sum_{g=1}^{NM_i} K_{grs}.VM_{ig} \tag{4-7}$$

Where:

$msat_{is}$ = saturation capacity for species s in Cell i (M)
sol_{sr} = solubility of species s in the Reference Fluid r (M/L^3)
K_{grs} = partition coefficient between medium g and Reference Fluid r for species s ([L^3/L^3] for Fluids or [L^3/M] for Solids)
VM_{ig} = quantity (volume or mass) of medium g in Cell I (L^3 for Fluids or M for Solids)
NM_i = the number of media in Cell i.

All or a portion of the mass within the Source can be specified to exist within the waste matrix, such that species that are bound in such a matrix are not released until the matrix itself degraded in some manner. Release of mass from the matrix is assumed to be congruent with the degradation of the matrix. Degradation rates are specified by the user. The rate at which the waste is exposed for release is calculated as:

$$e_s(n,t) = M_s(t) \,.\, k_s(t) \,.\, I_s(n,t) \tag{4-8}$$

Where:

$e_s(n,t)$ = the exposure rate for species n in bound inventory s for the Source at time t (M/T)

$M_s(t)$ = fraction of unprotected but undegraded matrix (unitless)
$k_s(t)$ = fractional degradation rate of waste matrix for bound inventory s (1/T)
$I_s(n,t)$ = mass of species n in bound inventory s at time (M).

When applying a fractional degradation rate to the matrix (such as for release of ^{99}Tc), the fraction of undegraded matrix $M_s(t)$ can be determined by solving the following differential equation:

$$\frac{dM_s(t)}{dt} = h(t) - M_s(0)\,.\,k_s(t) \tag{4-9}$$

Where:

$h(t)$ = rate at which matrix is being unprotected (T^{-1})
$k_s(t)$ = rate at which unprotected matrix is being degraded (T^{-1}).

If $h(t)$ and $k_s(t)$ are constant, the solution to the above equation is:

$$M_s(t) = \frac{h}{k_s}(1 - e^{-k_s t}) + M_s(0)e^{-k_s t} \tag{4-10}$$

4.3 ABSTRACTION APPROACH FOR IMPLEMENTING GROUNDWATER TRANSPORT PATHWAY

The flow field for the vadose zone is derived from the 3-D STOMP©-based model calculations, abstracted to provide a close approximation to the full STOMP©-based solution. The objective of the system model is to evaluate the interaction of various submodels within the overall system. This is carried out by conducting transport analyses within the vadose zone and saturated zone for each source type (tank, ancillary equipment, and pipeline). It has been found adequate to simplify and model the transport in one dimension (1-D) along the predominant transport pathway. The reasonableness of the abstraction approach was corroborated by comparisons of the results of the transport analysis conducted using the 1-D abstracted model to the full 3-D STOMP©-based model.

The flow field generated from the STOMP©-based model was evaluated prior to abstraction. Following aspects were considered during abstraction of flow field:

1. Variable HSU thickness within the model domain and its impact on flow velocity
2. Spatial and temporal variability in imposed recharge rates
3. Spatial and temporal variability in flow underneath the tank
4. Variable distances of tanks from the compliance location boundary.

The GoldSim©-based system model relies on the user to provide the moisture content, saturation, and Darcy flux as inputs. These flow field-related parameters were extracted from the STOMP©-based model. For the abstraction of the flow field, the primary regions of interest were the ones underneath the various source locations within WMA C.

First, the approximate thicknesses of the HSUs were extracted from the STOMP©-based model under each of the twelve 100-series tank and four 200-series tank locations. Figure 4-1 shows the location of the nodes, along with the cross-section lines used in extracting the HSU thickness. Figure 4-2 shows the northwest-southeast trending geologic cross-sections through the tank farm area, while Table 4-1 summarizes the thicknesses of the HSUs directly underneath the tanks, along with the median values of the HSU thicknesses. The median value of the 100-series tanks is very similar to the HSU thickness below tank C-105. Similarly, median value for 200-series tanks is close to the thickness below tank C-203. Therefore, tanks C-105 and C-203 were selected as representative columns for the flow-field abstraction for the 100-series tanks and the 200-series tanks, respectively.

The flow-field abstractions were performed separately for the 100-series and 200-series tanks because (a) 100-series tanks are 75 ft in diameter compared to 20 ft in diameter for the 200-series tanks, which leads to different flow paths, and (b) the thickness of HSU below the 100-series tanks differs from the 200-series tanks.

For the base case calculations, the recharge rates within the STOMP©-based model domain were varied spatially and temporally. During the operational period defined from year 1945 to 2020 (pre-barrier), a recharge rate of 100 mm/yr was applied over the WMA C area, followed by a reduced rate of 0.5 mm/yr to reflect the hydrologic barrier impact of surface cover for 500-year design life (year 2020 to 2520). During the post-barrier design period (year 2520 onwards), the recharge rate was changed to background recharge of 3.5 mm/yr. Due to these varying boundary conditions, the moisture content and Darcy flux profiles within the soil column vary with depth and respond differently at different times as shown in Figures 4-3 and 4-4, respectively. While the surface barrier is effective (between year 2020 and 2520), moisture content and Darcy fluxes decrease with time as they respond to the change in the recharge rate from 100 mm/yr to 0.50 mm/yr. After the barrier design period (year 2520 onwards), moisture content and Darcy fluxes equilibrate quickly to the change in recharge rate from 0.50 mm/yr to 3.5 mm/yr. The flow-field abstraction process was implemented to capture these trends.

The representative hydrostratigraphic columns for the 100-series tanks and 200-series tanks are compared against the vertical discretization chosen for the system-level model in Figure 4-5. Also presented is the vertical discretization implemented in the STOMP©-based model. For the system-level model, finer discretization was chosen at shallow depths with increasingly coarser discretization at deeper depths. However, near the HSU contacts, finer discretization was used to produce improved numerical results near the interface. Coarser discretization was allowable in the deeper portion of the vadose zone (e.g., H3 gravelly sand) because the flow field was not found to change appreciably with depth.

The STOMP©-based model nodes that were used to represent the moisture content and Darcy flux for the grid cells in the system model are highlighted in brown color in Figure 4-5. For example, the H1 Gravelly Sand unit in the representative column for the 100-series tank has a total thickness of 9.25 m and is divided into three grid cells of 2 m, 3.5 m and 3.75 m thickness. The flow field (moisture content and Darcy flux) extracted from STOMP© model node 69 is applied in the first cell of this unit in the system-level abstraction model. Similarly, the flow field from STOMP© model node 66 and node 63 is applied to the second and third cell of this

unit in the system model. The H2 Sand unit is the thickest HSU in the vertical profile. It is discretized into a 3.75-m grid cell at the top and 5-m grid cell at the bottom. The middle 40 m is discretized into 80 grid cells, each being 0.5 m in length to match the 0.25 m longitudinal dispersivity applied within the H2 Sand unit (the numerical dispersivity in GoldSim© cell is calculated to be equal to half the cell length). The top and bottom grid cells for the H2 Sand unit are assigned the flow field extracted from STOMP© nodes 61 and 24, respectively, while the middle 40 m length (consisting of 20 grid cells) is represented by the flow field from STOMP© node 47. A single flow field over the 40 m length is used, since the flow field varies little for the corresponding STOMP© nodes at depth. A similar discretization scheme is adopted for the 200-series tanks as shown in Figure 4-5. The details of the grid discretization are presented in Table 4-2.

Figure 4-6 provides an overview of how the moisture content and Darcy flux vary over time for the selected STOMP© nodes in relation to the location in the vertical direction in the system model under an intact 100-series tank. This flow field is applied to model the transport underneath the 100-series tank. The representative flow field underneath an intact 200-series tank is presented in Figure 4-7. In the early time period, the moisture content and Darcy flux decreases due to the decrease in recharge rate from 100 mm/yr to 0.50 mm/yr associated with the emplacement of the surface barrier. As the surface barrier is assumed to be degraded 500 years after closure, the recharge rate transitions from a barrier rate of 0.5 mm/yr to a natural background rate of 3.5 mm/yr, and reaches steady state by year 3000. The STOMP© node 14 used to set the flow field for the grid cell at the base of the H3 Gravelly Sand unit shows high moisture content because it is located in the capillary fringe just above the water table.

The above results are applied when the grout is structurally stable and provides a hydraulic barrier. However, a number of the sensitivity cases evaluate conditions where the effectiveness of the grout as a hydraulic barrier is assumed to degrade at different times. Under degraded grout conditions, the grout is assumed to be highly fractured, and the infill material in the tank is assumed to behave like a porous material with hydraulic properties the same as the H2 Sand unit. The STOMP©-based model is run with the H2 Sand hydraulic properties for the tank, and the flow field is calculated and abstracted in a manner similar to that described earlier for the intact tank. The flow field is calculated separately for the degraded tank conditions for the 100-series and 200-series tanks, as shown in Figure 4-8. One additional STOMP© node result (node 73) is extracted and added to the system model to represent the flow conditions inside the tank. In the sensitivity cases, when the tank degradation occurs, the flow field is switched from the intact tank flow field to the degraded tank flow field. As a result, the contaminants are released via advection at the time when the tank is degraded in addition to the ongoing diffusive release mechanism.

The flow field applied to pipeline releases is calculated separately. Vertical Darcy fluxes and volumetric moisture contents from the STOMP© nodes that fall within the pipeline source area (150 m by 150 m) but outside the tank footprint are averaged to calculate the pipeline flow field. The representative hydrostratigraphic column for the 100-series tanks is applied to the pipeline source area. Advective flow occurs through the pipelines for all time periods. The hydraulic effect of the presence of buried pipelines in the vadose zone are not modeled explicitly, and the areas occupied by the pipelines are modeled with hydraulic properties of soil backfill material.

Figure 4-1. Three-Dimensional Subsurface Transport Over Multiple Phases (STOMP©)-Based Model Node Locations for Waste Management Area C along with Location of Cross-section Lines.

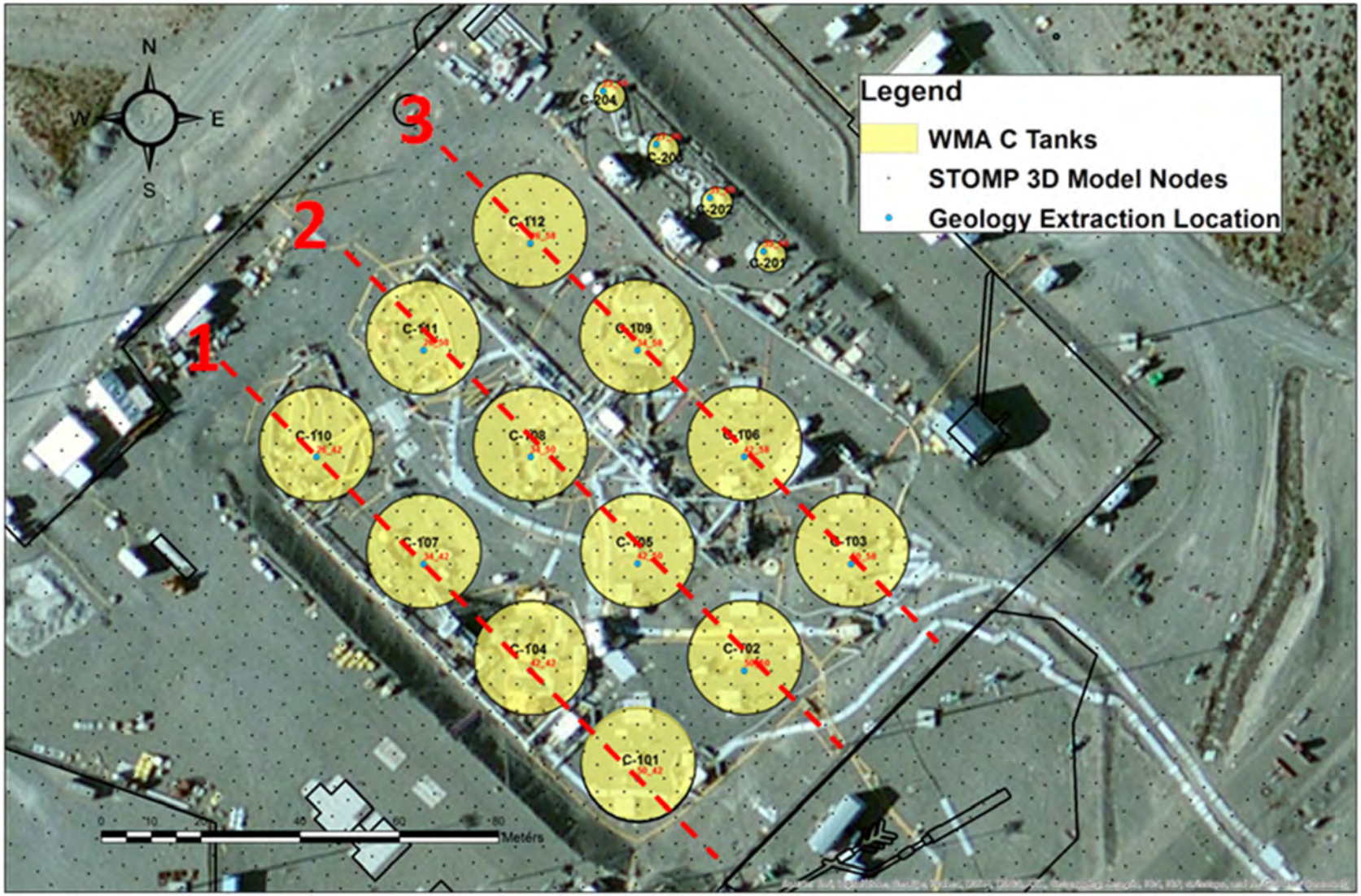

STOMP© 3D = Subsurface Transport Over Multiple Phases (code) three-dimensional WMA = Waste Management Area

Figure 4-2. Northwest-Southeast Trending Geologic Cross-sections Through the Tank Farm Using Information from Three-Dimensional Subsurface Transport Over Multiple Phases (STOMP©)-Based Model.

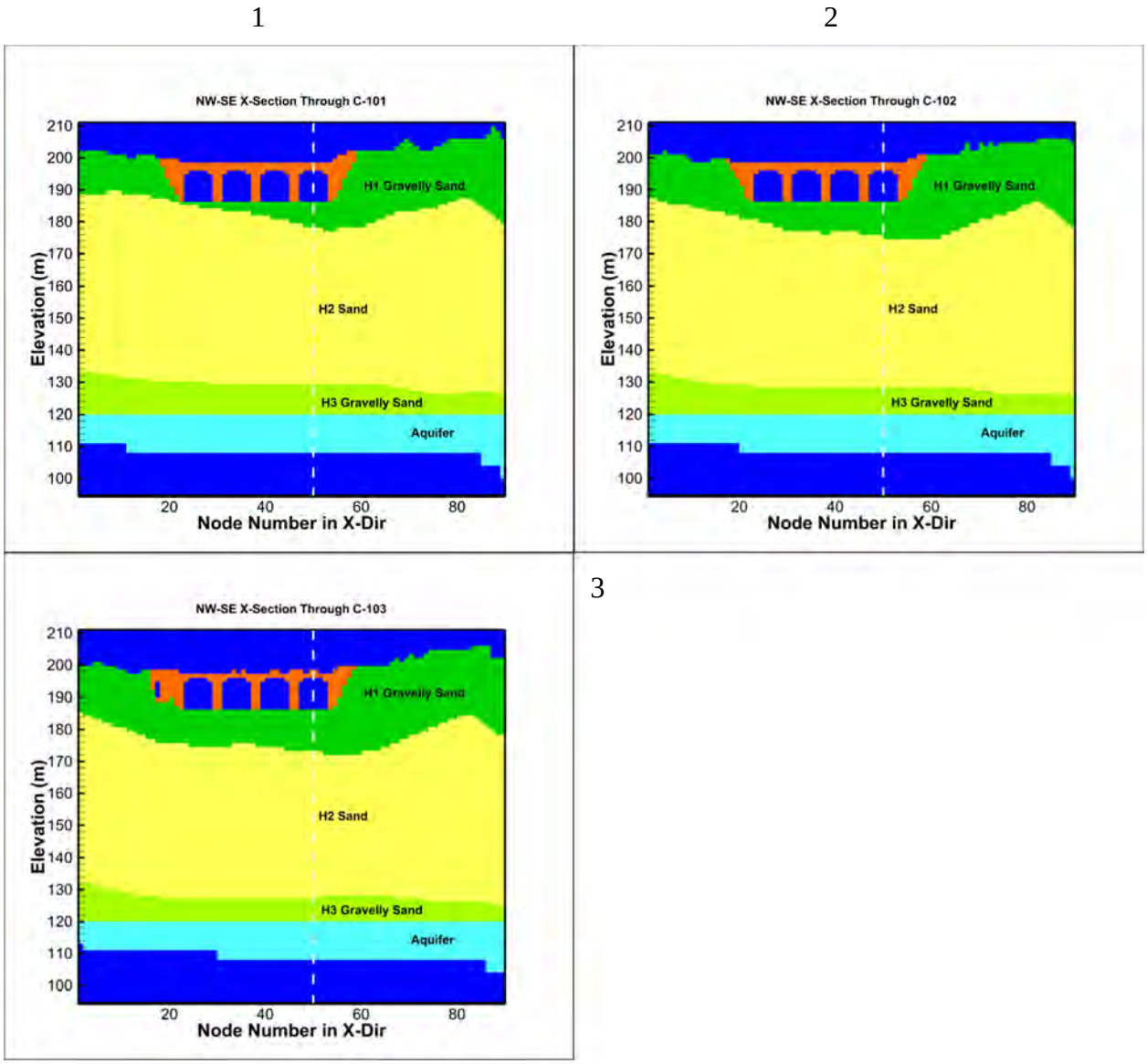

The saturated zone is modeled as a 1-D aquifer oriented along the primary flow direction using the aquifer pathway capability in GoldSim©. The volumetric flow rate through the aquifer is calculated based on the hydraulic gradient under steady-state conditions and saturated hydraulic conductivity consistent with the values used in the STOMP©-based model. The saturated zone thickness for the 100-series tanks is chosen to be 12 m, while that for the 200-series tanks is chosen to be 9 m (Table 4-1).

The mass flux from the vadose zone for each source term (each of the 100- and 200-series tanks, the C-301 catch tank, the 244-CR vault, and pipelines) is calculated separately. Each source term is then transported to the aquifer, assuming that vertical mass transport in the vadose zone

stays within the footprint of the source area, ignoring any lateral dispersion as shown in Figure 4-9. The aquifer pathway from each source area starts under its associated source in WMA C and extends to the point of calculation, 100 m downgradient from the WMA C fenceline along the groundwater flow direction. The width of the aquifer pathway is taken to be the width of the source area. The length of the aquifer pathway varies depending on the location of the source area being modeled (tanks and ancillary equipment), relative to the point of calculation 100 m downgradient from the WMA C fenceline along the groundwater flow path. As an example, the total length of the aquifer pathway from tank C-102 is ~144 m, compared with ~174 m for tank C-105, and ~235 m for tank C-111. For the pipeline source area, the aquifer pathway is assumed to begin at the center of the WMA C area to account for some vadose zone contribution occurring earlier, and in other cases later along the flow path length, leading to a total length of 175 m.

Table 4-1. Hydrostratigraphic Unit Thickness Under the Tanks Taken From the Three-Dimensional Subsurface Transport Over Multiple Phases (STOMP©)-Based Model.

Tank	STOMP_NODE (I_J)	H1 Gravelly Sand (m)	H2 Sand (m)	H3 Gravelly Sand (m)	Aquifer (m)
241-C-101	50_42	8.00	49.00	9.25	12.00
241-C-102	50_50	11.75	46.25	8.25	12.00
241-C-103	50_58	13.00	46.00	7.25	12.00
241-C-104	42_42	5.50	51.50	9.25	12.00
241-C-105	42_50	9.25	48.75	8.25	12.00
241-C-106	42_58	11.75	47.25	7.25	12.00
241-C-107	34_42	3.00	54.00	9.25	12.00
241-C-108	34_50	9.25	48.75	8.25	12.00
241-C-109	34_58	10.50	48.50	7.25	12.00
241-C-110	26_42	2.00	54.00	10.25	12.00
241-C-111	26_50	6.75	51.25	8.25	12.00
241-C-112	26_58	11.75	47.25	7.25	9.00
241-C-201	35_66	13.00	47.00	6.25	9.00
241-C-202	31_66	13.00	48.00	5.25	9.00
241-C-203	27_66	14.25	46.75	5.25	9.00
241-C-204	23_66	14.25	46.75	5.25	9.00
Median	100-Series Tank	9.2	48.7	8.2	12.0
Median	200-Series Tank	13.6	47.1	5.5	9.0

Figure 4-3. Moisture Content Distribution below Tank 241-C-105 at Various Times during (a) Surface Barrier Design Time Period of 500 years Following Closure and (b) Post-Surface Barrier Design Time Period.

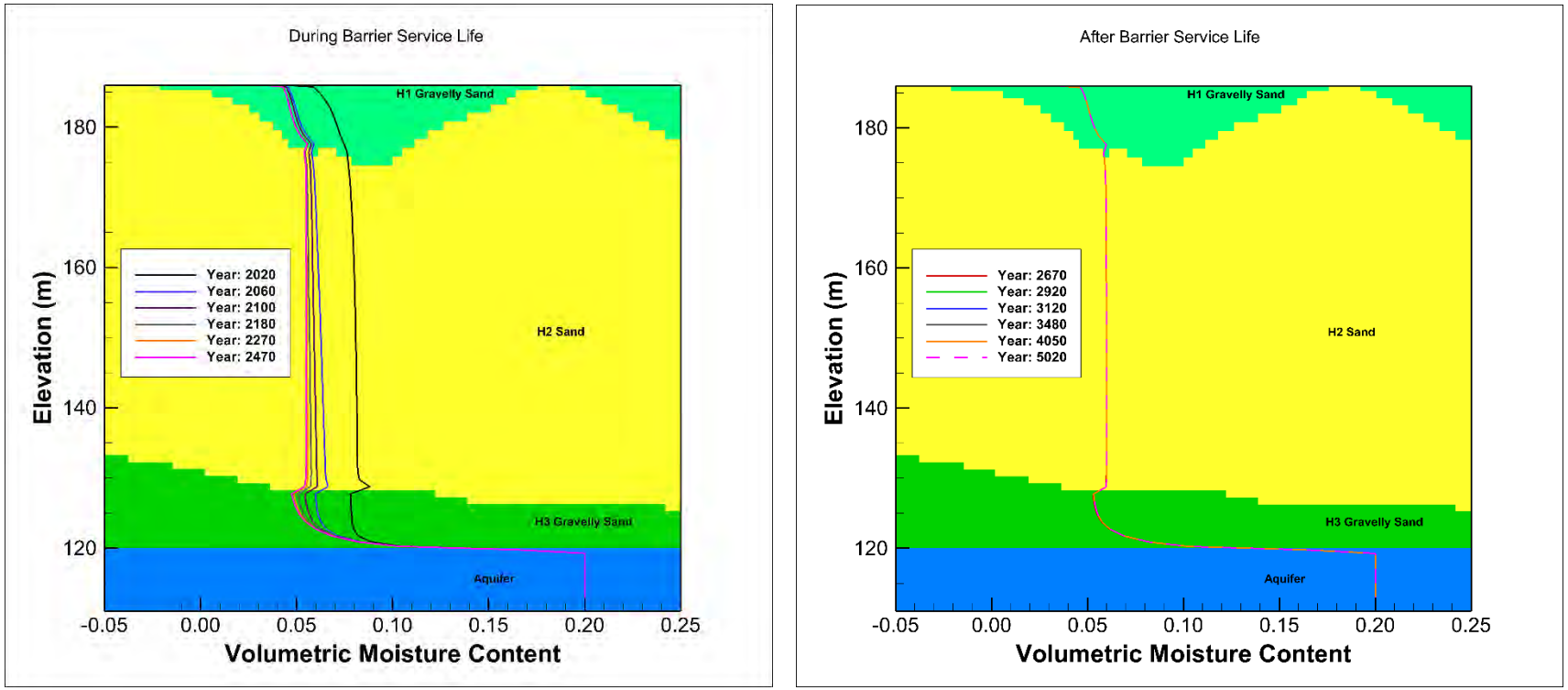

(a) (b)

Note: Barrier Service Life assumes intact surface cover leading to reduced net infiltration while Post-Barrier Service Life assumes degraded surface cover.

Figure 4-4. Vertical Darcy Flux Distribution below Tank 241-C-105 at Various Times.

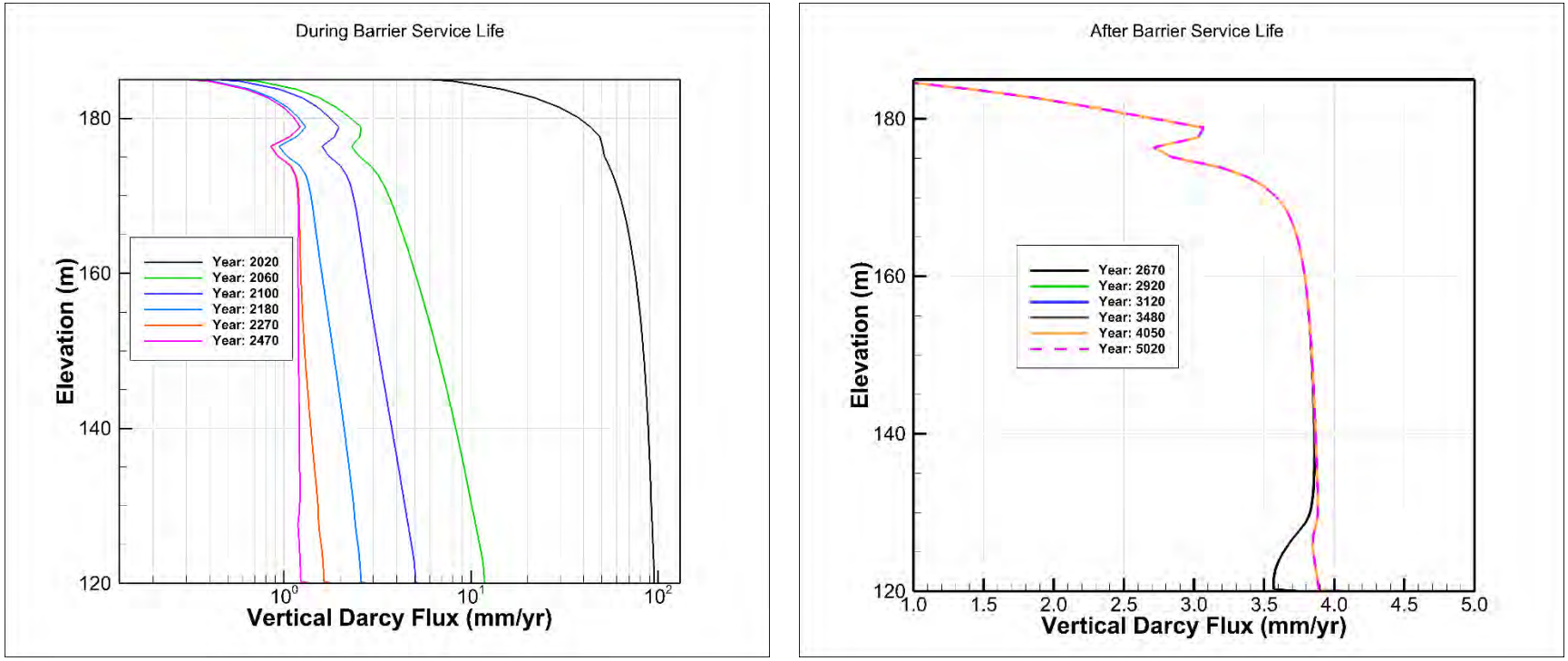

(a) (b)

Figure 4-5. Representative Hydrostratigraphic Column for (a) 100-Series and (b) 200-Series Tanks.

Hydrostratigraphy Below C-105	STOMP Node Elevation (m)	STOMP Node Numbers	STOMP Vertical Discretization (m)	GoldSim Vertical Discretization (m)
H1 Gravelly Sand	185.75	69	1.00	2 m
	184.75	68	1.00	
	183.75	67	1.00	3.5 m
	182.625	66	1.25	
	181.375	65	1.25	
	180.125	64	1.25	8.75 m
	178.875	63	1.25	
	177.625	62	1.25	
	176.375	61	1.25	3.75 m
	175.125	60	1.25	
	173.875	59	1.25	
H2 Sand	172.625	58	1.25	2 m (over 40 m thickness)
	171.375	57	1.25	
	170.125	56	1.25	
	168.875	55	1.25	
	167.625	54	1.25	
	166.375	53	1.25	
	165.125	52	1.25	
	163.875	51	1.25	
	162.625	50	1.25	
	161.375	49	1.25	
	160.125	48	1.25	
	158.875	47	1.25	
	157.625	46	1.25	
	156.375	45	1.25	
	155.125	44	1.25	
	153.875	43	1.25	
	152.625	42	1.25	
	151.375	41	1.25	
	150.125	40	1.25	
	148.875	39	1.25	
	147.625	38	1.25	
	146.375	37	1.25	
	145.125	36	1.25	
	143.875	35	1.25	
	142.625	34	1.25	
	141.375	33	1.25	
	140.125	32	1.25	
	138.875	31	1.25	
	137.625	30	1.25	
	136.375	29	1.25	
	135.125	28	1.25	
	133.875	27	1.25	
	132.75	26	1.00	5 m
	131.75	25	1.00	
	130.75	24	1.00	
	129.75	23	1.00	
	128.75	22	1.00	
H3 Gravelly Sand	127.75	21	1.00	7 m
	126.75	20	1.00	
	125.75	19	1.00	
	124.75	18	1.00	
	123.75	17	1.00	
	122.75	16	1.00	
	121.75	15	1.00	
	120.875	14	0.75	1.25 m
	120.25	13	0.50	
Aquifer	119.75	12	0.50	12 m
	119.25	11	0.50	
	118.625	10	0.75	
	117.75	9	1.00	
	116.625	8	1.25	
	115.25	7	1.50	
	113.75	6	1.50	
	112	5	2.00	
	109.5	4	3.00	
Inactive	106	3	4.00	
	102	2	4.00	
	97.5	1	5.00	

Node used in Flow-Field abstraction

(a)

Hydrostratigraphy Below C-203	STOMP Node Elevation (m)	STOMP Node Numbers	STOMP Vertical Discretization (m)	GoldSim Vertical Discretization (m)
H1 Gravelly Sand	185.75	69	1.00	2 m
	184.75	68	1.00	
	183.75	67	1.00	3.5 m
	182.625	66	1.25	
	181.375	65	1.25	
	180.125	64	1.25	8.75 m
	178.875	63	1.25	
	177.625	62	1.25	
	176.375	61	1.25	
	175.125	60	1.25	
	173.875	59	1.25	
	172.625	58	1.25	
H2 Sand	171.375	57	1.25	3.75 m
	170.125	56	1.25	
	168.875	55	1.25	
	167.625	54	1.25	2 m (over 40 m thickness)
	166.375	53	1.25	
	165.125	52	1.25	
	163.875	51	1.25	
	162.625	50	1.25	
	161.375	49	1.25	
	160.125	48	1.25	
	158.875	47	1.25	
	157.625	46	1.25	
	156.375	45	1.25	
	155.125	44	1.25	
	153.875	43	1.25	
	152.625	42	1.25	
	151.375	41	1.25	
	150.125	40	1.25	
	148.875	39	1.25	
	147.625	38	1.25	
	146.375	37	1.25	
	145.125	36	1.25	
	143.875	35	1.25	
	142.625	34	1.25	
	141.375	33	1.25	
	140.125	32	1.25	
	138.875	31	1.25	
	137.625	30	1.25	
	136.375	29	1.25	
	135.125	28	1.25	
	133.875	27	1.25	
	132.75	26	1.00	
	131.75	25	1.00	
	130.75	24	1.00	
	129.75	23	1.00	
	128.75	22	1.00	
	127.75	21	1.00	3
	126.75	20	1.00	
	125.75	19	1.00	
H3 Gravelly Sand	124.75	18	1.00	4
	123.75	17	1.00	
	122.75	16	1.00	
	121.75	15	1.00	
	120.875	14	0.75	1.25
	120.25	13	0.50	
Aquifer	119.75	12	0.50	9
	119.25	11	0.50	
	118.625	10	0.75	
	117.75	9	1.00	
	116.625	8	1.25	
	115.25	7	1.50	
	113.75	6	1.50	
	112	5	2.00	
Inactive	109.5	4	3.00	
	106	3	4.00	
	102	2	4.00	
	97.5	1	5.00	

Node used in Flow-Field abstraction

(b)

The mass loading on the aquifer pathway from the vadose zone occurs over the length of the source parallel to the flow path. For the tank sources, this is equivalent to the diameter of the tank. For the pipeline source, the source loading from the vadose zone to the aquifer is conservatively assumed to occur over the 75 m that represents the half-length of the pipeline source area along the flow path.

Table 4-2. Vertical Grid Discretization and Flow Field for the System-Level Model.

	Unit	Thickness (m)	Number of Grid Block Cells	Grid Discretization	Flow Field Discretization (Moisture Content and Vertical Darcy Flux)
100-Series Tanks	H1 Gravelly Sand	9.25	3	1 at 2 m, 1 at 3.5 m, 1 at 3.75 m	One flow field for each cell
	H2 Sand	48.75	22	1 at 3.75 m, 20 cells of 2 m thickness each for a total of 40 m 1 at 5 m	One flow field for the first cell. One flow field for the next 20 cells and One flow field for the remaining one cell
	H3 Gravelly Sand	8.25	2	1 at 7 m, 1 at 1.25 m.	One flow field for each cell
	Saturated Zone	12.00		Aquifer pathway	One flow field
200-Series Tanks	H1 Gravelly Sand	14.25	3	1 at 2 m, 1 at 3.5 m, 1 at 8.75 m	One flow field for each cell
	H2 Sand	46.75	22	1 at 3.75 m, 20 cells of 2 m thickness each for a total of 40 m 1 at 3 m	One flow field for the first cell. One flow field for the next 20 cells and One flow field for the remaining one cell
	H3 Gravelly Sand	5.50	2	1 at 4 m, 1 at 1.25 m.	One flow field per cell
	Saturated Zone	9.00		Aquifer pathway	One flow field

The average aquifer pathway concentrations at the 100 m downgradient boundary are calculated for each source separately, by assuming that the mass within the defined 1-D aquifer stream tube configuration does not laterally disperse. This 1-D approach tends to maximize the concentrations for a given source term, but it does not take account of overlapping plumes from lateral dispersion from other sources that are on parallel flow paths (Figure 4-9). To determine the maximum concentration, a separate calculation is performed. Since the highest concentrations were expected to occur along the centerline of the WMA C width, extended to the 100 m boundary due to location of highest residual inventory tanks along the centerline, the calculated concentrations for the C-102, C-105, 241-C-108, and C-111 tank sources at the 100 m boundary were combined to calculate the highest concentration. These four tanks fall along a single flow path (stream tube), since the flow direction is aligned with the orientation of these tanks. The amount of additional contaminant mass from lateral dispersion along adjacent flow paths is included by using an analytical solution (*Plume function* within GoldSim©) that calculates the concentration away from the centerline of the plume. Using this approach, the concentration from surrounding aquifer pathways are calculated and added to the combined concentration for the aquifer pathway that includes C-102, C-105, 241-C-108, and C-111 tank

sources. The two laterally adjacent and parallel aquifer pathways are (a) along the orientation of tanks 241-C-101, 241-C-104, 241-C-107, and 241-C-110, and (b) along the orientation of tanks 241-C-103, 241-C-106, 241-C-109, and 241-C-112 (C-112). The primary groundwater flow path on which the 200-series tanks occur is deemed too far to influence the concentrations along the centerline, and therefore is not considered based on evaluation of STOMP© 3-D model results.

A spatial-variability study was undertaken to evaluate the adequacy of using one representative flow field for all of the 100-series tanks. For this purpose, the vertical Darcy flux from STOMP©-based model nodes located underneath intact tanks were compared. The vertical Darcy flux underneath tank C-105 (located near the center of the tank farm) was compared to tank C-112 (located at the northern edge of the tank farm). The vertical Darcy flux under a 200-series tank (241-C-201 [C-201]) located near tank C-112 was also compared. The comparison results are presented in Figure 4-10 for two nodes. Node 69 is located ~0.5 m below the base of the tank while node 63 is located ~3 m below node 69. The results indicate that for node 69 the vertical Darcy flux for tank C-105 matches closely with tank C-112, and is quite different from that of tank C-201. For node 63, which is deeper, the differences among the three tanks are minor. The large difference observed for node 63 is attributed to its location near the base of the tank where the amount of flow diversion around the tank is influenced by its diameter. The smaller diameter of tank C-201 (20 ft) exhibits small flow diversion, and the Darcy flux under the tank is relatively high compared to the larger flow diversion observed for the larger-diameter (75 ft) C-105 and C-112 tanks. These observations support the use of one representative flow field for all 100-series tanks and another for all 200-series tanks.

Confirmation of the abstraction modeling approach for evaluating system performance was undertaken by comparing the contaminant transport results to the STOMP©-based model results for the base case. Due to coarser vertical discretization employed in the 1-D abstraction model, the results from those nodes that are closest to the STOMP©-based model grid nodes are compared. The diffusive mass flux of ^{99}Tc calculated using the source term parameters for tank C-105 was applied as boundary conditions to both models. A comparison between the dissolved concentration of ^{99}Tc in the vadose zone using a STOMP© 3-D model and a GoldSim© 1-D model are presented for selected locations in the vadose zone (Figures 4-11 and 4-12). There is a good match between the 3-D process model and 1-D abstraction model throughout the full thickness of the vadose zone under the tank (~66 m).

For the saturated zone, the groundwater concentration predicted by the STOMP©-based model (at the highest concentration point of calculation) is compared to the GoldSim©-based abstraction model results at 100 m downgradient of the WMA C fenceline along the tank C-105 aquifer pathway (Figure 4-13). The first breakthrough times match well, but the 1-D model produces slightly higher concentrations following the peak. This result is expected, as the 1-D aquifer pathway does not allow lateral dispersion of the mass and assumes constant flow rate through the steam tube. Given these differences in the conceptual model used in the two analyses, the agreement is very reasonable. This result indicates that the abstraction model is appropriate and sufficiently accurate for its intended use in evaluating system performance.

Figure 4-6. Representative Flow Field Applied Under 100-Series Tank for the Base Case (Intact Tank condition).

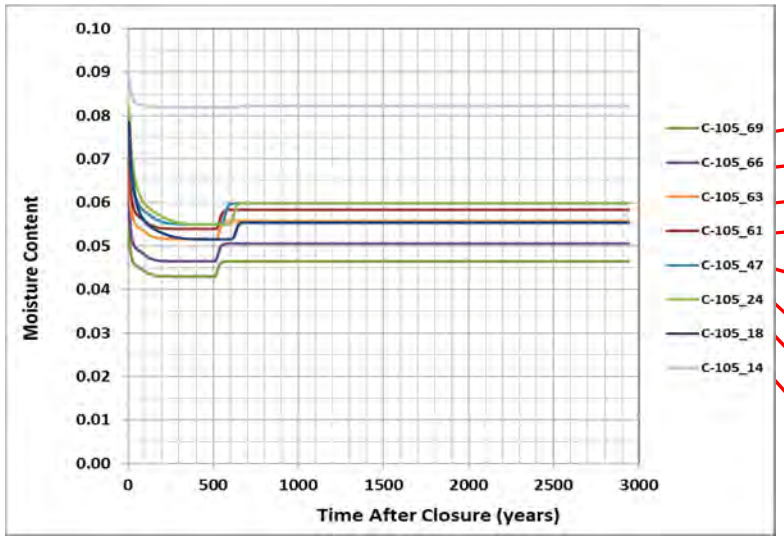

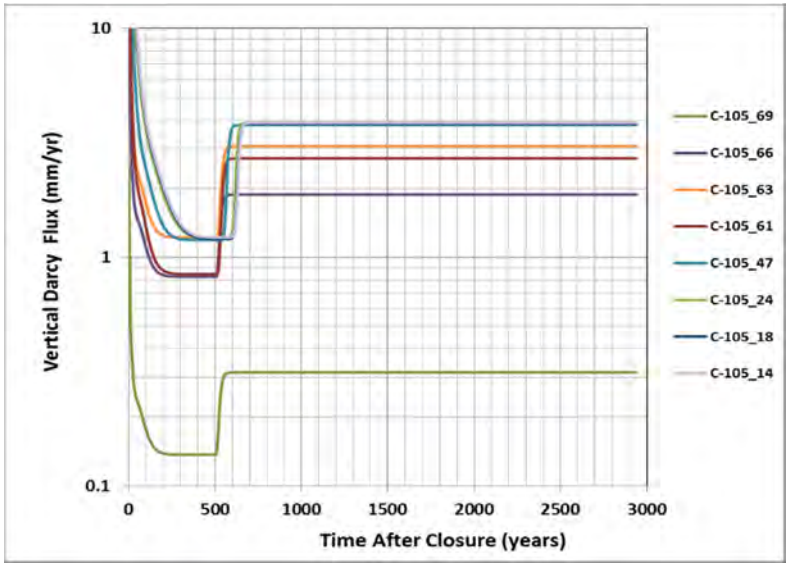

Hydrostratigraphy Below C-105	STOMP Node Elevation (m)	STOMP Node Numbers	STOMP Vertical Discretization (m)	GoldSim Vertical Discretization (m)
H1 Gravelly Sand	185.75	69	1.00	2 m
	184.75	68	1.00	
	183.75	67	1.00	
	182.625	66	1.25	3.5 m
	181.375	65	1.25	
	180.125	64	1.25	
	178.875	63	1.25	1.75 m
	177.625	62	1.25	
	176.375	61	1.25	
	175.125	60	1.25	3.75 m
	173.875	59	1.25	
H2 Sand	172.625	58	1.25	2 m (over 40 m thickness)
	171.375	57	1.25	
	170.125	56	1.25	
	168.875	55	1.25	
	167.625	54	1.25	
	166.375	53	1.25	
	165.125	52	1.25	
	163.875	51	1.25	
	162.625	50	1.25	
	161.375	49	1.25	
	160.125	48	1.25	
	158.875	47	1.25	
	157.625	46	1.25	
	156.375	45	1.25	
	155.125	44	1.25	
	153.875	43	1.25	
	152.625	42	1.25	
	151.375	41	1.25	
	150.125	40	1.25	
	148.875	39	1.25	
	147.625	38	1.25	
	146.375	37	1.25	
	145.125	36	1.25	
	143.875	35	1.25	
	142.625	34	1.25	
	141.375	33	1.25	
	140.125	32	1.25	
	138.875	31	1.25	
	137.625	30	1.25	
	136.375	29	1.25	
	135.125	28	1.25	
	133.875	27	1.25	
	132.75	26	1.00	5 m
	131.75	25	1.00	
	130.75	24	1.00	
	129.75	23	1.00	
	128.75	22	1.00	
H3 Gravelly Sand	127.75	21	1.00	7 m
	126.75	20	1.00	
	125.75	19	1.00	
	124.75	18	1.00	
	123.75	17	1.00	
	122.75	16	1.00	
	121.75	15	1.00	
	120.875	14	0.75	1.25 m
	120.25	13	0.50	
Aquifer	119.75	12	0.50	12 m
	119.25	11	0.50	
	118.625	10	0.75	
	117.75	9	1.00	
	116.625	8	1.25	
	115.25	7	1.50	
	113.75	6	1.50	
	112	5	2.00	
	109.5	4	3.00	
Inactive	106	3	4.00	
	102	2	4.00	
	97.5	1	5.00	

Node used in Flow Field abstraction

Figure 4-7. Representative Flow Field Applied Under 200-Series Tank for the Base Case (Intact Tank condition).

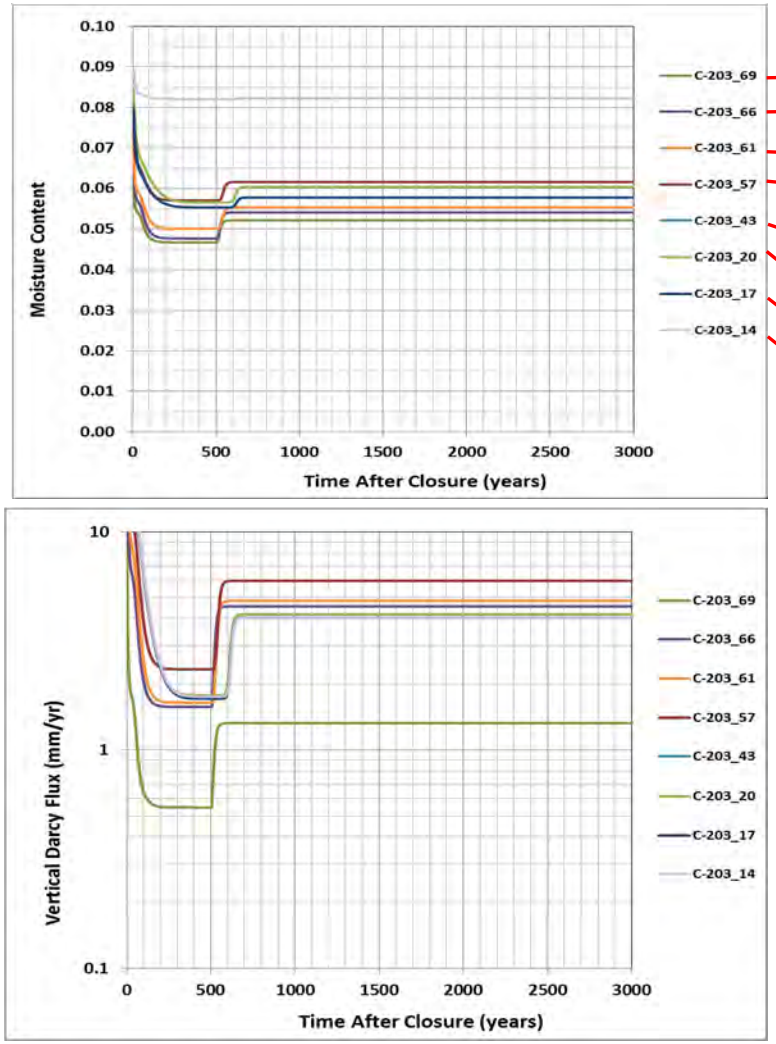

Hydrostratigraphy Below C-203	STOMP Node Elevation (m)	STOMP Node Numbers	STOMP Vertical Discretization (m)	GoldSim Vertical Discretization (m)
H1 Gravelly Sand	185.375	69	1.00	2
	184.75	68	1.00	
	183.75	67	1.00	3.5
	182.625	66	1.25	
	181.375	65	1.25	
	180.125	64	1.25	8.75
	178.875	63	1.25	
	177.625	62	1.25	
	176.375	61	1.25	
	175.125	60	1.25	
	173.875	59	1.25	
	172.625	58	1.25	
H2 Sand	171.375	57	1.25	3.75
	170.125	56	1.25	
	168.875	55	1.25	
	167.625	54	1.25	2 m (over 40 m thickness)
	166.375	53	1.25	
	165.125	52	1.25	
	163.875	51	1.25	
	162.625	50	1.25	
	161.375	49	1.25	
	160.125	48	1.25	
	158.875	47	1.25	
	157.625	46	1.25	
	156.375	45	1.25	
	155.125	44	1.25	
	153.875	43	1.25	
	152.625	42	1.25	
	151.375	41	1.25	
	150.125	40	1.25	
	148.875	39	1.25	
	147.625	38	1.25	
	146.375	37	1.25	
	145.125	36	1.25	
	143.875	35	1.25	
	142.625	34	1.25	
	141.375	33	1.25	
	140.125	32	1.25	
	138.875	31	1.25	
	137.625	30	1.25	
	136.375	29	1.25	
	135.125	28	1.25	
	133.875	27	1.25	
	132.75	26	1.00	
	131.75	25	1.00	
	130.75	24	1.00	
	129.75	23	1.00	
	128.75	22	1.00	
	127.75	21	1.00	
	126.75	20	1.00	
	125.75	19	1.00	
H3 Gravelly Sand	124.75	18	1.00	4
	123.75	17	1.00	
	122.75	16	1.00	
	121.75	15	1.00	
	120.875	14	0.75	1.25
	120.25	13	0.50	
Aquifer	119.75	12	0.50	9
	119.25	11	0.50	
	118.625	10	0.75	
	117.75	9	1.00	
	116.625	8	1.25	
	115.25	7	1.50	
	113.75	6	1.50	
	112	5	2.00	
Inactive	109.5	4	3.00	
	106	3	4.00	
	102	2	4.00	
	97.5	1	5.00	

Node used in Flow-Field abstraction

Figure 4-8. Representative Flow Field Applied for Degraded Tank Conditions for (a) 100-Series Tank and (b) 200-Series Tank.

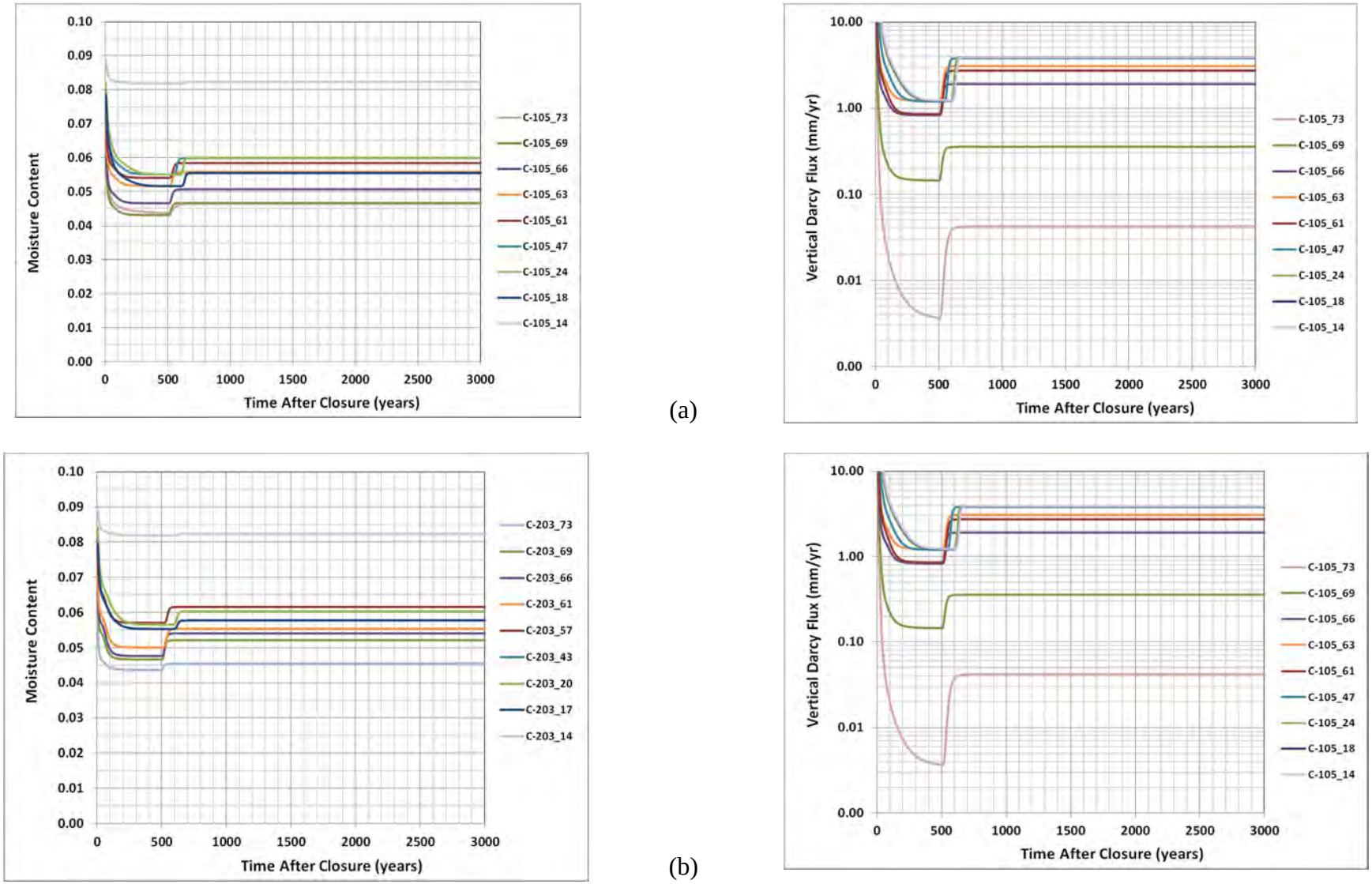

Figure 4-9. Implementation of Aquifer Pathway for a Given Source Area Along with Points of Evaluation of Concentrations.

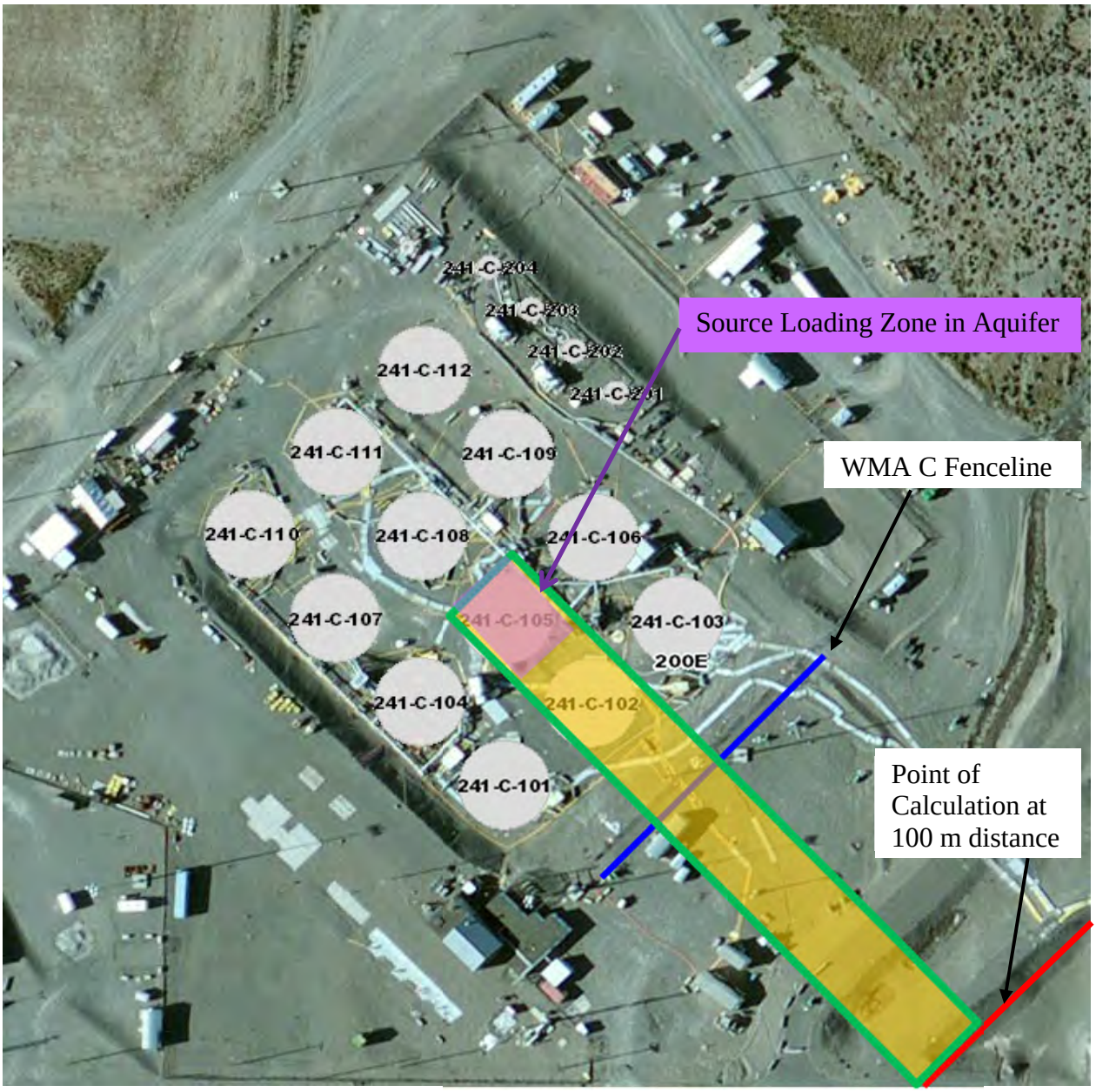

WMA = Waste Management Area

4.4 IMPLEMENTATION OF ATMOSPHERIC TRANSPORT PATHWAY

Gases and vapors could travel upward from the residual inventory within tanks and ancillary equipment through the surface barrier to the ground surface. The principal mechanism by which gaseous nuclides would migrate from the waste to the ground surface is gaseous diffusion. For

tanks, in which the residual waste is predominantly on the bottom of the tank, this means that the gases must be transported through the tank infill grout, the tank dome, the soil overburden, and the surface barrier. For pipelines, the diffusion would occur through the soil overburden and the surface barrier.

Releases to the atmospheric pathway are competitive with the groundwater pathway. The partitioning of inventory into the aqueous and gaseous phase occurs within the source term model (in the residual waste layer). The mass partitioned into the aqueous phase is then available for transport to the underlying vadose zone, while the partitioned fraction in the gas phase is available for upward transport to the atmosphere. Once partitioned, the transport within each pathway is maximized. Only the aqueous phase is considered in the vadose zone to maximize transport along the groundwater pathway. Similarly, to maximize the upward transport through the gas phase, the downward flow of water above the residual waste location is not modeled. In addition, any physical effect of surface barrier on gaseous flux is ignored.

Of the radionuclides contained in residual inventory at closure, four could potentially originate as gas:

- Carbon-14 as CO_2 gas
- Hydrogen-3 (tritium) as H_2 gas
- Iodine-129 as I_2 gas
- Radon-222 as radon gas.

A fraction of the radon atoms formed from the decay of radium escape from the solid phase into the gas phase between the solid grains, mainly because of alpha recoil. The fraction of radon atoms produced that ends up in the gas phase, and so available for transport in the gas phase, is known as the emanation coefficient. The emanation coefficient is highly variable from one material to another. This depends on a variety of specific features of the contaminated material, including the distribution of radium within the material particles, grain size and pore size distributions, and moisture content of the contaminated material ("A comprehensive review of radon emanation measurements for mineral, rock, soil, and fly ash" [Sakoda et al. 2011]). Emanation coefficients have not been measured for residual wastes. For the purposes of this assessment, the residual wastes are assumed to have emanation properties comparable to soils. NCRP Report No. 103, "Control of Radon in Houses" has recommended a nominal emanation coefficient of about 0.2 for soils and this value is adopted for this PA. The target emanation coefficient is implemented in the model as the fractional mass of radon produced in the residual waste that enters the gas phase.

The binary diffusion coefficients of the different gases of concern in air have been calculated using the EPA methodology (United States Environmental Protection Agency, [EPA On-line Tools for Site Assessment Calculation], http://www.epa.gov/athens/learn2model/part-two/onsite/estdiffusion-ext.html) considering an atmospheric pressure of 1 atm and a temperature of 20 °C. The calculated diffusion coefficients are reported in Table 4-3, together with the gas boiling point estimates used in the calculations. For radon, another reference has been considered (Radon and Its Decay Products in Indoor Air [Nazaroff and Nero 1988]) as EPA (2012) did not consider diffusion coefficient calculation for this gas.

Figure 4-10. Vertical Darcy Flux Extracted from Three-Dimensional Subsurface Transport Over Multiple Phases (STOMP©)-Based Model Nodes Located below Tanks 241-C-105, 241-C-112, and 241-C-201 along with Their Location in Waste Management Area C. Node 69 is located 0.5 m below the tank bottom while node 63 is located about 3 m below node 69.

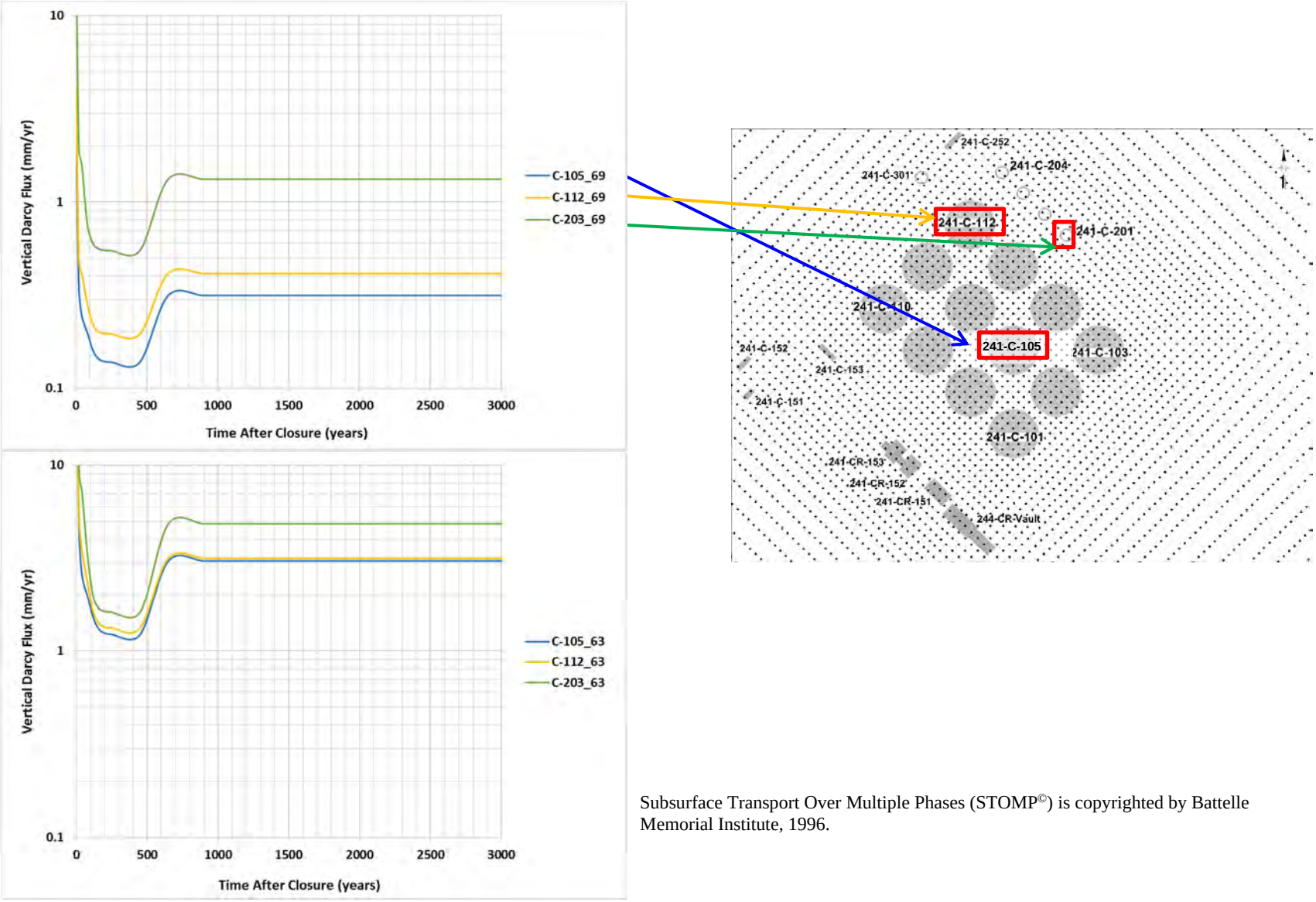

Subsurface Transport Over Multiple Phases (STOMP©) is copyrighted by Battelle Memorial Institute, 1996.

Figure 4-11. Comparison between Three-Dimensional Subsurface Transport Over Multiple Phases (STOMP©)-Based Model Prediction and GoldSim©-Based One-Dimensional Abstraction Model Prediction for Nodes Located in H1 Gravelly Sand Unit.

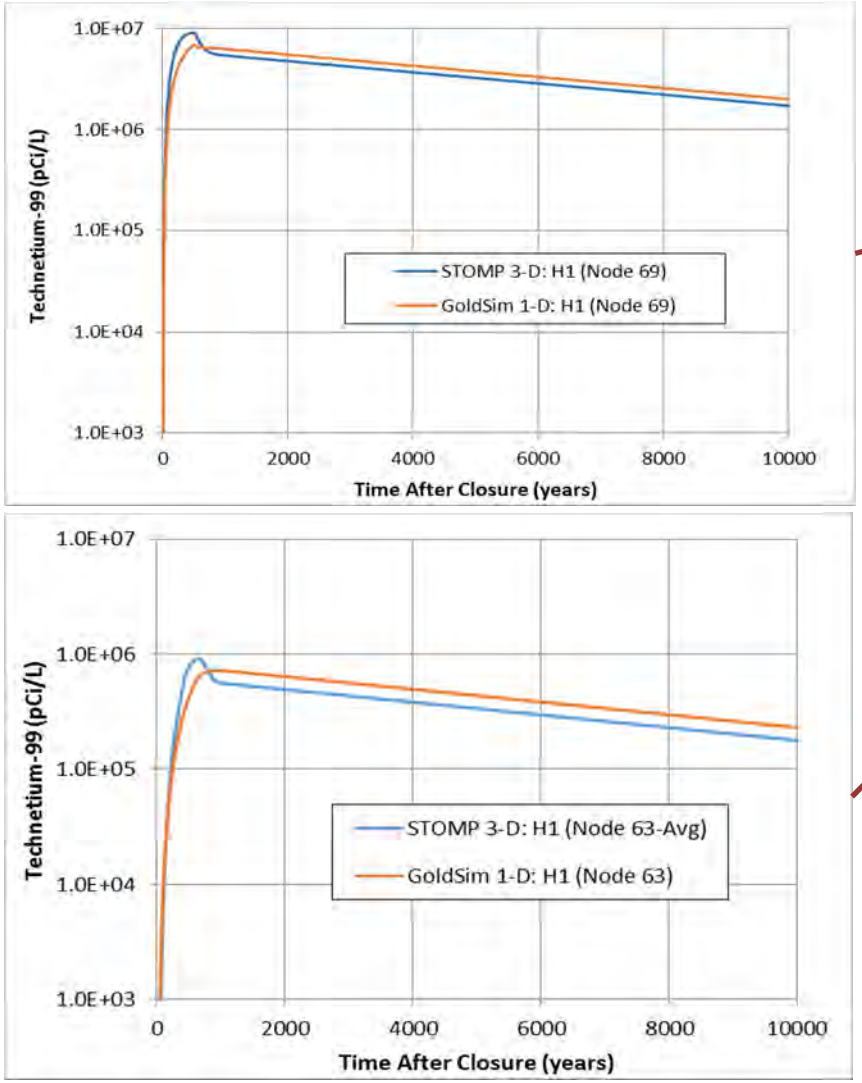

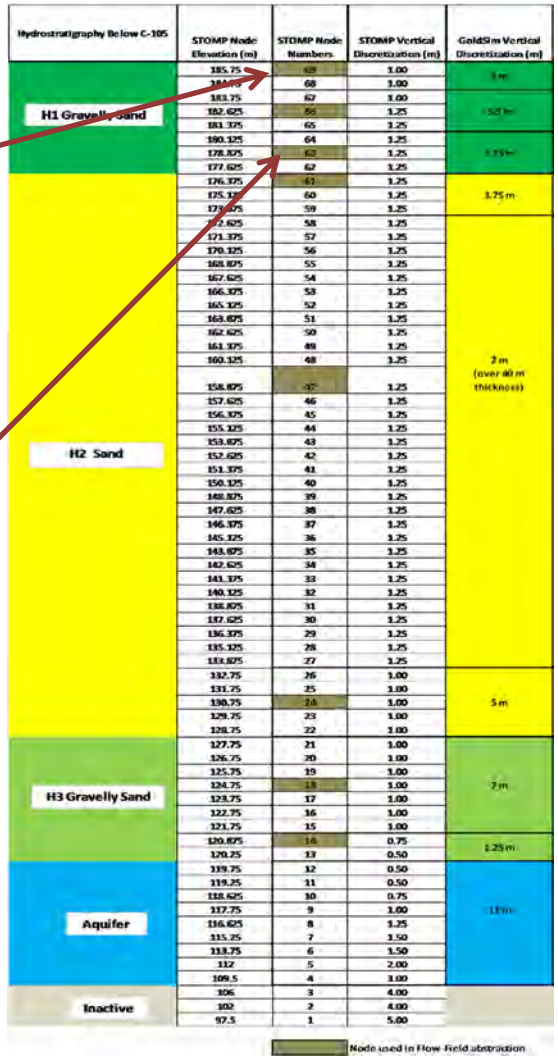

GoldSim© simulation software is copyrighted by GoldSim Technology Group LLC of Issaquah, Washington (see http://www.goldsim.com).
Subsurface Transport Over Multiple Phases (STOMP©) is copyrighted by Battelle Memorial Institute, 1996.

Figure 4-12. Comparison between Three-Dimensional Subsurface Transport Over Multiple Phases (STOMP©)-Based Model Prediction and GoldSim©-Based One-Dimensional Abstraction Model Prediction for Nodes Located in H2 Sand Unit and H3 Gravelly Sand Unit.

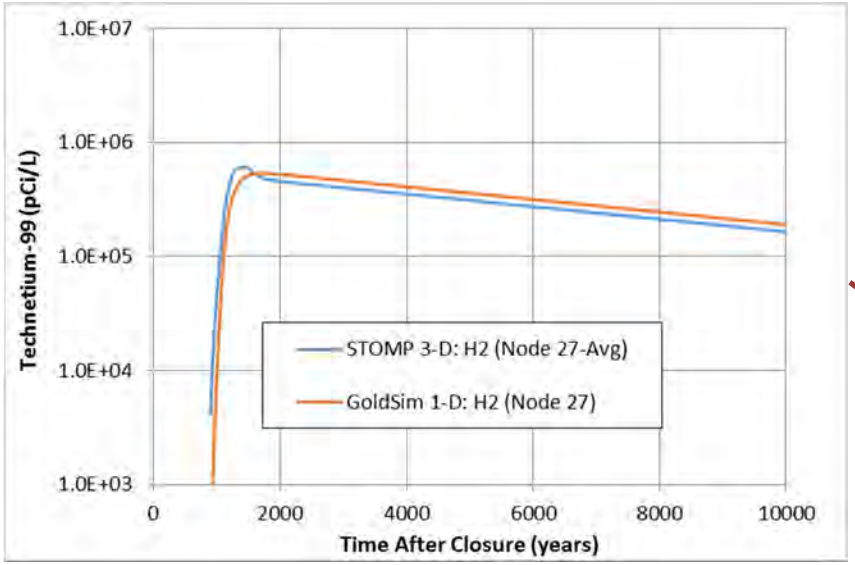

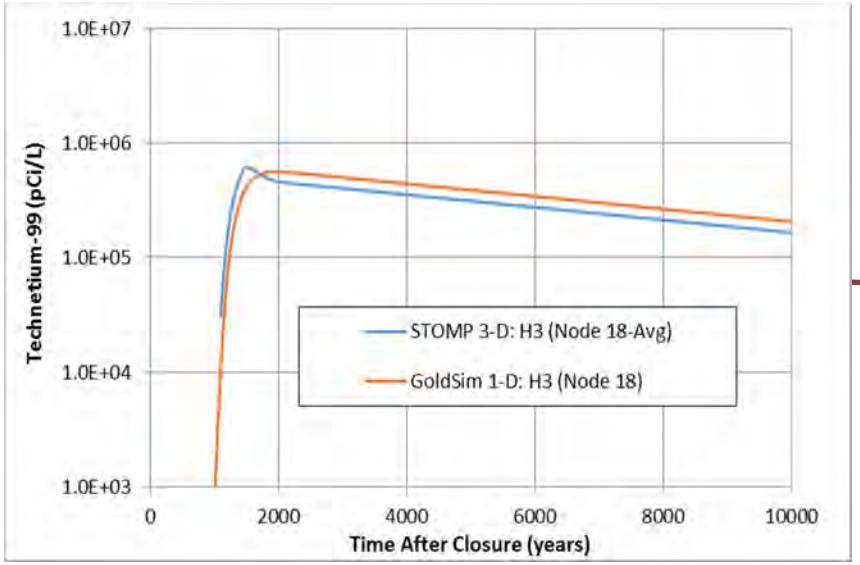

GoldSim© simulation software is copyrighted by GoldSim Technology Group LLC of Issaquah, Washington (see http://www.goldsim.com). Subsurface Transport Over Multiple Phases (STOMP©) is copyrighted by Battelle Memorial Institute, 1996.

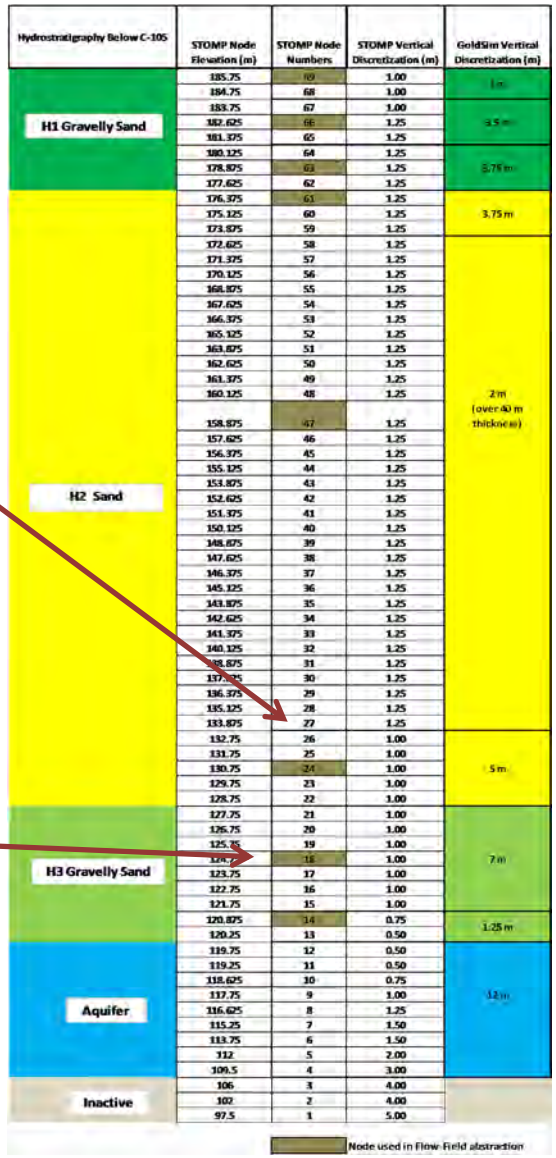

Hydrostratigraphy Below C-105	STOMP Node Elevation (m)	STOMP Node Numbers	STOMP Vertical Discretization (m)	GoldSim Vertical Discretization (m)
H1 Gravelly Sand	185.75	69	1.00	1 m
	184.75	68	1.00	
	183.75	67	1.00	4.5 m
	182.625	66	1.25	
	181.375	65	1.25	
	180.125	64	1.25	3.75 m
	178.875	63	1.25	
	177.625	62	1.25	
	176.375	61	1.25	3.75 m
H2 Sand	175.125	60	1.25	
	173.875	59	1.25	
	172.625	58	1.25	2 m (over 40 m thickness)
	171.375	57	1.25	
	170.125	56	1.25	
	168.875	55	1.25	
	167.625	54	1.25	
	166.375	53	1.25	
	165.125	52	1.25	
	163.875	51	1.25	
	162.625	50	1.25	
	161.375	49	1.25	
	160.125	48	1.25	
	158.875	47	1.25	
	157.625	46	1.25	
	156.375	45	1.25	
	155.125	44	1.25	
	153.875	43	1.25	
	152.625	42	1.25	
	151.375	41	1.25	
	150.125	40	1.25	
	148.875	39	1.25	
	147.625	38	1.25	
	146.375	37	1.25	
	145.125	36	1.25	
	143.875	35	1.25	
	142.625	34	1.25	
	141.375	33	1.25	
	140.125	32	1.25	
	138.875	31	1.25	
	137.625	30	1.25	
	136.375	29	1.25	
	135.125	28	1.25	
	133.875	27	1.25	
	132.75	26	1.00	5 m
	131.75	25	1.00	
	130.75	24	1.00	
	129.75	23	1.00	
	128.75	22	1.00	
H3 Gravelly Sand	127.75	21	1.00	7 m
	126.75	20	1.00	
	125.75	19	1.00	
	124.75	18	1.00	
	123.75	17	1.00	
	122.75	16	1.00	
	121.75	15	1.00	
	120.875	14	0.75	1.25 m
	120.25	13	0.50	
Aquifer	119.75	12	0.50	12 m
	119.25	11	0.50	
	118.625	10	0.75	
	117.75	9	1.00	
	116.625	8	1.25	
	115.25	7	1.50	
	113.75	6	1.50	
	112	5	2.00	
	109.5	4	3.00	
Inactive	106	3	4.00	
	102	2	4.00	
	97.5	1	5.00	

Node used in Flow-Field abstraction

These releases are controlled by the partitioning of the radionuclides among the solid fraction of the porous medium (sorbed fraction), aqueous dissolved fraction (grout/water partitioning), and the gaseous fraction (air/water partitioning) by considering the following equilibrium coefficients:

- K_d representing grout-to-water partitioning

- Henry's law constant (K_h) for representing air-to-water partitioning (see Table 4-4 for the constant used for the constituents above).

The atmospheric transport pathway calculations are conducted in the following three steps.

1. First, a calculation is performed to compute the upward diffusive flux from each source term to the surface. A zero-concentration boundary condition at the surface is imposed for purpose of calculating the gaseous flux. This is conceptually equivalent to having a large enough wind speed above WMA C such that the air parcel is renewed constantly, thereby maximizing the diffusive gradient.

    - For all sources except pipelines, while the infill grout is intact, upward gaseous diffusion of volatile contaminants is modeled from the residual waste layer towards the atmosphere. Upward diffusive gas phase transport through the tanks (or 244-CR vault) is modeled to occur along a 10-m-long pathway towards the land surface (Figure 4-14). This pathway is split into a lower 5 m thickness composed of infill grout material, followed by another 5 m thickness of soil overburden. For the pipeline source area, the diffusive length chosen is the pipeline diameter (0.076 m [3 in.]) and the 5 m thickness of the soil overburden.

    - A surface barrier that will be emplaced at closure over the tank farm will provide additional depth to the waste and therefore greater diffusive length. For the purpose of performing the air pathway calculations, this additional thickness is conservatively ignored.

    - For all grouted facilities, the air content within the infill grout is assumed to be 6% based on characterization information for possible Hanford grout formulations (WSRC-TR-2005-00195). The porosity and saturation of the infill grout for the purpose of diffusive release calculations are fixed over time. This is deemed to be conservative, as studies have indicated that chemical transformation of initial grout minerals will likely cause porosity reduction over time due to increased molar volume of the newly formed mineral phases.

Figure 4-13. Comparison between Three-Dimensional Subsurface Transport Over Multiple Phases (STOMP©)-Based Model Prediction and GoldSim©-Based One-Dimensional Abstraction Model Prediction in the Saturated Zone at 100 meter Distance from the Waste Management Area C Fenceline.

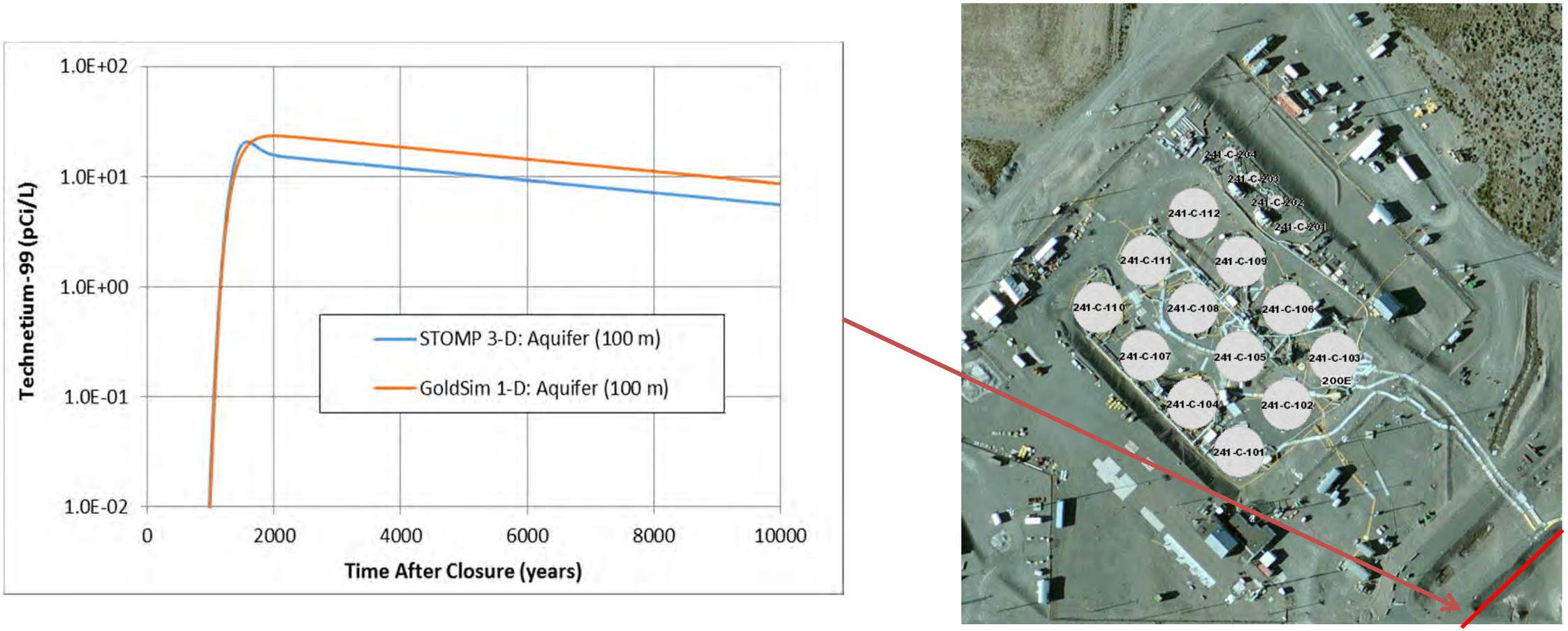

1-D = one-dimensional 3-D = three-dimensional

GoldSim© simulation software is copyrighted by GoldSim Technology Group LLC of Issaquah, Washington (see http://www.goldsim.com).
Subsurface Transport Over Multiple Phases (STOMP©) is copyrighted by Battelle Memorial Institute, 1996.

Table 4-3. Diffusion Coefficients in Air at 20 °C and 1 Atm.

Radionuclide	Gas Form	Diffusion Coefficient in Air (cm^2s^{-1})	Reference	Boiling Point (°C) Used in EPA Calculations (Haynes and Lide 2011)
^{14}C	CO_2	0.160	EPA 2012 (average method)	-78.55
^{3}H	H_2	0.819	EPA 2012 (average method)	-252.76
^{129}I	I_2	0.0897	EPA 2012 (FSG/LaBas method)	184.45
^{222}Rn	Rn	0.11	Nazaroff and Nero (1988) cited in ANL/EAD-4	(-)

EPA = U.S. Environmental Protection Agency

References:
ANL/EAD-4, "User's Manual for RESRAD Version 6."
CRC Handbook of Chemistry and Physics, 92nd Edition (Haynes and Lide 2011).
Radon and Its Decay Products in Indoor Air (Nazaroff and Nero 1988).
United States Environmental Protection Agency, Queried 01/2012, [EPA On-line Tools for Site Assessment Calculation], http://www.epa.gov/athens/learn2model/part-two/onsite/estdiffusion-ext.html.

Table 4-4. Henry's Law Constants.

Radionuclide	Gas Form	Aqueous-to-Gas Henry's Constant	Reference	Calculated Gas-to-Aqueous Dimensionless Henry's Constant at 20 °C
^{14}C	CO_2	4.5 (-)	Plummer et al. 2004	0.22
^{3}H	H_2	7.80E-4 (mol $atm^{-1}L^{-1}$)	Sander 1999	53.36
^{129}I	I_2	3.10E+0 (mol $atm^{-1}L^{-1}$)	Sander 1999	0.013
^{222}Rn	Rn	9.30E-3 (mol $atm^{-1}L^{-1}$)	Sander 1999	4.47

References:
"Transport of Carbon-14 in a Large Unsaturated Soil Column" (Plummer et al. 2004).
"Compilation of Henry's Law Constants for Inorganic and Organic Species of Potential Importance in Environmental Chemistry," Version 3 (Sander 1999).

2. Second, for each source area, the radionuclide transport in air along the downwind direction is performed using a Gaussian plume model, where advection and dispersion occur via wind movement to the receptor placed 100 m downwind at the point of calculation as conceptualized in Figure 4-15. As a continuous stream of gas (pollutants) is released into the steady wind in open atmosphere, the gas plume will travel with the mean wind speed. The plume will also disperse in the horizontal and vertical directions along the centerline. A schematic is presented in Figure 4-16 for a single source based on effective stack height (includes plume rise).

3. In order to evaluate the effect of commingling of gas plumes from different sources that could lead to increased concentration at the receptor location located 100 m downwind, a

separate calculation is performed where the upward diffusive flux emanating from various sources (described in Step 1) are combined into a point source, with the location near the approximate center point of the WMA C area. This is conceptually equivalent to a point source (i.e., stack source), but with the release rate (emission rate) equal to all the sources within the WMA C area. This point location is chosen to be the center of the pipeline area, which is 75 m from the WMA C fenceline. The total distance to the receptor is therefore 175 m.

- The predominant wind direction in the 200 East Area is towards southeast, and therefore in the general direction of groundwater flow. The average annual wind speed of 3.4 m/s (average from 1944 to 2004) is applied to the pathway for transport. The air mixing height is assumed to be 2 m, which is the approximate average height of an adult. The calculated air concentrations at the receptor location are used for evaluating air-pathway dose.

Figure 4-14. Atmospheric Transport Pathway Considered for Release from Tank Sources.

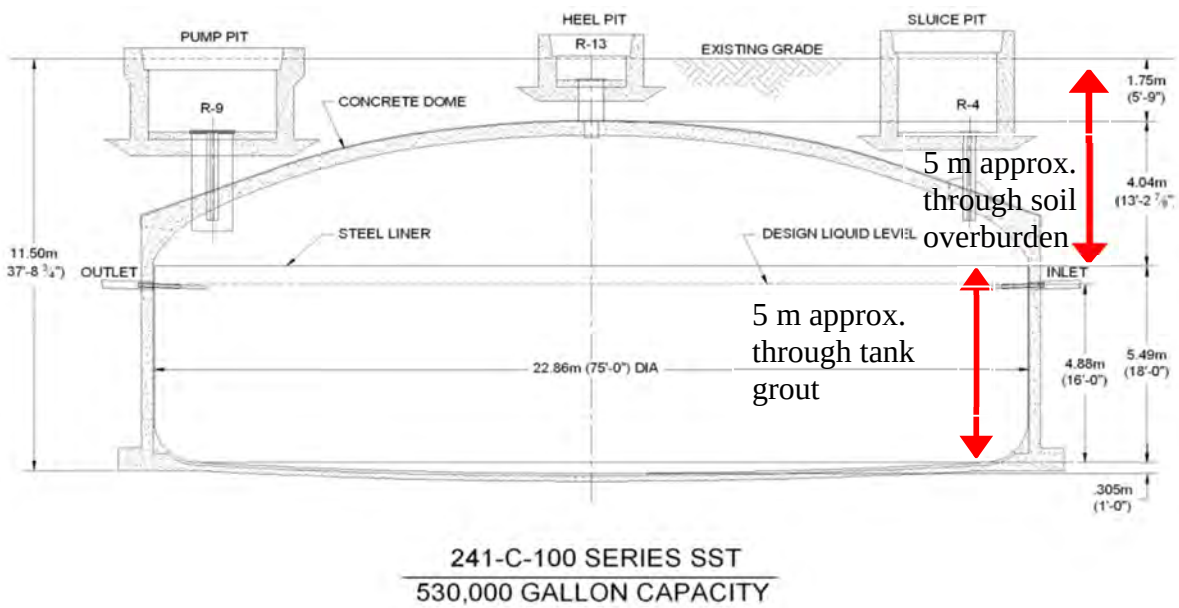

4.4.1 Mathematical Modeling of First Step

To calculate the diffusive flux releasing at the surface from a given source (buried tank or ancillary equipment), a 1-D model is developed using a finite-difference network of batch-reactor cells. The following transport equation (Fick's second law) is numerically solved to compute the mass flux and concentration.

$$R_d \frac{\partial(\theta_a C)}{\partial t} = D_{ef} \frac{\partial^2 C}{\partial x^2} \tag{4-11}$$

Where:

$C(x,t)$	=	the air concentration (kg/m^3) in the pore network of a given gas at the distance x (m) from the residual waste layer and time t (s) from assumed closure at WMA C
D_{ef} (m^2/s)	=	the effective diffusion coefficient of a given gas through the tortuous air pathway of the porous medium
R_d	=	the retardation coefficient of a given gas due to partitioning among different phases (air, water and solids) of the porous medium
θ_a (-)	=	the air content (or air-filled porosity) of the porous medium.

The diffusion coefficient for various gases of concern (CO_2, H_2, I_2, and radon) through the tortuous air pathway of the porous medium is calculated as follows.

$$D_{ef} = D_0 \tau \tag{4-12}$$

Where:

D_{ef} (m^2/s)	=	the effective diffusion coefficient through the tortuous air pathway of the porous medium for a given gas
D_0 (m^2/s)	=	the binary diffusion coefficient of the gas of concern in the air
τ	=	the tortuosity of the porous medium for air pathway.

An effective zero concentration boundary condition is imposed above WMA C to maximize the diffusive flux of gases. The diffusive area varies by the source geometry.

Separate modeling calculation is performed for estimating radon flux. The analysis is conducted assuming there is no downward migration of the parent radionuclide ^{226}Ra. This assumption was made to keep the ^{226}Ra fixed in the residual waste, with a constant diffusion path for the duration of the analysis. The ^{222}Rn release rate from the ground surface is estimated using the diffusion equation (Equation 4-11).

4.4.2 Gas Tortuosity

"Simulating the Gas Diffusion Coefficient in Macropore Network Images: Influence of Soil Pore Morphology" (Liu et al. 2006) compiled data sets and presented the experimentally determined gas tortuosity (ratio of the effective diffusion coefficient in soil [$\boldsymbol{D_{ef}}$] to that in free air [$\boldsymbol{D_0}$]) as a function of the air-filled porosity (air content) for various soil types. It also provided the best fit lines and bounding estimates based on models presented by "Transport in porous media" (Millington and Quirk 1960) and "Permeability of Porous Solids" (Millington and Quirk 1961). The results from Liu et al. (2006) are reproduced in Figure 4-17.

Figure 4-15. Atmospheric Transport Pathway from a Source to the Receptor Located at the Point of Calculation Along the Centerline of the Gas Plume.

Using the Millington and Quirk (1960) gas tortuosity equation below (Equation 4-13), Liu et al. (2006) found the best fit to the experimental data set by varying the value of the total porosity in the denominator and finally selecting a value of 0.8:

$$\tau = \frac{\theta_a^2}{\Phi^{2/3}} = \frac{(\phi - \theta_w)^2}{\Phi^{2/3}} \tag{4-13}$$

Where:

τ = the tortuosity
θ_a = the air content (or air-filled porosity) of the porous medium
θ_w = the water content (or water-filled porosity) of the porous medium
ϕ = the total porosity (measured)
Φ = fitted total porosity; set equal to 0.8 for best fit (Liu et al. 2006).

Figure 4-16. A Schematic of Gaseous Plume Movement Based on Gaussian Distribution in the Horizontal and Vertical Directions.

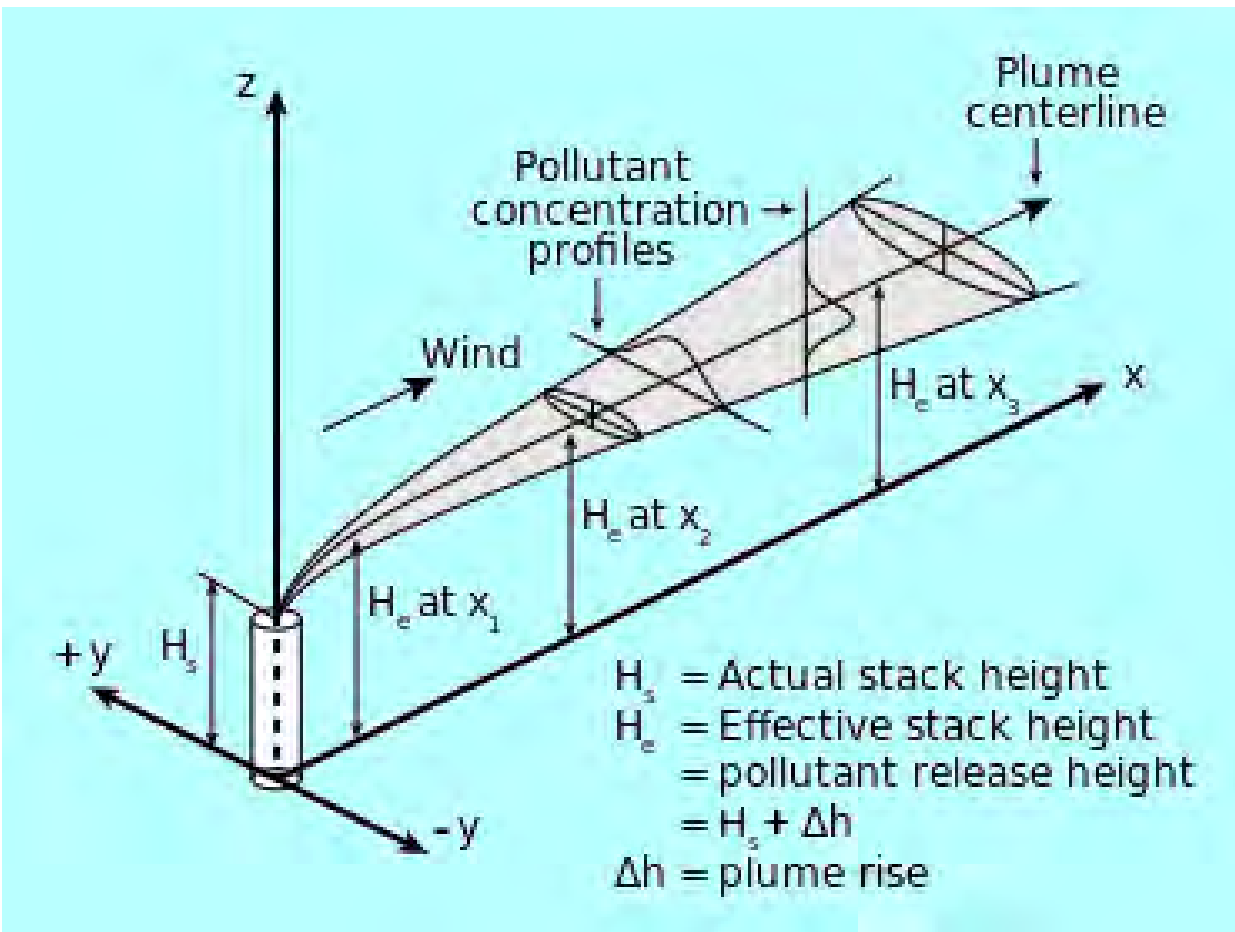

The tortuosity in the infill grout material is calculated from the first equality of the above equation using a fixed value of θ_a (6%), while the second equality is used for calculating the tortuosity for the backfill material (soil overburden) where the θ_w (and hence tortuosity) varies as a function of time. Note that Liu et al. (2006) made an error in referencing Millington and Quirk papers. They reversed a referenced paper's date ("1961" instead of correct date 1960) in the text and in the figure; the error is now corrected.

Figure 4-17. Comparison of Measured Tortuosity (i.e., Ratio of Diffusion Coefficient in Soil [D_{ef}] to that in Free Air [D_0]) with Fitted Tortuosity Models.

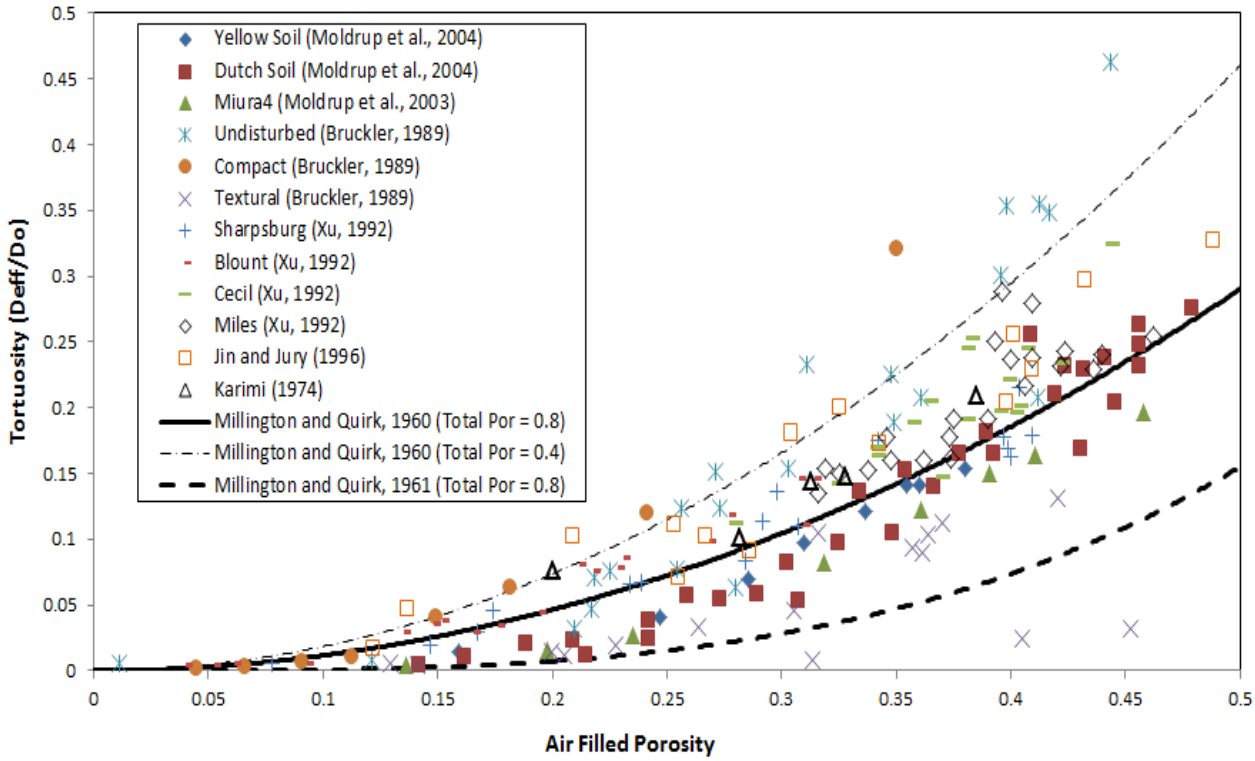

Source: "Simulating the Gas Diffusion Coefficient in Macropore Network Images: Influence of Soil Pore Morphology" (Liu et al. 2006).

References:
"Characterizing the Dependence of Gas Diffusion Coefficient on Soil Properties" (Jin and Jury 1996).
"Compaction Effect on the Gas Diffusion Coefficient in Soils" (Xu et al. 1992).
"Gas Diffusivity in Undisturbed Volcanic Ash Soils: Test of Soil-Water-Characteristic-Based Prediction Models" (Moldrup et al. 2003).
"Laboratory Estimation of Gas Diffusion Coefficient and Effective Porosity in Soils" (Bruckler et al. 1989).
"Permeability of Porous Solids" (Millington and Quirk 1961).
"Three-Porosity Model for Predicting the Gas Diffusion Coefficient in Undisturbed Soil" (Moldrup et al. 2004).
"Transport in porous media" (Millington and Quirk 1960).
"Vapor-phase Diffusion of Benzene in Soil" (Karimi et al. 1987).

The solid surface within the tank and ancillary equipment (except for pipelines) is considered to be the infill grout. The K_d value for ^{222}Rn is set to zero because it is a noble gas and unreactive with its surroundings.

Sorption on the backfill could be considered but is conservatively ignored since it is typically much smaller than on the grout.

4.4.3 Mathematical Modeling of Second Step

Once the gaseous diffusive flux from the source area is calculated, a plume dispersion model is applied to evaluate the concentrations at the receptor (point of calculation) using the double Gaussian plume equation of "The Estimation of the Dispersion of Windborne Material"

(Pasquill 1961) as discussed in the CAP88-PC Version 4.0 User Guide (EPA 2014). This equation (which models the dispersion of a non-reactive gaseous pollutant from an emission point) is given below in a form that predicts the steady-state concentration as a point (x, y, z) located downwind from the source as shown in Figure 4-16.

$$C = \frac{Q}{2\,\pi\,u\,\sigma_y\sigma_z}\,\exp\left(-\frac{1}{2}\frac{y^2}{\sigma_y{}^2}\right)\left\{\exp\left(-\frac{1}{2}\frac{(z-H)^2}{\sigma_z{}^2}\right)+\exp\left(-\frac{1}{2}\frac{(z+H)^2}{\sigma_z{}^2}\right)\right\} \qquad (4\text{-}14)$$

Where:

C	=	steady-state concentration at x meters downwind, y meters crosswind, and z meters above ground (Ci/m^3)
Q	=	release rate (emission rate) from source (Ci/sec)
u	=	average wind speed at stack height (m/sec)
σ_y, σ_z	=	horizontal and vertical dispersion coefficient (spread parameters) (m)
z	=	vertical distance from ground level (m)
H	=	effective stack height (m) that includes physical stack height and plume rise.

In this model, the highest concentration occurs along the centerline of the plume. For the purpose of estimating the concentration in air at exposure location, the receptor is assumed to be located at the centerline (y = 0 m) of the plume. The effective stack height (H), which includes the plume rise, and the vertical distance from ground level (z) are each taken to be 2 m (assumed approximate height of the adult person). The above equation simplifies to:

$$C = \frac{Q}{2\,\pi\,u\,\sigma_y\sigma_z}\left\{1+\exp\left(-\frac{1}{2}\frac{(z+H)^2}{\sigma_z{}^2}\right)\right\} \qquad (4\text{-}15)$$

Where z + H = 4 m, and u (the average wind speed) is chosen to be 3.4 m/s.

4.4.4 Horizontal and Vertical Plume Dispersivity in Air

Horizontal and vertical dispersivities of the plume in air are required to calculate air concentrations downwind from WMA C to simulate the effect of dispersion due to wind flow over a horizontal 1-D pathway.

EPA (2014) provides equations to calculate the horizontal dispersion coefficient (σ_y) and the vertical dispersion coefficient (σ_z) for dispersion calculations using the Gaussian plume model. In these equations, the dispersion coefficient is a function of the downwind distance, x, from a point source for different atmospheric turbulence classes under open-country conditions. These atmospheric turbulence classes are categorized according to the Pasquill classification (Pasquill 1961). This classification defines six stability classes named A, B, C, D, E, and F, with class A being the most turbulent and class F the most stable or least turbulent class. According to the wind speeds observed on the Hanford Site, which usually range from 2.7 m/s during winter to 4 m/s during summer (monthly average), the most conservative Pasquill class for a moderate solar radiation above WMA C is Class C (i.e., “slightly unstable class”). The following

equations are used to calculate the horizontal and vertical dispersion coefficient for Class C (EPA 2014).

$$\sigma_y = 0.11\, x\, (1 + 0.0001x)^{-½} \quad (4\text{-}16)$$

$$\sigma_z = 0.08\, x\, (1 + 0.0002x)^{-½} \quad (4\text{-}17)$$

Where σ_y and σ_z are the horizontal and vertical dispersion coefficients (m) for Pasquill class C and x is the downwind distance (m) from the point source.

The dispersion coefficient estimates for air transport to the fenceline vary by the distance of the source (tank and ancillary equipment) from the fenceline using the above equation. The air pathway calculations are performed for each source term (tank and ancillary equipment) separately, where the distance to the point of calculation at 100 m boundary is calculated based on the location of the source.

4.5 IMPLEMENTATION OF INADVERTENT INTRUDER SCENARIO

Hypothetical inadvertent intruder analysis is undertaken to meet the requirements of the DOE O 435.1. Guidance for the inadvertent intruder analysis comes from DOE G 435.1-1, Implementation Guide for Use with DOE M 435.1-1, which states the following:

> "Although DOE is committed to retaining control of land containing residual radioactive material, such as disposed low-level waste, it is nonetheless appropriate to consider the impacts of potential inadvertent intrusion. Intrusion should be considered as an accident scenario which could occur during lapses of institutional controls. It is a hypothetical situation assumed simply to provide a basis for determining the acceptability of waste for near-surface disposal and may be used for establishing concentrations of radioactive material in a near-surface disposal facility."

Two types of exposure scenarios are considered to estimate dose to the hypothetical intruder: (1) acute scenarios and (2) chronic scenarios. Acute scenarios evaluate the dose received from well drilling and subsequent exposure to residual waste in the drill cuttings; exposure is evaluated over a short time period. Chronic scenarios evaluate the dose received from spreading the drill cuttings over the surface followed by living and/or working on that area. One acute exposure scenario and three chronic exposure scenarios are evaluated in the system model and brief descriptions of each scenario are provided in Table 4-5. The equations and input parameters are presented in the following sections and additional details are provided in RPP-ENV-58813, "Exposure Scenarios for Risk and Performance Assessments in Tank Farms at the Hanford Site, Washington."

The calculations are performed using the same model set-up that is described in Section 4.2. The only difference is that contaminant transport and release is not allowed out of the tanks or ancillary equipment. The residual inventory for radionuclide undergoes decay and ingrowth and the radionuclide concentration is calculated at the time of the intrusion.

Table 4-5. Descriptions of the Inadvertent Intruder Scenarios Evaluated in the Waste Management Area C Performance Assessment.

Scenario	Description
Acute Exposure: Well Driller	Dose is the result of drilling through WMA C. Exposure pathways include external exposure, inhalation of soil particulates, and incidental soil ingestion. Exposure occurs during the drilling operation while in contact with the drill cuttings. Exposure does not depend on the borehole diameter.
Chronic Exposure: Rural Pasture	Dose is the result of drilling a well that serves a rural pasture. Contaminated drill cuttings are mixed with the soil over the pasture area. Exposure pathways include external exposure, inhalation of soil particulates, incidental soil ingestion, and milk consumption.
Chronic Exposure: Suburban Garden	Dose is the result of drilling a well that serves a suburban garden. Contaminated drill cuttings are mixed with the soil over the area where a residence and a garden are constructed. Exposure pathways include external exposure, inhalation of soil particulates, incidental soil ingestion, and fruit and vegetable consumption.
Chronic Exposure: Commercial Farm	Dose is the result of drilling a well that serves a commercial farm. Contaminated drill cuttings are mixed with the soil over the commercial farm area. Exposure pathways are external exposure, inhalation of soil particulates, and incidental soil ingestion.

Reference: RPP-ENV-58813, "Exposure Scenarios for Risk and Performance Assessments in Tank Farms at the Hanford Site, Washington."

For the acute exposure "Well driller" scenario, the driller is assumed to drill through the residual waste and all the way to the water table. Radionuclide concentrations in the drill cuttings are calculated as shown in Equations 4-18 through 4-20.

$$A_{well} = \pi \times \left(\frac{d_{well}}{2}\right)^2 \tag{4-18}$$

$$C_{ds} = \frac{C_{ws} \times A_{well} \times Z_{ws} \times \rho_{ws}}{A_{well} \times Z_{ws} \times \rho_{ws} + A_{well} \times (Z_{gw} - Z_{ws}) \times \rho_{sl}} = \frac{C_{ws} \times Z_{ws} \times \rho_{ws}}{Z_{ws} \times \rho_{ws} + (Z_{gw} - Z_{ws}) \times \rho_{sl}} \tag{4-19}$$

Because bulk density of residual waste and the soil is very similar, to simplify the equations it is assumed that $\rho_{ws} = \rho_{sl}$. As a result, the above equation simplifies to:

$$C_{ds} = \frac{C_{ws} \times Z_{ws}}{Z_{gw}} \tag{4-20}$$

Where:

C_{ds} = radionuclide concentration in drill cuttings (pCi/g)
C_{ws} = radionuclide concentration in the residual tank waste (pCi/g), varies as a function of time due to radioactive decay and ingrowth
A_{well} = area of well (cm^2)
d_{well} = diameter of well (cm)
Z_{gw} = depth to groundwater (cm)
Z_{ws} = thickness of waste intercepted by borehole (cm)

ρ_{sl} = soil dry bulk density for soil layers below WMA C (g/cm^3)
ρ_{ws} = residual tank waste bulk density (g/cm^3).

In the three chronic exposure scenarios, the drill cuttings from the borehole are spread and mixed over a target field that varies based on the type of land use, and long-term exposure is considered. The differences in radionuclide activities for each scenario are the well diameters and the area of the target field within which the drill cuttings are tilled into the soil.

The following equation is used to calculate the total radionuclide activity in the drill cuttings for the chronic scenario.

$$S_A = T_A \times \left(\frac{A_{well}}{A_{source_term}}\right) \tag{4-21}$$

Where:

S_A = radionuclide activity in soil from drill cuttings (pCi) at any given time
T_A = residual radionuclide activity in the tank waste(pCi), varies with time due to radioactive decay and ingrowth
A_{well} = area of the well (cm^2)
A_{source_term} = area over which the residual waste is spread at base of the tank (cm^2).

For the pipeline source term, the activity in the drill cuttings is based on the contaminated pipeline area that is interrogated by the borehole. If the borehole diameter is greater than the pipeline diameter, then the width of the contaminated zone is restricted to the pipeline diameter. Note that the borehole diameter varies based on the chronic scenario being evaluated.

The waste transfer pipelines cover 98% of the total pipeline length within WMA C while remaining pipelines are gravity-fed cascade lines between the 100-series SSTs (RPP-PLAN-47559). The waste transfer pipelines are likely to be intruded and therefore the calculations are based on the residual inventory within these pipelines, which are assumed to be 5% full of waste (RPP-PLAN-47559).

The following equation is used to calculate the radionuclide concentration in the chronic scenario.

$$C_{ps} = \frac{S_A}{A_p \times Z_p \times \rho_p + A_{well} \times Z_{gw} \times \rho_s} \tag{4-22}$$

Where:

C_{ps} = radionuclide concentration in pasture soil (pCi/g) at any given time
S_A = radionuclide activity in soil from drill cuttings (pCi) at any given time
A_p = area of the target field (cm^2)
Z_p = depth the drill cuttings are tilled into the pasture (cm)
ρ_p = soil dry bulk density in the pasture (g/cm^3)

A_{well} = area of the well (cm^2)
Z_{gw} = depth to groundwater (cm)
ρ_s = dry bulk density of the drill cuttings (g/cm^3).

The inadvertent intruder calculations are performed for all 19 sources (tanks and ancillary equipment). Although inadvertent intrusions into many of the tanks lead to potential doses, the likelihood of intrusion is considered to be very small due to the significant mechanical barrier to drilling from the large thickness of grout that will fill tanks at closure compared to drilling outside of grouted tank area. On the other hand, the inadvertent intrusion through pipelines is more likely as pipelines would not provide any appreciable mechanical barrier to drilling compared to drilling through the Hanford unit sediments.

4.6 PARAMETERIZATION

4.6.1 Selection of Radionuclides for System-Level Model

The approach taken for identifying specific radionuclides for more detailed analysis in the PA based on evaluation of inventory-related information is discussed below.

- This evaluation began with all radionuclides for which WMA C tank inventory information is available in the Best-Basis Inventory (BBI) within the official Tank Waste Information Network System (TWINS). The BBI contains inventory estimates for 46 radionuclides.

- A second step in the evaluation considered radioactive decay. The BBI list contains some very short-lived radionuclides (half-lives less than three years), such as ^{90}Y, ^{106}Ru, ^{125}Sb, ^{134}Cs, ^{137m}Ba, and ^{242}Cm. These six radionuclides were removed because either they were assumed to decay to negligible concentrations (^{106}Ru, ^{125}Sb, ^{134}Cs, ^{242}Cm) or their parents were already included in the PA calculations (^{90}Y, ^{137m}Ba). When the parent is included in the PA calculations, the contribution of the progeny is included in the dose calculation for the parent.

- An additional evaluation was conducted to identify any supplemental radionuclides that were not included in the BBI estimates for retrieved tanks but may be of interest for the PA evaluations. For this, the residual inventory estimates for retrieved tanks were obtained from RPP-RPT-42323, Table D-1. Radionuclides identified in RPP-RPT-42323, Table D-1 were reduced by eliminating inventory of radionuclides with half-lives of less than three years and those that are not directly related to Hanford Site operations or are non-detects. This led to the assumption of zero initial mass of ^{228}Th (naturally occurring with half-life of 1.91 years) and ^{230}Th (naturally occurring/ non-detect). Only the tank 241-C-106 nominal inventory for ^{230}Th was above the detection limit and was included.

- The next step was to include radionuclides needed to complete the uranium decay chain to calculate radon flux. This step identified ^{222}Rn along with intermediate parent ^{230}Th

that forms during the decay from ^{234}U. In addition, ^{210}Pb was identified as it is the decay product of ^{222}Rn. The initial mass of all three radionuclides (^{230}Th, ^{222}Rn, and ^{210}Pb) is assumed to be zero at closure (except for ^{230}Th for tank 241-C-106).

- The next step in the evaluation was to ensure that the daughter radionuclides that are part of the decay chain are included and tracked in PA calculations. Necessary radionuclide data (atomic weights, decay rates, and daughter products stoichiometry) needed for this evaluation are taken from ICRP (2008). This source of information is consistent with the information in DOE's Derived Concentration Technical Standard (DOE-STD-1196-2011). Progeny radionuclides with a half-life of less than two years are assumed to be in secular equilibrium with their parent, which allows for a reduction in the number of species tracked but still accounts for the radiological effects of the progeny.

The results of this overall screening process identified a total of 43 radionuclides for more detailed analysis. The final set of radionuclides are presented in Table 4-6.

The initial inventory estimates are decay corrected to the assumed closure date of January 1, 2020. Furthermore, the residual inventory of pits is not considered due to very small estimated residual volume, which is a factor of 50 times smaller than that estimated for the pipeline. The radionuclide inventory is used in the calculation is presented in Table 4-7.

4.6.2 Selection of Chemicals for System-Level Model

Chemical constituents of potential concern (COPCs) were identified using two types of COPC identification evaluations: 1) an evaluation that considered inventory-related information including constituent-specific availability of toxicity information and mass estimates, and 2) an evaluation that considered information on the groundwater pathway including travel times to the accessible environment and constituent-specific mobility. These evaluations and their results are described in the following sections.

The approach taken for identifying specific chemical constituents for more detailed analysis based on evaluation of inventory-related information is discussed below.

- The evaluation began with all chemicals for which WMA C tank inventory information is available in the BBI within the official TWINS database. The BBI contains inventory estimates for 24 chemicals.

- The next step in the evaluation process considered known toxicity information. Chemicals tracked in the BBI with no known toxicity information were excluded as COPCs. Twelve constituents were excluded from further consideration.

The results of this overall COPC identification process identified a total of 11 chemical COPCs (Al, Cr, F, Fe, Hg, Mn, Ni, NO_2, NO_3, Pb, and Sr) for further evaluation in the RCA.

Table 4-6. List of Radionuclides Considered for the Performance Assessment. (2 sheets)

Number	Species ID	Description	Atomic Weight	Half-life	Daughter1	Stoichiometry 1	Daughter2	Stoichiometry 2
1	Ac227	Actinium-227	227.028	21.772 yr				
2	Am241	Americium-241	241.057	432.2 yr	Np237	1		
3	Am243	Americium-243	243.061	7,370 yr	Pu239	1		
4	C14	Carbon-14	14.0032	5,700 yr				
5	Cd113m	Cadmium-113	112.904	14.1 yr				
6	Cm243	Curium-243	243.061	29.1 yr	Pu239	0.9976	Am243	0.0024
7	Cm244	Curium-244	244.063	18.1 yr	Pu240	1		
8	Co60	Cobalt-60	59.9338	5.2713 yr				
9	Cs137	Cesium-137	136.907	30.167 yr				
10	Eu152	Europium-152	151.922	13.537 yr				
11	Eu154	Europium-154	153.923	8.593 yr				
12	Eu155	Europium-155	154.923	4.7611 yr				
13	H3	Hydrogen-3	3.01605	12.32 yr				
14	I129	Iodine-129	128.905	1.57E+7 yr				
15	Nb93m	Niobium-93	92.9064	16.13 yr				
16	Ni59	Nickel-59	58.9343	1.01E+5 yr				
17	Ni63	Nickel-63	62.9297	100.1 yr				
18	Np237	Neptunium-237	237.048	2.144E+6 yr	U233	1		
19	Pa231	Protactinium-231	231.036	32,760 yr	Ac227	1		
20	Pb210	Lead-210	209.984	22.2 yr				
21	Pu238	Plutonium-238	238.05	87.7 yr	U234	1		
22	Pu239	Plutonium-239	239.052	24,110 yr	U235	1		
23	Pu240	Plutonium-240	240.054	6,564 yr	U236	1		

Table 4-6. List of Radionuclides Considered for the Performance Assessment. (2 sheets)

Number	Species ID	Description	Atomic Weight	Half-life	Daughter1	Stoichiometry 1	Daughter2	Stoichiometry 2
24	Pu241	Plutonium-241	241.057	14.35 yr	Am241	0.99998	Np237	2.45E-05
25	Pu242	Plutonium-242	242.059	3.75E+5 yr	U238	1		
26	Ra226	Radium-226	226.025	1,600 yr	Rn222	1		
27	Ra228	Radium-228	228.031	5.75 yr				
28	Rn222	Radon-222	222.018	3.8235 day	Pb210	0.9998		
29	Se79	Selenium-79	78.9185	2.95E+5 yr				
30	Sm151	Samarium-151	150.92	90 yr				
31	Sn126	Tin-126	125.908	2.3E+5 yr				
32	Sr90	Strontium-90	89.9077	28.79 yr				
33	Tc99	Technetium-99	98.9063	2.111E+5 yr				
34	Th229	Thorium-229	229.032	7340 yr				
35	Th230	Thorium-230	230.033	75,380 yr	Ra226	1		
36	Th232	Thorium-232	232.038	1.405E+10 yr	Ra228	1		
37	U232	Uranium-232	232.037	68.9 yr				
38	U233	Uranium-233	233.04	1.592E+5 yr	Th229	1		
39	U234	Uranium-234	234.041	2.455E+5 yr	Th230	1		
40	U235	Uranium-235	235.044	7.04E+8 yr	Pa231	1		
41	U236	Uranium-236	236.046	2.342E+7 yr	Th232	1		
42	U238	Uranium-238	238.051	4.468E+9 yr	U234	1		
43	Zr93	Zirconium-93	92.9065	1.53E+6 yr	Nb93m	0.975		

Table 4-7. Estimated Inventory of Radionuclides (in Curies) at Closure of Waste Management Area C (Decay Corrected to January 1, 2020) Used in the Calculation.

Tank/ Equipment	Ac-227	Am-241	Am-243	C-14	Cd-113m	Cm-243	Cm-244	Co-60	Cs-137	Eu-152	Eu-154	Eu-155	H-3	I-129	Nb-93m	Ni-59	Ni-63	Np-237	Pa-231	Pb-210	Pu-238	Pu-239
241-C-101	1.58E-06	9.91E+00	1.43E-03	2.76E-03	1.47E-03	1.86E-05	3.32E-04	1.76E-04	3.61E+02	6.38E-05	2.77E-03	4.69E-04	2.45E-02	5.55E-05	1.83E-05	7.23E-04	5.53E-02	3.45E-04	2.48E-08	0.00E+00	1.13E-01	1.83E+01
241-C-102	1.93E-02	2.12E+01	7.93E-04	9.88E-04	1.78E-02	6.22E-05	1.28E-03	2.14E-01	8.07E+01	1.26E-04	1.36E-01	2.62E-02	2.15E-05	2.56E-03	1.10E-02	1.62E-01	1.36E+01	5.16E-05	2.12E-03	0.00E+00	1.48E+00	6.49E+01
241-C-103	6.39E-08	4.83E+00	3.70E-05	6.99E-03	1.49E-02	7.66E-07	1.52E-05	1.83E-02	6.07E+02	2.58E-05	1.41E+00	4.37E-01	3.98E-03	3.00E-03	3.69E-04	1.12E-01	1.86E+01	1.35E-02	1.66E-07	0.00E+00	1.30E+00	4.99E+00
241-C-104	1.11E-05	8.46E+00	5.25E-03	3.08E-03	5.11E-02	3.64E-03	6.69E-02	4.66E-01	6.22E+02	3.54E-02	1.57E+00	2.29E-01	9.32E-03	4.84E-04	3.16E-02	8.64E-02	9.95E+01	7.97E-02	7.47E-05	0.00E+00	5.89E-01	5.15E+00
241-C-105	5.17E-07	2.84E+01	6.73E-04	4.86E-02	5.87E-02	9.11E-06	1.56E-04	6.83E-01	5.08E+03	1.12E-04	4.68E-03	6.08E-04	4.08E+00	8.95E-03	1.45E-03	4.41E-01	3.61E+01	1.93E-04	6.57E-07	0.00E+00	7.50E-01	5.28E+01
241-C-106	1.74E-03	6.38E+01	3.05E-03	8.21E-03	2.13E+00	5.55E-02	7.39E-01	2.23E+00	1.00E+03	2.02E+00	2.25E+01	7.65E+00	4.17E-03	6.31E-04	5.92E+00	1.05E+01	6.53E+01	5.41E-02	2.53E-03	0.00E+00	2.38E+00	1.67E+01
241-C-107	6.20E-06	3.70E+02	3.86E-02	2.16E-02	2.50E-03	5.02E-04	8.95E-03	9.14E-04	2.32E+03	1.35E-04	5.70E-03	8.66E-04	1.44E-02	4.07E-02	8.45E-02	1.18E-03	1.46E-01	2.08E-04	3.83E-05	0.00E+00	8.05E-01	1.30E+02
241-C-108	7.78E-07	9.46E-01	9.78E-05	8.18E-03	1.97E-03	1.50E-06	2.96E-05	7.22E-04	8.57E+01	1.07E-04	4.52E-03	6.84E-04	1.94E-02	3.81E-05	4.80E-02	9.30E-04	2.80E+00	2.17E-05	3.02E-05	0.00E+00	4.37E-03	6.68E-01
241-C-109	3.40E-06	3.71E-01	3.91E-05	7.65E-04	1.37E-03	5.09E-07	9.09E-06	5.02E-04	4.31E+01	7.41E-05	3.13E-03	4.74E-04	3.51E-03	2.65E-05	4.64E-02	6.46E-04	8.78E-01	6.46E-04	2.10E-05	0.00E+00	1.56E-02	4.01E-01
241-C-110	9.62E-07	4.94E-02	5.54E-06	1.51E-03	3.89E-04	7.22E-08	1.29E-06	1.42E-04	2.02E+01	2.11E-05	8.89E-04	1.35E-04	1.80E-03	2.65E-04	1.32E-02	1.83E-04	4.08E-01	1.09E-03	5.96E-06	0.00E+00	1.56E-02	1.17E+00
241-C-111	1.82E-05	8.32E+01	1.15E-02	1.04E-01	5.99E-02	1.82E-03	3.26E-02	1.03E-01	7.14E+03	5.38E-02	2.41E+00	3.70E-01	2.58E+00	1.41E-02	9.78E-02	1.40E+00	1.13E+02	3.32E-03	4.99E-05	0.00E+00	1.70E+00	9.45E+01
241-C-112	4.57E-06	9.42E-01	9.72E-05	1.60E-02	1.84E-03	1.26E-06	2.25E-05	6.75E-04	7.66E+02	1.00E-04	4.22E-03	6.39E-04	1.06E-02	3.57E-05	6.26E-02	8.69E-04	1.08E-01	1.54E-04	2.82E-05	0.00E+00	3.59E-02	5.79E+00
241-C-201	3.45E-09	2.46E+00	9.76E-04	7.64E-04	5.77E-04	3.10E-03	5.55E-02	2.37E-03	7.01E+00	2.10E-03	9.42E-02	1.45E-02	1.57E-04	4.57E-07	7.46E-04	4.07E-03	8.33E-01	3.42E-03	6.79E-09	0.00E+00	4.42E-01	1.58E+01
241-C-202	3.51E-09	1.21E+00	4.71E-04	2.03E-04	5.88E-04	1.50E-03	2.68E-02	2.44E-03	6.18E+00	2.14E-03	9.61E-02	1.48E-02	1.60E-04	7.35E-06	7.64E-04	4.16E-03	2.00E-01	2.90E-03	6.93E-09	0.00E+00	3.99E-01	1.43E+01
241-C-203	2.87E-09	3.16E-02	1.22E-05	1.66E-04	4.80E-04	3.88E-05	6.95E-04	2.15E-03	9.10E+00	1.75E-03	1.50E-02	1.81E-02	1.31E-04	1.47E-05	6.26E-04	3.40E-03	5.54E-02	2.70E-05	5.67E-09	0.00E+00	1.36E-02	4.86E-01
241-C-204	2.69E-09	3.16E-03	1.22E-06	1.88E-04	4.50E-04	3.87E-06	6.95E-05	1.86E-03	4.13E+00	1.64E-03	5.62E-02	1.13E-02	1.13E-04	3.57E-07	5.84E-04	3.18E-03	1.46E-02	2.16E-02	5.30E-09	0.00E+00	2.76E-04	9.84E-03
C-301	6.62E-05	5.54E+00	1.37E-03	2.04E-03	8.49E-02	5.33E-03	8.60E-02	1.16E-01	1.21E+02	8.31E-02	1.17E+00	3.60E-01	2.09E-03	2.06E-04	2.30E-01	4.14E-01	9.54E+00	2.82E-02	1.01E-04	0.00E+00	7.40E-01	2.13E+01
244-CR vault	1.20E-04	1.01E+01	2.49E-03	3.71E-03	1.54E-01	9.68E-03	1.56E-01	2.11E-01	2.21E+02	1.51E-01	2.13E+00	6.54E-01	3.80E-03	3.75E-04	4.18E-01	7.52E-01	1.73E+01	5.13E-02	1.84E-04	0.00E+00	1.34E+00	3.88E+01
Pipelines	1.02E-04	8.52E+00	2.11E-03	3.14E-03	1.31E-01	8.19E-03	1.32E-01	1.79E-01	1.87E+02	1.28E-01	1.80E+00	5.54E-01	3.22E-03	3.17E-04	3.54E-01	6.37E-01	1.47E+01	4.34E-02	1.56E-04	0.00E+00	1.14E+00	3.28E+01

Tank/ Equipment	Pu-240	Pu-241	Pu-242	Ra-226	Ra-228	Rn-222	Se-79	Sm-151	Sn-126	Sr-90	Tc-99	Th-229	Th-230	Th-232	U-232	U-233	U-234	U-235	U-236	U-238	Zr-93
241-C-101	1.96E+00	1.54E+00	2.70E-05	5.90E-07	2.64E-13	0.00E+00	2.80E-04	4.00E+00	5.13E-04	3.29E+03	4.34E-02	1.33E-10	0.00E+00	1.12E-12	1.75E-06	1.71E-07	1.69E-01	7.54E-03	1.93E-03	1.72E-01	3.35E-05
241-C-102	1.55E+01	4.87E+01	9.00E-04	2.88E-07	3.64E-01	0.00E+00	1.60E-06	9.72E-01	1.83E-04	2.94E+02	3.56E-03	1.06E-02	0.00E+00	2.29E-02	2.83E-02	2.17E+00	1.13E-01	4.27E-03	1.43E-03	9.78E-02	4.22E-03
241-C-103	1.04E+00	1.80E+00	3.24E-05	1.54E-08	4.70E-05	0.00E+00	2.64E-05	4.30E-01	5.27E-05	6.78E+03	4.48E-02	2.60E-11	0.00E+00	1.99E-04	4.29E-06	5.85E-03	1.36E-02	7.10E-04	3.74E-04	1.64E-02	7.03E-04
241-C-104	1.55E+00	1.14E+01	1.97E-02	3.24E-07	8.73E-04	0.00E+00	8.56E-03	3.17E+03	8.81E-03	4.89E+03	3.04E-01	8.56E-08	0.00E+00	3.70E-03	3.53E-02	2.18E+00	4.17E-01	1.98E-02	4.85E-03	4.39E-01	6.24E-02
241-C-105	1.04E+01	1.75E+01	3.14E-04	1.60E-07	2.36E-13	0.00E+00	1.51E-04	2.37E+00	2.93E-04	2.89E+04	7.83E+00	1.25E-10	0.00E+00	1.00E-12	8.62E-06	5.02E-07	2.39E-01	1.02E-02	5.17E-03	2.44E-01	2.77E-03
241-C-106	3.57E+00	1.84E+01	4.16E-04	5.13E-04	1.32E-04	0.00E+00	9.57E-03	7.82E+03	1.76E+00	4.50E+04	1.64E-01	1.91E-05	9.38E-04	5.60E-04	4.87E-04	1.82E-03	9.40E-04	3.86E-05	1.73E-05	9.02E-04	1.04E+01
241-C-107	1.42E+01	1.10E+01	1.97E-04	5.95E-07	9.70E-04	0.00E+00	2.70E-04	1.04E+04	4.94E-04	2.42E+04	2.14E+00	1.89E-09	0.00E+00	4.11E-03	2.20E-06	2.15E-07	2.07E-01	9.24E-03	2.31E-03	2.11E-01	1.55E-01
241-C-108	7.27E-02	7.91E-02	1.01E-06	4.73E-07	3.70E-06	0.00E+00	1.62E-03	6.66E+00	3.91E-04	1.25E+03	4.87E-02	1.50E-09	0.00E+00	1.57E-05	4.50E-07	4.10E-08	3.25E-02	1.82E-03	2.85E-04	4.03E-02	1.22E-01
241-C-109	4.36E-02	5.09E-01	6.07E-07	3.26E-07	2.06E-12	0.00E+00	1.48E-04	4.65E+00	2.71E-04	2.33E+03	8.77E-03	1.04E-09	0.00E+00	8.72E-12	9.94E-08	9.69E-09	9.35E-03	4.01E-04	9.61E-05	9.53E-03	8.45E-02
241-C-110	1.27E-01	3.58E-01	1.77E-06	9.27E-08	5.85E-13	0.00E+00	4.21E-05	1.32E+00	2.38E-02	2.62E+03	4.46E-02	2.95E-10	0.00E+00	2.48E-12	1.91E-08	1.86E-09	2.64E-03	1.14E-04	2.93E-05	2.59E-03	2.41E-02
241-C-111	1.85E+01	3.54E+01	6.54E-04	4.51E-06	6.54E-12	0.00E+00	3.53E-03	6.39E+02	6.72E-03	3.05E+05	2.19E+00	3.56E-09	0.00E+00	2.77E-11	2.22E-05	4.80E-05	7.74E-01	3.37E-02	1.32E-02	7.88E-01	1.81E-01
241-C-112	6.29E-01	4.91E-01	8.76E-06	4.40E-07	2.78E-12	0.00E+00	1.99E-04	6.25E+00	3.65E-04	2.28E+02	1.69E+00	1.40E-09	0.00E+00	1.18E-11	4.50E-07	4.39E-08	4.23E-02	1.89E-03	4.73E-04	4.32E-02	1.14E-01
241-C-201	3.40E+00	8.36E+00	1.60E-04	1.00E-09	9.51E-07	0.00E+00	5.49E-05	2.39E+01	1.10E-04	1.71E+02	2.63E-03	1.18E-11	0.00E+00	4.03E-06	2.25E-06	1.14E-05	3.65E-02	1.48E-03	5.23E-04	3.69E-02	1.46E-03
241-C-202	3.08E+00	7.52E+00	1.45E-04	1.02E-09	9.70E-07	0.00E+00	5.61E-05	2.43E+01	1.13E-04	3.31E+02	2.50E-03	1.20E-11	0.00E+00	4.11E-06	2.00E-06	1.02E-05	3.52E-02	1.42E-03	3.52E-04	3.28E-02	1.49E-03
241-C-203	1.05E-01	2.58E-01	4.94E-06	8.40E-10	4.48E-07	0.00E+00	4.58E-05	1.99E+01	9.21E-05	1.56E+02	2.32E-03	9.81E-12	0.00E+00	1.90E-06	6.60E-06	3.37E-05	1.13E-01	4.79E-03	8.33E-04	1.09E-01	1.22E-03
241-C-204	2.12E-03	5.21E-03	9.98E-08	7.86E-10	3.35E-06	0.00E+00	4.29E-05	1.86E+01	8.61E-05	1.03E+02	3.18E-03	9.17E-12	0.00E+00	1.42E-05	4.93E-06	2.51E-05	8.27E-02	3.42E-03	5.13E-04	8.13E-02	1.14E-03
C-301	4.60E+00	1.21E+01	1.30E-03	1.93E-05	5.90E-05	0.00E+00	1.03E-03	5.29E+02	6.80E-02	3.06E+03	3.64E-02	7.21E-07	0.00E+00	2.50E-04	1.96E-03	1.20E-01	2.26E-01	9.56E-03	1.93E-03	2.22E-01	4.07E-01
244-CR vault	8.36E+00	2.19E+01	2.36E-03	3.51E-05	1.07E-04	0.00E+00	1.87E-03	9.62E+02	1.24E-01	5.55E+03	6.62E-02	1.31E-06	0.00E+00	4.54E-04	3.57E-03	2.17E-01	4.11E-01	1.74E-02	3.51E-03	4.04E-01	7.39E-01
Pipelines	7.08E+00	1.86E+01	2.00E-03	2.97E-05	9.08E-05	0.00E+00	1.58E-03	8.15E+02	1.05E-01	4.70E+03	5.61E-02	1.11E-06	0.00E+00	3.85E-04	3.02E-03	1.84E-01	3.48E-01	1.47E-02	2.97E-03	3.42E-01	6.26E-01

An additional evaluation was conducted to identify any supplemental analytes in residual inventory estimates for retrieved tanks that were not included in the BBI but may be of interest for the RCA calculations. Residual inventory estimates for retrieved tanks were obtained from RPP-RPT-42323, Table D-1. A comprehensive list of C Farm analytes is provided in RPP-RPT-42323, Table D-1; this list of analytes was reduced to identify supplemental analytes based on the following exclusion criteria:

- analytes not required to be sampled in RPP-23403,
- analytes without known toxicity information,
- analytes with K_d values greater than 2 mL/g (see Sections 6.3.2.3 and 7.2.1), and
- analytes with nominal inventories less than 0.1 kg at each retrieved tank; such small numbers were judged to have insignificant effect on the system performance.

The process of identifying supplemental analytes resulted in six analytes (B, Co, CN, Se, Sn, and tributyl phosphate) being identified for further evaluation.

Additional COPC identification was performed using the 3-D STOMP©-based flow and transport model to determine the maximum K_d value of COPCs in the WMA C tank residuals that are capable of reaching the water table in 1,000 and 10,000 years.

In summary, the total number of chemical COPCs identified for more detailed analysis in the RCA is 18. The final set of chemicals used for the more detailed analysis in the RCA are presented in Table 4-8. The final best-estimate inventory for chemicals considered is presented in Table 4-9.

Table 4-10 provides a list of parameters used in developing source term release calculations.

A linear sorption isotherm (using a K_d approach) is used for representing sorption within the grout and concrete layer for various contaminants as they undergo diffusive (and advective) transport through the tank. The K_d values are presented in Table 4-11 in terms of best estimate and the uncertainty range that are derived from relevant published literature for chemical conditions that are likely to exist within the grout/concrete layer within the tanks.

For contaminant transport calculations along the groundwater pathway, the flow parameters are not directly used in the system model; rather, as described in Section 4.3, the flow field is abstracted from the process-level model. However, for transport calculations in the vadose zone and saturated zone, the transport is affected by sorption and retardation from interaction of contaminant with the sediment. An equilibrium sorption isotherm is applied that is described by the K_d value (partitioning coefficient equal to the sorbed concentration to the dissolved concentration). The best-estimate K_d values are presented for the sand material in Table 4-12 that are then scaled based on the gravel fraction.

Table 4-8. List of Chemicals Considered for the RCRA Closure Analysis.

Number	Species ID	Description	Atomic Weight
1	Al	Aluminum	26.98
2	Cr	Chromium	51.99
3	F	Fluoride	18.99
4	Fe	Iron	55.85
5	Hg	Mercury	200.6
6	Mn	Manganese	54.94
7	Ni	Nickel	58.7
8	NO_2	Nitrite	46
9	NO_3	Nitrate	62
10	Pb	Lead	207.2
11	Sr	Strontium	87.6
12	B	Boron	10.8
13	Co	Cobalt	58.9
14	CN	Cyanide	26
15	Se	Selenium	78.9
16	Sn	Tin	118.7
17	TBP	Tributyl phosphate	266.3

RCRA = Resource Conservation and Recovery Act of 1976

Table 4-9. Estimated Inventory of Chemicals (in Kilograms) at Closure at Waste Management Area C Used in the RCRA Closure Analysis Calculations.

Tank/ Equipment	Al	Cr	F	Fe	Hg	Mn	Ni	NO_2	NO_3	Pb	Sr	U_Total	B	Co	CN	Se	Sn	Tributyl Phosphate
241-C-101	7.93E+01	7.23E+00	3.46E+01	8.77E+02	2.98E+00	7.14E+00	3.27E+00	5.64E+02	8.20E+03	2.07E+01	2.34E+01	5.16E+02	0.00E+00	0.00E+00	0.00E+00	0.00E+00	0.00E+00	0.00E+00
241-C-102	9.45E+04	2.19E+02	1.41E+03	5.98E+03	2.06E+00	5.10E+02	2.18E+03	6.46E+03	2.22E+04	5.47E+02	5.24E+01	5.27E+03	0.00E+00	0.00E+00	0.00E+00	0.00E+00	0.00E+00	0.00E+00
241-C-103	3.63E+03	2.38E+00	1.62E-01	1.19E+02	1.06E+00	4.42E+00	4.58E+00	4.82E-01	8.71E-01	8.50E+00	2.41E+00	4.91E+01	1.95E-01	8.63E-02	1.12E-02	6.90E-01	1.14E+00	1.04E+00
241-C-104	1.14E+03	3.06E+00	1.54E+01	3.24E+02	1.35E+00	4.29E+01	6.00E+00	5.06E+00	9.38E+00	6.48E+00	9.35E-01	1.32E+03	0.00E+00	2.05E-02	1.05E-02	7.73E-02	2.13E-01	1.06E-02
241-C-105	1.49E+04	3.70E+01	7.92E+01	3.92E+02	5.03E-01	1.83E+02	1.60E+02	6.47E+02	7.83E+02	3.45E+01	1.38E+01	7.34E+02	0.00E+00	0.00E+00	0.00E+00	0.00E+00	0.00E+00	0.00E+00
241-C-106	3.82E+02	3.78E+00	5.43E-01	2.07E+02	1.93E+00	5.49E+02	3.02E+01	4.14E+01	3.48E+01	2.56E+01	1.83E+00	2.70E+00	1.19E+00	3.75E-01	7.80E-02	2.94E+00	2.40E+00	0.00E+00
241-C-107	1.98E+03	5.54E+01	6.05E+02	4.37E+03	3.78E+00	1.93E+02	9.86E+01	2.15E+03	3.59E+03	3.62E+02	1.71E+01	6.32E+02	0.00E+00	0.00E+00	0.00E+00	0.00E+00	0.00E+00	0.00E+00
241-C-108	3.47E+03	6.31E-01	1.21E+02	2.82E+02	2.03E-02	4.08E+00	7.45E+01	5.78E+00	9.16E+00	1.71E+01	1.97E+01	1.21E+02	4.20E-02	4.20E-02	1.34E-01	2.52E-01	1.26E-01	4.42E-02
241-C-109	2.15E+03	1.76E-01	9.68E+01	9.28E+01	1.84E-02	5.63E-01	1.33E+01	3.83E+00	4.52E+00	5.39E+00	4.91E-01	2.86E+01	1.12E-02	1.12E-02	3.37E-01	6.72E-02	3.36E-02	7.42E-03
241-C-110	1.29E+03	1.12E+00	1.38E+02	1.90E+02	1.07E-01	7.61E-01	4.13E-01	2.74E+00	6.73E+00	5.62E+00	5.63E+01	5.49E+00	2.33E-02	2.35E-02	8.12E-03	3.99E-02	8.42E-01	1.01E-01
241-C-111	1.60E+04	7.33E+01	8.07E+02	7.53E+03	4.69E+01	4.68E+01	2.65E+03	5.50E+03	1.47E+04	7.65E+02	3.58E+01	2.36E+03	0.00E+00	0.00E+00	0.00E+00	0.00E+00	0.00E+00	0.00E+00
241-C-112	3.32E+02	5.78E+01	7.09E+02	7.02E+02	2.63E-02	6.52E+00	1.46E+00	6.75E+02	8.76E+03	1.36E+01	1.00E+01	1.29E+02	0.00E+00	0.00E+00	0.00E+00	0.00E+00	0.00E+00	0.00E+00
241-C-201	4.11E+00	1.22E+01	2.69E+00	1.10E+02	1.07E-01	1.90E+01	6.15E+00	5.27E-01	1.35E+00	6.25E+00	9.09E-01	1.11E+02	4.69E-02	8.56E-02	2.08E-03	1.16E-01	1.32E-01	2.02E+01
241-C-202	8.48E+00	9.09E+00	2.26E+00	8.70E+01	2.87E-01	1.69E+01	7.28E+00	4.52E-01	1.25E+00	5.84E+00	1.22E+00	9.88E+01	2.78E-02	7.84E-02	4.04E-03	9.27E-02	3.84E-01	5.41E+00
241-C-203	0.00E+00	2.60E+00	1.64E+00	1.28E+01	2.23E-03	5.13E-01	2.04E-01	9.94E-01	3.76E+00	3.07E+00	2.30E-01	3.26E+02	6.03E-02	2.64E-02	4.59E-03	2.01E-01	1.61E-01	9.54E+00
241-C-204	5.88E+00	1.36E+00	8.05E-03	3.21E+01	1.47E-01	2.39E-01	8.01E-01	3.13E-02	2.22E-02	1.02E+00	3.67E-01	2.43E+02	1.24E-01	4.13E-02	7.06E-04	4.13E-01	2.07E-01	6.69E+01
C-301	5.20E+02	1.76E+01	2.09E+01	2.18E+02	5.73E-01	4.75E+01	1.42E+01	3.81E+00	7.38E+00	1.39E+01	5.48E+00	6.65E+02	0.00E+00	0.00E+00	0.00E+00	0.00E+00	0.00E+00	0.00E+00
244-CR vault	9.44E+02	3.19E+01	3.80E+01	3.96E+02	1.04E+00	8.63E+01	2.59E+01	6.92E+00	1.34E+01	2.52E+01	9.96E+00	1.21E+03	0.00E+00	0.00E+00	0.00E+00	0.00E+00	0.00E+00	0.00E+00
Pipelines	7.99E+02	2.70E+01	3.22E+01	3.35E+02	8.81E-01	7.30E+01	2.19E+01	5.86E+00	1.14E+01	2.14E+01	8.43E+00	1.02E+03	0.00E+00	0.00E+00	0.00E+00	0.00E+00	0.00E+00	0.00E+00

RCRA = Resource Conservation and Recovery Act of 1976

Table 4-10. Parameters Used in Developing Source Term Model. (2 sheets)

Parameter	Value	Reference
Porosity of Residual Waste Layer	0.4	Assumed
Saturation of Residual Waste Layer	1	Assumed fully saturated to maximize diffusive release
Residual Waste Volume	Variable by source	Section 3.1
Porosity of Concrete and Grout layer below the waste layer	0.11	SRNL-STI-2008-00421, Table 39
Porosity of in-fill Grout within the tank (at closure)	0.269	WSRC-STI-2007-00369, Table 29; Strong grout assumed.
Saturation of Concrete and Grout layer below the waste layer	1	Assumed to maximize diffusive release
Bulk Density of Concrete and Grout layer below the waste layer	2.41 g/cm^3	RPP-RPT-50934, p. C-3 (241-C-107 dome core density of 151 lb/ft^3)
Diffusive Length of Waste form layer	0 m	Assumed to maximize diffusive release
Diffusive Length of Concrete and Grout layer below the waste layer	0.203 m (8 in.)	Minimum diffusive thickness based on tank bottom geometry
Diffusive Area for source term release	410.4 m^2 for 100-Series Tanks; 29.2 m^2 for 200-Series Tanks and C-301 catch tank; 162.4 m^2 for CR-Vaults; 22,500 m^2 for Pipelines	Base area for tanks based on circular geometry; area of CR-Vault is based on rectangular area with length of 92 ft and average width of 19 ft; area of Pipeline assumed to be 150 m × 150 m.
Effective Diffusion Coefficient through grout and concrete layer (incorporates effects of tortuosity)	3×10^{-8} cm^2/s	PNNL-23841
Uranium solubility for intact tank conditions	1×10^{-4} M for 1,000 years; 1×10^{-6} M for time >1,000 years	
Uranium solubility for degraded tank conditions	1×10^{-4} M for 1,000 years; 2×10^{-5} M for time >1,000 years	
Technetium-99 release	6% of the waste inventory available for release instantaneously; remaining 94% waste form inventory made available based on first order fractional release rate of 6×10^{-4} day^{-1}.	
Chromium dissolved concentration limit	2,000 µg/L dissolved concentration limit imposed	
Contaminant K_d values for transport through the grout and concrete layer	Variable	

Table 4-10. Parameters Used in Developing Source Term Model. (2 sheets)

Parameter	Value	Reference
Release Type	Diffusive release from the tanks and CR-Vaults under intact conditions; Both advective and diffusive release for the Pipelines Both advective and diffusive release for tanks and CR-Vaults under degraded conditions	

References:
PNNL-23841, "Radionuclide Migration through Sediment and Concrete: 16 Years of Investigations."
RPP-RPT-50934, "Inspection and Test Report for the Removed 241-C-107 Dome Concrete."
SRNL-STI-2008-00421, "Hydraulic and Physical Properties of Saltstone Grouts and Vault Concretes."
WSRC-STI-2007-00369, "Hydraulic and Physical Properties of Tank Grouts and Base Mat Surrogate Concrete for FTF Closure."

Table 4-11. K_d Values (mL/g) for Grout/Concrete Used for Waste Management Area C Performance Assessment. (2 sheets)

Element	Best	Minimum	Maximum	Reference
Ac	1.00E+05	3.00E+03	3.30E+05	NAGRA NTB 02-20
Al	0.00E+00	0.00E+00	0.00E+00	No relevant information
Am	1.00E+03	2.00E+02	5.00E+03	SKB R-05-75
B	0.00E+00	0.00E+00	0.00E+00	No relevant information
C	2.00E+02	1.00E+02	4.00E+03	SKB R-05-75
Cd	4.00E+01	2.00E+00	8.00E+02	SKB R-05-75
Cm	1.00E+03	2.00E+02	5.00E+03	SKB R-05-75
CN	0.00E+00	0.00E+00	0.00E+00	No relevant information
Co	4.00E+01	4.00E+00	4.00E+02	SKB R-05-75
Cr	0.00E+00	0.00E+00	0.00E+00	No relevant information
Cs	1.00E+00	1.00E-01	1.00E+01	SKB R-05-75
Eu	5.00E+03	1.00E+03	2.50E+04	SKB R-05-75
F	0.00E+00	0.00E+00	0.00E+00	No relevant information
Fe	0.00E+00	0.00E+00	0.00E+00	No relevant information
H	1.00E-01	7.10E-02	1.40E-01	NAGRA NTB 02-20
Hg	0.00E+00	0.00E+00	0.00E+00	No relevant information
I	3.00E+00	3.00E-01	3.00E+01	SKB R-05-75

Table 4-11. K_d Values (mL/g) for Grout/Concrete Used for Waste Management Area C Performance Assessment. (2 sheets)

Element	Best	Minimum	Maximum	Reference
Mn	0.00E+00	0.00E+00	0.00E+00	No relevant information
Nb	5.00E+02	1.00E+02	2.50E+04	SKB R-05-75
Ni	4.00E+01	8.00E+00	2.00E+02	SKB R-05-75
NO_2	0.00E+00	0.00E+00	0.00E+00	No relevant information
NO_3	0.00E+00	0.00E+00	0.00E+00	No relevant information
Np	1.00E+02	7.10E+01	1.40E+02	NAGRA NTB 02-20
Pa	1.00E+02	7.10E+01	1.40E+02	NAGRA NTB 02-20
Pb	5.00E+02	3.60E+02	7.10E+02	NAGRA NTB 02-20
Pu	1.00E+02	7.14E+01	1.40E+02	NAGRA NTB 02-20
Ra	5.00E+01	5.00E+00	5.00E+02	SKB R-05-75
Rn	0.00E+00	0.00E+00	0.00E+00	No relevant information
Se	6.00E+00	1.00E-01	4.00E+02	SKB R-05-75
Sm	5.00E+03	1.00E+03	2.50E+04	SKB R-05-75
Sn	5.00E+02	2.50E+01	1.00E+04	SKB R-05-75
Sr	1.00E+00	5.00E-01	5.00E+01	SKB R-05-75
Tributyl phosphate	0.00E+00	0.00E+00	0.00E+00	No relevant information
Tc	1.00E+00	7.10E-01	1.40E+00	NAGRA NTB 02-20
Th	3.00E+04	1.00E+03	1.00E+06	NIROND-TR 2008-23 E
U	2.00E+03	1.40E+03	2.80E+03	NAGRA NTB 02-20
Zr	1.00E+04	3.00E+03	3.30E+04	NAGRA NTB 02-20

References:
NAGRA NTB 02-20, “Cementitious Near-Field Sorption Data Base for Performance Assessment of an ILW Repository in Opalinus Clay.”
NIROND-TR 2008-23 E, “Review of sorption values for the cementitious near field of a near surface radioactive waste disposal facility, Project near surface disposal of category A waste at Dessel.”
PSI Bericht Nr. 95-06, “Sorption Databases for the Cementitious Near-Field of a L/ILW Repository for Performance Assessment.”
SKB Rapport R-05-75, “Assessment of uncertainty intervals for sorption coefficients SFR-1 uppföljning av SAFE.”

Table 4-12. K_d Values (mL/g) for Sand Material. (2 sheets)

Element	Best Estimate	Reference
Ac	350	PNNL-16663
Al	1,500	RPP-RPT-46088
Am	600	PNNL-17154
B	3	RPP-RPT-46088
C	1	PNNL-17154
Cd	6.7	RPP-RPT-46088
Cm	350	PNNL-16663
CN	0	RPP-RPT-46088
Co	0	PNNL-17154
Cr	0	PNNL-17154
Cs	100	PNNL-17154
Eu	10	PNNL-17154
F	0	PNNL-17154
Fe	25	RPP-RPT-46088
H	0	PNNL-17154
Hg	52	RPP-RPT-46088
I	0.2	PNNL-17154
Mn	65	RPP-RPT-46088
Nb	0	PNNL-16663
Ni	3	PNNL-17154
NO_2	0	PNNL-17154
NO_3	0	PNNL-17154
Np	10	PNNL-17154
Pa	300	PNNL-17154
Pb	10	PNNL-17154
Pu	600	PNNL-17154
Ra	10	PNNL-17154
Rn	0	No relevant information available
Se	0.1	PNNL-17154
Sm	10	PNNL-17154
Sn	0.5	PNNL-17154

Table 4-12. K_d Values (mL/g) for Sand Material. (2 sheets)

Element	Best Estimate	Reference
Sr	10	PNNL-17154
Tributyl phosphate	1.89	RPP-RPT-46088
Tc	0	PNNL-16663
Th	300	PNNL-16663
U	0.6	RPP-RPT-46088
Zr	300	PNNL-16663

References:
PNNL-16663, "Geochemical Processes Data Package for the Vadose Zone in the Single-Shell Tank Waste Management Areas at the Hanford Site."
PNNL-17154, "Geochemical Characterization Data Package for the Vadose Zone in the Single-Shell Tank Waste Management Areas at the Hanford Site."
RPP-RPT-46088, "Flow and Transport in the Natural System at Waste Management Area C."

This page intentionally left blank.

5 MODEL SENSITIVITY AND UNCERTAINTY ANALYSIS

Projections of environmental processes are inherently uncertain. Assessment of uncertainty in model results arising from assumptions and parameter values is necessary to support the determination that there is reasonable expectation of meeting the performance objectives. The objective of the uncertainty analysis is to estimate the plausible range of radionuclide dose that results from selecting parameter values within their uncertainty ranges. When a sufficient number of parameter combinations is evaluated over their plausible range, the calculated range of potential radionuclide dose can be used to quantify the uncertainty in the dose estimates. This analysis supports the demonstration of meeting the requirements of DOE M 435.1-1.

NCRP Report No. 152, "Performance Assessment of Near-Surface Facilities for Disposal of Low-Level Radioactive Waste" notes that "methods of uncertainty and sensitivity analysis have been studied extensively, and a large body of scientific literature is devoted to each. However, that literature and the experience developed from it must be used with caution in the context of performance assessment, due to the unusual nature of this type of assessment and the significant amount of judgment that must be exercised. Results of uncertainty and sensitivity analyses of performance assessments need to be interpreted carefully, lest an erroneous and unwarranted implication of precision in calculations be imputed." NCRP emphasized that the goal of the uncertainty analysis is to support the regulatory decision, and that its nature and structure is therefore different than an uncertainty analysis focused solely on understanding uncertainties in model results.

5.1 SENSITIVITY ANALYSIS

The sensitivity analyses conducted using the system-level model for WMA C are documented in the environmental model calculation file RPP-CALC-60451, "WMA C System Model for Performance Assessment of Base Case, Uncertainty Analysis, and Sensitivity Analysis." The sensitivity analyses quantify the ranges of calculated groundwater concentration outcomes due to single-parameter or multiple-parameter changes that represent an underlying shift in the conceptual model. The analyses quantify the impacts that alternative views of the natural and engineered barriers have on groundwater concentrations in the evaluation of total system performance. In particular, the system model was used to evaluate the sensitivity to alternative inventory assumptions, effects of degradation of grouted tanks at various times, and the effect of varying diffusion coefficients in the grouted tanks.

5.2 UNCERTAINTY ANALYSIS

The objective of this section is to develop uncertainty ranges and probability distributions of input parameter values for use in the PA and to perform a fully probabilistic uncertainty analysis. The methodology that will be applied to propagate uncertainty through these models is first presented, followed by a discussion of the rationale that has guided the assignment of probability distribution functions of input parameters. Uncertainty in model parameters is subsequently examined followed by evaluation of uncertainty in the groundwater and air pathways.

The uncertainty analysis is conducted using the model and abstractions described earlier in this report.

As discussed previously, the vadose zone flow rates as a function of time were abstracted from the process-level models, developed using the STOMP© code that solves the Richards' equation for the unsaturated media. Outputs calculated by the 3-D STOMP©-based model were used to generate the flow field (spatially and temporally varying Darcy flux and moisture content), which were abstracted along with their uncertainty estimates for use in GoldSim©-based models. Because uncertainty in hydraulic properties and recharge rates affect the flow field in a complex manner, the abstraction was performed by first propagating the uncertainty in flow parameters using the STOMP©-based model and then evaluating the resulting flow field. Since running 3-D STOMP©-based models is numerically intensive, a selected combination of pre-determined hydraulic properties and recharge rates were used by setting the parameter values at various percentiles of their distribution. This approach led to development of a range of flow fields (vertical Darcy flux and moisture contents) that were abstracted as inputs to the transport calculations using the GoldSim©-based system model for uncertainty analysis.

5.2.1 Parameter Uncertainty Distributions

This section provides a description of each of the areas of parameter uncertainty distributions evaluated in the uncertainty analysis for the WMA C PA.

5.2.1.1 Uncertainty in Recharge Rates. Recharge rates have been estimated from studies conducted at the Hanford Site over the last 30 years. Recharge rates are based on estimate of downward water flux below the evapotranspiration zone representing deep drainage. Recharge rates are available for natural and disturbed soils, for soils with and without vegetation, and for various plant communities. In addition, recharge has been estimated for surface covers with varying plant communities. These estimates are based on lysimeter records, tracer tests (chloride mass balance), and computer simulations to match field data. PNNL-16688, "Recharge Data Package for Hanford Single-Shell Tank Waste Management Areas" and PNNL-14702, "Vadose Zone Hydrogeology Data Package for Hanford Assessments" provide primary sources of information on recharge estimates for the Hanford Site that are relevant to tank farms. There is limited information specific to WMA C.

Both spatial and temporal uncertainty in recharge need to be estimated. The spatial variability in recharge occurs because WMA C and surrounding areas have had varying vegetative cover and disturbed surface conditions. Spatially, two zones have been identified with different disturbed surface conditions: one within the WMA C fenceline, designated as the WMA C Disturbed Surface, and the other outside the WMA C fenceline, which is designated as the Non-Tank Farm Disturbed Surface. Although spatial variability in recharge has existed due to varying surface conditions, it is expected that after closure the disturbed areas will revegetate fully within 30 years.

The temporal uncertainty in recharge occurs due to time-varying changes resulting from construction and operations at WMA C and future changes anticipated after closure. These temporal recharge estimates have been grouped into a pre-operational phase, an operational

phase, a post-closure phase with intact surface cover, and a post-closure phase with degraded surface. While both spatial and past temporal changes have influenced the recharge rates at WMA C and needs to be considered, the focus of the PA is on developing uncertainty in long-term post-closure recharge rates, since that will influence the transport of contaminants from the residual waste in the future.

The area outside the WMA C fenceline, designated as the Non-Tank Farm Disturbed Surface, is not likely to influence the contaminant transport in the vadose zone, and therefore, constant best-estimate values are used for those areas in the following manner.

- Disturbed areas observed during the operations phase using aerial photographs, where vegetation appears to have grown, are assigned a value of 22 mm/yr based on estimates presented in PNNL-14702. These areas include surfaces where the existing shrub-steppe vegetation has been destroyed (e.g., by fire or Hanford operations), but shallow-rooted plants have been allowed, or were reintroduced, to re-vegetate the land.

- Disturbed areas observed during the operations phase using aerial photographs that appear to be reworked such that vegetation does not grow are assigned a value of 63 mm/yr based on estimates presented in PNNL-14702. These disturbed areas include construction and operations outside WMA C that removed the surface soil, broke up any near-surface layering, and exposed Hanford formation sands. These sediments tend to be coarser than the original soil, and, as indicated in photographs of the area around WMA C, plants have difficulty growing on them. The selected recharge rate is supported by drainage data collected from the 300 North Lysimeter, which contains coarse Hanford formation material screened to less than 1% gravel, where the long-term recharge rate averaged 62 mm/yr from 1981 to 2005 (PNNL-16688).

- Disturbed areas are allowed 30 years to fully revegetate after closure. Therefore, over time the disturbed area recharge changes to that assigned for the undisturbed natural vegetated land surface.

For the area within the WMA C fenceline, designated WMA C Disturbed Surface, the temporal evolution is presented below with the uncertainty estimates.

5.2.1.1.1 Pre-Operation Period. During the time prior to construction (before 1945), the area currently occupied by WMA C appears to have been covered by a mature shrub-steppe plant community growing in Rupert sand or Burbank loamy sand soil. It is difficult to distinguish between the two soil types because the divide between the Rupert sand and Burbank loamy sand soil appears to coincide with the northeastern boundary of WMA C.

For the vegetated Rupert sand, PNNL-14702 recommended using a value estimated using the Wye Barricade data (4 mm/yr) as the best-estimate value, although the surface is described as a stabilized dune area with low shrub cover. PNNL-16688 later revised the estimate of PNNL-14702 by considering an average of the three available tracer estimates (4, 0.26, and 0.9 mm/yr). Moreover, they reported a good agreement between their suggested mean value (1.7 mm/yr) and their modeling results that considered a 50-year weather record (including the

two wettest years: 1995 and 1996) and yielded a rate of 1.9 mm/yr. Consequently, they recommended using an estimate of 1.7 mm/yr for vegetated Rupert sand soil.

For the vegetated Burbank loamy sand, PNNL-14702 recommended the average value of 3.0 mm/yr based on three chloride tracer-based estimates of recharge (0.66 mm/yr, 2.8 mm/yr, and 5.5 mm/yr). PNNL-16688 augmented these data with five additional tracer-based estimates that decreased the average to 1.9 mm/yr, along with a simulation that suggested a rate of 5.2 mm/yr, which is near the upper end of the range of tracer estimates.

Based on the available information, uncertainty in pre-operational (natural vegetation) recharge is developed through selection of a triangular distribution, with a minimum value of 0.5 mm/yr, maximum value of 5.2 mm/yr, and mode of 1.9 mm/yr.

5.2.1.1.2 Operations Period. During the operations period, which started in 1945 and is assumed to last until 2020, two recharge zones have been defined within the WMA C fenceline: one that is disturbed, has no vegetation, and is covered with gravel; and the other that is largely undisturbed and characterized by a vegetative cover. For the latter, the same uncertainty distribution and range is considered that is developed for the pre-operations phase. For the former (the disturbed zone without vegetation [bare soil]), the range in recharge is based on the following discussion.

Disturbed zone recharge rates for the tank farms have been estimated to vary from 40 mm/yr to 140 mm/yr. A reasonably conservative estimate of 100 mm/yr was recommended for disturbed Rupert sand zone without vegetation and with gravel cover ("Variations in Recharge at the Hanford Site" [Gee et al. 1992]). The upper bound value of 140 mm/year results from an enhanced precipitation experiment on the "sandy gravel side slope" of the Hanford Prototype Barrier installed at the 216-B-57 Crib. This treatment is referenced as being "useful for characterizing deep drainage at the high-level waste tank farms at Hanford" (PNNL-14744, "Recharge Data Package for the 2005 Integrated Disposal Facility Performance Assessment"). Enhanced precipitation represented three times the average precipitation. Approximately 140 mm of the applied precipitation was observed to have infiltrated. For a lower bounding value, CP-14873, "200-BP-1 Prototype Hanford Barrier Annual Monitoring Report for Fiscal Year 2002" reported that 21.5% of precipitation (37.8 mm/yr) became recharge through sparsely vegetated sandy gravel representing the "sandy gravel side slope." Such a percentage (i.e., 21.5%) represents a lower value of approximately 40 mm/yr.

Based on the available information, uncertainty in the operational period recharge for the disturbed zone within WMA C is developed through selection of a triangular distribution, with a minimum value of 40 mm/yr, maximum value of 140 mm/yr, and mode of 100 mm/yr.

5.2.1.1.3 Post-Closure Period with Intact Surface Cover. For the area covered by the intact surface barrier, the recharge rate is expected to decline to nearly zero, as the modified RCRA-compliant surface cover is designed to prevent or significantly limit recharge. The design criteria of such a barrier are identified in BHI-00007, "Prototype Hanford Surface Barrier: Design Basis Document" and DOE/RL-93-33, Focused Feasibility Study of Engineered Barriers

for Waste Management Units in the 200 Areas, and include limiting recharge to 0.5 mm/yr. The design life of surface cover as a recharge barrier is assumed to be 500 years (DOE/RL-93-33).

Extensive laboratory and modeling work, and limited field testing of surface barriers, have been performed with results summarized in PNNL-14744. Lysimeter testing has been performed for different surface barrier concepts, including a Modified RCRA Subtitle C Barrier with silt-loam layers having depths between 1 and 2 m. Lysimeter data from the prototype Hanford barrier ("Quest for the Perfect Cap" [Wing and Gee 1994]) have also been collected and analyzed. Finally, modeling has been performed to address potential climate change impacts and no vegetation impacts on surface barrier performance.

The lysimeter drainage data that have been collected since 1989 suggest that the recharge rate beneath surface barriers having at least 1 m of silt loam is zero under ambient precipitation conditions. Most of these lysimeters did not contain an asphalt layer. Simulation results reported in PNNL-14744 investigated the sensitivity of the lysimeter data to climate change, silt-loam hydraulic properties, vegetation changes, erosion, and dune formation above the surface barrier. Results indicated that the performance of these surface barriers was robust in that the estimated recharge rates remained below 0.1 mm/yr. For the cases investigated, only in the case of dune formation and no vegetation on the surface barrier were the simulated recharge rates above 0.1 mm/yr. To account for such uncertainty (dune formation and no vegetation) within the design life of the barrier, an upper-bound recharge of 0.9 mm/yr is considered as suggested by PNNL-14744 for the post-barrier design life.

Based on the available information, uncertainty in recharge during the post-closure period with intact surface is developed through selection of a triangular distribution, with a minimum value of 0.1 mm/yr, a maximum value of 0.9 mm/yr, and mode of 0.5 mm/yr.

5.2.1.1.4 Post-Closure Period with Degraded Surface Cover. In the post-closure period after 500 years, the recharge barrier capability of the surface cover is assumed to be degraded. This recharge rate is applicable to the entire simulated duration (except for the first 500 years after closure) and influences the contaminant transport of residual tank waste through the vadose zone. It is expected that once the surface cover is degraded, the recharge will be similar to the recharge during the pre-operational phase, since the surface will most likely be indistinguishable from the surrounding surface in terms of vegetative cover. PNNL-14744 suggests that the performance of the barrier is not expected to change after its design life. Conclusions in PNNL-14744 indicate that the possibility of the most likely natural failure mechanisms (i.e., bioturbation of the silt loam layer, wind erosion, and accretion of windblown sand) of these natural systems is quite low with an appropriate design. The emplaced silt-loam soils should continue to perform as long as they remain in place.

To propagate uncertainty in post-closure recharge rate following degraded surface cover, a triangular distribution is chosen, with a minimum value of 0.5 mm/yr, a mode value of 1.9 mm/yr, and a maximum value of 5.2 mm/yr. This uncertainty range is the same as that chosen for the pre-operational phase recharge rates.

The uncertainties in recharge rates selected for the various time periods are summarized in Table 5-1.

Table 5-1. Spatial and Temporal Uncertainty in Recharge Rates Considered for Waste Management Area C.

Spatially Distinct Zone	Uncertainty in Recharge Estimate (mm/yr)		
	Minimum	**Maximum**	**Most Likely**
Pre-operations Period (Prior to Year 1945)			
Undisturbed (Natural Vegetation)[a]	0.5	5.2	1.9
Operations Period (Years 1945 – 2020)			
Undisturbed (Natural Vegetation)[a]	0.5	5.2	1.9
Waste Management Area C Disturbed Surface	40	140	100
Non-Tank Farm Disturbed Surface[b]	22 / 63	22 / 63	—
Post-Closure Period with Intact Surface Cover (Years 2020 – 2520)			
Undisturbed (Natural Vegetation)[a]	0.5	5.2	1.9
Waste Management Area C Surface Barrier	0.1	0.9	0.5
Non-Tank Farm Disturbed Surface[a,c]	0.5	5.2	1.9
Late Post-Closure Period with Degraded Surface Cover (Years > 2520)			
Undisturbed (Natural Vegetation)[a]	0.5	5.2	1.9
Waste Management Area C Surface Barrier	0.5	5.2	1.9
Non-Tank Farm Disturbed Surface[a]	0.5	5.2	1.9

[a]Waste Management Area C late post-closure surface barrier assumed to acquire natural vegetation recharge rate.
[b]Disturbed areas that allow vegetation are assigned 22 mm/yr. Disturbed areas that are reworked such that vegetation does not grow are assigned 63 mm/yr.
[c]Disturbed areas are allowed 30 years to revegetate fully.

5.2.1.2 Uncertainty in Residual Inventory Estimates. A best estimate of the residual inventory for tanks and ancillary equipment was developed and evaluated in the PA (Section 3.2.2). However, considerable uncertainty exists in estimating the residual inventory due to mixing of various waste types, differentiation between inventory associated with sludge and salt-cake, and the limited availability of direct measurements of contaminant concentrations. These uncertainties have been recognized in the BBI database, which is the official database for tank waste inventory. Uncertainties in concentration, waste volume, and waste density for each tank are accounted by developing standard deviation (SD) estimates in those parameters (assuming a normal distribution), which are then propagated to calculate the inventory uncertainty in 46 radionuclides and 25 chemicals that are tracked in the BBI. For the retrieved tanks, the uncertainty is based primarily on sample-based results. However, where information

is lacking for a particular analyte, a template based on process knowledge is used to fill in the gaps.

For WMA C, the BBI database currently contains residual inventory information from 10 retrieved tanks: 241-C-103, 241-C-104, 241-C-106, 241-C-108, 241-C-109, 241-C-110, C-201, 241-C-202, C-203, and C-204. These are the tanks from which post-retrieval samples were collected, and uncertainty in concentration (in solid phase), residual volume, and density is quantified in terms of relative standard deviation (RSD), which is the SD divided by the mean value. All the relevant information related to 46 radionuclides and 25 chemicals from the BBI was downloaded for these 10 tanks. The following steps were undertaken to reduce the dataset.

- Removal of the analytes that were below detection limits. This resulted in 25 radionuclides and 12 chemicals.

- Identification of mean solid-phase concentration, residual volume, and waste density for each analyte for the sludge waste form for each tank.

- Identification of the RSD of concentration for each analyte, residual volume, and waste density for the sludge waste form for each tank.

- Calculation of SDs in concentration, residual volume, and waste density from the RSDs by multiplying by the mean values.

Since the residual inventory for a given analyte is calculated by multiplying the concentration in solid phase (sludge) with the residual waste volume and waste density, the mean inventory is calculated based on the mean values of these parameters.

Next, normal probability distributions were developed for the concentration of each analyte, residual volume, and density for each tank. This was done by defining the mean and SD for the parameter and implementing them in the GoldSim©-based system model. Following this, 10,000 realizations were run using Latin Hypercube Sampling, leading to 10,000 realizations of inventory for each analyte for each tank. The sampled inventory estimates were normalized by dividing by the mean inventory, leading to 10,000 normalized inventories for each analyte for each tank. These results can be expressed as a cumulative distribution function (CDF) of the normalized inventory. An example CDF for ^{99}Tc is presented in Figure 5-1 for each tank. In addition, an average CDF was calculated by averaging the CDF values for all the tanks.

Development of a normalized inventory CDF is attractive because the sampled value can be multiplied with the mean inventory to estimate inventory for a given realization. As shown in Figure 5-1, the average normalized inventory CDF for ^{99}Tc ranges from 0.4 to 1.75 and therefore indicates the factor by which the mean inventory can vary. Since the CDF of normalized inventory is calculated separately for each analyte for each tank, each CDF could be separately sampled for each tank to determine the multiplier factor for the inventory. However, this approach leads to a very large number of uncertain parameters related to inventory, due to the large number of analytes considered per source term. The analysis has therefore been simplified by sampling the analyte-specific average CDF (averaged over the tanks) and then multiplying the

sampled value by the mean inventory for a given analyte for each source term. This approach significantly simplifies the analysis while preserving the uncertainty in the analyte inventory.

Figure 5-1. Cumulative Distribution Function of Normalized Inventory of Technetium-99 for Retrieved Tanks, and the Average Cumulative Distribution Function.

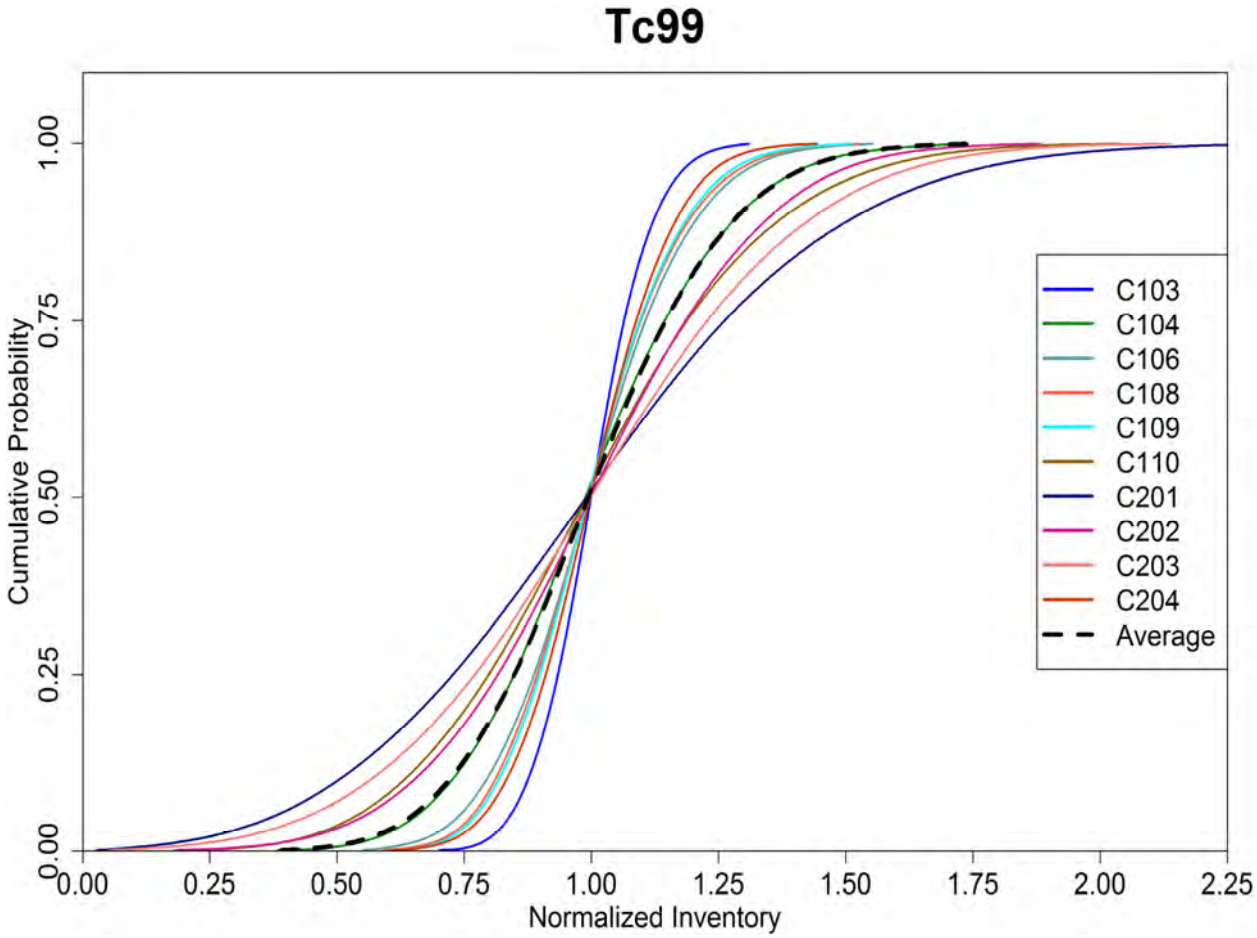

The uncertainties in inventory for various analytes are presented in Figure 5-2. Not all the tanks have uncertainty in all the analytes quantified. This is because some analytes are below detection limits in some of the tanks. In such cases, the average CDF is calculated based on the CDF of the tanks for which uncertainty estimates were available. For analytes for which uncertainty information is not available in the BBI, no uncertainty is propagated in the inventory. For the tanks where post-retrieval sampling-based inventory uncertainty estimates were not available in the BBI database, the uncertainty estimates based on average normalized CDF presented earlier are applied. This is a reasonable approximation, given that several tanks within WMA C have similar waste types and were operated in a similar manner.

Figure 5-2. Cumulative Distribution Function of Normalized Inventory of Various Analytes for the Retrieved Tanks along with the Average Cumulative Distribution Function. (sheet 1 of 10)

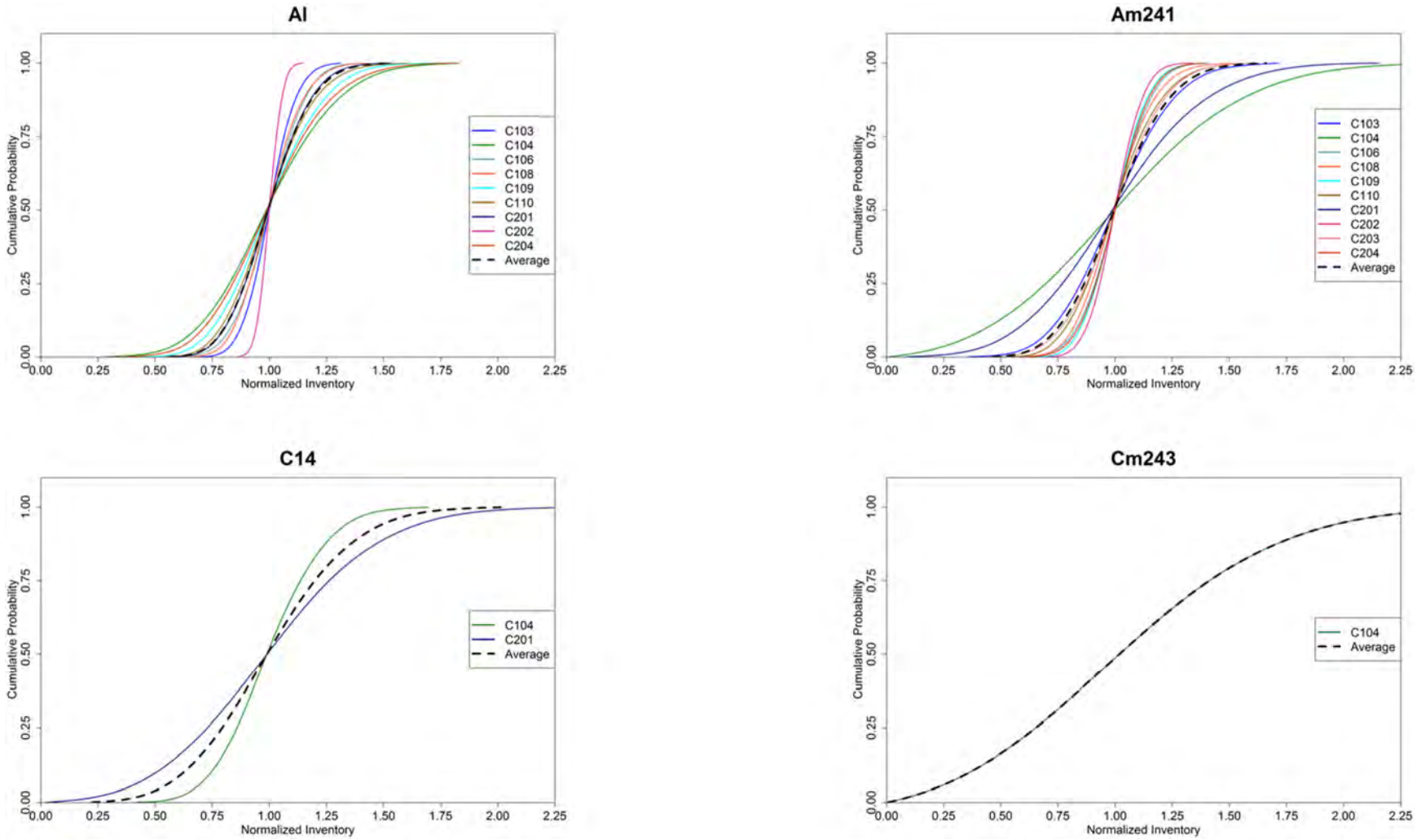

Figure 5-2. Cumulative Distribution Function of Normalized Inventory of Various Analytes for the Retrieved Tanks along with the Average Cumulative Distribution Function. (sheet 2 of 10)

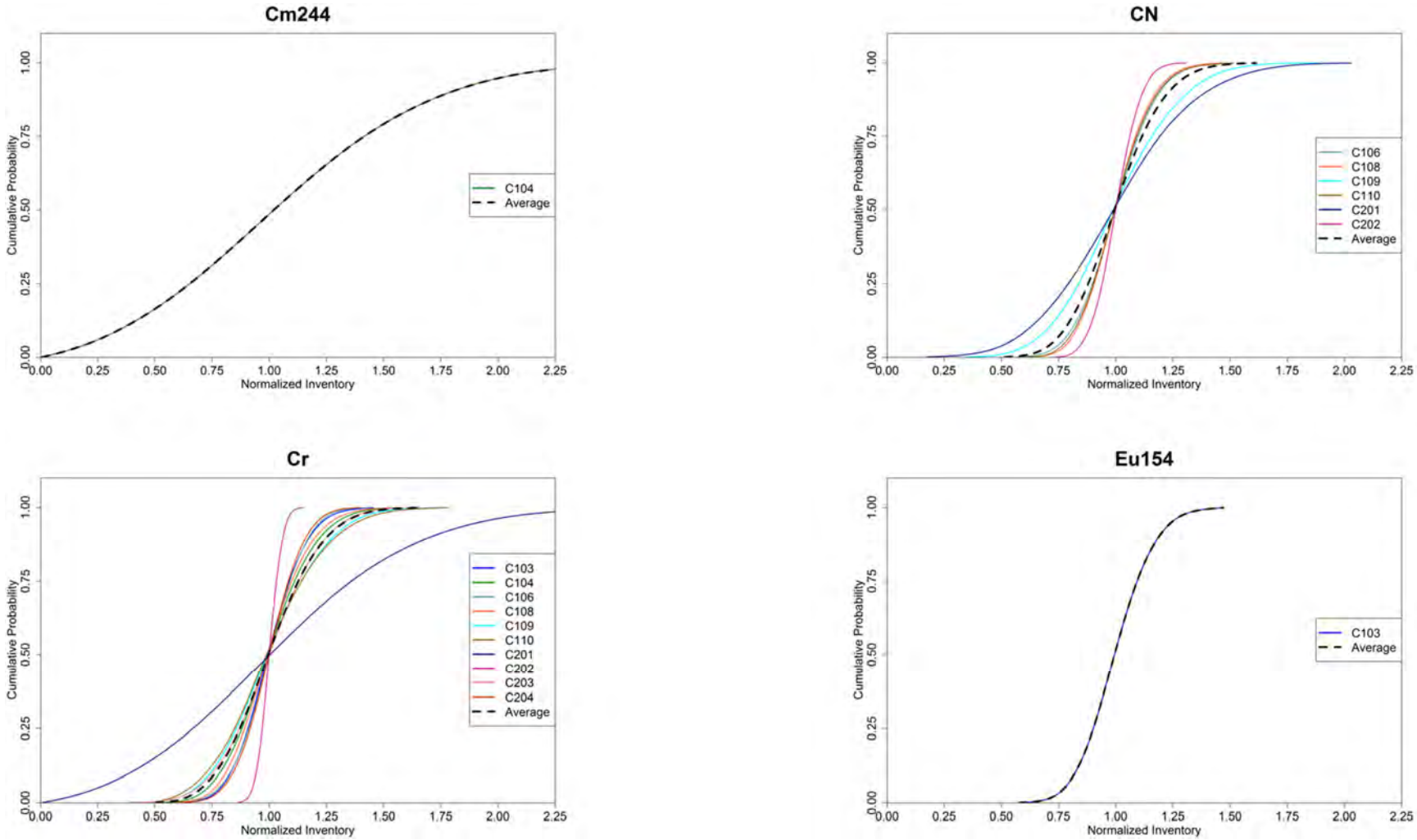

Figure 5-2. Cumulative Distribution Function of Normalized Inventory of Various Analytes for the Retrieved Tanks along with the Average Cumulative Distribution Function. (sheet 3 of 10)

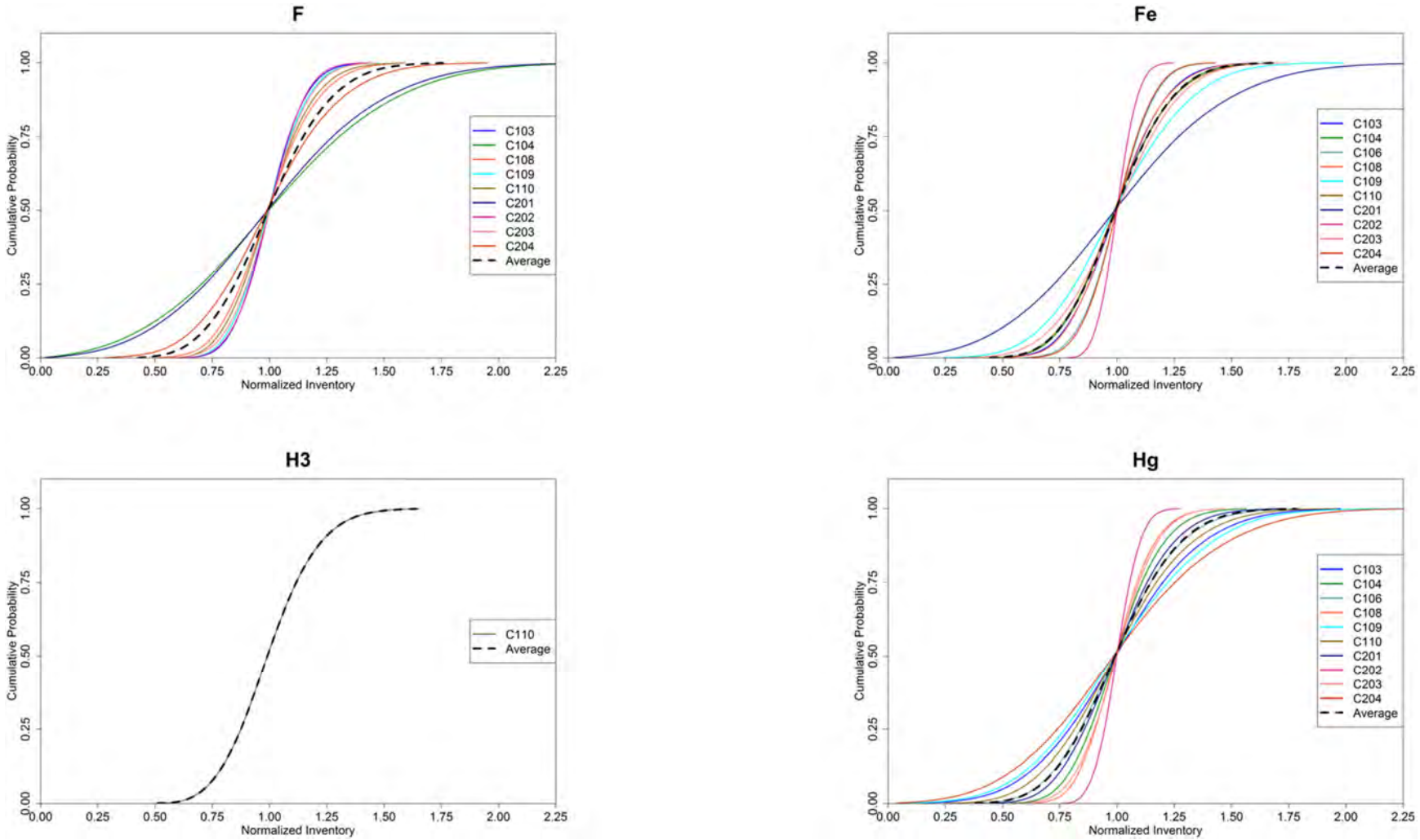

Figure 5-2. Cumulative Distribution Function of Normalized Inventory of Various Analytes for the Retrieved Tanks along with the Average Cumulative Distribution Function. (sheet 4 of 10)

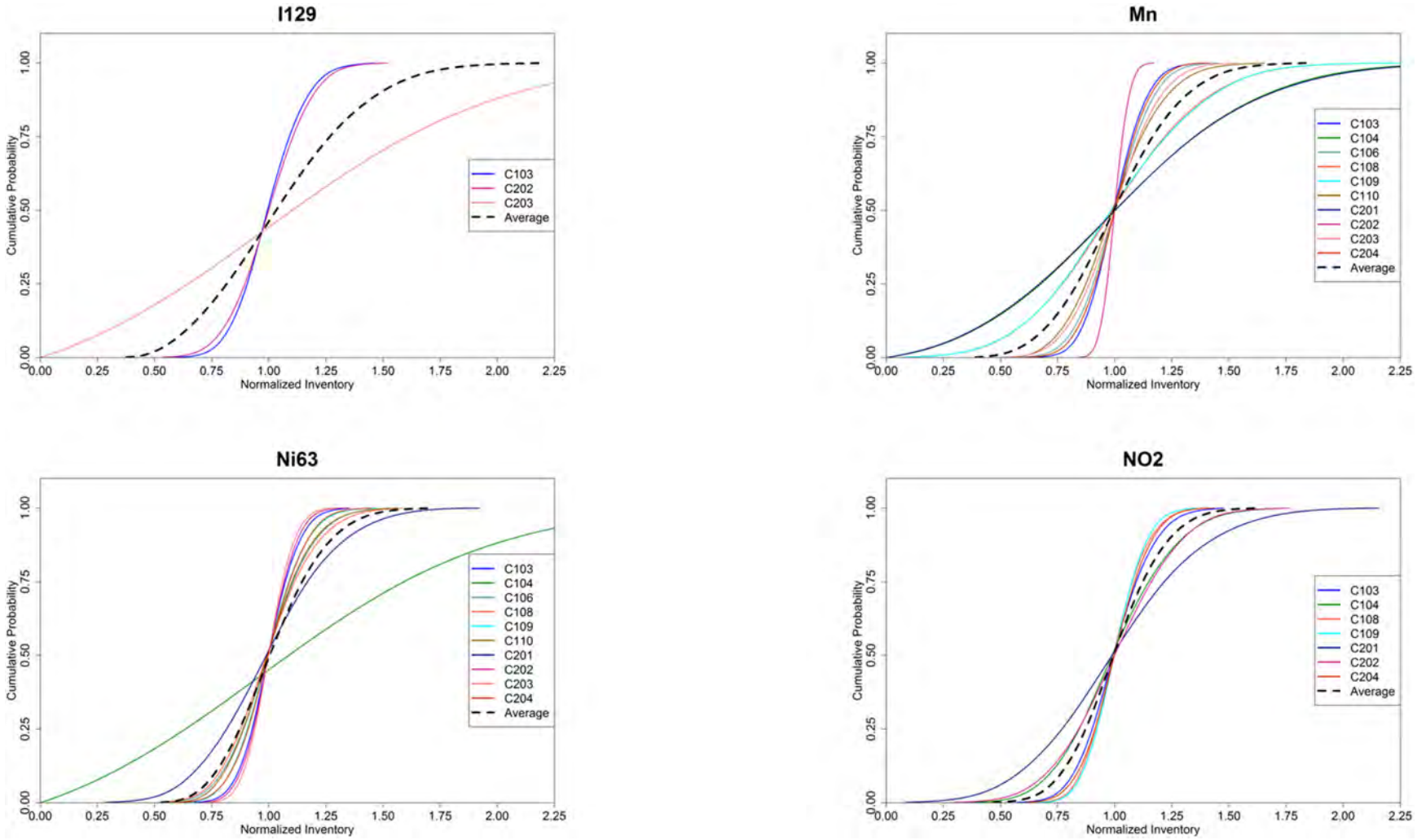

Figure 5-2. Cumulative Distribution Function of Normalized Inventory of Various Analytes for the Retrieved Tanks along with the Average Cumulative Distribution Function. (sheet 5 of 10)

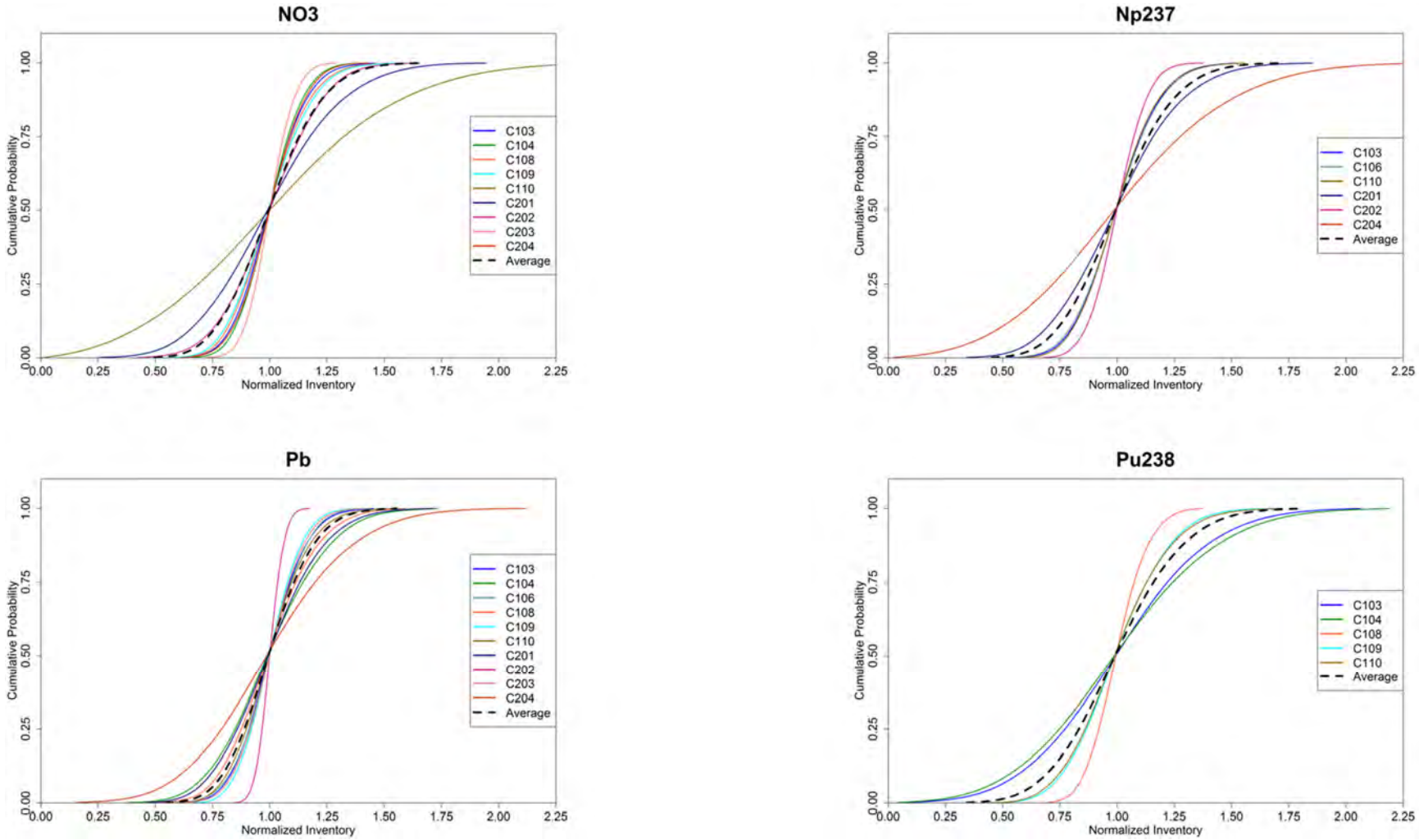

Figure 5-2. Cumulative Distribution Function of Normalized Inventory of Various Analytes for the Retrieved Tanks along with the Average Cumulative Distribution Function. (sheet 6 of 10)

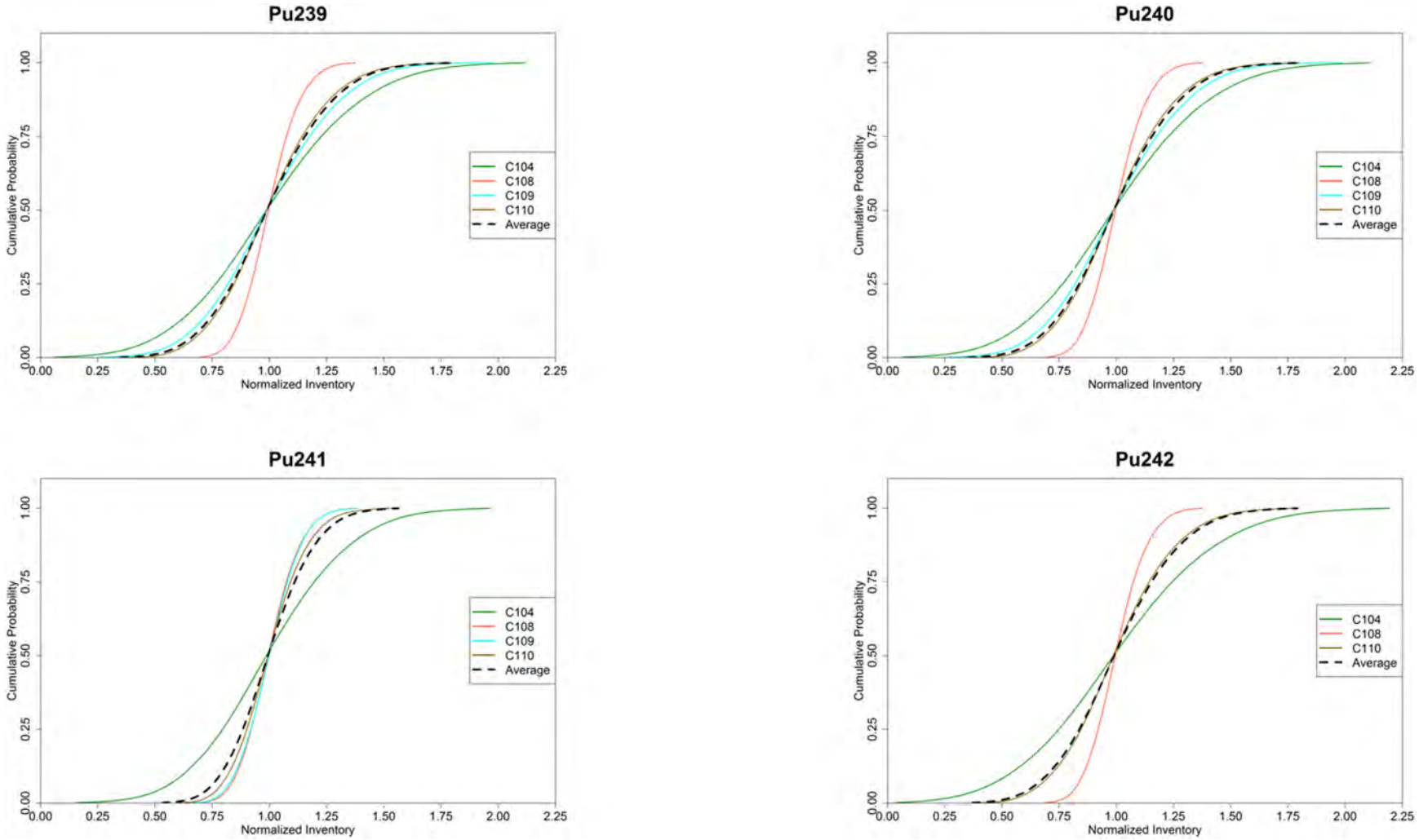

Figure 5-2. Cumulative Distribution Function of Normalized Inventory of Various Analytes for the Retrieved Tanks along with the Average Cumulative Distribution Function. (sheet 7 of 10)

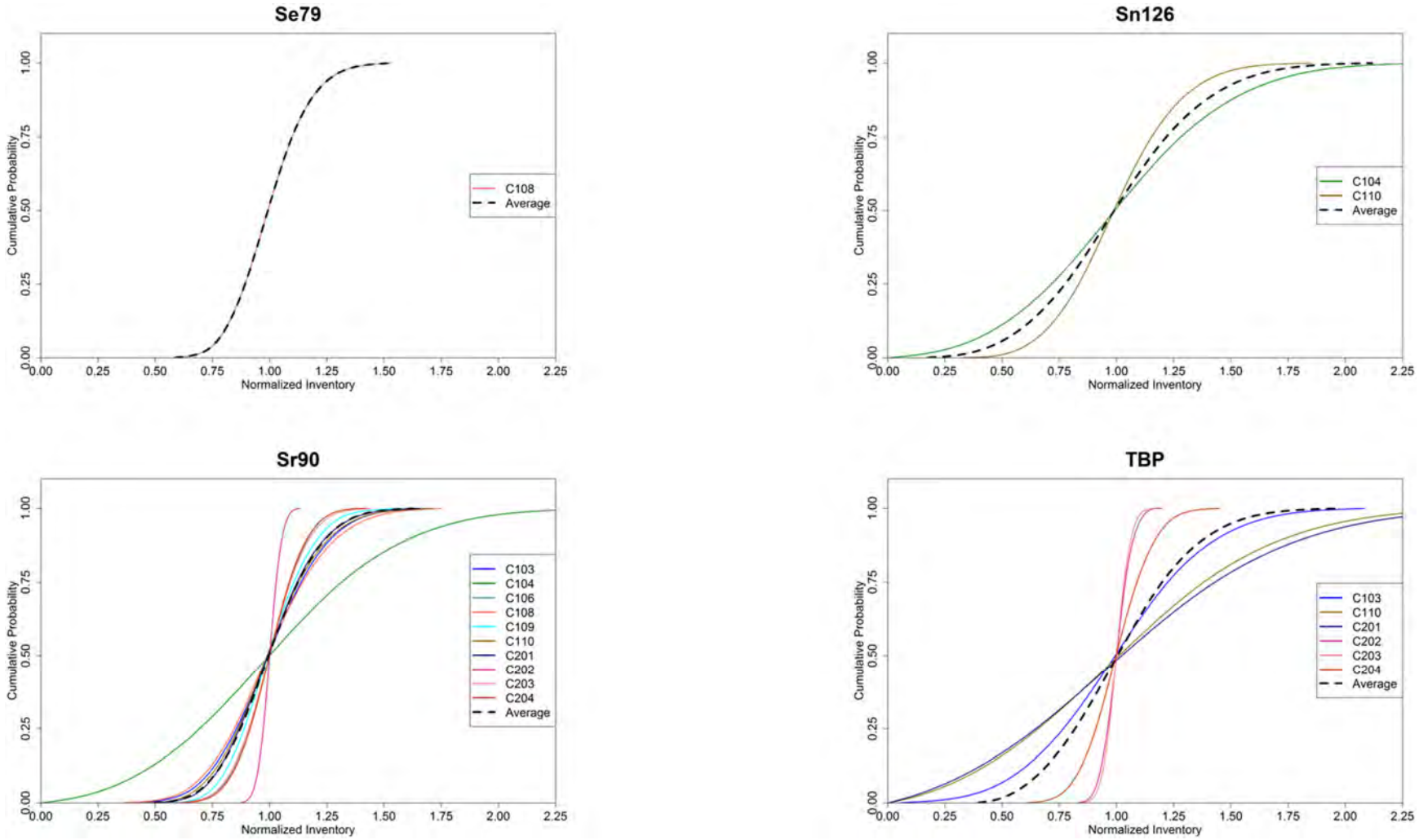

Figure 5-2. Cumulative Distribution Function of Normalized Inventory of Various Analytes for the Retrieved Tanks along with the Average Cumulative Distribution Function. (sheet 8 of 10)

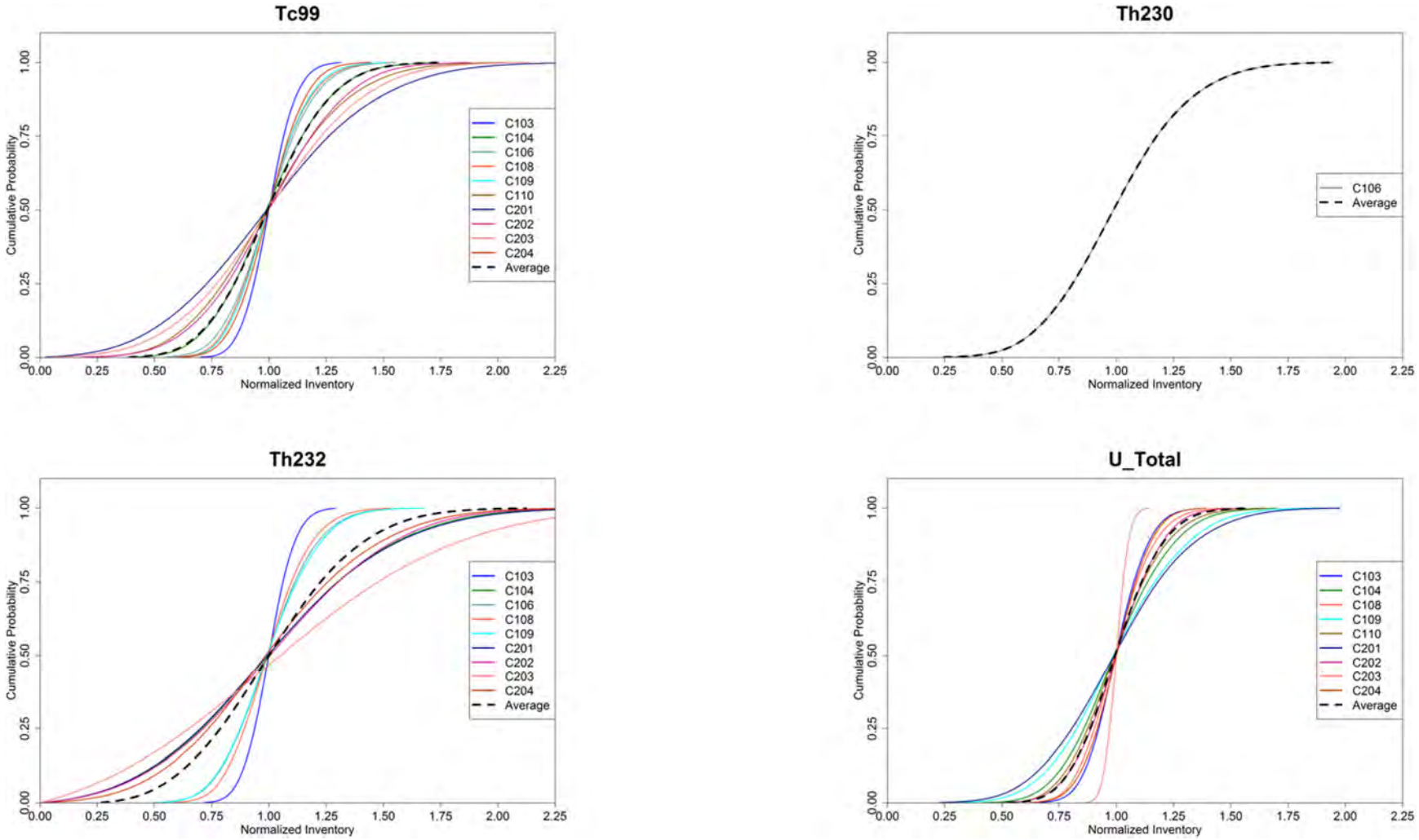

Figure 5-2. Cumulative Distribution Function of Normalized Inventory of Various Analytes for the Retrieved Tanks along with the Average Cumulative Distribution Function. (sheet 9 of 10)

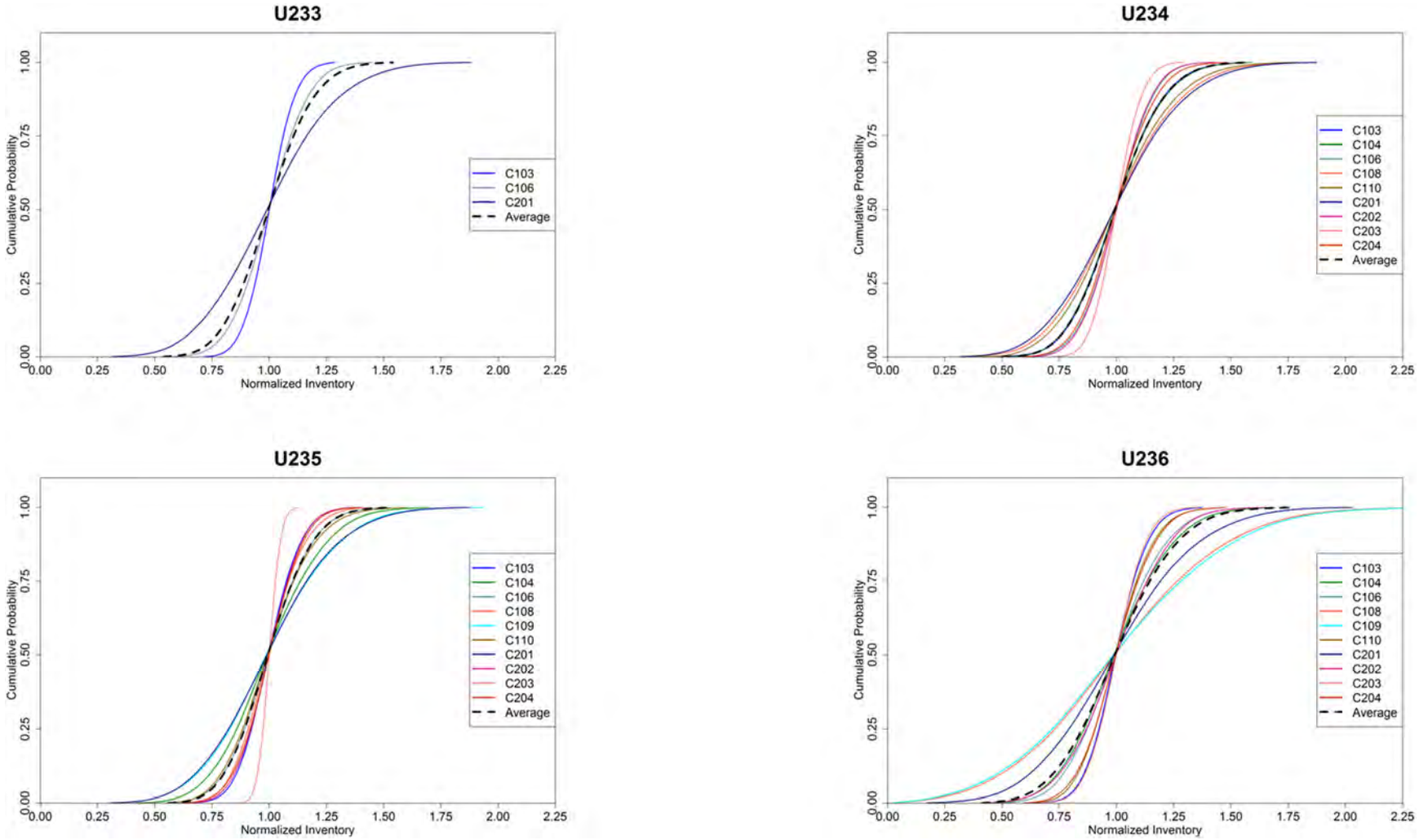

Figure 5-2. Cumulative Distribution Function of Normalized Inventory of Various Analytes for the Retrieved Tanks along with the Average Cumulative Distribution Function. (sheet 10 of 10)

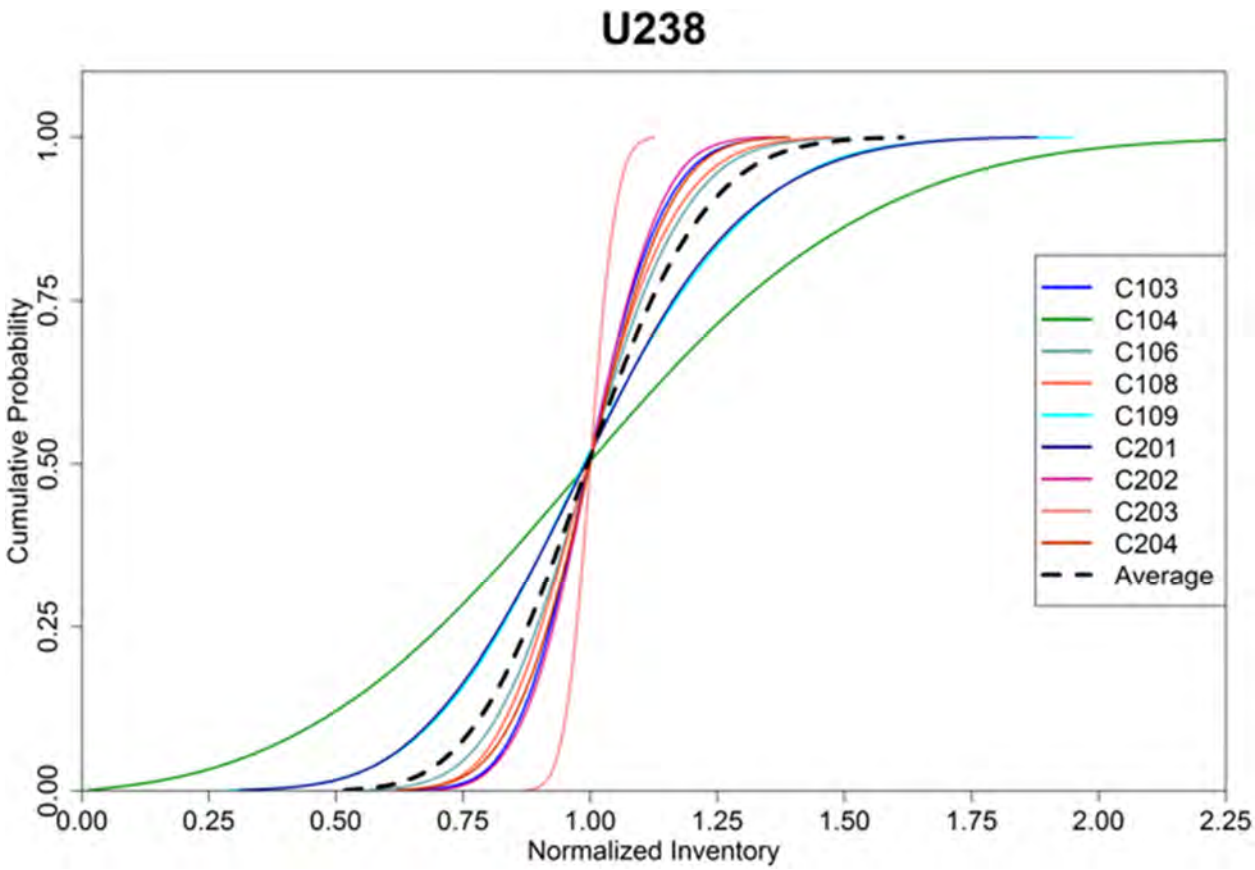

In addition to developing uncertainty in the inventory, uncertainty is also propagated separately in the residual volume, as it is a key parameter in the contaminant transport calculations. The methodology for deriving the uncertainty in residual volume is similar to that for the inventory derivation and is based on the same dataset. The normalized residual waste volume is derived from 10,000 Latin Hypercube Sampling realizations of the same GoldSim© model file used for inventory uncertainty. The model file samples the underlying normal distribution for each tank and divides by the mean residual volume for that tank. The CDF of normalized residual waste volume uncertainty is presented in Figure 5-3 for each tank, along with the average CDF (average of all tanks). The average CDF of normalized waste volume is sampled to scale the mean residual volume for each source term. As shown in Figure 5-3, the normalized values in the average CDF vary from 0.75 to 1.25. Because some correlation is expected between residual waste volume and the residual inventory, the uncertainty distribution of residual waste volume is correlated to the uncertainty distribution of the residual uranium inventory, since it is the dominant radionuclide in terms of mass and forms mineral phases that contribute to the residual volume.

Figure 5-3. Cumulative Distribution Function of Normalized Residual Volume for the Retrieved Tanks along with the Average Cumulative Distribution Function.

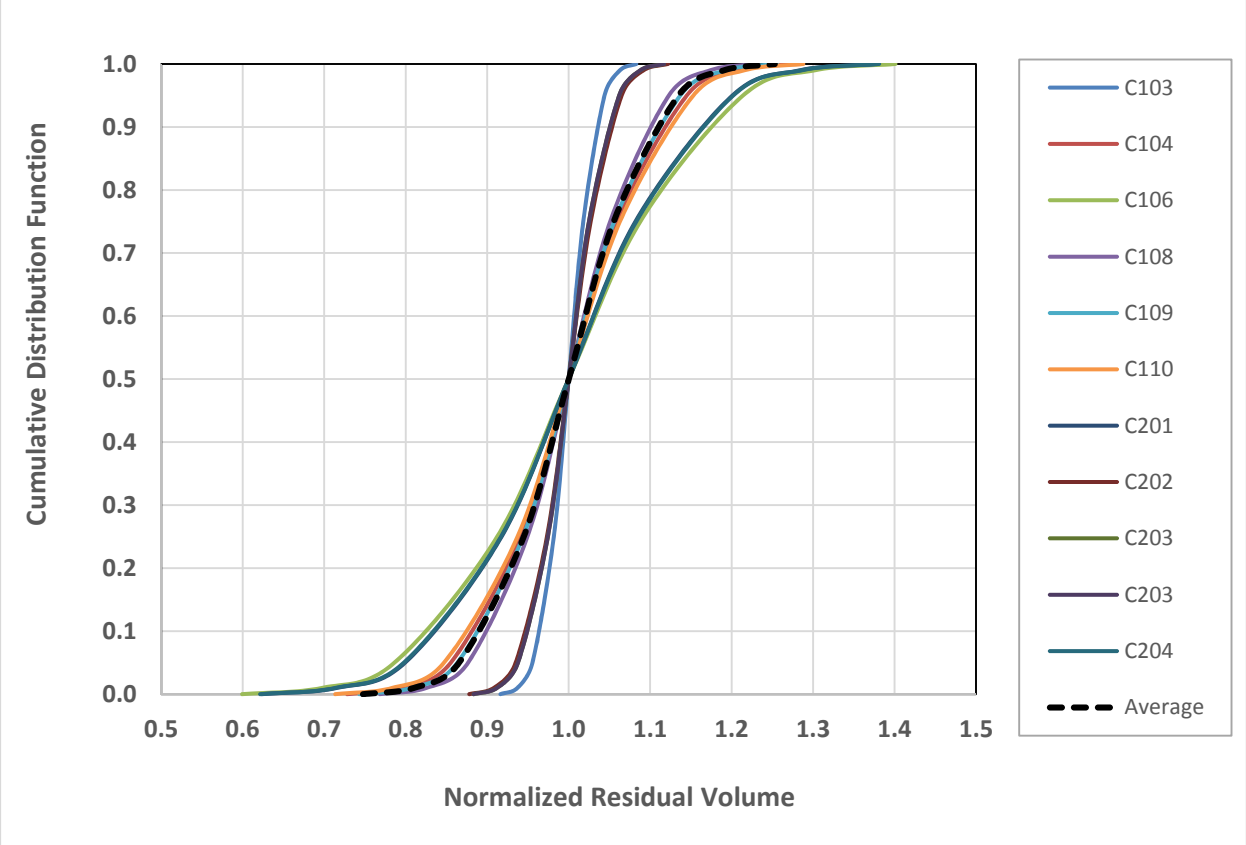

5.2.1.3 Uncertainty in Source Term Transport Parameters. The waste form degradation and release mechanisms from the source term are described in Section 4.2. Several interacting parameters determine the release rate from the base of the tanks and ancillary equipment into the underlying vadose zone. The uncertainty in these parameter estimates is summarized below.

- The initial release fraction of ^{99}Tc is observed to vary between 4.5% and 15%. Without additional information, a uniform distribution is applied.

- The remaining fraction of ^{99}Tc undergoes a slower release that is modeled using a first order reaction rate. The available information was used to identify a uniform distribution with a minimum of 5×10^{-4} day^{-1} and a maximum of 8×10^{-4} day^{-1}.

- The solubility of uranium is also considered to be uncertain. The uncertainties arise from both the value of the solubility at any time and the mineral phases assumed to be controlling the solubility. The mean solubility is assumed to change from 10^{-4} M to 10^{-6} M at 1,000 years, based on the assumption that solubility will be controlled by amorphous mineral phases early on, and later by a $CaUO_4$ mineral phase under $Ca(OH)_2$-saturated conditions. A factor of two uncertainty multiplier to solubility is imposed by assigning a log-uniform distribution varying from 0.5 to 2. This distribution

is chosen because the median value of this distribution is 1 (and mean is about 1.1); therefore, the mean/median sampled multiplier will retain the base case solubility value.

- Uncertainty in dissolved concentration limit for chromium is applied the same way as that for uranium, using a separate log-uniform distribution varying from 0.5 to 2.

- Uncertainty in the effective diffusion coefficient through the base mat is propagated through a log-uniform distribution with a minimum and maximum value of 6×10^{-9} cm^2/s and 2×10^{-7} cm^2/s, based on the range of effective diffusion coefficients measured for ^{99}Tc (PNNL-23841). This distribution leads to a median value of 3.5×10^{-8} cm^2/s, which is close to the best-estimate value of 3×10^{-8} cm^2/s.

- Uncertainty in sorption on cementitious material is represented using a triangular distribution of K_d values for each analyte (see Table 4-11). This distribution is appropriate for representing the available literature information, which provides mean values and ranges. Where information is not available, a zero K_d value is used.

5.2.1.4 Uncertainties in Vadose Zone Hydraulic Properties. Uncertainties in vadose zone hydraulic properties are derived from a set of laboratory (core-scale) experiments conducted on sediments representative of Hanford H1, H2, and H3 units and backfill material. The laboratory-measured soil-moisture retention and unsaturated hydraulic conductivity datasets were fit using van Genuchten-Mualem constitutive relationships to derive uncertainty in the following parameters[5]:

- The fitted saturated hydraulic conductivity K_s

- The van Genuchten fitting parameter α, which is proportional to the inverse of air-entry matric potential (cm^{-1})

- The van Genuchten fitting parameter n, which is a dimensionless fitting parameter commonly taken to be the inverse of the pore-size SD

- The saturated and residual moisture contents (θ_s and θ_r).

A single, large, internally consistent soil-moisture retention and unsaturated hydraulic conductivity dataset consisting of 44 soil samples from the nearby IDF was analyzed for the H2 sand-dominated unit. The IDF is located southwest of WMA C within 200 East Area, and the dataset is the largest appropriate database for evaluating uncertainty and to derive probability distribution functions for K_s, α, n, θ_s, and θ_r for the H2 sand-dominated unit.

Similar uncertainty analyses were undertaken for the gravel-dominated Hanford H1 and H3 units and for the backfill sediments based on the hydraulic properties dataset from other representative samples.

[5] The pore size distribution factor, ℓ (Mualem 1976) was kept fixed at 0.5 in this exercise.

5.2.1.4.1 Uncertainty in Saturated Hydraulic Conductivity (K_s) Parameter for H2 Unit. The derived K_s values from each of the 44 laboratory-measured, soil-moisture retention and unsaturated hydraulic conductivity datasets were fit to a log-normal distribution (Figure 5-4), as the number of samples allow an estimate of a mean and standard deviation. The distribution was truncated at the minimum and maximum values of the dataset. The K_s distribution has the following characteristics:

- Geometric mean = 4.2E-3 cm/s
- Geometric SD = 4.3
- Minimum = 2.5E-4 cm/s and Maximum = 5E-2 cm/s.

Figure 5-4. Fitted Log-Normal Distribution to the Saturated Hydraulic Conductivity Dataset Used for H2 Unit.

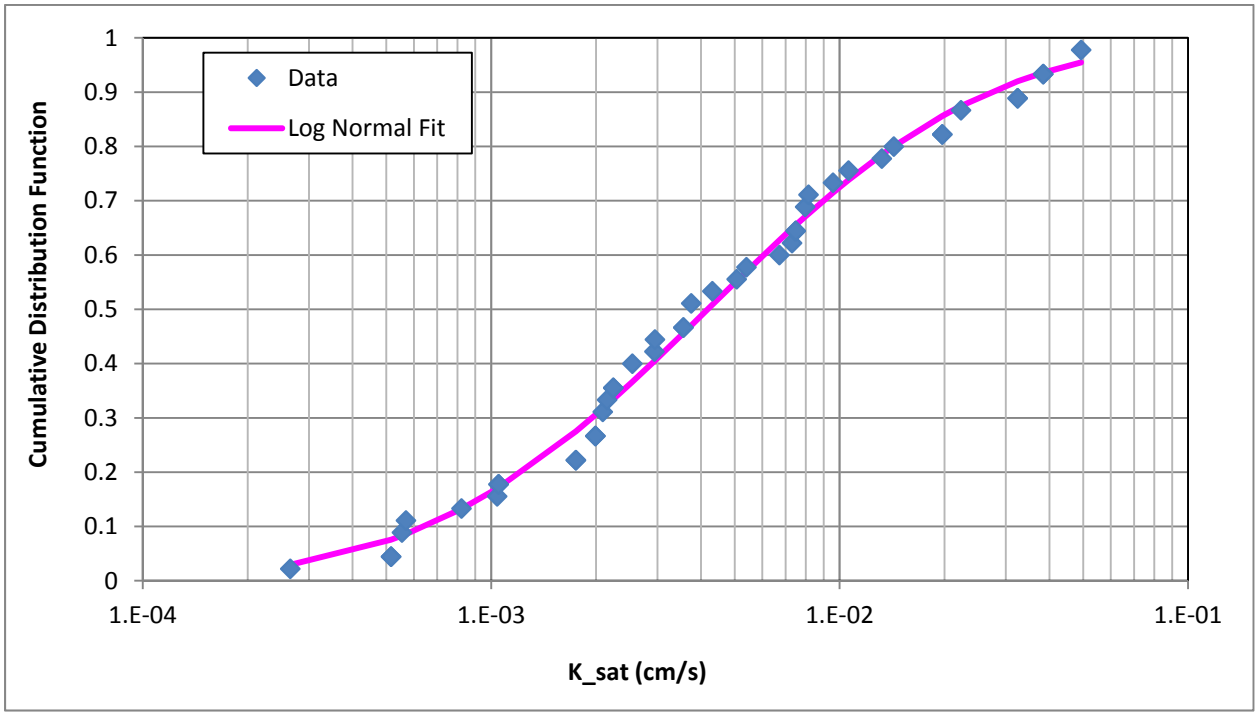

5.2.1.4.2 Uncertainty in van Genuchten Alpha (α) Parameter for H2 Unit. The derived van Genuchten alpha (α) values from each of the 44 laboratory-measured, soil-moisture retention and unsaturated hydraulic conductivity datasets were fit to a log-normal distribution (Figure 5-5). The distribution was truncated at the minimum and maximum values of the dataset. The α distribution has the following characteristics:

- Geometric mean = 0.060 cm^{-1}
- Geometric SD = 1.85
- Minimum = 0.0058 cm^{-1} and Maximum = 0.201 cm^{-1}.

5.2.1.4.3 Uncertainty in van Genuchten n Parameter for H2 Unit. The derived van Genuchten *n* parameter values from each of the 44 laboratory–measured, soil-moisture

retention and unsaturated hydraulic conductivity datasets were fit to a log-normal distribution (Figure 5-6). The distribution is truncated at the minimum and maximum values of the dataset. The *n* distribution has the following characteristics:

- Geometric mean = 1.81
- Geometric SD = 1.15
- Minimum = 1.5 and Maximum = 3.18.

Figure 5-5. Fitted Log-Normal Distribution to the van Genuchten "Alpha" Parameter Dataset Used for H2 Unit.

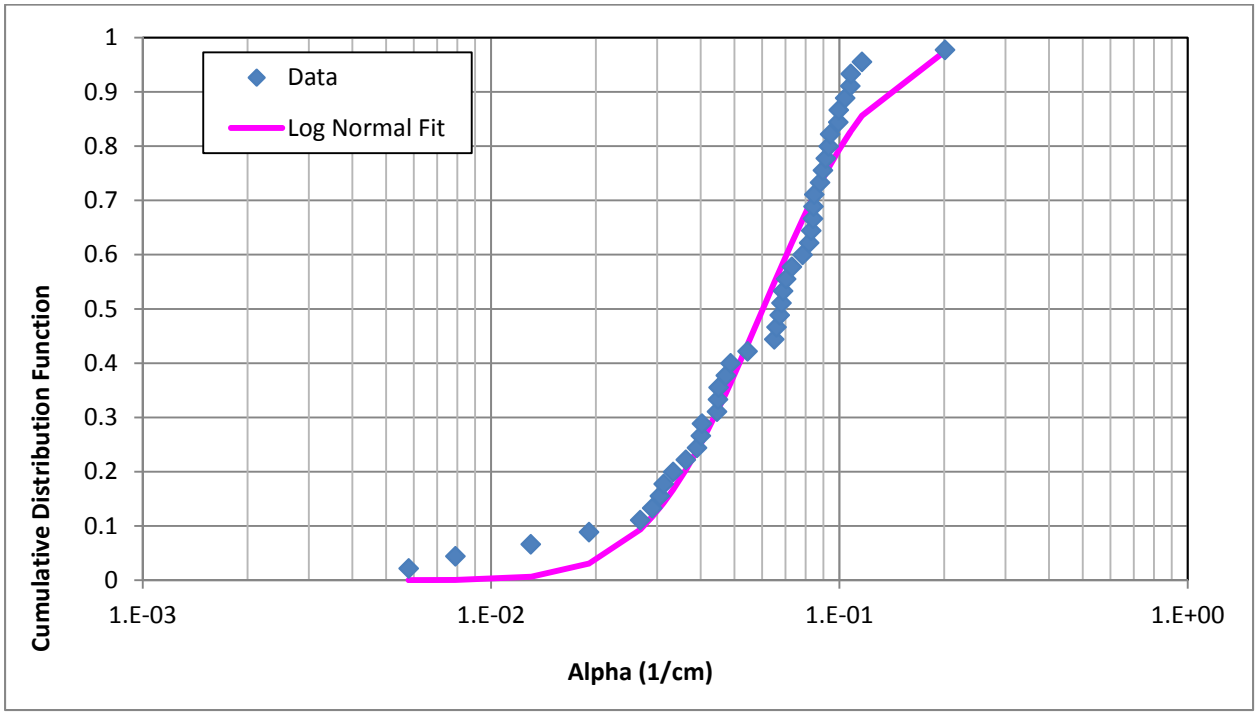

5.2.1.4.4 Uncertainty in Saturated and Residual Moisture Content (θ_s and θ_r) for H2 Unit. The derived saturated and residual moisture content values (θ_s and θ_r) from each of the 44 laboratory-measured, soil-moisture retention datasets were considered with a 20% gravel correction for WMA C. The values have a small range, and as a result, a uniform distribution was assumed with the following minimum and maximum values:

- Saturated moisture content (θ_s): Minimum = 0.239 and Maximum = 0.355
- Residual moisture content (θ_r): Minimum = 0 and Maximum = 0.037.

5.2.1.4.5 Correlation between Parameters. The K_s, α, and *n* parameters were evaluated to see if any correlation exists within them that needs to be preserved. Based on rank correlation, it was found that α and K_s have a correlation coefficient of 0.77, while α and *n* have a correlation coefficient of -0.33. This correlation was implemented while sampling the above-defined log-normal distributions to preserve the relationships in the measured dataset.

Figure 5-6. Fitted Log-Normal Distribution to the van Genuchten "*n*" Parameter Dataset Used for H2 Unit.

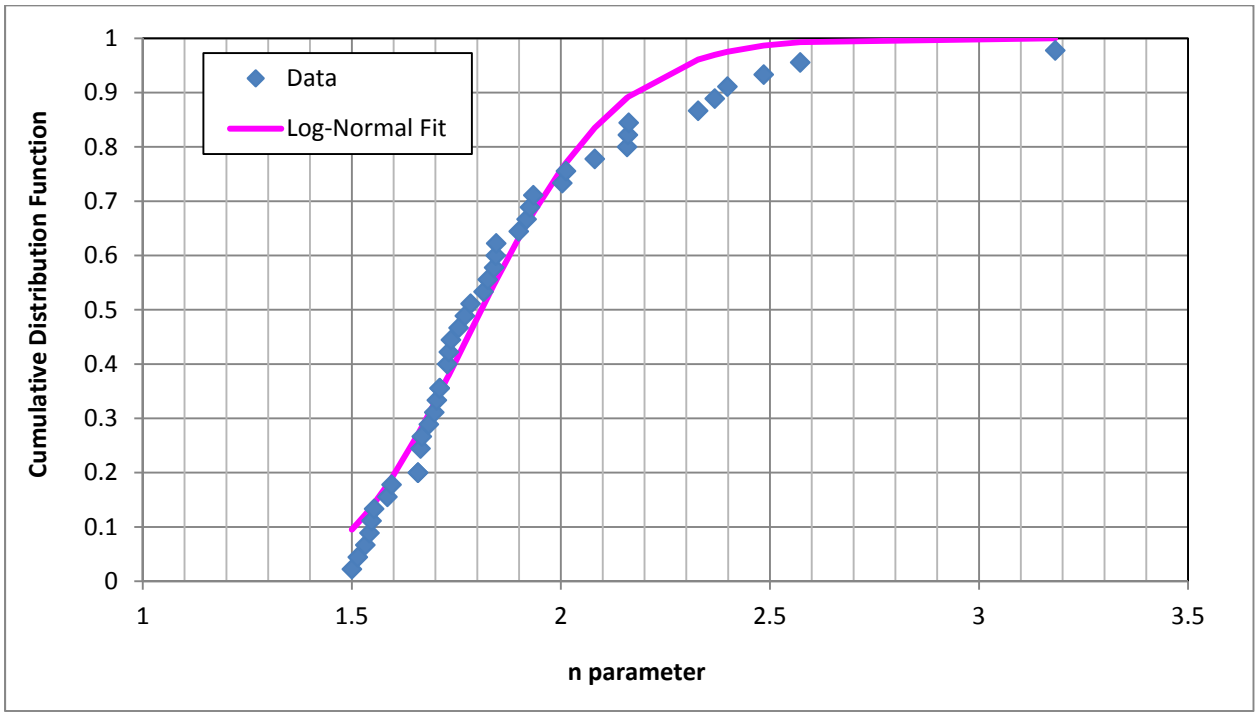

Using Monte Carlo analysis with a Latin Hypercube Sampling distribution, functions of the van Genuchten parameters (including the correlation between parameters) were sampled 200 times. Using the van Genuchten-Mualem constitutive relationship functions, 200 realizations were generated of unsaturated hydraulic conductivity as a function of matric potential, and soil-moisture characteristic curves. These realizations are shown in Figure 5-7 and Figure 5-8 for the H2 unit.

Similar to the sand-dominated H2 unit, uncertainty in the hydraulic properties for the gravel-dominated H1 and H3 units (assumed to take the same values) and the backfill material was developed. For the H1/H3 unit, the derived uncertainty distributions are summarized in Table 5-2. The fitted log-normal distributions are presented in Figures 5-9 through 5-11. Using the van Genuchten-Mualem constitutive relationship functions, 200 realizations of unsaturated hydraulic conductivity as a function of matric potential and soil-moisture characteristic curves were generated, which are shown in Figure 5-12 and Figure 5-13.

For the backfill material, the uncertainty distributions are summarized in Table 5-3.

5.2.1.5 Uncertainty in Sorption Parameter for Natural System. A linear sorption isotherm (K_d) was implemented for evaluating the interaction of contaminants with soils, as discussed in Section 6.3.8. These values represent intermediate impact zones, which are defined as zones (or areas) in which the acidic or basic nature of the released waste was expected to have been largely neutralized by reaction with the natural sediment.

Figure 5-7. 200 Realizations of Unsaturated Hydraulic Conductivity as a Function of Matric Potential for H2 Unit. Red line indicates the Composite curve used in the Base Case.

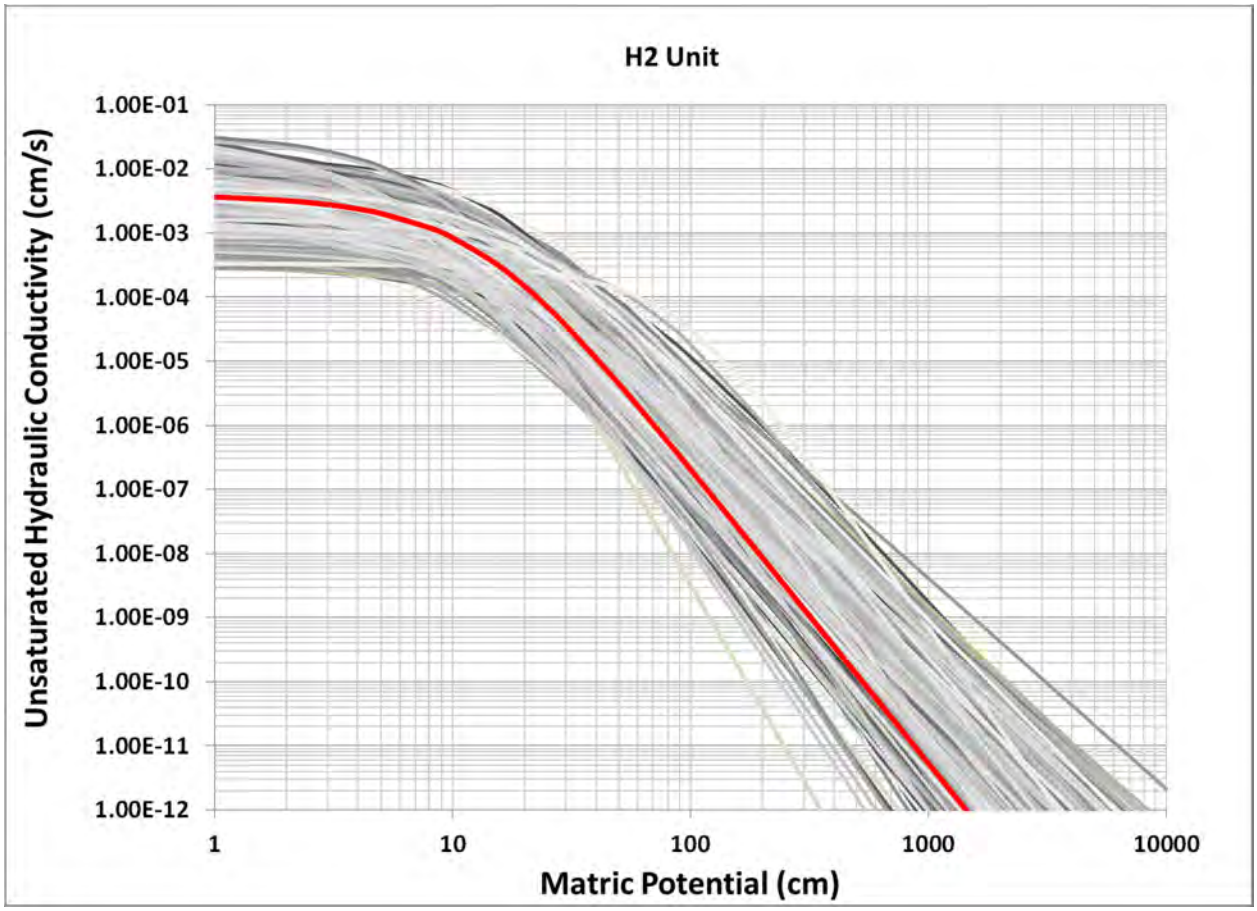

Uncertainties in K_d values were developed for sand using a triangular distribution as shown in Table 5-4. The sampled K_d value is then corrected for gravel fraction based on the average gravel content. To be consistent with the hydraulic properties, the average gravel content for H2 unit is 20% and for H1 and H3 units is 42%.

5.2.1.6 Uncertainty in Darcy Flux in Saturated Zone. Uncertainty exists in determination of the saturated hydraulic conductivity and the future hydraulic gradient within the aquifer. As discussed in RPP-RPT-58949, the base case effective hydraulic conductivity was derived from the current calibrated Central Plateau Groundwater Model (CPGWM). The CPGWM provides calibrated hydraulic conductivity estimates for the model layers and HSUs present within the aquifer in the vicinity of WMA C. The weighted average hydraulic conductivity of the CPGWM HSUs mapped onto the WMA C flow domain provides the base case estimate of approximately 11,000 m/day. However, estimates based on pumping tests and other modeling studies have indicated values both lower and higher than the CPGWM calibrated value. The uncertainty in saturated zone hydraulic conductivity was chosen to range from 1,000 m/day to 21,000 m/day based on evaluation of all available information (RPP-RPT-58949).

Figure 5-8. 200 Realizations of Soil-Moisture as a Function of Matric Potential for H2 Unit. Red line indicates the Composite curve used in the Base Case.

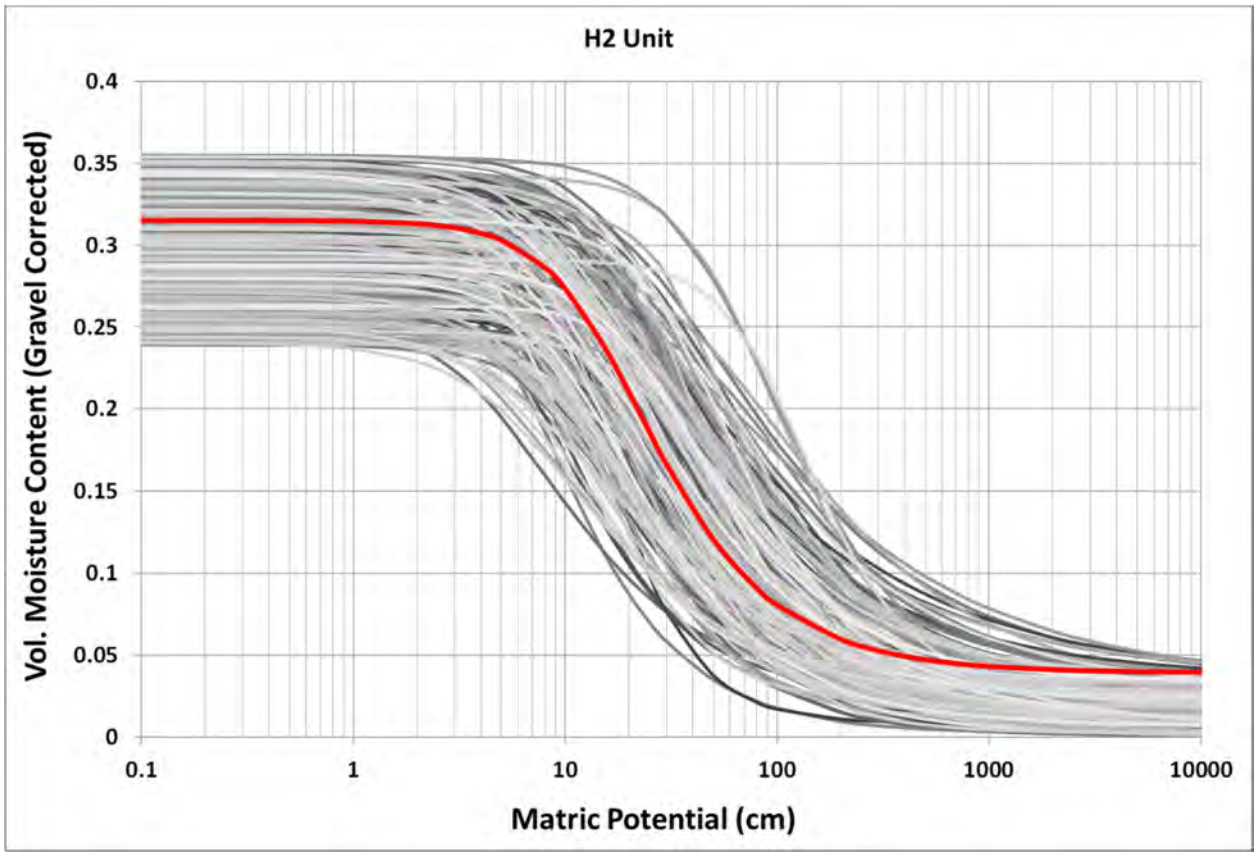

Uncertainty also exists in the hydraulic gradient within 200 East Area. Even though the hydraulic gradients are likely to remain very small (around 10^{-5} m/m) as the water table declines in the future, current monitoring has indicated that a factor of two change is possible due to Columbia River stage fluctuations and interconnections to the aquifer in the Central Plateau.

While the uncertainties in hydraulic conductivity and gradient can be defined, as discussed above, the two are not independent. As a result, it has been found useful to combine the two into a single uncertainty estimate in Darcy flux in the aquifer, which has been implemented as a factor that is multiplied to the base case Darcy flux at the upgradient boundary of the WMA C system model.

The uncertainty in the Darcy flux multiplier is dominated by uncertainty in the saturated zone hydraulic conductivity, which varies by more than an order of magnitude. The factor of two uncertainty in hydraulic gradient is comparatively smaller, and was considered to be included within the uncertainty magnitude of Darcy flux. To derive the Darcy flux multiplier,

the saturated hydraulic conductivity range (1,000 to 21,000 m/day) was divided by the best-estimate value (11,000 m/day) and a triangular distribution was chosen with the following parameters:

- Minimum = 0.09
- Most Likely = 1
- Maximum = 1.91.

Table 5-2. Uncertainty Distributions Developed for H1/H3 Hydraulic Properties.

Hydraulic Property	Selected Uncertainty Distribution	Parameters for Defining Uncertainty Distribution
Saturated hydraulic conductivity (K_s)	Log-Normal (truncated)	Geometric Mean = 1.95E-4 cm/s Geometric Standard Deviation = 8.37 Minimum = 1E-6 cm/s; Maximum = 7.77E-3 cm/s
van-Genuchten Alpha (α) parameter	Log-Normal (truncated)	Geometric Mean = 0.015 cm^{-1} Geometric Standard Deviation = 2.42 Minimum = 0.0043 cm^{-1}; Maximum = 0.0438 cm^{-1}
van-Genuchten *n* parameter	Log-Normal (truncated)	Geometric Mean = 1.58 Geometric Standard Deviation = 1.13 Minimum = 1.31; Maximum = 2.25
Saturated Moisture Content (θ_s)	Uniform	Minimum = 0.1; Maximum = 0.357
Residual Moisture Content (θ_r)	Uniform	Minimum = 0; Maximum = 0.033
Rank Correlation between hydraulic properties		Alpha and K_s = 0.92 Alpha and n = 0.38

5.2.1.7 Uncertainty in Macrodispersivity in the Vadose Zone and the Saturated Zone. In unsaturated media, the longitudinal macrodispersivity is dependent on soil moisture content (or matric potential) and differs when the primary flow and transport is parallel to the bedding plane versus being primarily perpendicular to the bedding. A range of estimates are presented in RPP-RPT-58949. These estimates are based on numerical simulations, stochastic theory, and experimental observations applicable to the relatively dry conditions observed in the vadose zone at WMA C. A range from 25 cm to 100 cm is recommended for longitudinal macrodispersivity. Under the relatively dry conditions within the WMA C vadose zone, and because the primary flow and transport direction is vertical (perpendicular to the bedding plane in the H2 unit), the lower value of 25 cm is deemed the best estimate. Consequently, a triangular distribution is used for the H2 unit with the following parameters:

- Minimum = 25 cm
- Most Likely = 25 cm
- Maximum = 100 cm.

A range in the saturated zone macrodispersivity is discussed in RPP-RPT-58949, based on a review of literature-based, scale-dependence relationships. The range in saturated zone macrodispersivity at the scale of the WMA C model is estimated to be from 1 m to 20 m. In the

system model, it is necessary to use different macrodispersivity values for each source, as the transport distance in the saturated zone to the 100 m boundary varies by the location of the source (tank and ancillary equipment), and the appropriate macrodispersivity is dependent on the distance. It is therefore necessary to use different macrodispersivities for each source so that the results match with the STOMP© 3-D process level model results for each source term. This is best accomplished by defining an uncertain parameter that multiplies (scales) the chosen macrodispersivity values for each source. To propagate uncertainty in macrodispersivity multiplier, a uniform distribution was chosen by taking the minimum and maximum values of the macrodispersivity range and dividing by the median value. This results in the following parameters that define the uniform distribution:

- Minimum = 0.095
- Maximum = 1.9.

Figure 5-9. Fitted Log-Normal Distribution to the Saturated Hydraulic Conductivity Dataset Used for H1/H3 Units.

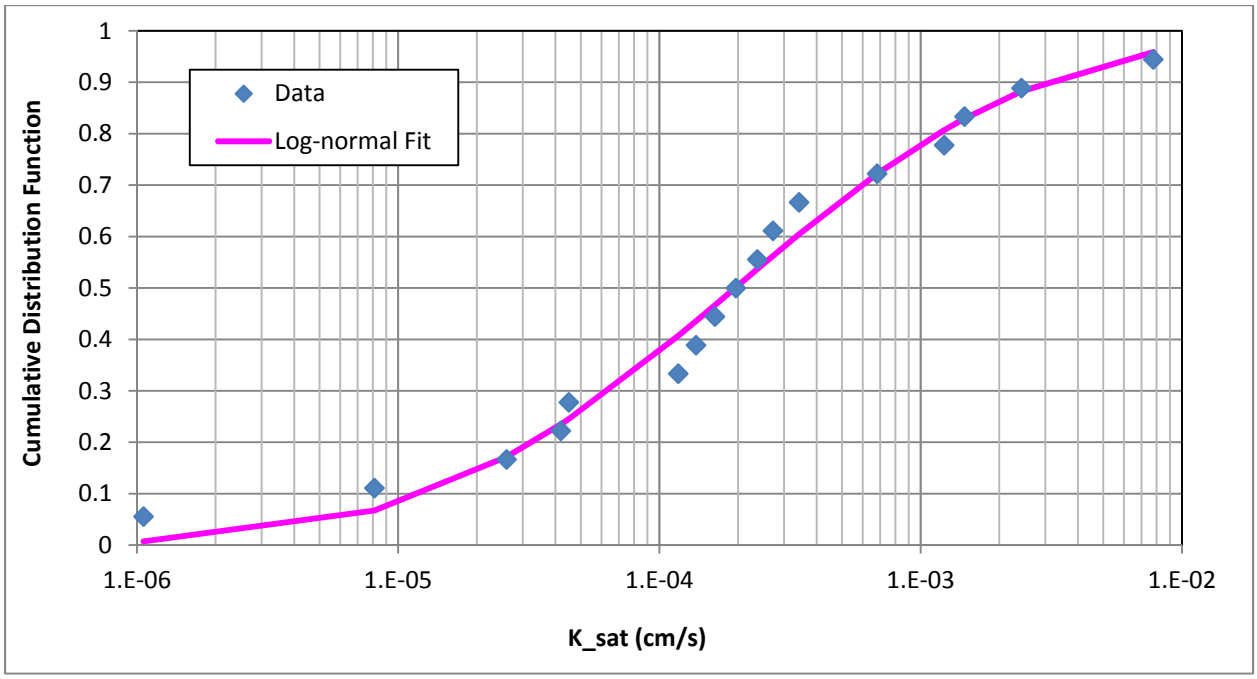

5.2.1.8 Uncertainty in Gas-Phase Tortuosity. Gas-phase tortuosity is considered to be a key parameter in the air-pathway transport calculation. Uncertainty in this parameter was implemented as a triangular distribution based on the fitted tortuosity models shown in Figure 4-17 (and discussed in Section 4.4). The most likely value of the triangular distribution is based on the best fit line given by Equation 6-18. The minimum and maximum values are described below:

- The minimum envelope curve obtained with the model of Millington and Quirk (1961) with Φ, fitted total porosity = 0.8

$$\tau = \frac{\theta_a^{10/3}}{\Phi^2} = \frac{(\phi-\theta_w)^{10/3}}{\Phi^2} \quad (8\text{-}1)$$

- The maximum envelope curve obtained with the model of Millington and Quirk (1960) with Φ, fitted total porosity = 0.4.

$$\tau = \frac{\theta_a^{2}}{\Phi^{2/3}} = \frac{(\phi-\theta_w)^{2}}{\Phi^{2/3}} \quad (8\text{-}2)$$

Where:

τ = the tortuosity
θ_a = the air content (or air-filled porosity) of the porous medium
θ_w = the water content (or water-filled porosity) of the porous medium
ϕ = the total porosity (measured)
Φ = fitted total porosity.

Two different triangular distributions were implemented related to gas-phase tortuosity, one for the gaseous transport through the tank grout and the other through the soil overburden due to different air contents.

Figure 5-10. Fitted Log-Normal Distribution to the van Genuchten "Alpha" Parameter Dataset Used for H1/H3 Units.

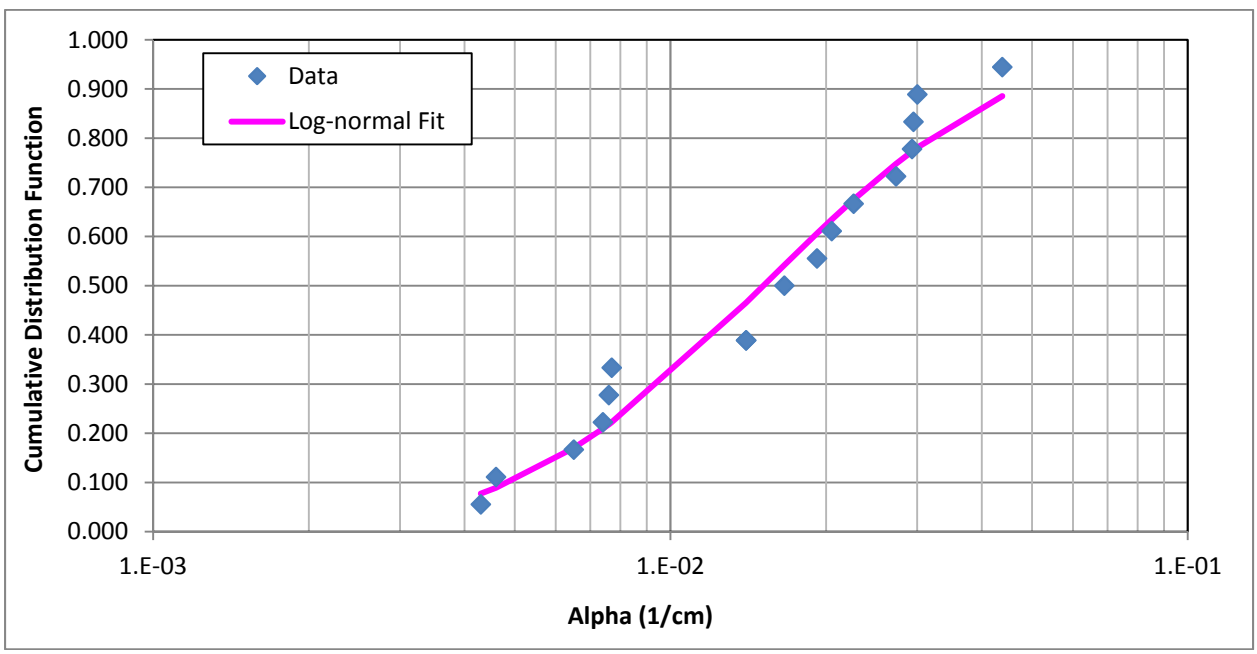

5.2.1.9 Uncertainty in Annual Wind Speed. The wind speed at Hanford varies on a monthly basis, with speeds being higher in summer and lower during winter months. The monthly and annual average speeds from Year 1945 through 2004 are summarized in Tables 5.1 through 5.4 of PNNL-15160, "Hanford Site Climatological Summary 2004 with Historical Data." The annual average wind speed for meteorological records kept from 1945 to 2004 is calculated to be

about 3.4 m/s (7.6 mi/hr) at 15.2 m (50 ft) above the ground, with a maximum annual average value of 3.9 m/s (8.8 mi/hr) and a minimum annual average value of 2.8 m/s (6.2 mi/hr). Although seasonal variability in wind speed is observed, since the dose evaluations are performed on an annual basis, the annual averaged wind speeds are considered for evaluating the effect of uncertainty in this parameter. Based on the available information, a triangular distribution was implemented with the following parameters:

- Minimum = 2.8 m/s
- Most Likely = 3.4 m/s
- Maximum = 3.9 m/s.

Figure 5-11. Fitted Log-Normal Distribution to the van Genuchten "*n*" Parameter Dataset Used for H1/H3 Units.

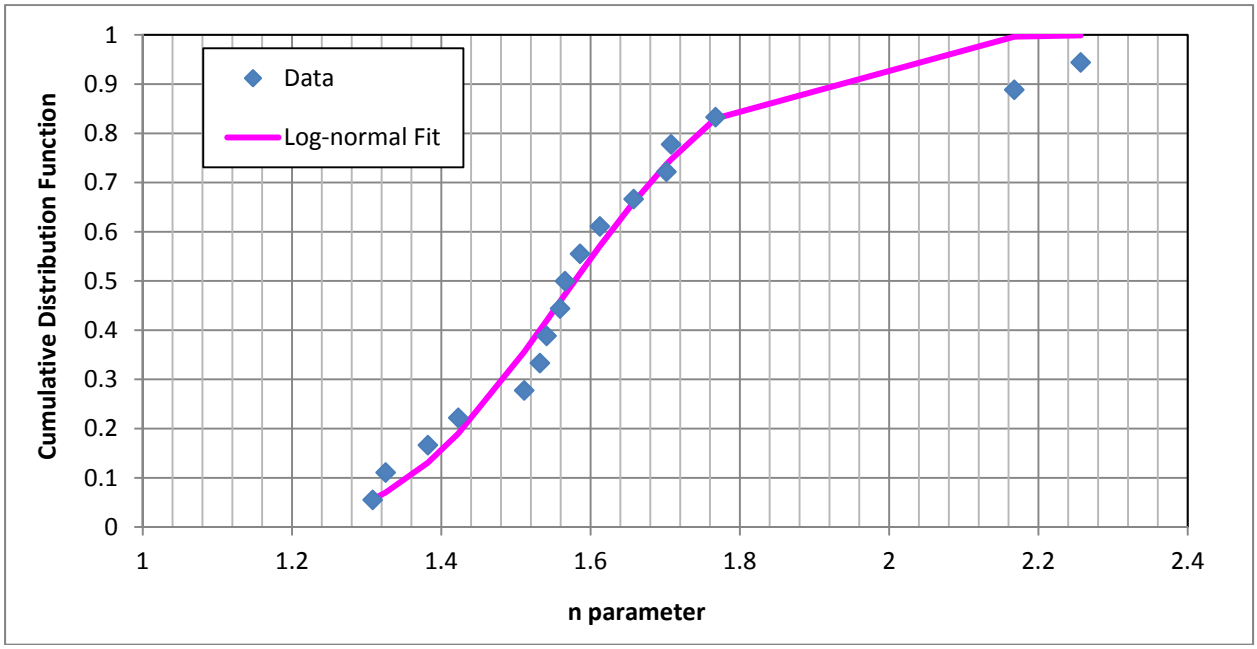

5.2.2 Development of Vadose Zone Flow Fields and Propagation of Uncertainty

The flow field for the vadose zone was abstracted from the 3-D STOMP© results as a way to efficiently evaluate the effects of uncertainty in the vadose-zone flow using the GoldSim©-based system model. The 1-D transport model implemented in GoldSim© relies on the user to provide the time-varying vertical Darcy flux and volumetric moisture content as inputs. These flow field-related parameters were extracted from the 3-D STOMP©-based model. The flow-field abstractions were performed separately for the 100-series and 200-series tanks because of different tank dimensions and thickness of HSUs within the vadose zone. The details of the flow-field abstraction approach are discussed in Section 4.3. The reasonableness of the abstraction approach was corroborated by comparisons of the results of the transport analysis conducted using the 1-D abstracted system model to the full 3-D STOMP©-based model.

Figure 5-12. 200 Realizations of Unsaturated Hydraulic Conductivity as a Function of Matric Potential for H1/H3 Units. Red line indicates the Composite curve used in the Base Case.

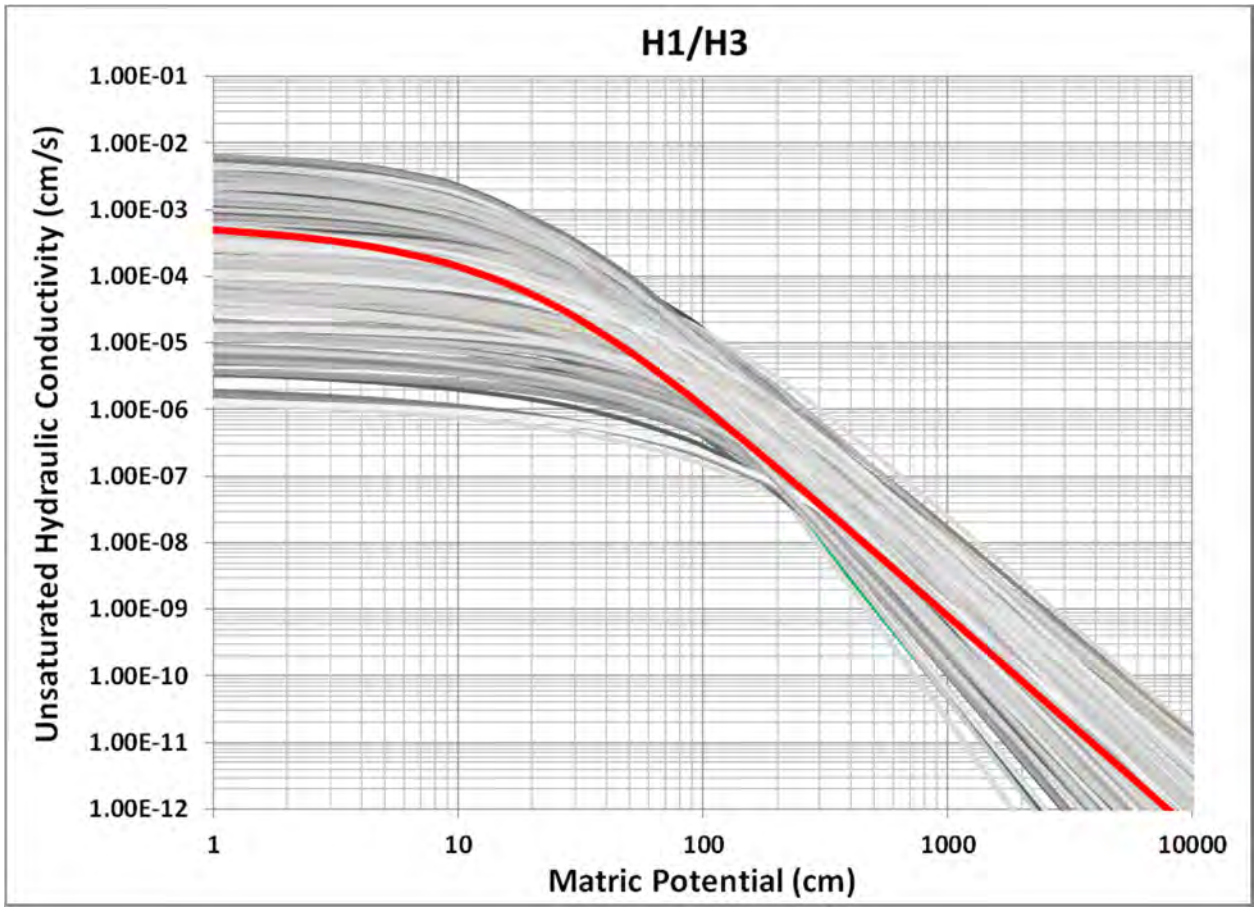

In this section, the methodology for propagating uncertainty in the flow field is discussed. The vadose zone flow field is a function of the imposed recharge rate and vadose zone hydraulic properties. The uncertainties in these two parameters are discussed in an earlier section. The uncertainty in the flow field is propagated by jointly considering the uncertainty in vadose zone hydraulic properties and the uncertainty in recharge rates. A comprehensive Monte Carlo analysis using the 3-D STOMP©-based model was deemed to be too computationally intensive and impractical for propagating the uncertainty in the flow field. Instead, the Monte Carlo analysis has been approximated by a discrete number of analyses that are intended to span the range of behavior of the flow fields in a limited number of runs. To do this, five discrete hydraulic properties were chosen along with three discrete recharge rates to cover the uncertainty range. Five sets of hydraulic properties are chosen owing to the larger uncertainty range in the flow parameters compared to a relatively smaller range in recharge rates, where three discrete parameter values were judged adequate to represent the uncertainty range. The combination of five hydraulic properties with three recharge rates results in a matrix of fifteen parameter sets. These fifteen combinations of flow parameters were each run using the 3-D STOMP© model. For each STOMP© calculation, the resulting flow field was abstracted using the methodology

discussed in Section 4.3. It was then used as an input in the 1-D transport model implemented in the GoldSim©-based system model.

Figure 5-13. 200 Realizations of Soil-Moisture as a Function of Matric Potential for H1/H3 Units. Red line indicates the Composite curve used in the Base Case.

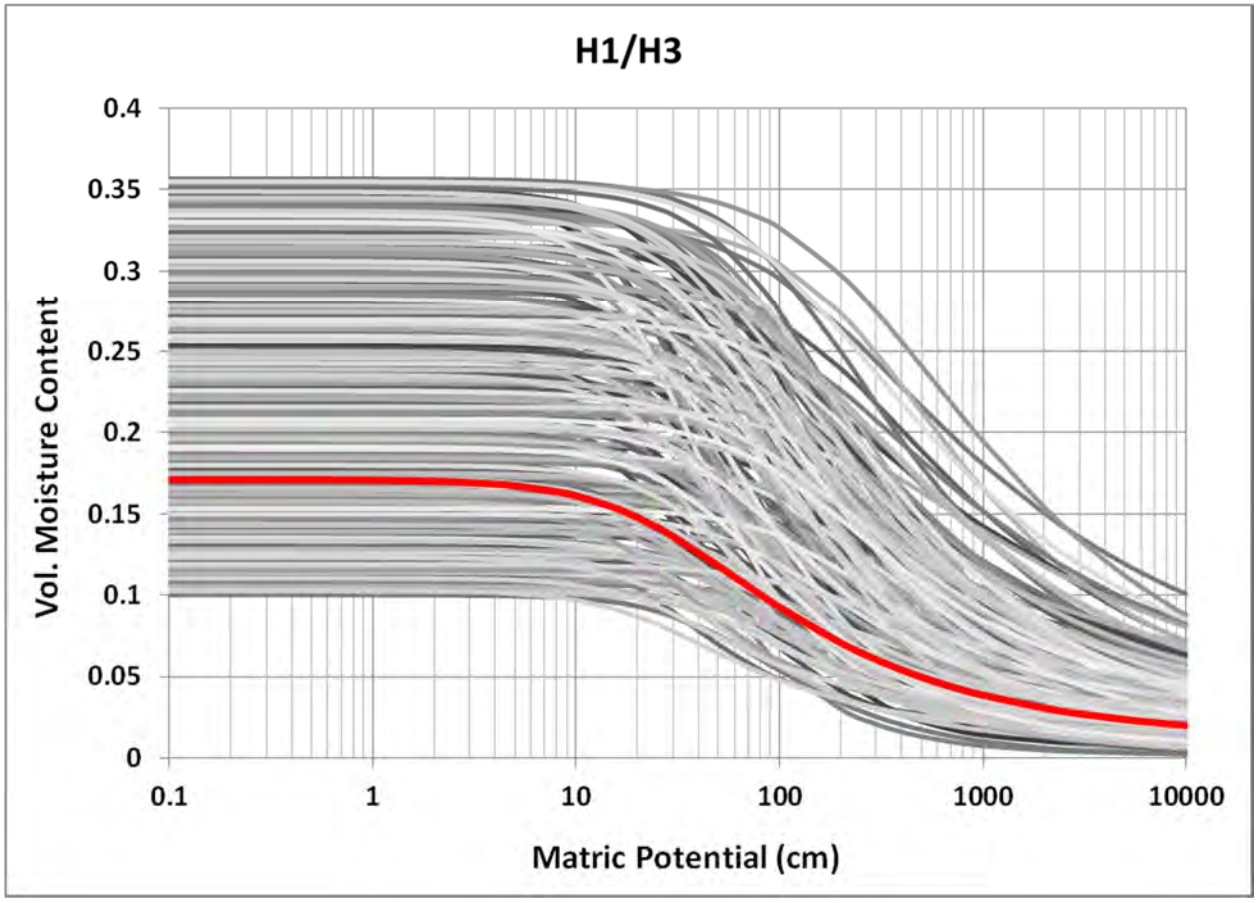

A simplification of the flow-field sampling approach was identified by observing that variations in recharge could be reproduced using an appropriate scaling method. Therefore, instead of implementing 15 flow fields, only 5 flow fields had to be implemented, defined by the combination of 5 hydraulic parameters with base case recharge rate. Therefore, the remaining 10 flow fields calculated by the 3-D STOMP©-based model were used to corroborate the scaling approach, but were not directly used in the GoldSim©-based system model.

The details of flow-field abstraction approach are described below, broken into five steps.

Step 1 – Selection of Vadose Zone Hydraulic Properties:

The uncertainty in the vadose zone hydraulic properties is discussed in an earlier section. For each HSU in the vadose zone, 200 realizations of unsaturated hydraulic conductivity (as a function of matric potential) and soil-moisture characteristic curves were generated. Although different curves could be randomly selected from the 200 realizations by using insights regarding

the flow fields, the uncertainties relevant to the PA could be more tightly defined. First is the recognition that under the post-closure conditions, the flow will closely approach a unit gradient flow field as the vertical Darcy flux equilibrates with the imposed recharge rate. Using the long-term base recharge rate of 3.5 mm/yr as an estimate of vertical Darcy flux, and with the unit hydraulic gradient assumption, the associated unsaturated hydraulic conductivity is approximately 1×10^{-8} cm/s. This allows the analysis to focus on a specific part of the characteristic curves (see Figure 5-7) in which the range of uncertainties is smaller than the full range over all conditions.

Fixing the unsaturated hydraulic conductivity, the following procedure was undertaken to derive uncertainty in hydraulic properties.

- The 200 realizations of the unsaturated hydraulic conductivity as a function of matric potential were first interrogated (for example, see Figure 5-7 for H2 unit). For each realization, the matric potential corresponding to 1×10^{-8} cm/s unsaturated hydraulic conductivity was determined.

- Next, the 200 realizations of the soil-moisture characteristic curves (for example, see Figure 5-8 for H2 unit) were interrogated based on the matric potential determined in the previous step, to determine the corresponding volumetric moisture content for that realization.

- The vertical pore water velocity was calculated for each realization by dividing the 1×10^{-8} cm/s unsaturated hydraulic conductivity by the corresponding volumetric moisture content.

- The resulting 200 vertical pore water velocity estimates were then sorted, and an empirical CDF was developed. For example, see the CDF shown in Figure 5-14 for the H2 unit.

- The above steps were repeated for each HSU, and the CDFs are presented in Figures 5-14 through 5-16.

- From the CDF, five pore water velocity values associated with the 5th, 25th, 50th, 75th, and 95th percentiles were chosen to represent the uncertainty in pore water velocity for a given HSU. The realizations associated with these percentiles were selected, and the hydraulic properties associated with the realization are noted for the HSU. Table 5-5 summarizes the hydraulic properties associated with the various percentiles in terms of the sampled van Genuchten-Mualem parameters. For the purpose of comparison, the parameters chosen for the base case are also presented.

Step 2 – Selection of Recharge Rates:

Recharge rate varies both temporally and spatially as discussed in an earlier section. Table 5-1 presents the uncertainty distribution in recharge rates for various time periods. For the purpose of abstracting the flow field, the time periods of interest are operational and post-closure periods,

and the spatial area of interest is the one designated as WMA C since all of the contaminant sources are within this area. From the triangular distributions developed for each time period, the 5th percentile and the maximum recharge values are selected along with the base case recharge values for the flow-field calculations. These values are representative of the uncertainty in recharge rates (the minimum value was not used due to very low probability of occurrence). The selected recharge rates are summarized in Table 5-6.

Table 5-3. Uncertainty Distributions Developed for Backfill Hydraulic Properties.

Hydraulic Property	Selected Uncertainty Distribution	Parameters for Defining Uncertainty Distribution
Saturated hydraulic conductivity (K_s)	Log-Normal (truncated)	Geometric Mean = 5.52E-5 cm/s Geometric Standard Deviation = 5.48 Minimum = 1E-6 cm/s; Maximum = 3.42E-4 cm/s
van-Genuchten Alpha (α) parameter	Log-Normal (truncated)	Geometric Mean = 0.0086 cm^{-1} Geometric Standard Deviation = 2.63 Minimum = 0.0025 cm^{-1}; Maximum = 0.030 cm^{-1}
van-Genuchten *n* parameter	Log-Normal (truncated)	Geometric Mean = 1.53 Geometric Standard Deviation = 1.07 Minimum = 1.31; Maximum = 1.66
Saturated Moisture Content (θ_s)	Uniform	Minimum = 0.1; Maximum = 0.236
Residual Moisture Content (θ_r)	Uniform	Minimum = 0; Maximum = 0.018
Rank Correlation between hydraulic properties		Alpha and K_s = 0.71 Alpha and n = 0.47

Step 3 – Flow-Field Abstraction:

The five hydraulic properties corresponding to the vertical pore velocity percentiles and the three recharge rates were used to develop 15 combinations of flow-field inputs. The 3-D STOMP©-based model was used to calculate the flow field for each input combination. The results from the 3-D model were abstracted to generate separate flow fields for the 100-series and 200-series tanks. Each flow field contains time-dependent vertical Darcy flux and volumetric moisture content that is applicable to the vertical grid discretization used in the GoldSim©-based system model (Table 4-2).

Step 4 – Scaling of Flow Field by Recharge Rate:

Upon evaluation of the 15 flow fields, it was found that a linear relationship exists between vertical Darcy flux and the recharge rate when hydraulic properties remain unchanged. Similarly, a linear relationship exists between volumetric moisture content and recharge rate. This information was used to reduce the number of flow fields being implemented in the system model to only five flow fields. The five flow fields were generated based on the combination of five hydraulic properties with the base case recharge rate. These flow fields are scaled based on sampled recharge rate using the regression equations. This approach allows for directly

estimating the Darcy flux and volumetric moisture content for any sampled recharge rate without going through a demanding abstraction process.

Table 5-4. Uncertainty in K_d Values (mL/g) for Sand As a Triangular Distribution. (2 sheets)

Element	Most Likely	Minimum	Maximum	Reference
Ac	350	100	1,500	PNNL-16663
Al	1,500	1,500	1,500	RPP-RPT-46088
Am	600	200	2,000	PNNL-17154
B	3	3	3	RPP-RPT-46088
C	1	0	100	PNNL-17154
Cd	6.7	6.7	6.7	RPP-RPT-46088
Cm	350	100	1,500	PNNL-16663
CN	0	0	0	RPP-RPT-46088
Co	0	0	10	PNNL-17154
Cr	0	0	3	PNNL-17154
Cs	100	10	1,000	PNNL-17154
Eu	10	3	100	PNNL-17154
F	0	0	1	PNNL-17154
Fe	25	25	25	RPP-RPT-46088
H	0	0	0	PNNL-17154
Hg	52	52	100	RPP-RPT-46088
I	0.2	0	2	PNNL-17154
Mn	65	65	65	RPP-RPT-46088
Nb	0	0	0.1	PNNL-16663
Ni	3	1	20	PNNL-17154
NO_2	0	0	0.1	PNNL-17154
NO_3	0	0	0.1	PNNL-17154
Np	10	2	30	PNNL-17154
Pa	300	40	500	PNNL-17154
Pb	10	3	100	PNNL-17154
Pu	600	200	2,000	PNNL-17154
Ra	10	5	20	PNNL-17154
Rn	0	0	0	No relevant information available

Table 5-4. Uncertainty in K_d Values (mL/g) for Sand As a Triangular Distribution. (2 sheets)

Element	Most Likely	Minimum	Maximum	Reference
Se	0.1	0	3	PNNL-17154
Sm	10	3	100	PNNL-17154
Sn	0.5	0	20	PNNL-17154
Sr	10	5	100	PNNL-17154
Tributyl phosphate	1.89	1.89	1.89	RPP-RPT-46088
Tc	0	0	0.1	PNNL-16663
Th	300	40	500	PNNL-16663
U	0.6	0.2	2	RPP-RPT-46088
U_total	0.6	0.2	2	PNNL-17154
Zr	300	40	500	PNNL-16663

References:
PNNL-16663, "Geochemical Processes Data Package for the Vadose Zone in the Single-Shell Tank Waste Management Areas at the Hanford Site."
PNNL-17154, "Geochemical Characterization Data Package for the Vadose Zone in the Single-Shell Tank Waste Management Areas at the Hanford Site."
RPP-RPT-46088, "Flow and Transport in the Natural System at Waste Management Area C."

The development of the regression equations was done as follows.

- For a selected hydraulic property percentile, the 3-D STOMP© model was used for three recharge rates presented in Table 5-6.

- Vertical Darcy flux and volumetric moisture content values were abstracted from STOMP© model nodes that correspond to the GoldSim© 1-D discretization. This was done for Calendar Year 2300 (to represent early the post-closure time period from Calendar Year 2020 to 2520 while the surface cover is intact) and at Calendar Year 5020 (to represent the late post-closure period beyond Calendar Year 2520 following surface barrier degradation).

- For the set of flow fields where the hydraulic property is held constant but recharge rate varies, the extracted vertical Darcy flux and volumetric moisture content were normalized by dividing by the values obtained from the base case recharge flow field. Table 5-7 provides an example of normalized Darcy flux for Calendar Year 2300 below tank C-105 for the 3-D STOMP© simulations with 5th percentile hydraulic properties at different recharge rates. This analysis was done for each time period.

- Normalized Darcy flux was plotted against the normalized recharge rates, and a linear regression analysis was performed to determine the relationships shown in Figures 5-17 and 5-18. These relationships are representative of the H1 unit and the deeper H2 and

H3 units. Results of the regression analysis shown in Figure 5-17 are based on a STOMP© node located in H1 unit (node 66), and are used to scale the flow field for all other nodes in H1 unit in the GoldSim©-based system model. For the deeper H2 and H3 units, the regression analysis shown in Figure 5-18 was performed after averaging the results of several STOMP© nodes located in H2 and H3 units (nodes 63, 61, 55, 47, 39, 31, 24, 18, and 14). Results of the regression analysis were used to scale the flow field for all nodes that define H2 and H3 in the GoldSim©-based system model.

- A regression equation was also developed between normalized volumetric moisture content and normalized recharge rate in the same way. This is shown in Figures 5-19 and 5-20.

- These steps were repeated for each of the five hydraulic properties. This resulted in the development of linear relationships between normalized Darcy flux and normalized recharge rate, and between normalized volumetric moisture content and normalized recharge rate.

Figure 5-14. Cumulative Distribution Function of Pore Water Velocity from 200 Realizations for the H2 Unit.

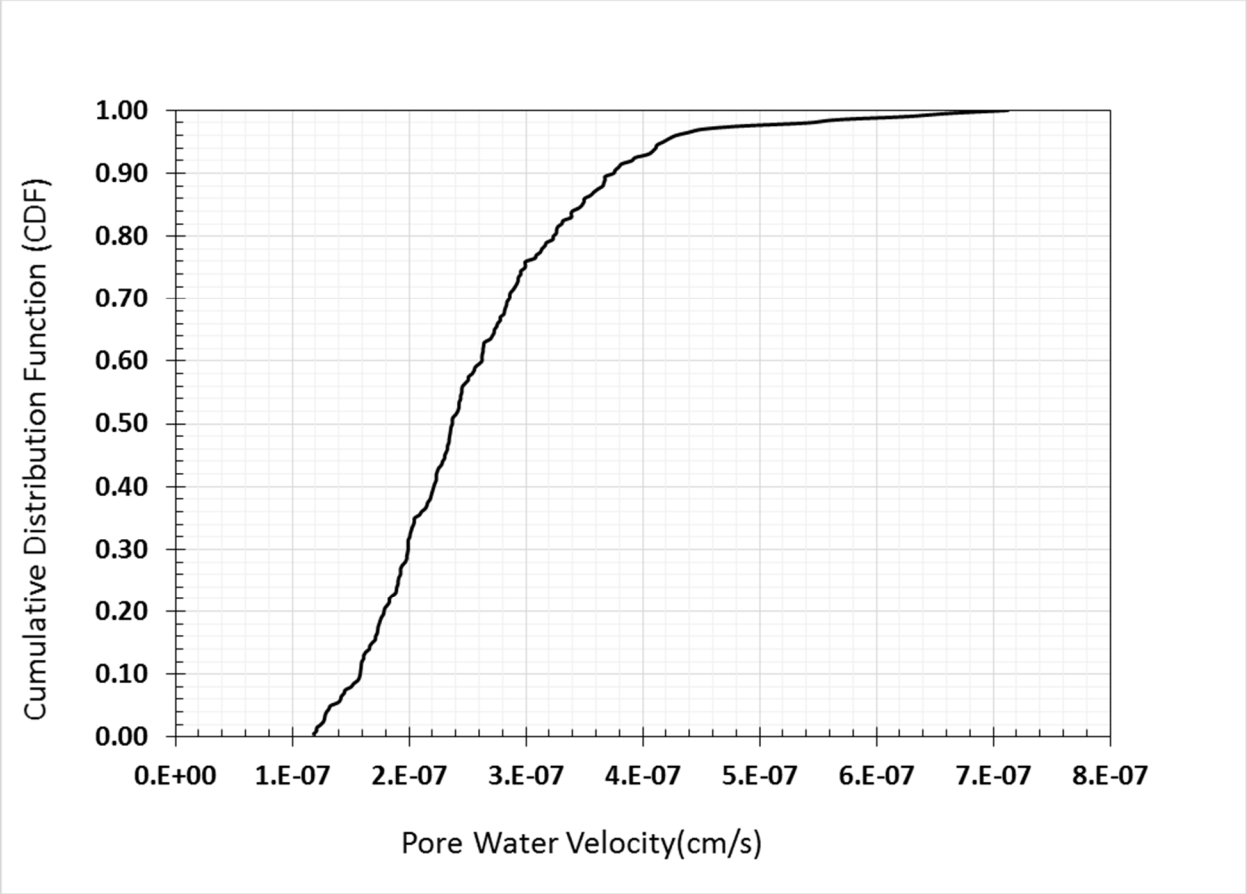

Figure 5-15. Cumulative Distribution Function of Pore Water Velocity from 200 Realizations for the H1/H3 Unit.

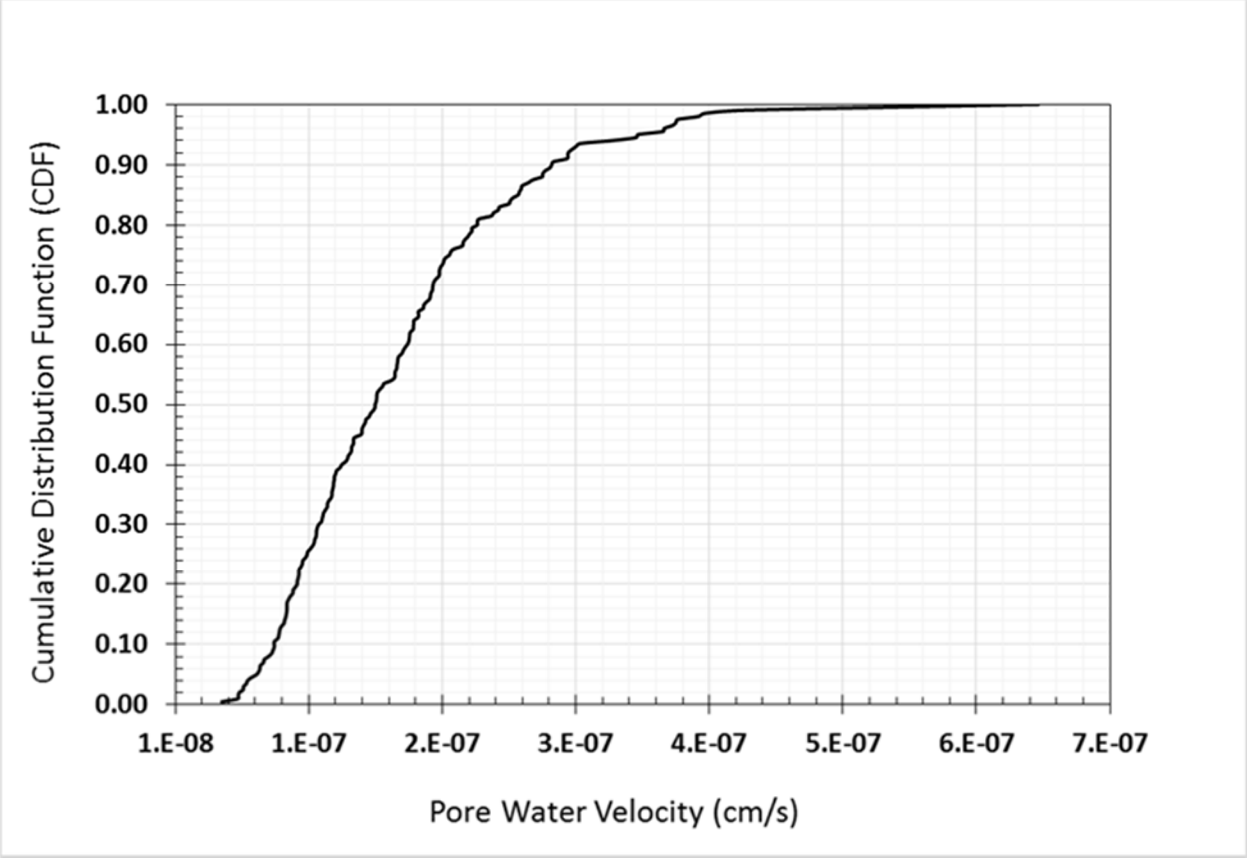

This algorithm resulted in a total of 40 regression equations, which were implemented in the GoldSim©-based system model for Darcy flux scaling calculations. The large number of regression equations was the result of separate regression relationships for the early post-closure time period (while the surface cover was intact) and the late post-closure time period (after surface cover is degraded), and then calculated separately for H1 unit and H2/H3 units for the 100-series tanks and 200-series tanks. The regression equations are presented in Table 5-8 for the 100-series tanks and in Table 5-9 for the 200-series tanks. Once a value is calculated from the regression equation, the Darcy flux derived from the base case recharge rate abstraction process can be scaled by multiplying with this value to generate a new Darcy flux for the selected hydraulic property.

During the regression analyses, it was observed that linear regression relationships for normalized volumetric moisture content and normalized recharge rate do not vary appreciably when different hydraulic properties were used, and between 100-series and 200-series tanks. As a result, only four regression equations are needed for scaling the volumetric moisture content. These are calculated separately for the H1 unit and the H2/H3 units for early post-closure and late post-closure time periods, and are summarized in Table 5-10. Once a value is calculated from the regression equation, the volumetric moisture content derived from the base case

recharge rate can be scaled by multiplying with this value to generate the new volumetric moisture content.

Figure 5-16. Cumulative Distribution Function of Pore Water Velocity from 200 Realizations for the Backfill Unit.

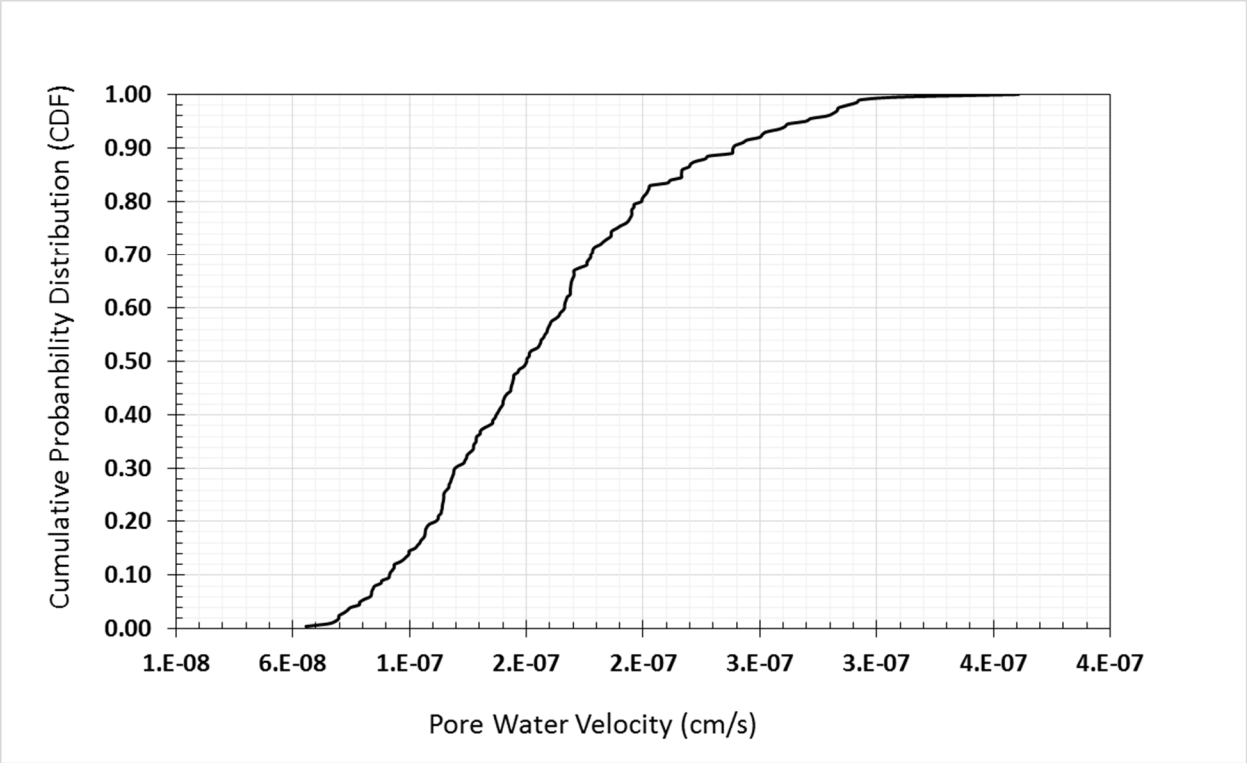

This scaling method was verified by comparing flow fields calculated using the regression equation with the flow field from 3-D STOMP© simulations for each of the hydraulic properties. An example of the comparison for the 5th percentile hydraulic property case is shown in Figure 5-21(a-d) for representative nodes from H1 and H2 units under 100-series and 200-series tanks. Very good agreement is observed between vertical Darcy flux calculated using the regression equation and that obtained from STOMP©.

Note that the scaling multipliers developed for vertical Darcy flux and volumetric moisture content are dimensionless and are applied to values calculated under base recharge conditions, as abstracted from the 3-D STOMP© model results for each of the five hydraulic properties. The results of using the regression equations over the minimum and maximum recharge rates are presented in Appendix A. The purpose of Appendix A is to illustrate the uncertainty range in vertical average linear pore water velocities within the vadose zone for the post-closure time period. Based on the uncertainty ranges calculated for each hydraulic property under minimum and maximum recharge rates, it is found that the range in vertical linear pore water velocities is the largest for the 95th percentile hydraulic property (around a factor of 6.5) and minimum for the 25th percentile hydraulic property (factor of 2 to 2.5). For other hydraulic properties, the range varies from factor of 3 to 4. These results indicate that for realizations where 95th percentile

hydraulic property is selected during uncertainty analysis, greater variance in travel times can be expected compared to other hydraulic properties (under similar recharge rate range).

Table 5-5. van Genuchten-Mualem Parameters Corresponding to the Percentiles Selected from the Vertical Pore Water Velocity Cumulative Distribution Functions.

Strata (tension)	Percentile	K_s (cm/s)	θ_s	θ_r	α (1/cm)	n
Backfill	5th Percentile	7.91E-06	0.2217	1.23E-02	0.0026	1.441
	25th Percentile	1.08E-05	0.1319	1.57E-02	0.0031	1.31
	50th Percentile	7.31E-05	0.203	5.94E-03	0.0086	1.577
	75th Percentile	1.98E-04	0.1409	1.42E-02	0.0123	1.47
	95th Percentile	3.13E-04	0.1287	1.35E-02	0.0298	1.635
	Base Case	5.60E-04	0.138	1.00E-02	0.021	1.374
Hanford H1/H3	5th Percentile	7.78E-05	0.2887	3.24E-02	0.0121	1.335
	25th Percentile	5.14E-06	0.2118	2.08E-02	0.0062	1.733
	50th Percentile	1.49E-04	0.1735	3.06E-02	0.0124	1.603
	75th Percentile	1.58E-03	0.3094	7.01E-03	0.0238	1.717
	95th Percentile	2.99E-04	0.1024	1.45E-02	0.0152	1.76
	Base Case	7.70E-04	0.1712	1.11E-02	0.036	1.491
Hanford H2	5th Percentile	1.79E-03	0.3541	2.89E-02	0.0402	1.633
	25th Percentile	1.15E-03	0.2893	2.99E-02	0.0266	1.971
	50th Percentile	2.20E-02	0.3304	2.72E-02	0.1253	1.889
	75th Percentile	3.79E-02	0.3474	2.05E-02	0.0966	1.966
	95th Percentile	1.68E-02	0.2652	2.11E-03	0.1076	1.724
	Base Case	4.15E-03	0.3152	3.92E-02	0.0631	2.047

Note: The connectivity parameter ℓ is assumed to be 0.5 for all strata and all percentile values.

Table 5-6. Recharge Rate Used in Scaling Flow Field.

	Base Case Recharge Rate	5th Percentile Recharge Rate	Maximum Recharge Rate
Operational Period (Calendar Year 1945-2020)	100 mm/yr	57.30 mm/yr	140 mm/yr
Early Post-Closure (Calendar Year 2020-2520)	0.5 mm/yr	0.23 mm/yr	0.9 mm/yr
Late Post-Closure (Calendar Year >2520)	3.5 mm/yr	1.07 mm/yr	5.2 mm/yr

Table 5-7. Example of Normalized Darcy Flux at Calendar Year 2300 from Selected Three-Dimensional STOMP©-based Model Nodes under Tank 241-C-105 Using 5th Percentile Hydraulic Property.

Node Location	Normalized Darcy Flux: Base Recharge Rate	Normalized Darcy Flux: 5th Percentile Recharge Rate	Normalized Darcy Flux: Maximum Recharge Rate
C-105_66	1	0.5012	1.3086
C-105_63	1	0.5079	1.2964
C-105_61	1	0.4588	1.3587
C-105_55	1	0.4936	1.3802
C-105_47	1	0.5427	1.3820
C-105_39	1	0.5947	1.3560
C-105_31	1	0.6407	1.3188
C-105_24	1	0.6765	1.2864
C-105_18	1	0.6759	1.2861
C-105_14	1	0.6832	1.2791

Subsurface Transport Over Multiple Phases (STOMP)© is copyrighted by Battelle Memorial Institute, 1996.

Step 5 – Sampling of Flow Fields:

In the Monte Carlo analysis for the system model, a flow field is selected for each realization. Using the approach described in Steps 1 through 4, the flow fields are developed for five hydraulic properties based on the selection of various percentiles from the vertical pore water velocity CDF (for example, see Figure 5-14 for the H2 unit). The percentiles selected were 5th, 25th, 50th, 75th, and 95th to discretely represent the uncertainty in the CDF. A discrete probability distribution was developed for sampling the five hydraulic properties (flow fields). The 5th and 95th percentile hydraulic properties were given a probability of 0.1 each, the 25th and 75th percentile hydraulic properties were given a probability of 0.25 each, and the 50th percentile hydraulic property was given a probability of 0.3, leading to a discrete probability distribution with a median value being represented by the 50th percentile hydraulic property. The rationale for this probability weighting was based on the understanding that the 5th and 95th percentile hydraulic properties represent the extremes of the pore water velocity distribution, and should have a lower probability of being selected compared to the other percentile hydraulic properties, with the 50th percentile hydraulic property being the most probable. As a result, the 25th and 75th percentile hydraulic properties are given slightly lower weighting than the 50th percentile hydraulic property. The selected discrete probability distribution results in the median being the 50th percentile hydraulic property, which is also the most probable flow field.

Figure 5-17. Normalized Darcy Flux for Node 66 during (a) Early Post-Closure Period (b) Late Post-Closure Period.

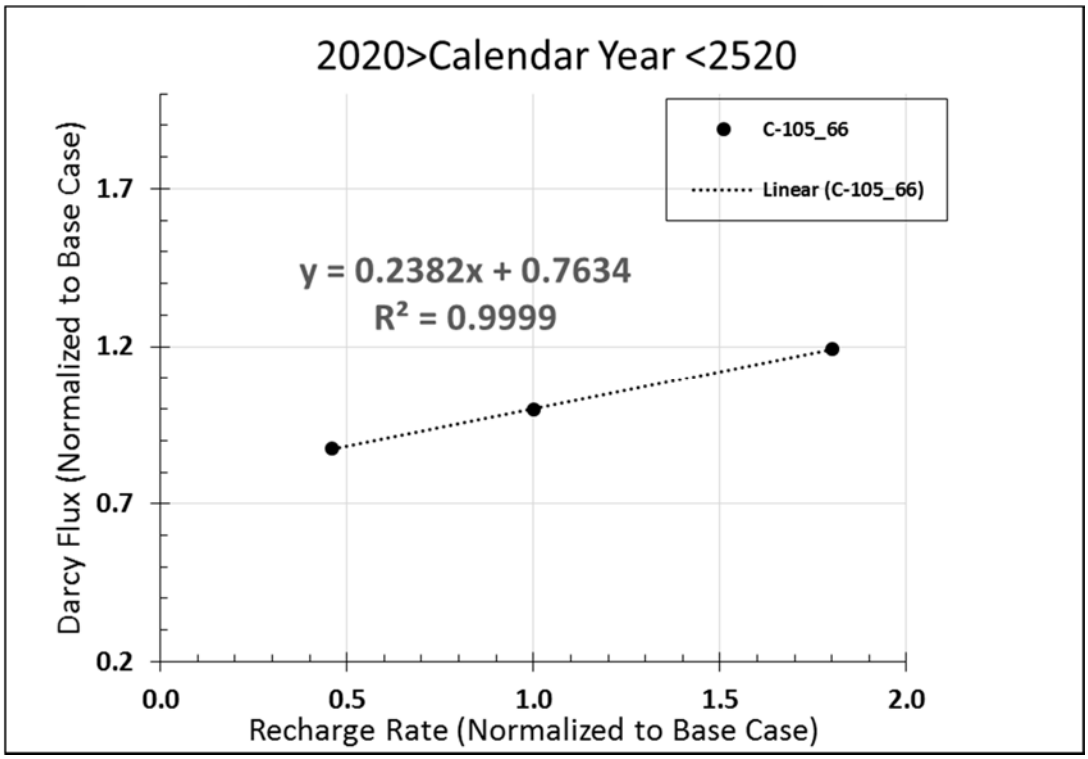

(a)

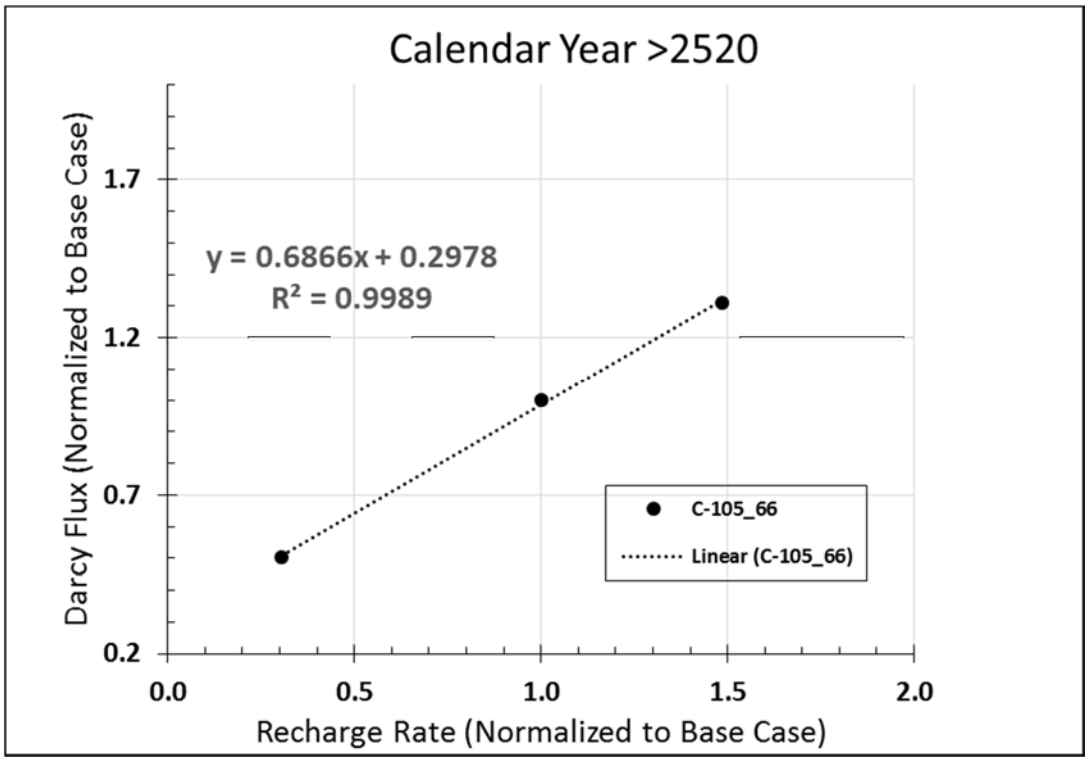

(b)

Figure 5-18. Normalized Darcy Flux for Deeper Nodes during (a) Early Post-Closure Period (b) Late Post-Closure Period.

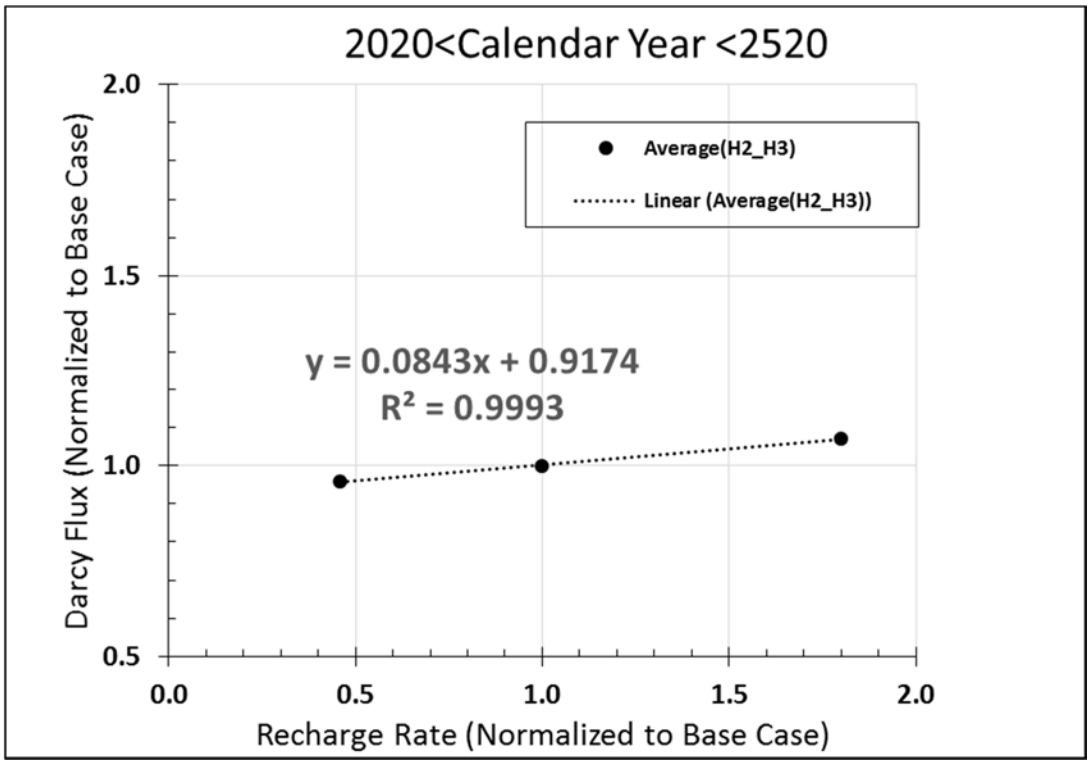

(a)

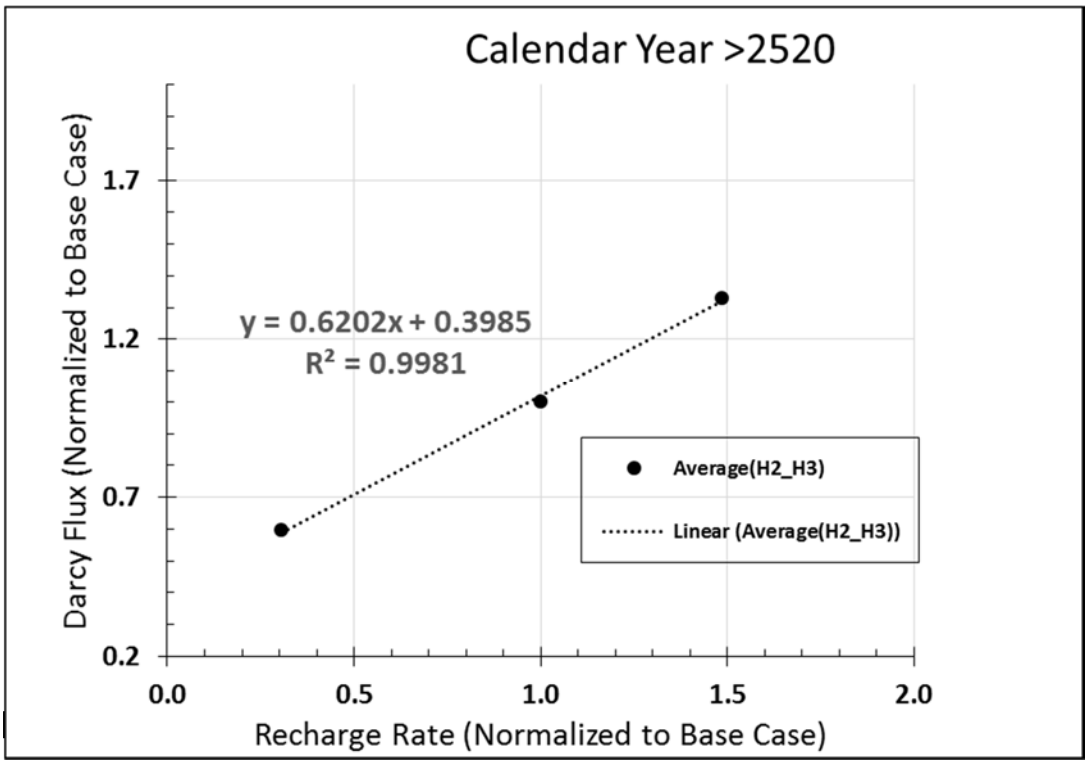

(b)

Figure 5-19. Normalized Moisture Content for Node 66 during (a) Early Post-Closure Period (b) Late Post-Closure Period.

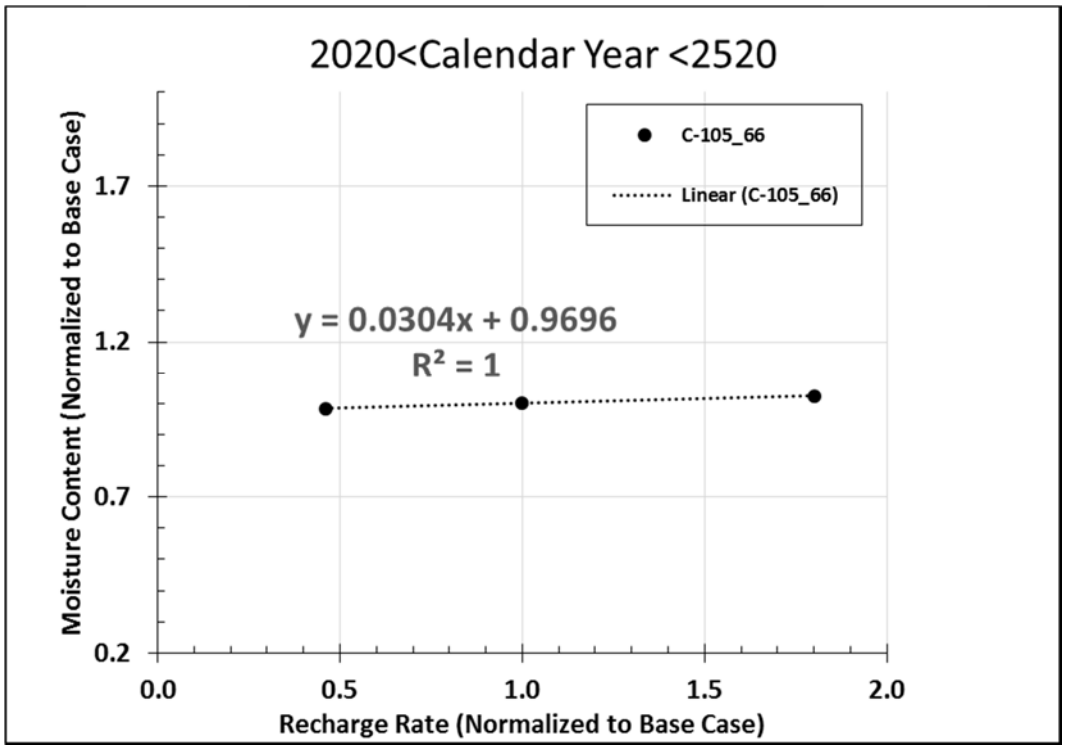

(a)

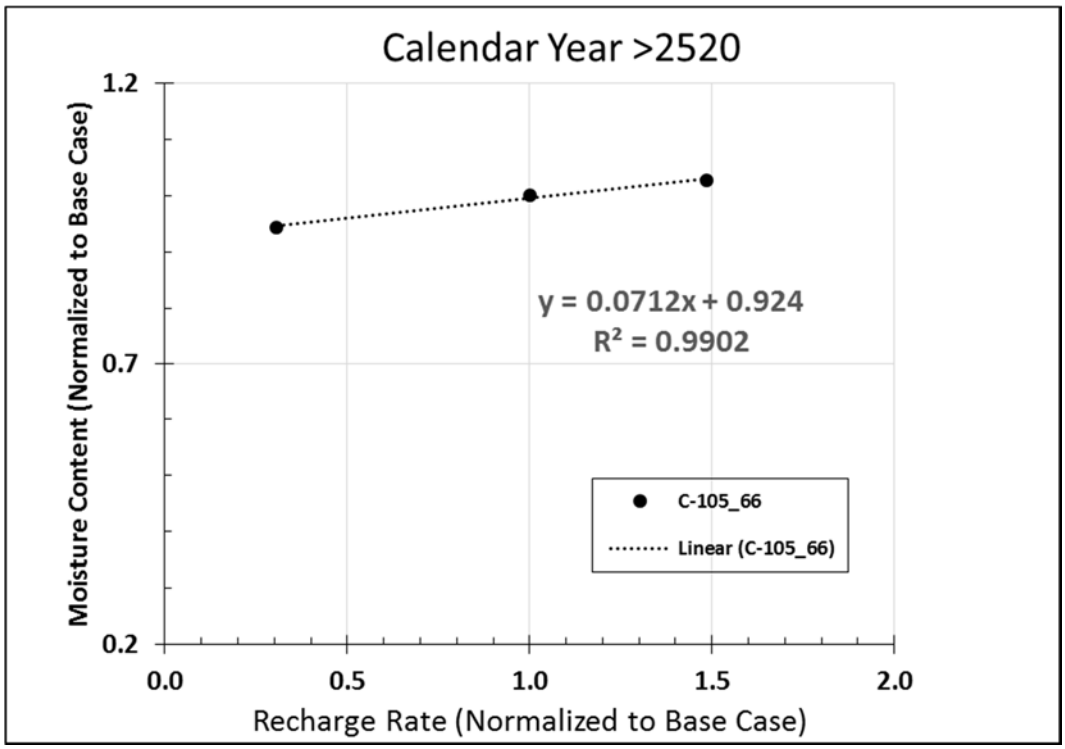

(b)

Figure 5-20. Normalized Moisture Content for Deeper Nodes during (a) Early Post-Closure Period (b) Late Post-Closure Period.

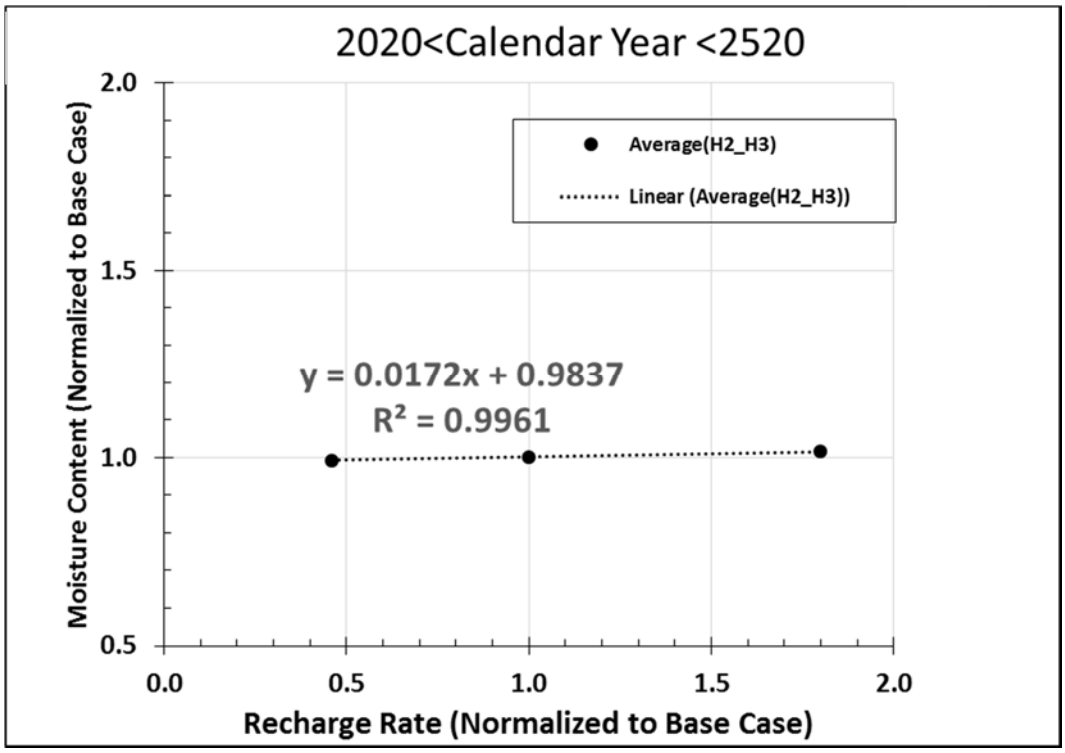

(a)

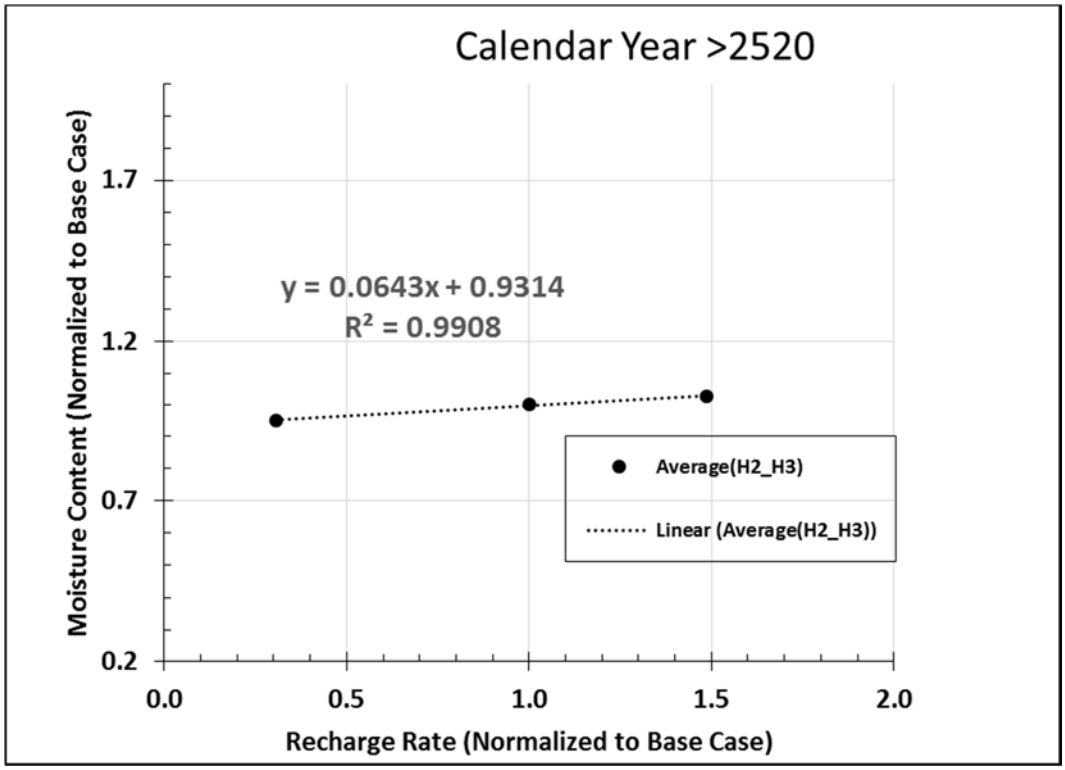

(b)

Table 5-8. Regression Equations for Scaling Darcy Flux for 100-Series Tank.

Vadose Zone Hydraulic Properties	Normalized Darcy Flux: 100 Series Tank			
	H1 Unit		H2/H3 Unit	
	2020<Calendar Year<2520	Calendar Year>2520	2020<Calendar Year<2520	Calendar Year>2520
5th Percentile Case Hydraulic Properties	0.2382*x+0.7634	0.6866*x+0.2978	0.0843*x+0.9174	0.6202*x+0.3985
25th Percentile Case Hydraulic Properties	0.2562*x+0.7406	0.5083*x+0.4701	0.1261*x+0.8763	0.7149*x+0.3032
50th Percentile Case Hydraulic Properties	0.2652*x+0.7363	0.7305*x+0.2670	0.2243*x+0.7829	0.8141*x+0.1940
75th Percentile Case Hydraulic Properties	0.3265*x+0.6721	0.7233*x+0.2580	0.2602*x+0.7474	0.8109*x+0.1946
95th Percentile Case Hydraulic Properties	0.8006*x+0.2164	0.899*x+0.0660	0.2795*x+0.7409	0.9497*x+0.0775

x = Sampled recharge rate / Base case recharge rate

Table 5-9. Regression Equations for Scaling Darcy Flux for 200-Series Tank.

Vadose Zone Hydraulic Properties	Normalized Darcy Flux: 200 Series Tank			
	H1 Unit		H2/H3 Unit	
	2020<Calendar Year<2520	Calendar Year>2520	2020<Calendar Year<2520	Calendar Year>2520
5th Percentile Case Hydraulic Properties	0.2456*x+0.7566	0.7221*x+0.2714	0.0485*x+0.9523	0.4389*x+0.5651
25th Percentile Case Hydraulic Properties	0.2832*x+0.7155	0.7253*x+0.2754	0.0781*x+0.9237	0.5536*x+0.4573
50th Percentile Case Hydraulic Properties	0.2604*x+0.7415	0.7512*x+0.2540	0.1236*x+0.8783	0.5572*x+0.4463
75th Percentile Case Hydraulic Properties	0.3260*x+0.6735	0.7614*x+0.2361	0.1472*x+0.8554	0.6110*x+0.3950
95th Percentile Case Hydraulic Properties	0.3731*x+0.6336	0.8759*x+0.1345	0.1480*x+0.8567	0.6252*x+0.3798

x = Sampled recharge rate / Base case recharge rate

Table 5-10. Regression Equations for Scaling Volumetric Moisture Content.

Normalized Volumetric Moisture Content			
H1 Unit		**H2/H3 Unit**	
2020<Calendar Year<2520	**Calendar Year>2520**	**2020<Calendar Year<2520**	**Calendar Year>2520**
0.0304*x+0.9696	0.0712*x+0.9240	0.0172*x+0.9837	0.0643*x+0.9314

x = Sampled recharge rate / Base case recharge rate

Figure 5-21. Comparison between Darcy Flux Calculated using Regression Equation and that Obtained from Three-Dimensional Subsurface Transport Over Multiple Phases Based Model Simulation for the 5th Percentile Hydraulic Property Case for (a) H1 Unit under 100-Series Tank (Node 66); (b) H2 Unit under 100-Series Tank (Node 47); (c) H1 Unit under 200-Series Tank (Node 66); and (d) H2 Unit under 200-Series Tank (Node 43). (sheet 1 of 4)

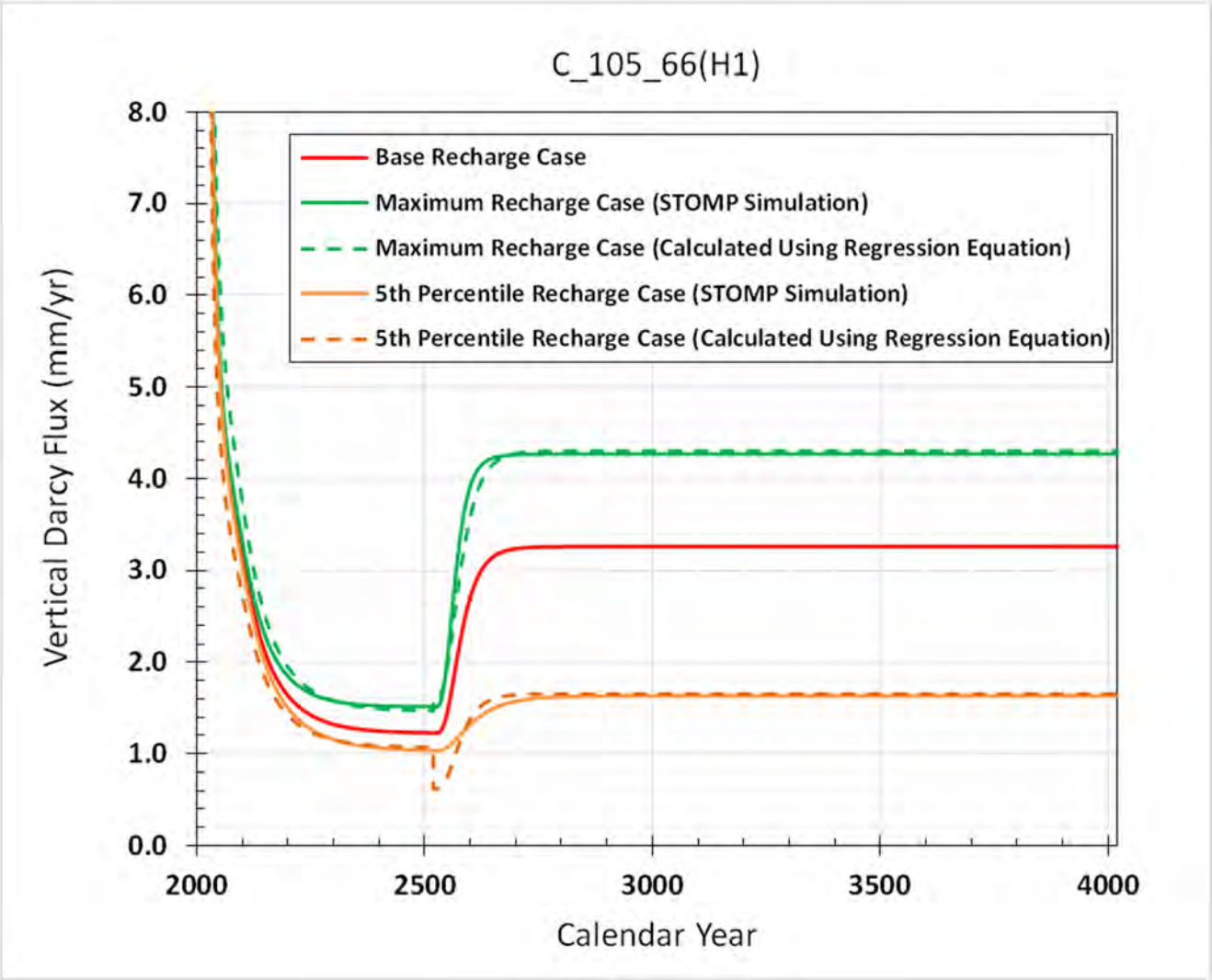

Figure 5-21. Comparison between Darcy Flux Calculated using Regression Equation and that Obtained from Three-Dimensional Subsurface Transport Over Multiple Phases Based Model Simulation for the 5th Percentile Hydraulic Property Case for (a) H1 Unit under 100-Series Tank (Node 66); (b) H2 Unit under 100-Series Tank (Node 47); (c) H1 Unit under 200-Series Tank (Node 66); and (d) H2 Unit under 200-Series Tank (Node 43). (sheet 2 of 4)

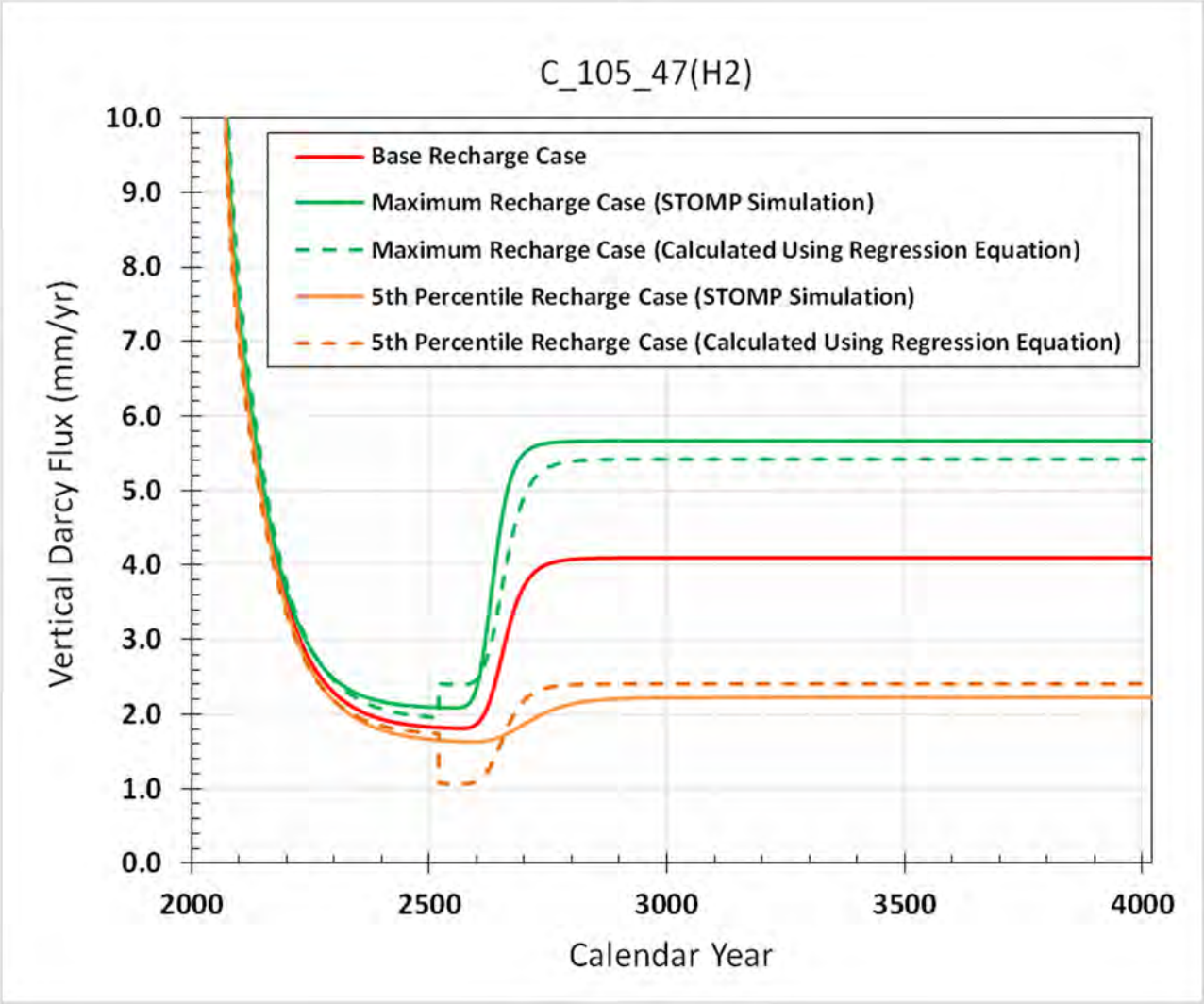

Figure 5-21. Comparison between Darcy Flux Calculated using Regression Equation and that Obtained from Three-Dimensional Subsurface Transport Over Multiple Phases Based Model Simulation for the 5th Percentile Hydraulic Property Case for (a) H1 Unit under 100-Series Tank (Node 66); (b) H2 Unit under 100-Series Tank (Node 47); (c) H1 Unit under 200-Series Tank (Node 66); and (d) H2 Unit under 200-Series Tank (Node 43). (sheet 3 of 4)

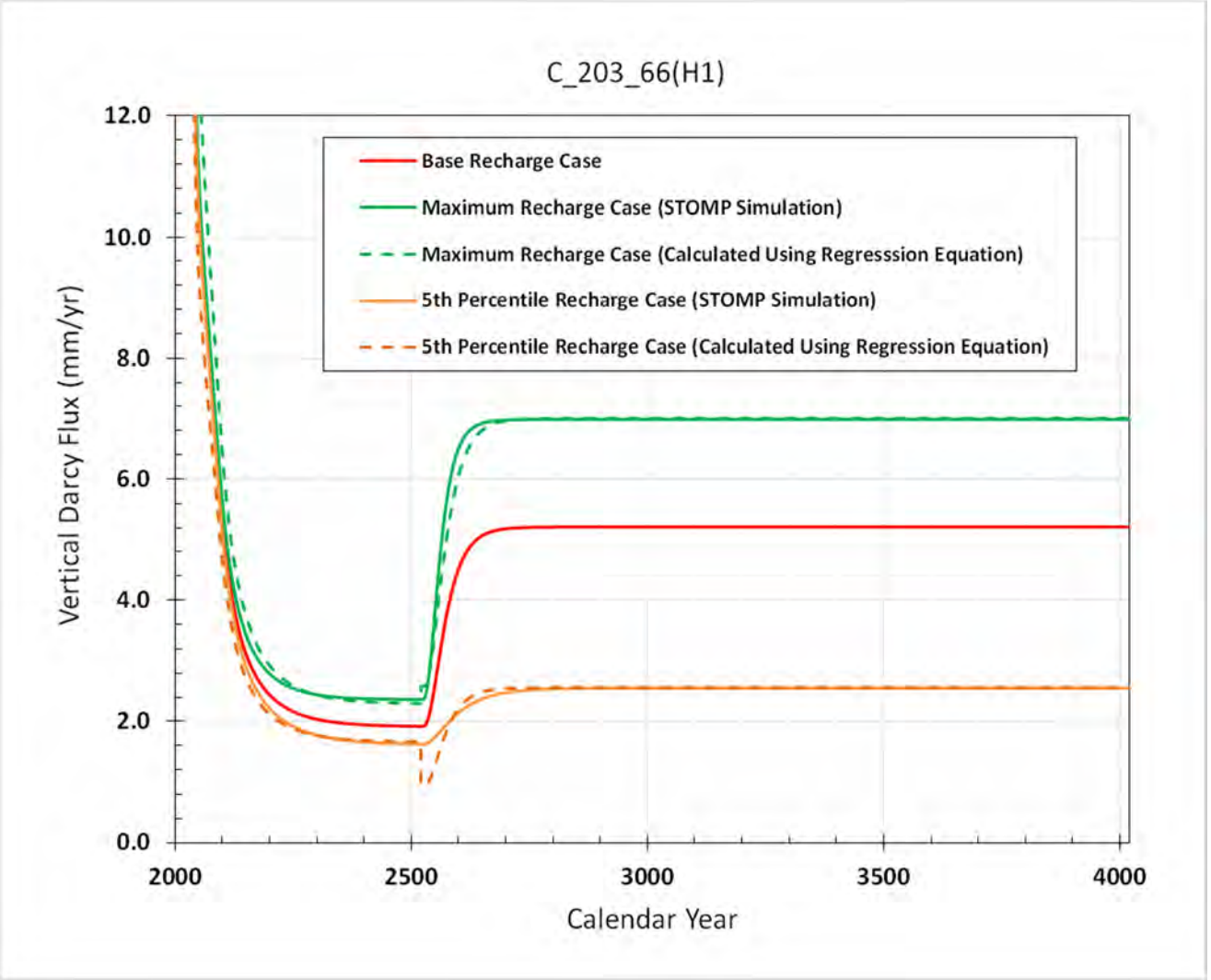

Figure 5-21. Comparison between Darcy Flux Calculated using Regression Equation and that Obtained from Three-Dimensional Subsurface Transport Over Multiple Phases Based Model Simulation for the 5th Percentile Hydraulic Property Case for (a) H1 Unit under 100-Series Tank (Node 66); (b) H2 Unit under 100-Series Tank (Node 47); (c) H1 Unit under 200-Series Tank (Node 66); and (d) H2 Unit under 200-Series Tank (Node 43). (sheet 4 of 4)

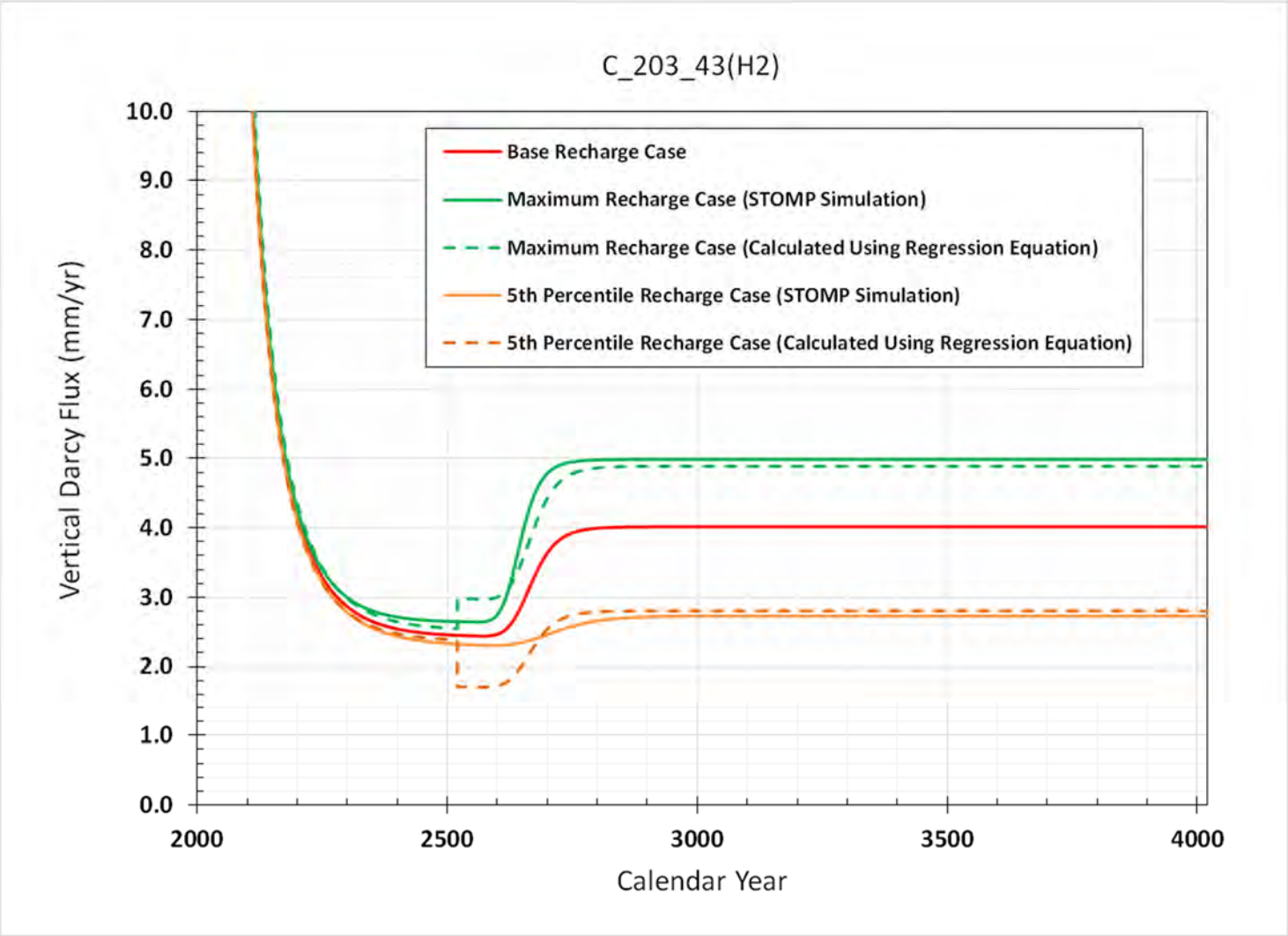

6 MODEL LIMITATIONS

The system model described in the report is developed specifically to evaluate the long-term impact of releases to the biosphere from residual waste in WMA C tanks and ancillary equipment. The system model is developed for the site-specific conditions at WMA C and should not be used for other tank farms without performing necessary adjustments/modification.

This page intentionally left blank.

7 GOLDSIM© SOFTWARE

GoldSim© Pro use at the Hanford Site is managed and controlled such that the computational needs filled by use of GoldSim© Pro (and any associated utility codes) and the specific roles and responsibilities for management and the modeling staff and subcontractors have been identified and traced. These responsibilities include the following:

- modeler training,
- source code installation and testing,
- preserving the software and verification test results,
- validation and verification that the GoldSim© Pro quality assurance documentation demonstrate that GoldSim© Pro meets identified modeling needs and purposes,
- reporting and documenting any software errors (none were encountered during the development of the WMA C PA),
- management of the GoldSim© Pro input files, and
- contingency and disaster recovery (which was not encountered during the development of the WMA C PA).

Acceptance and installation tests of the GoldSim© Pro simulation software demonstrate that it is appropriate for its intended uses for the WMA C PA and that it has been successfully installed on the computing systems used to conduct WMA C PA modeling.

This page intentionally left blank.

8 MODEL CONFIGURATION MANAGEMENT

All inputs and outputs for the development of the WMA C PA GoldSim©-based system model are archived to the CH2M HILL Plateau Remediation Company (CHPRC) Environmental Model Management Archive (EMMA) to maintain and preserve models, input and select output files under configuration management. Inputs include the input files used in the GoldSim© simulations and the input parameters. Basis information (that information collected to form the basis for model input parameterization) is also stored in the EMMA for traceability purposes.

This page intentionally left blank.

9 MODEL RECOMMENDATIONS

None at this time.

This page intentionally left blank.

10 REFERENCES

ANL/EAD-4, 2001, "User's Manual for RESRAD Version 6," Environmental Assessment Division, Argonne National Laboratory, Argonne, Illinois.

ASME NQA-1, 2000, "Quality Assurance Requirements for Nuclear Facility Applications," American National Standards Institute/American Society of Mechanical Engineers, New York, New York.

BHI-00007, 1994, "Prototype Hanford Surface Barrier: Design Basis Document," Rev. 00, Bechtel Hanford, Inc., Richland, Washington.

BPF-73550, 1944, "Specifications For Construction of Composite Storage Tanks Bldg. No. 241 Hanford Engineer Works Project 9536," Rev. 2, Richland, Washington.

Bruckler, L., B. C. Ball, and P. Renault, 1989, "Laboratory Estimation of Gas Diffusion Coefficient and Effective Porosity in Soils," Soil Science, Vol. 147, pp. 1–10.

Cantrell, K. J., K. C. Carroll, E. C. Buck, D. Neiner, K. N. Geiszler, 2013, "Single-pass flow-through test elucidation of weathering behavior and evaluation of contaminant release models for Hanford tank residual radioactive waste," Applied Geochemistry, Vol. 28, pp. 119–127.

Cantrell, K. J., W. J. Deutsch, and M. J. Lindberg, 2011, "Thermodynamic Model for Uranium Release from Hanford Site Tank Residual Waste," Environmental Science & Technology, Vol. 45, No. 4, pp. 1473–1480.

CP-14873, 2003, "200-BP-1 Prototype Hanford Barrier Annual Monitoring Report for Fiscal Year 2002," Rev. 0, Fluor Hanford, Inc., Richland, Washington.

DOE G 435.1-1, 1999, Implementation Guide for Use with DOE M 435.1-1, Radioactive Waste Management Manual, U.S. Department of Energy, Washington, D.C.

DOE O 414.1D, 2011, Quality Assurance, U.S. Department of Energy, Washington, D.C.

DOE O 435.1, 2001, Radioactive Waste Management, U.S. Department of Energy, Washington, D.C.

DOE/RL-93-33, 1996, Focused Feasibility Study of Engineered Barriers for Waste Management Units in the 200 Areas, Rev. 1, U.S. Department of Energy, Richland Operations Office, Richland, Washington.

DOE-STD-1196-2011, 2011, Derived Concentration Technical Standard, U.S. Department of Energy, Washington, D.C.

Ecology, EPA, and DOE, 1989, Hanford Federal Facility Agreement and Consent Order – Tri-Party Agreement, 2 vols., as amended, State of Washington Department of Ecology, U.S. Environmental Protection Agency, and U.S. Department of Energy, Olympia, Washington.

EPA, 2014, CAP88-PC Version 4.0 User Guide, U.S. Environmental Protection Agency, Washington, D.C.

Gee, G. W., M. J. Fayer, M. L. Rockhold, and M. D. Campbell, 1992, "Variations in Recharge at the Hanford Site," Northwest Science, Vol. 66, No. 4, pp. 237–250.

GoldSim Technology Group, 2014a, "GoldSim Contaminant Transport Module User's Guide," Version 6.4, GoldSim Technology Group, Issaquah, Washington.

GoldSim Technology Group, 2014b, "GoldSim Distributed Processing Module User's Guide," Version 11.1, GoldSim Technology Group LLC, Issaquah, Washington.

GoldSim Technology Group, 2014c, "GoldSim Probabilistic Simulation Environment User's Guide," Version 11.1, GoldSim Technology Group LLC, Issaquah, Washington.

Haynes, W. M. and D. R. Lide, 2011, CRC Handbook of Chemistry and Physics, 92nd Edition, CRC Press, Talyor & Francis Group, Boca Raton, Florida.

ICRP, 2008, "ICRP Publication 107: Nuclear Decay Data for Dosimetric Calculations," Annals of the ICRP, International Commission on Radiation Protection, Vol. 38, No. 3, pp. 7–96.

Jin, Y. and W. A. Jury, 1996, "Characterizing the Dependence of Gas Diffusion Coefficient on Soil Properties," Soil Science Society of America Journal, Vol. 60, No. 1, pp. 66–71.

Karimi, A. A., W. J. Farmer, and M. M. Cliath, 1987, "Vapor-phase Diffusion of Benzene in Soil," Journal of Environmental Quality, Vol. 16, No. 1, pp. 38–43.

Liu, G., B. Li, K. Hu, and M. T. van Genuchten, 2006, "Simulating the Gas Diffusion Coefficient in Macropore Network Images: Influence of Soil Pore Morphology," Soil Science Society of America Journal, Vol. 70, pp. 1252–1261.

Millington, R. J., and J. P. Quirk, 1960, "Transport in porous media," in Transactions of the 7th International Congress of Soil Science, Madison, Wisconsin, Vol. 1, pp. 97–106.

Millington, R. J. and J. P. Quirk, 1961, "Permeability of Porous Solids," Transactions of the Faraday Society, Vol. 57, pp. 1200–1207.

Moldrup, P., S. Yoshikawa, T. Olesen, T. Komatsu, and D. E. Rolston, 2003, "Gas Diffusivity in Undisturbed Volcanic Ash Soils: Test of Soil-Water-Characteristic-Based Prediction Models," Soil Science Society of America Journal, Vol. 67, No. 1, pp. 41–51.

Moldrup, P., T. Oleson, S. Yoshikawa, T. Komatsu, and D. E. Rolston, 2004, "Three-Porosity Model for Predicting the Gas Diffusion Coefficient in Undisturbed Soil," Soil Science Society of America Journal, Vol. 68, No. 3, pp. 750–759.

NAGRA NTB 02-20, 2002, "Cementitious Near-Field Sorption Data Base for Performance Assessment of an ILW Repository in Opalinus Clay," Technical Report 02-20, National Cooperative for the Disposal of Radioactive Waste, Hardstrasse, Zurich, Switzerland.

Nazaroff, W. W. and A. V. Nero, 1988, Radon and Its Decay Products in Indoor Air, John Wiley & Sons, New York, New York.

NCRP Report No. 103, 1989, "Control of Radon in Houses," National Council on Radiation Protection and Measurements, Bethesda, Maryland.

NCRP Report No. 152, 2005, "Performance Assessment of Near-Surface Facilities for Disposal of Low-Level Radioactive Waste," National Council on Radiation Protection and Measurements, Bethesda, Maryland.

NIROND-TR 2008-23 E, "Review of sorption values for the cementitious near field of a near surface radioactive waste disposal facility, Project near surface disposal of category A waste at Dessel," Belgian Agency for Radioactive Waste and Enriched Fissile Materials, Brussels, Belgium.

Pasquill, F., 1961, "The Estimation of the Dispersion of Windborne Material," The Meteorological Magazine, Vol. 90, No. 1063, pp. 33–49.

Plummer, M. A., L. C. Hull, and D. T. Fox, 2004, "Transport of Carbon-14 in a Large Unsaturated Soil Column," Vadose Zone Journal, Vol. 3, No. 1, pp. 109–121.

PNNL-14702, 2006, "Vadose Zone Hydrogeology Data Package for Hanford Assessments," Rev. 1, Pacific Northwest Laboratory, Richland, Washington.

PNNL-14744, 2004, "Recharge Data Package for the 2005 Integrated Disposal Facility Performance Assessment," Pacific Northwest National Laboratory, Richland, Washington.

PNNL-15160, 2005, "Hanford Site Climatological Summary 2004 with Historical Data," Pacific Northwest National Laboratory, Richland, Washington.

PNNL-16663, 2007, "Geochemical Processes Data Package for the Vadose Zone in the Single-Shell Tank Waste Management Areas at the Hanford Site," Pacific Northwest National Laboratory, Richland, Washington.

PNNL-16688, 2007, "Recharge Data Package for Hanford Single-Shell Tank Waste Management Areas," Pacific Northwest National Laboratory, Richland, Washington.

PNNL-17154, 2008, “Geochemical Characterization Data Package for the Vadose Zone in the Single-Shell Tank Waste Management Areas at the Hanford Site,” Pacific Northwest National Laboratory, Richland, Washington.

PNNL-23841, 2014, “Radionuclide Migration through Sediment and Concrete: 16 Years of Investigations,” Pacific Northwest National Laboratory, Richland, Washington.

PSI Bericht Nr. 95-06, 1995, “Sorption Databases for the Cementitious Near-Field of a L/ILW Repository for Performance Assessment,” Paul Scherrer Institute, Switzerland.

Resource Conservation and Recovery Act of 1976, 42 USC 6901, et seq.

RPP-CALC-54266, 2013, “Post-Hard Heel Retrieval Camera/CAD Modeling System Waste Volume Estimate for Tank 241-C-108,” Rev. 0, Washington River Protection Solutions, LLC, Richland, Washington.

RPP-CALC-60451, in process, “WMA C System Model for Performance Assessment of Base Case, Uncertainty Analysis, and Sensitivity Analysis,” Rev. 0, Washington River Protection Solutions, LLC, Richland, Washington.

RPP-ENV-58813, in process, “Exposure Scenarios for Risk and Performance Assessments in Tank Farms at the Hanford Site, Washington,” Rev. 0, Washington River Protection Solutions, LLC, Richland, Washington.

RPP-PLAN-47559, 2012, “Single-Shell Tank Waste Management Area C Pipeline Feasibility Evaluation,” Rev. 1, Washington River Protection Solutions, LLC/Cenibark International, Inc., Richland, Washington.

RPP-RPT-42323, 2015, “Hanford C-Farm Tank and Ancillary Equipment Residual Waste Inventory Estimates,” Rev. 3, Washington River Protection Solutions, LLC, Richland, Washington.

RPP-RPT-46088, 2010, “Flow and Transport in the Natural System at Waste Management Area C,” Rev. 1, Washington River Protection Solutions, LLC/GSI Water Solutions, Inc., Richland, Washington.

RPP-RPT-46879, 2011, “Corrosion and Structural Degradation within Engineered System in Waste Management Area C,” Rev. 2, Washington River Protection Solutions, LLC, Richland, Washington.

RPP-RPT-50934, 2012, “Inspection and Test Report for the Removed 241-C-107 Dome Concrete,” Rev. 0, Washington River Protection Solutions, LLC, Richland, Washington.

RPP-RPT-58949, in process, “Model Package Report Flow and Contaminant Transport Numerical Model used in WMA C Performance Assessment and RCRA Closure Analysis,” INTERA, Richland, Washington.

Sakoda, A., Y. Ishimori, and K. Yamaoka, 2011, "A comprehensive review of radon emanation measurements for mineral, rock, soil, and fly ash," Applied Radiation and Isotopes, Vol. 69, Issue 10, pp. 1422–1435.

Sander, R., 1999, "Compilation of Henry's Law Constants for Inorganic and Organic Species of Potential Importance in Environmental Chemistry," Version 3, Max-Planck Institute of Chemistry, Mainz, Germany.

SKB Rapport R-05-75, 2005, "Assessment of uncertainty intervals for sorption coefficients, SFR-1 uppföljning av SAFE," Swedish Nuclear Fuel and Waste Management Company, Stockholm, Sweden.

SRNL-STI-2008-00421, 2008, "Hydraulic and Physical Properties of Saltstone Grouts and Vault Concretes," Rev. 0, Savannah River National Laboratory, Savannah River Nuclear Solutions, Aiken, South Carolina.

Tank Waste Information Network System (TWINS), Queried 02/10/2014, [WMA C Tanks, wt% water in sludge/solid waste type], http://twins.pnl.gov/twins.htm.

United States Environmental Protection Agency, Queried 01/2012, [EPA On-line Tools for Site Assessment Calculation], http://www.epa.gov/athens/learn2model/part-two/onsite/estdiffusion-ext.html.

WHC-EP-0772, 1994, "Characterization of the Corrosion Behavior of the Carbon Steel Liner in Hanford Site Single-Shell Tanks," Rev. 0, Westinghouse Hanford Company, Richland, Washington.

Wing, N. R. and G. W. Gee, 1994, "Quest for the Perfect Cap," Civil Engineering, Vol. 64, No. 10, pp. 38-41.

WSRC-STI-2007-00369, 2007, "Hydraulic and Physical Properties of Tank Grouts and Base Mat Surrogate Concrete for FTF Closure," Rev. 0, Savannah River National Laboratory, Aiken, South Carolina.

WSRC-TR-2005-00195, 2005, "Summary of Grout Development and Testing for Single Shell Tank Closure at Hanford," Rev. 0, Savannah River National Laboratory, Aiken, South Carolina.

Xu, X., J. L. Nieber, and S. C. Gupta, 1992, "Compaction Effect on the Gas Diffusion Coefficient in Soils," Soil Science Society of America Journal, Vol. 56, No. 6, pp. 1743–1750.

This page intentionally left blank.

APPENDIX A

RESULTS ILLUSTRATING VADOSE ZONE FLOW-FIELD UNCERTAINTY RANGE

This page intentionally left blank.

TABLE OF CONTENTS

APPENDIX A – RESULTS ILLUSTRATING VADOSE ZONE FLOW-FIELD UNCERTAINTY RANGE A-1

LIST OF FIGURES

Figure A-1. Results for H1 Unit for Base Case Recharge Rates for Five Hydraulic Properties in Vadose Zone. A-3

Figure A-2. Results for H2 Unit for Base Case Recharge Rates for Five Hydraulic Properties in Vadose Zone. A-6

Figure A-3. Results for H3 Unit for Base Case Recharge Rates for Five Hydraulic Properties in Vadose Zone. A-9

This page intentionally left blank.

APPENDIX A

RESULTS ILLUSTRATING VADOSE ZONE FLOW-FIELD UNCERTAINTY RANGE

The purpose of this appendix is to present information on the uncertainty range in vertical Darcy flux and volumetric moisture content in order to illustrate the range and magnitude of vertical pore water velocities over the full range of uncertainty in recharge rates. Development of vadose zone flow field and propagation of uncertainty is discussed in detail in Section 5.2.

The flow fields are abstracted from the three-dimensional Subsurface Transport Over Multiple Phases (STOMP)©[1] modeling results as a way to efficiently evaluate the effect of uncertainty in the vadose zone flow using the GoldSim©[2]-based system model. The flow fields are developed for five different vadose zone hydraulic properties to represent the range of vertical linear pore water velocities in the vadose zone under base case recharge conditions (Figures 5-14, 5-15, and 5-16). In order to derive the vertical pore water velocity for other recharge conditions, regression equations are developed that are used to scale the vertical Darcy flux and volumetric moisture content estimates for each of the five hydraulic properties using base case recharge rates. The regression equations for scaling vertical Darcy flux underneath 100-series tanks are presented in Table 5-8 and that for the 200-series tanks is presented in Table 5-9 for H1, H2, and H3 units. The scaling of the volumetric moisture content is simpler and presented in Table 5-10. Note that these scaling multipliers are dimensionless and are applied to values calculated under base recharge conditions, as abstracted from three-dimensional STOMP© model results for each of the five hydraulic properties.

The results are presented by taking the regression equations shown in Tables 5-8 and 5-10 (for 100-series tanks) and performing the calculations over the minimum and maximum recharge rates over the post-closure time period to illustrate the uncertainty range in vertical average linear pore water velocities. The results from 200-series tanks are not presented as they lead to similar uncertainty range as the 100-series tanks. Since the recharge rates are estimated for two time periods, an early post-closure time period (first 500 years while the surface cover is intact) and late post-closure time period (for the remaining time period with degraded surface cover), the uncertainties in recharge rates are different for these two time periods. As presented in Table 5-1, for the early post-closure time period, the minimum recharge rate within the WMA C area is 0.1 mm/yr and the maximum is 0.9 mm/yr with the base case recharge rate being 0.5 mm/yr. For the late post-closure time period the minimum recharge rate is 0.5 mm/yr and the maximum is 5.2 mm/yr while the base case recharge rate is 3.5 mm/yr. The minimum and maximum recharge rates are applied in the regression equations to calculate the scaling of vertical Darcy flux and volumetric moisture content relative to those based on the base case recharge rates. From this the vertical average linear pore water velocities are estimated at a given time by dividing the vertical Darcy flux with the volumetric moisture content value for each unit (H1, H2, and H3). Although the vertical Darcy flux and volumetric moisture content for H2 and H3 are different, the scaling multipliers are the same as noted in Tables 5-8 and 5-10.

---

[1] Subsurface Transport Over Multiple Phases (STOMP)© is copyrighted by Battelle Memorial Institute, 1996.

[2] GoldSim© simulation software is copyrighted by GoldSim Technology Group LLC of Issaquah, Washington (see http://www.goldsim.com).

Results for each of the three units is presented below for the representative node within that unit to illustrate the uncertainty. For each unit, the time histories of vertical Darcy flux, volumetric moisture content, and vertical linear pore water velocity under base case recharge conditions are presented for each of the five hydraulic properties noted as 5th percentile, 25th percentile, 50th percentile, 75th percentile, and 95th percentile. Next, the scaling multiplier calculated for vertical Darcy flux is presented based on the regression equations for the minimum and maximum recharge rate cases for each of the five hydraulic properties (percentile cases). After that, the resulting vertical linear pore water velocities are presented for each of the five hydraulic properties evaluated under minimum and maximum recharge rates. The scaling multipliers and resulting vertical velocity values do not change at late times and, therefore, the results are only presented up to 1,000 years following closure.

The variation in volumetric moisture content is not appreciable for the various recharge cases within the early post-closure time period and vary marginally after that; the scaling of volumetric moisture content is either 0.93 (for minimum recharge case) or 1.3 (for maximum recharge case) for the post-closure time period. These results are not presented separately.

Results for H1 unit are presented in Figure A-1, while those for H2 and H3 units are presented in Figures A-2 and A-3. Figure A-1c shows the range in vertical linear pore water velocity for the H1 unit under base case recharge conditions. It represents the uncertainty range that could result from the choice of hydraulic properties alone. Figure A-1d shows the range in scaling multiplier for each of the five hydraulic properties over the minimum and maximum recharge rates while Figure A-1e presents the corresponding range in vertical linear pore water velocities, which affects transport of contaminants via advection. The uncertainty range (spread) in the vertical linear pore water velocities is the largest for the 95th percentile hydraulic property (factor of 6.5) and minimum for the 25th percentile hydraulic property (factor of 2). For other hydraulic properties the range varies by factor of 3 to 3.3.

For H2 and H3 units the result are similar. The uncertainty range (spread) in the vertical linear pore water velocities is the largest for the 95th percentile hydraulic property (factor of 6.4) and minimum for the 25th percentile hydraulic property (factor of 2.5). For other hydraulic properties the range varies by factor of 3 to 4.1.

These results indicate that for realizations where 95th percentile hydraulic property is selected during uncertainty analysis, greater variance in travel times can be expected compared to other hydraulic properties (under similar recharge rate range).

Figure A-22. Results for H1 Unit for Base Case Recharge Rates for Five Hydraulic Properties in Vadose Zone. (1 of 3 sheets)

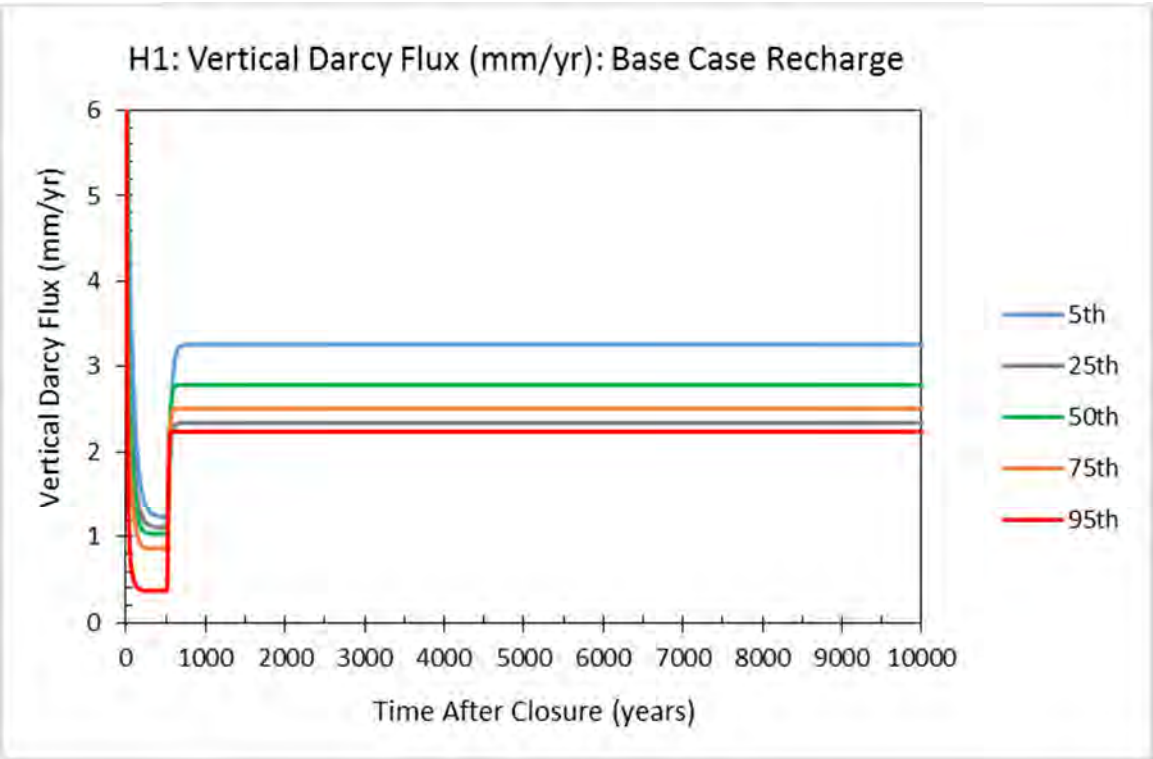

(a)

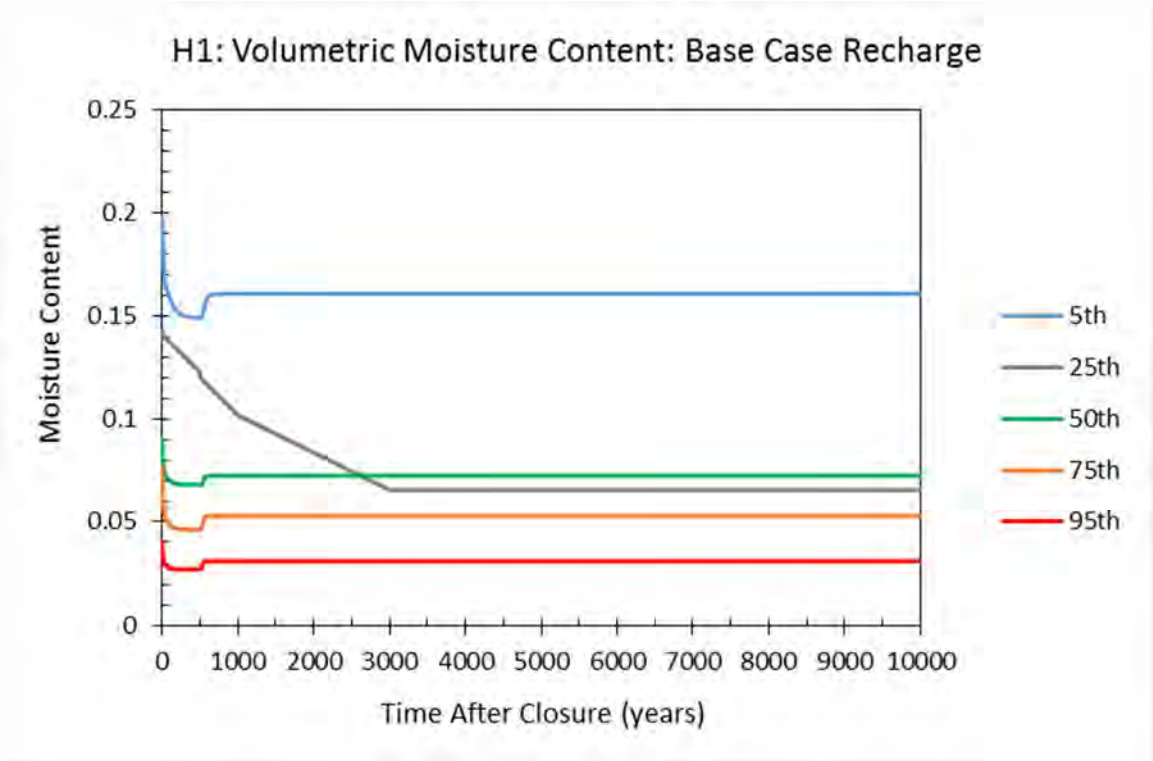

(b)

Figure A-1. Results for H1 Unit for Base Case Recharge Rates for Five Hydraulic Properties in Vadose Zone. (2 of 3 sheets)

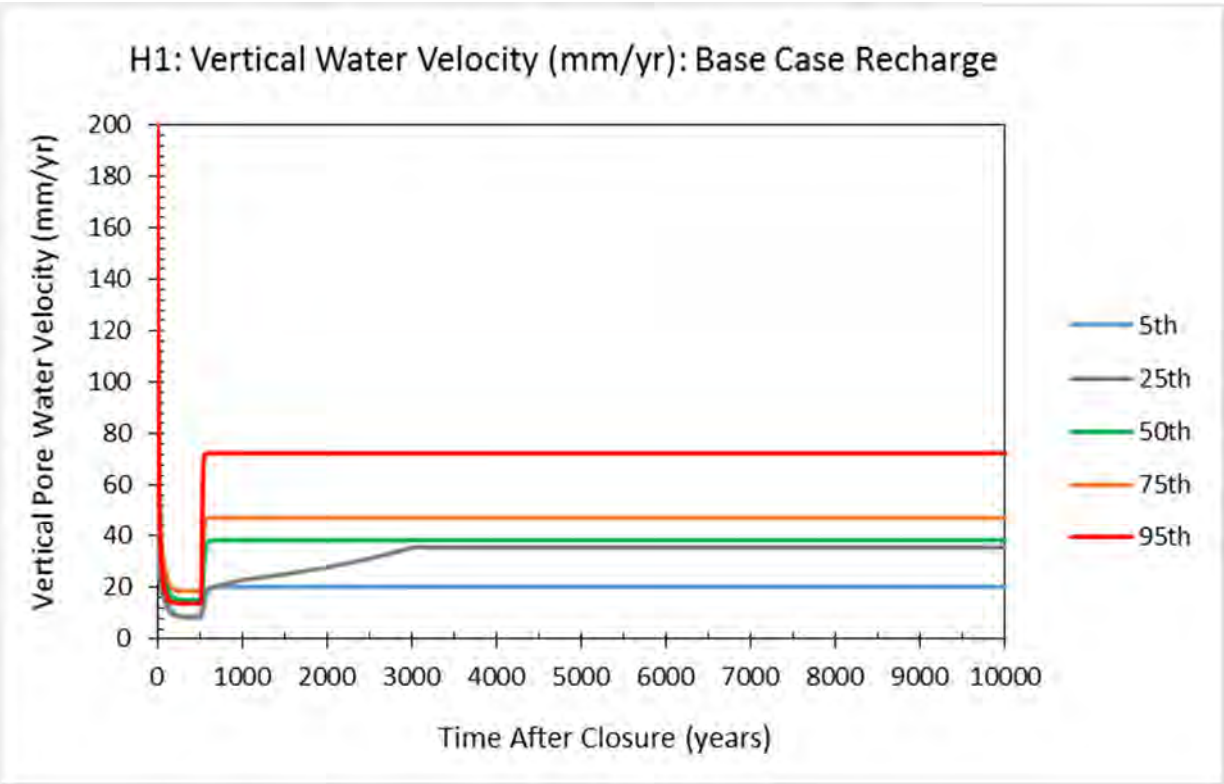

(c)

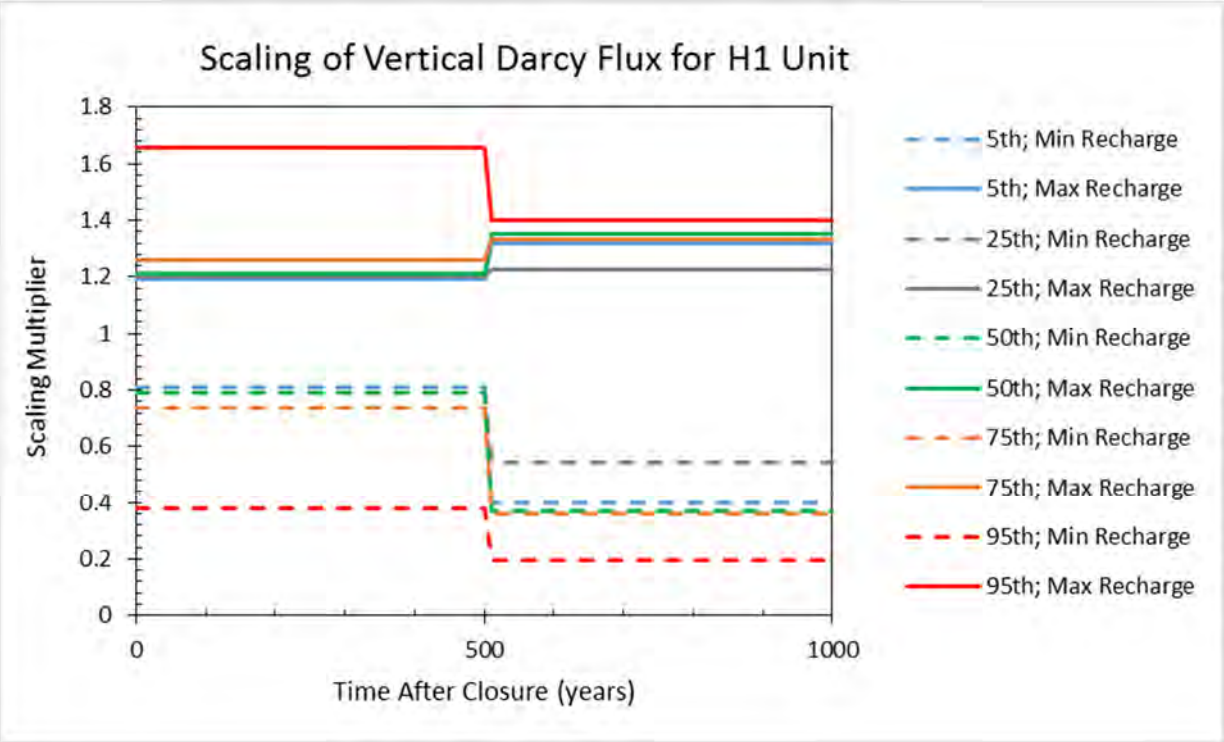

(d)

Figure A-1. Results for H1 Unit for Base Case Recharge Rates for Five Hydraulic Properties in Vadose Zone. (3 of 3 sheets)

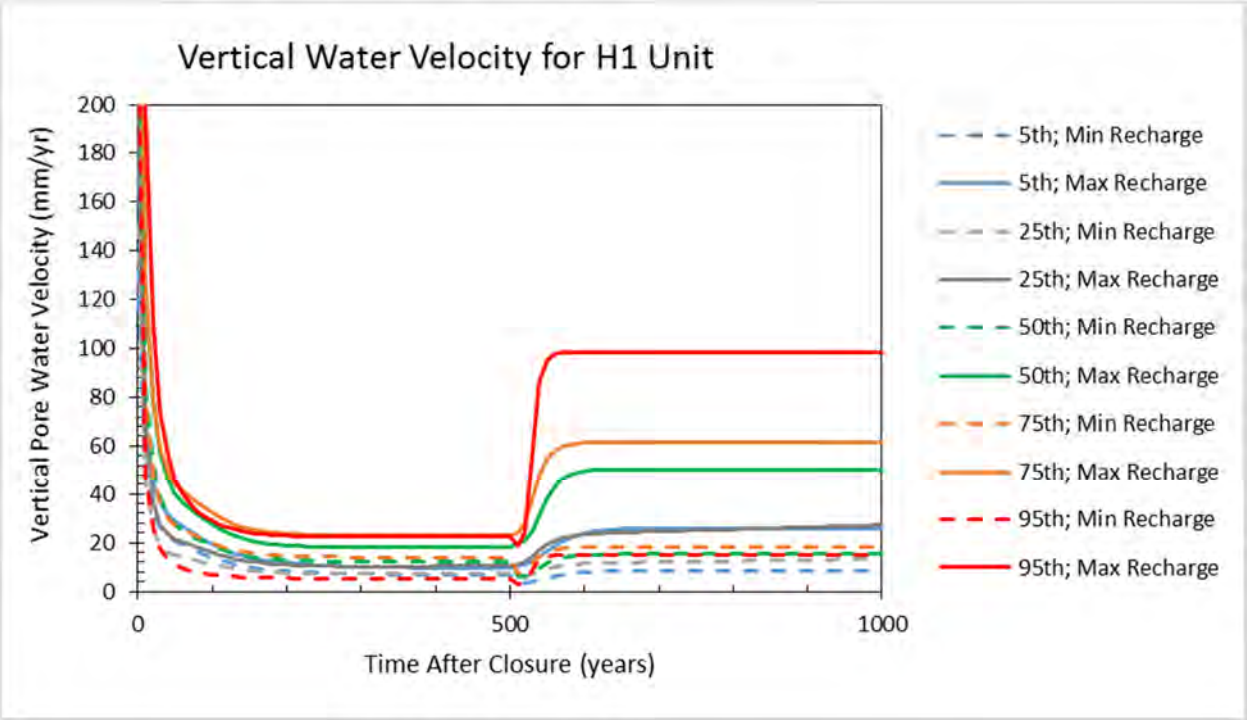

(e)

Figure A-23. Results for H2 Unit for Base Case Recharge Rates for Five Hydraulic Properties in Vadose Zone. (1 of 3 sheets)

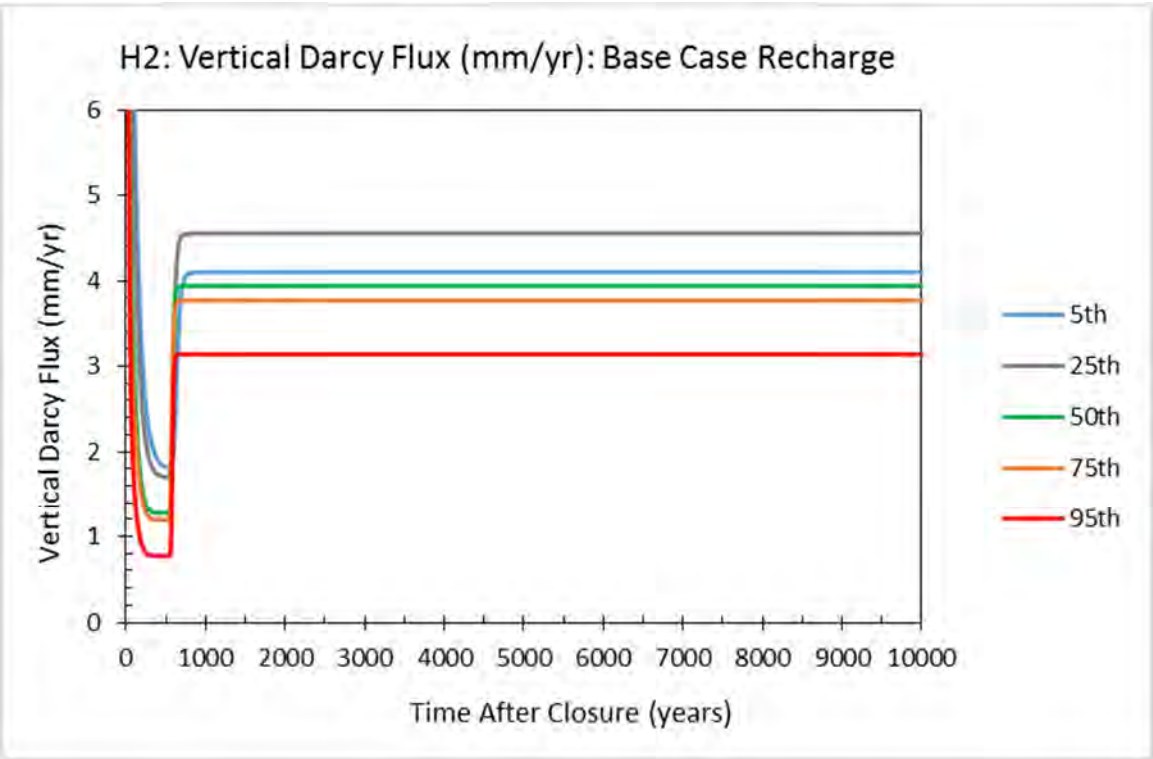

(a)

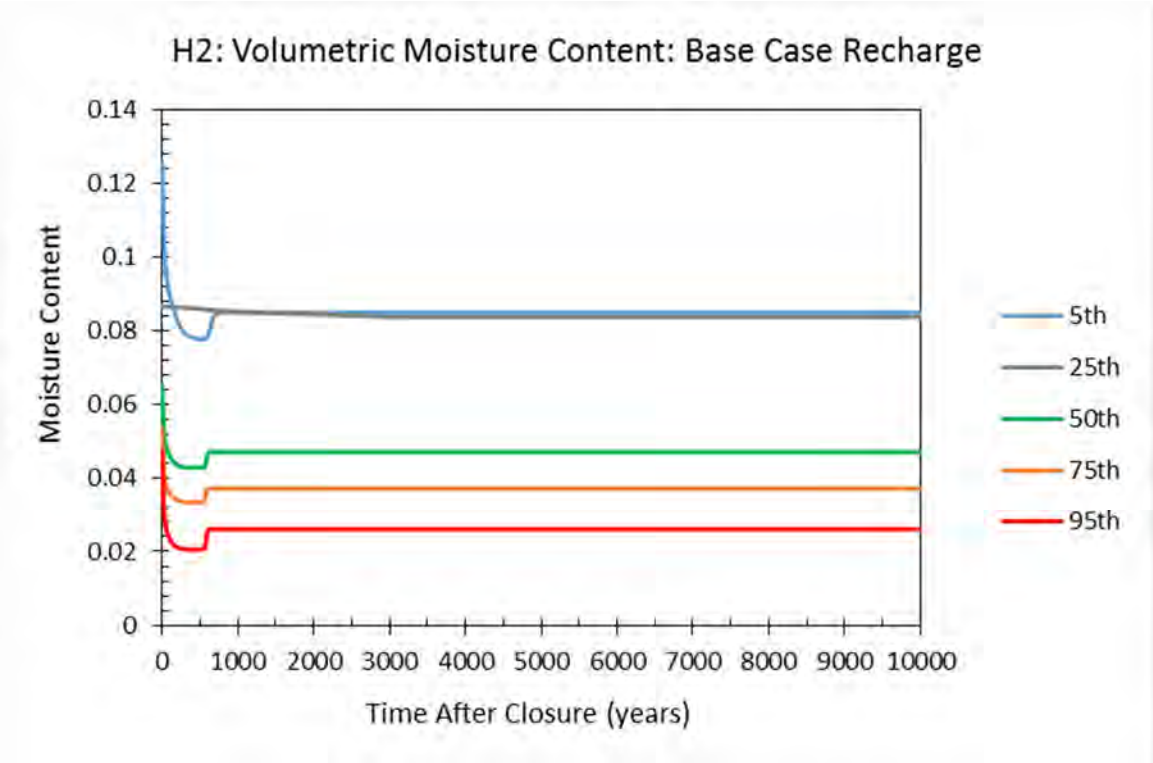

(b)

Figure A-2. Results for H2 Unit for Base Case Recharge Rates for Five Hydraulic Properties in Vadose Zone. (2 of 3 sheets)

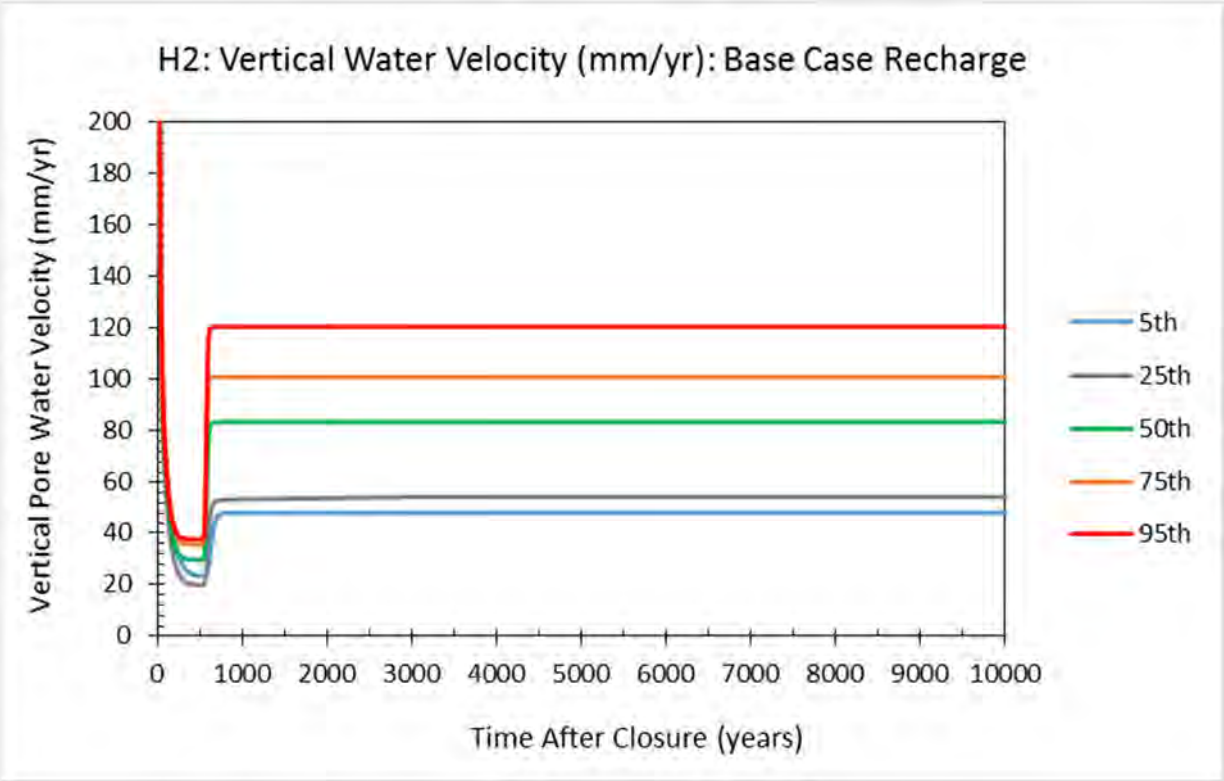

(c)

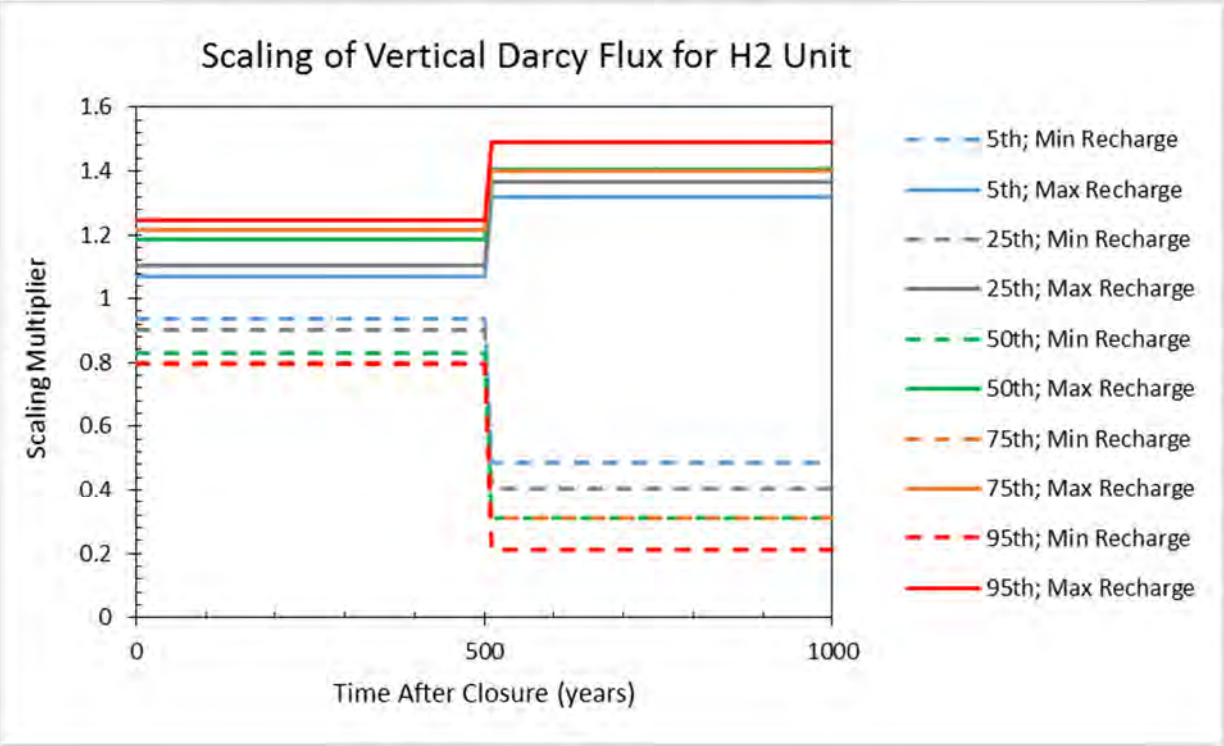

(d)

Figure A-2. Results for H2 Unit for Base Case Recharge Rates for Five Hydraulic Properties in Vadose Zone. (3 of 3 sheets)

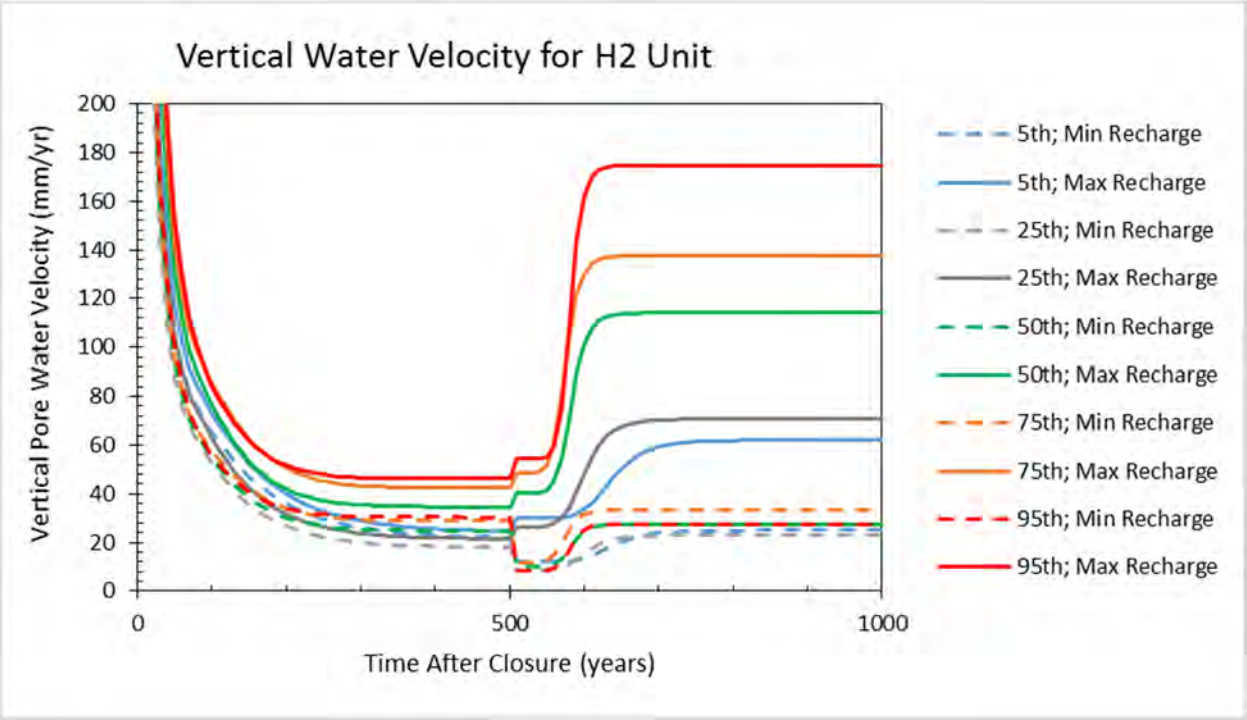

(e)

Figure A-3. Results for H3 Unit for Base Case Recharge Rates for Five Hydraulic Properties in Vadose Zone. (1 of 3 sheets)

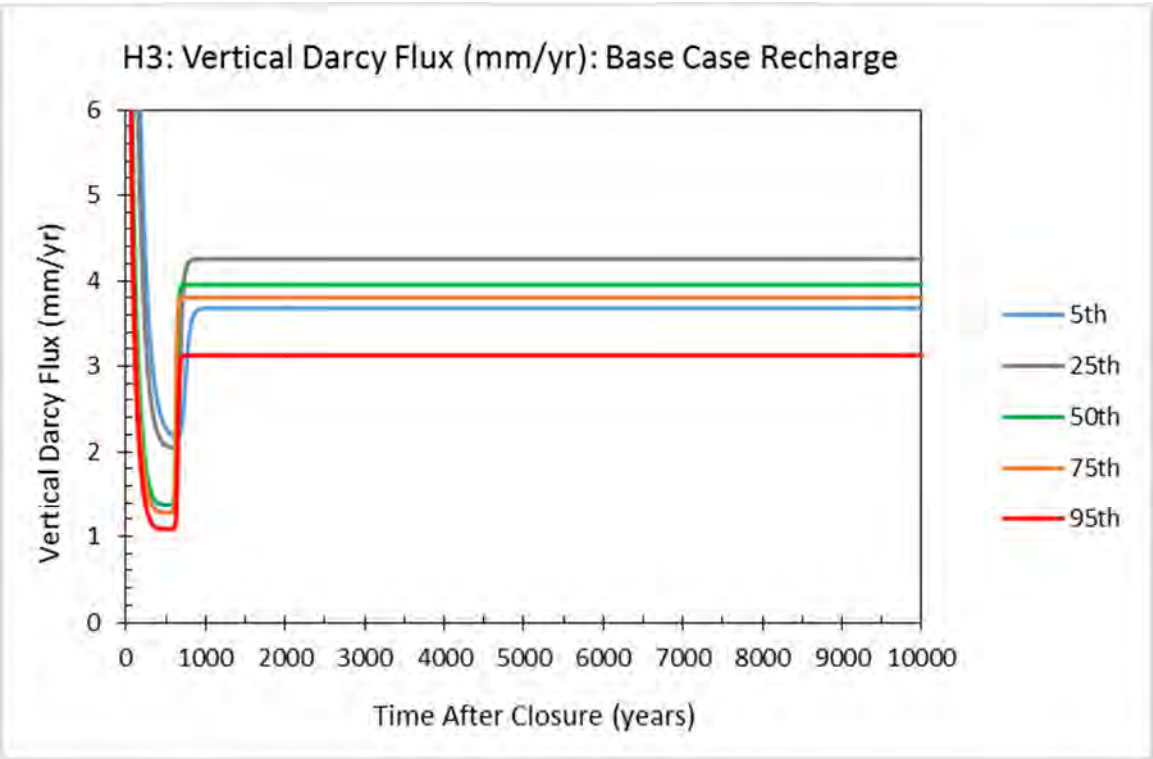

(a)

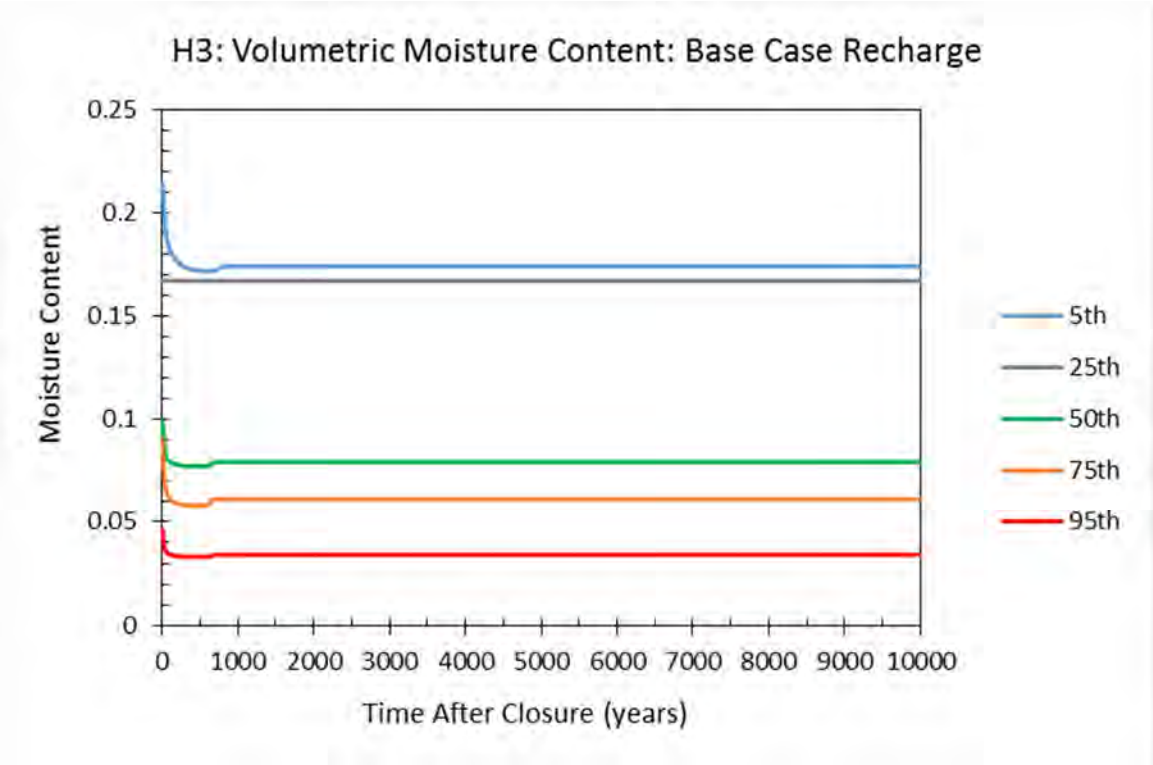

(b)

Figure A-3. Results for H3 Unit for Base Case Recharge Rates for Five Hydraulic Properties in Vadose Zone. (2 of 3 sheets)

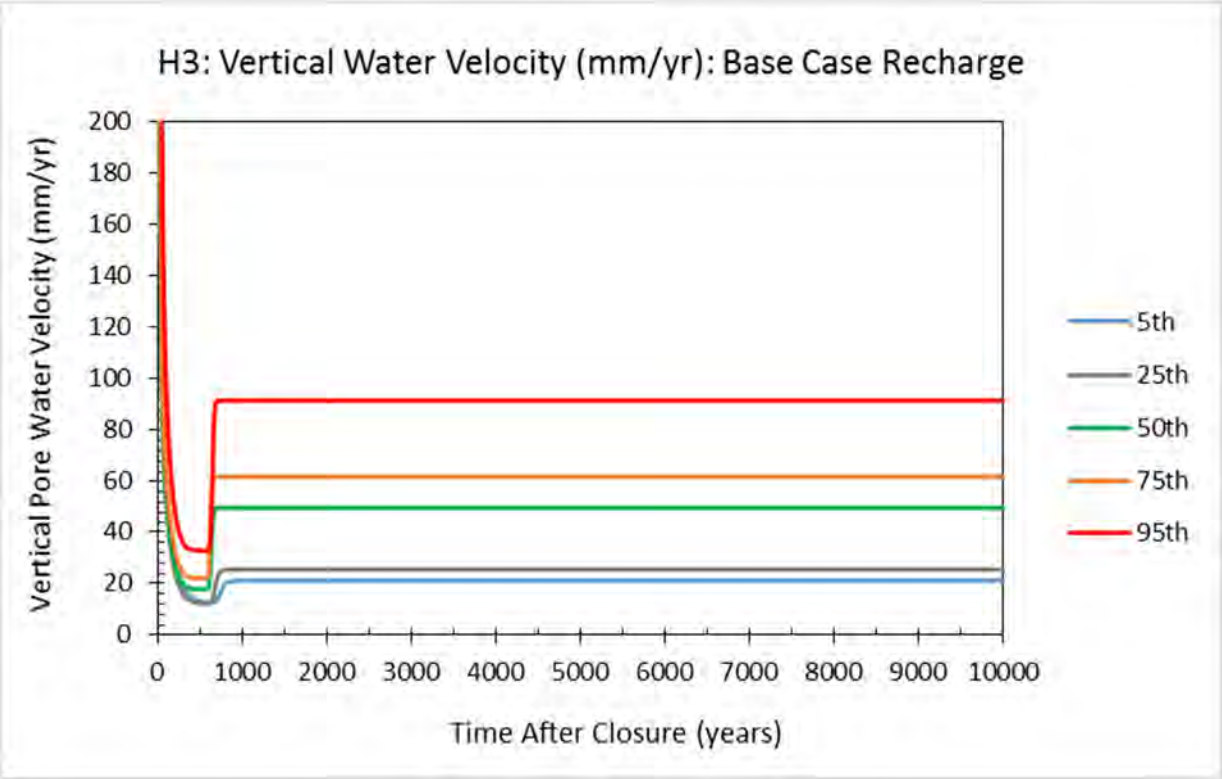

(c)

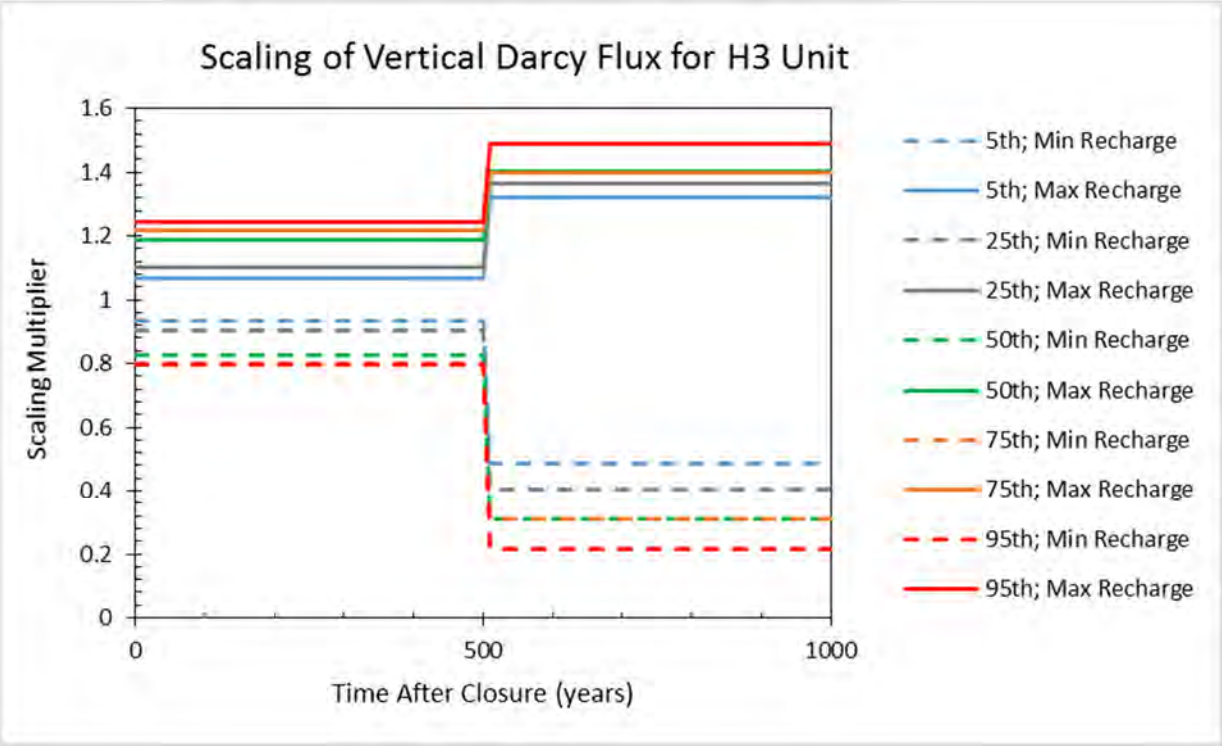

(d)

Figure A-3. Results for H3 Unit for Base Case Recharge Rates for Five Hydraulic Properties in Vadose Zone. (3 of 3 sheets)

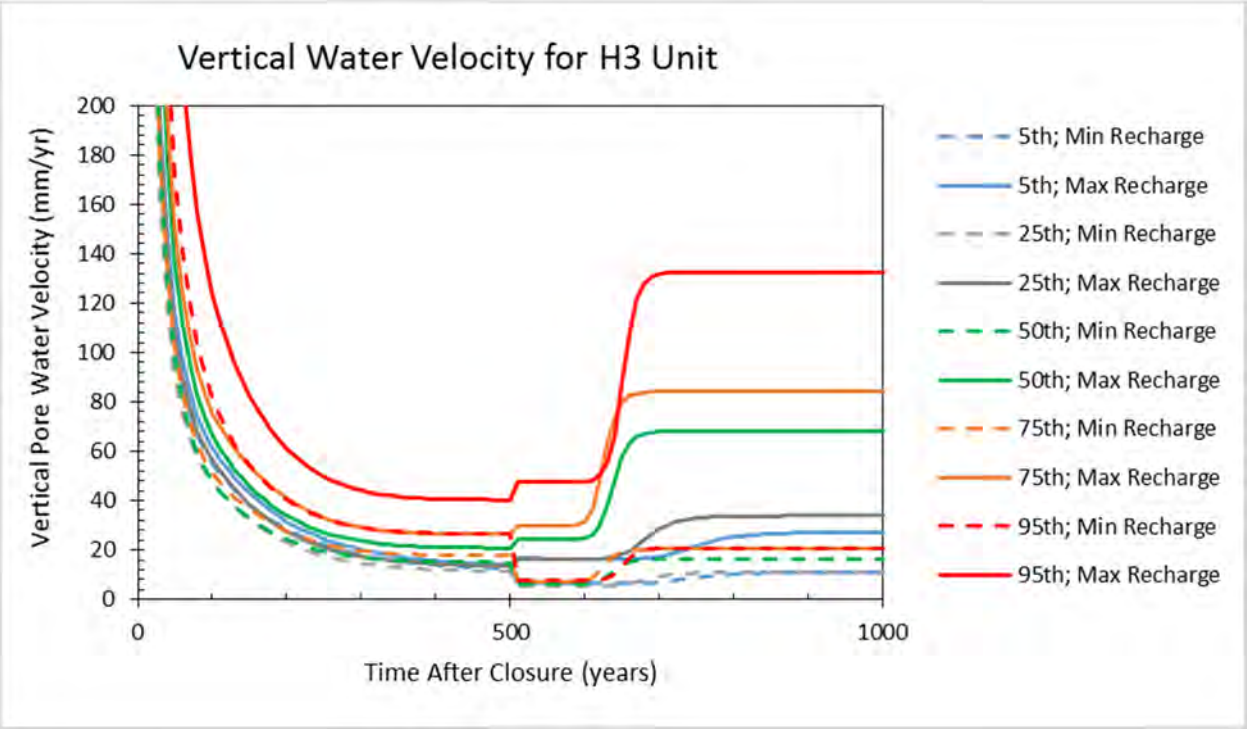

(e)

This page intentionally left blank.